Theoretical and *in vitro* analysis of iron acquisition in *Pasteurella multocida* A:3

Alexander James Macdonald

Ph.D.

The University of Edinburgh

2009

Declaration

This thesis is wholly my own work and no part of it has been submitted for any other degree or qualification.

Alexander James Macdonald, April 2009

Acknowledgements

I would like to acknowledge first my supervisors Chris Hodgson, Junli Liu, Frank Wright and Ian Poxton for all their invaluable help with every aspect of my work. Also, everyone at Moredun Research Institute for their friendliness and support, both scientific and social. In particular, Willie Donachie, Colin Bayne for passing on to me a fraction of his encyclopaedic knowledge, Malcolm Quirie for his bacteriological genius, Gordon Moon for… teaching me how to play skittles (and help in the lab), and everyone else in lab 3.060. Particular thanks go to David Frew and Gordon Moon for helping out with the Microreactor experiments despite destroying the compressor!

This work was part of a joint Systems Grant with the Scottish Crop Research Institute and as such I would like to thank Paul Birch, Ian Toth and Leighton Pritchard for their involvement in the collaborative aspects of the project. Similar thanks go BioSS, also partners in the Systems Grant. Funding from SEERAD is gratefully acknowledged.

Lastly, I'd like to thank my girlfriend Hazel, my dad and all the other members of my family and friends for being so supportive and helpful.

Abstract

A key bacterial virulence factor is the ability to acquire the micronutrient iron, required by a vast majority of micro-organisms for survival and proliferation within their hosts. The work described here focuses on acquisition of iron in *Pasteurella multocida* serotype A:3, a Gram-negative opportunistic pathogen that causes pneumonic pasteurellosis in cattle, a severe respiratory infection of significant economic burden and welfare concern. *P. multocida* A:3 acquires iron primarily from the host iron-chelating molecule transferrin through the expression of specific outer membrane receptors. The correlation between up-regulation of these receptors and of other iron-regulated outer membrane proteins (IROMPs) and an increase in bacterial virulence has been noted elsewhere. To date, there has been no systems analysis of the metabolic processes of iron acquisition published for any bacterial species. The work described here used a systems approach involving elementary flux modes analysis to derive a computational model of iron acquisition and reveal a number of key findings on the mechanisms of iron acquisition and links between iron uptake, glucose metabolism and protein synthesis. This *in silico* model was subjected to experimental validation through a range of *in vitro* experiments designed to investigate the links between iron restriction and growth and metabolism of *P. multocida*. This novel approach was only possible after the development and optimisation of a number of assays to measure key model parameters.

Key findings included:

1. An *in silico* description of iron acquisition by a bacterial pathogen with complementary *in vitro* analyses, allowing the identification and quantitation of the key pathways involved.
2. The Ton system, a membrane-associated energy-transducing complex was confirmed as playing a vital role in transmembrane iron transport in *P. multocida.*
3. The fundamental role of ATP in both protein synthesis and iron uptake was highlighted.
4. A greater understanding of the fundamental role played by iron acquisition in bacterial virulence.
5. Suggestions of key foci for potential future prophylactic or therapeutic strategies.
6. Perhaps most interestingly, the model suggested a constant low-level influx of iron into *P. multocida* driven by highly efficient pathways of short path length. Longer, less efficient pathways were utilised when iron was in short supply and increased uptake was required. In addition, an energy-efficient 'recycling' of previously expressed iron uptake proteins was shown to occur.

Contents

List of tables

Chapter 1

Chapter 2

Chapter 3

Chapter 4

Chapter 5

Chapter 6

List of figures

Chapter 1

Chapter 2

Chapter 3

Chapter 4

Chapter 5

Chapter 6

Chapter 7

List of abbreviations

ABC	ATP-Binding Cassette
API	Analytical Profile Index
BHI	Brain Heart Infusion
BLAST	Basic Local Alignment Search Tool
BRSV	Bovine Respiratory Syncitial Virus
CDM	Chemically Defined Medium
CEF	Control Effective Flux
CFU	Colony Forming Unit
CMK	Cell-Mediated Killing
COBRA	COnstraints Based Reconstruction and Analysis
CYTO	Cytoplasmic
EDDA	Ethylenediaminediacetic Acid
EDTA	Ethylenediaminetetraacetic Acid
EFM	Elementary Flux Mode
EM	Elementary Mode
ET	Electron Transport
EVC	Estimated Viable Count
FBA	Flux Balance Analysis
FbpA/B/C	Ferric-binding protein A/B/C
FC	Flux Contribution
FE	Iron
Fe^{2+}	Ferrous
Fe^{3+}	Ferric
FepA	Ferric enterobactin permease A
FhuA	Ferric hydroxamate uptake receptor A
Fur	Ferric uptake regulator
G	Glycolysis
gDW	grams Dry Weight
GLU	Glucose
HasR	Haemophore-specific outer membrane Receptor
HbBP	Haemoglobin-Binding Protein
HbpA	Haemin-binding Protein A
HgbA	Haemoglobin-Binding Protein A
HgbB	Haemoglobin-binding Protein B
HitA/B/C	*Haemophilus* iron transport A/B/C
HmBP	Haemin-Binding Protein
HS	Haemorrhagic Septicaemia
IBR	Infectious Bovine Rhinotracheitis
INCORP	Incorporated
IROMP	Iron-Regulated Outer Membrane Protein
IRP	Iron-Restricted/Regulated/Related Protein
kDa	kiloDalton

KEGG	Kyoto Encyclopedia of Genes and Genomes
LbpA/B	Lactoferrin-binding protein A/B
ND	No Data
OD	Optical Density
OMP	Outer Membrane Protein
OXY	Oxygen
P	Protein
PBS	Phosphate-Buffered Saline
PCR	Polymerase Chain Reaction
PfhA	Pertussis filamentous haemagglutinin A
PMF	Proton-Motive Force
PPP	Pentose Phosphate Pathway
qRT-PCR	quantitative Reverse Transcription-PCR
r	reversible
ROS	Reactive Oxygen Species
SBA	Sheep Blood Agar
SBML	Systems Biology Markup Language
TAE	Tris-Acetate EDTA
TbpA/B	Transferrin-binding protein A/B
TCA	Tri-Carboxylic Acid cycle
TSB/YE	Tryptic Soy Broth/Yeast Extract
TSE	Transmissable Spongiform Encephalopathy
VGRO	vGROWTH
VIDA	Veterinary Investigation Diagnosis Analysis

Chapter 1. Introduction

1.1 General introduction

The repertoire of virulence factors encoded by the genome of a bacterium is integral to its success as a pathogen and affects its ability to cause disease of varying severity. Before an invading micro-organism begins to cause disease, it must first establish a niche by adhering at the site of infection and proliferating. The host immune response, if primed and activated, can prevent initial colonisation, bacterial invasion and subsequent tissue damage and dissemination. Virulence factors may be thought of as any mechanism which enables the bacterium to evade eradication by the host (Sparling, 1983) and, as well as classic virulence factors such as those in the outer membrane that interact with the host (endotoxin, capsule, fimbriae), encompass mechanisms such as micronutrient uptake, considered often only in nutrient terms for growth. A prime example of this, highlighted in many studies, is the host micronutrient iron, acquisition of which is a fundamental survival mechanism for a majority of bacteria, allowing them to exert their pathogenicity and virulence (Andrews, Robinson and Rodriguez-Quinones, 2003), including commensal bacteria (Palyada, Threadgill and Stintzi, 2004).

1.2 Iron acquisition

Iron acquisition is a process which is crucial to the colonisation, survival and pathogenesis of bacteria *in vivo*. Whereas the bacterium can obtain most other required nutrients from the host (Mims *et al*, 1998a), the acquisition of iron poses a specific problem. In spite of the ubiquitous nature of iron, its physiological properties render it awkward for bacteria, and indeed host cells, to acquire and utilise. The reasons for this are 2-fold: the first being that the solubility and hence the availability of iron, in its most common ferric form, is very low and, secondly, that iron is toxic to cells in high concentrations. Accordingly, the process of iron acquisition in bacteria is a complex one, needing high affinity processes to out-compete host sequestration mechanisms and enable sufficient influx of iron, whilst being tightly regulated to prevent iron toxicity (Clarke, Tari and Vogel, 2001). A number of different mechanisms of bacterial iron acquisition exist. Iron is always found associated with protein or as part of larger molecules and is crucial to many host processes such as oxygen uptake by haemoglobin. With iron being one of the first and most important determinants of whether successful bacterial infection will occur, the host has developed mechanisms to limit the amount of iron available to invading microorganisms (Andrews, Robinson and Rodriguez-Quinones, 2003). Consequently, the amount of free iron available in the uninfected host has been shown to be of the order of $<10^{-18}$ M, an extremely low level, maintained through binding of free iron to Fe^{3+}-binding proteins and haemoproteins, and also due to its low solubility (Wandersman and Delepelaire, 2004). By contrast, the lowest concentration of iron permitting bacterial growth is approximately 10^{-7} M, clearly much higher than is available in the host (Palyada, Threadgill and Stintzi, 2004).

Iron has been implicated as having a role in the production of highly toxic reactive oxygen species (ROS) such as superoxide, hydroxyl, ferryl and perferryl radicals (Ghio *et al*, 2006; Stohs and Bagchi, 1995). This property is a second reason for the binding of iron to accessory molecules by the host: to limit possible oxidative stress caused by production of ROS. High iron concentrations in the lungs have been implicated in encouraging bacterial growth and causing pulmonary injury due to ROS formation (Ward, Bullen and Rogers, 1996). When host iron intake is high, excess iron is stored for use in times of iron deficit through binding to iron storage molecules such as ferritin. Binding of iron to ferritin is also known to limit the potential for production of ROS (Balla *et al*, 1992; Balla *et al*, 1995; Cozzi *et al*, 1990; Ward, Bullen and Rogers, 1996).

In response to host iron-restriction, bacteria have evolved highly competitive methods of obtaining iron from their hosts, either through secretion of iron-scavenging molecules or expression of specific outer membrane receptors which bind iron or iron-containing molecules (Andrews, Robinson and Rodriguez-Quinones, 2003). The subsequent sections will attempt to summarise the process of bacterial iron acquisition and present key findings on the mechanisms involved.

1.2.1 Iron-binding proteins - host

In addition to the intrinsically low level of circulating iron, the infected host restricts the availability of iron to the invading pathogen by synthesising proteins that chelate free iron. Ovalbumin was the first host iron chelator implicated in host defence to be discovered. Other chelators include the transferrins, a group of glycoproteins of

approximately 80 kDa comprising of 3 main types: lactoferrin, serum transferrin and ovotransferrin. Lactoferrin is found in mammalian milk, its presence increasing with decreasing pH, making its chelation more effective at the lower pH sometimes found at sites of infection, whilst ovotransferrin is found in egg whites where it constitutes approximately 12% of the total protein and functions both to transport iron and withhold it from bacteria. Serum transferrin is a major regulator and transporter of iron in mammalian systems and, in the work reported here, bovine serum transferrin is a major topic. A fourth member of the transferrin family, melanotransferrin, is found in a number of tissues and in serum, although details of its function are scant (Lambert, Perri and Meehan, 2005). Herein, transferrin will refer to serum transferrin. An excess of transferrin results in the binding of most free iron, and studies have shown that transferrin is commonly between 30 and 40% iron-saturated (Bullen *et al.*, 2005). This powerful chelation of free iron is due to the high association or binding constant of transferrin for ferric iron, approximately 10^{23} M (Williams *et al.*, 1978). In addition, the process of hypoferremia, initiated upon bacterial infection as part of the acute-phase response, is known to decrease host iron availability in conjunction with a rise in serum transferrin levels (Dinarello, 1984; Muller, Edwards and Smith, 1983; Weinberg, 1984). Despite this, bacteria have developed highly specialised methods of acquiring iron from their host, either directly or by the use of highly specific iron scavenging molecules known as siderophores which have a higher affinity for iron than transferrin. Once an iron-containing transferrin molecule has bound to the cell surface of the pathogen via the transferrin receptors, the iron is removed and must be transported across the cytoplasmic membrane in Gram-positive bacteria or both the outer and cytoplasmic

membranes in Gram-negative bacteria (Andrews, Robinson and Rodriguez-Quinones, 2003). It is known that *P. multocida* can acquire iron directly by removing bound iron from transferrin molecules (Ogunnariwo, Alcantara and Schryvers, 1991).

The transferrin molecule is bilobed, having 2 binding sites, designated the N and C-lobes, each of which can bind a ferric (Fe^{3+}) iron ion. The similarity of these 2 lobes has led to the suggestion that a distant evolutionary gene duplication event resulted in the bilobed structure of transferrin, and that serum transferrin and melanotransferrin are descended from a common ancestor (Park *et al*, 1985). Further evidence indicates that gene duplication events are biased for genes which evolve slowly (Davis and Petrov, 2004). This would be consistent with the knowledge that the structure of melanotransferrin, the member of the transferrin family currently most similar to the original ancestral transferrin, has evolved little since its emergence, estimated to be approximately 850 million years ago (Lambert, Perri and Meehan, 2005). Structural and mechanistic studies have revealed that binding of iron by transferrin is only favourable when a synergistic anion, specifically carbonate, is bound to the respective transferrin lobe (Schlabach and Bates, 1975).

Transferrin is commonly designated holo-transferrin when iron is bound to it, or apo-transferrin when it has no iron bound. It is known that a solution of transferrin will consist of a mixture of apo-transferrin and both mono and bi-ferric holo-transferrin, that is, transferrin with 1 or 2 ferric iron ions bound respectively. *P. multocida* A:3 when causing bovine pneumonic pasteurellosis has been shown to

remove only the ferric ion bound to the N-lobe of the transferrin molecule leaving the C-lobe ferric ion behind (Ogunnariwo and Schryvers, 2001). Furthermore, the same group observed that the principal form of bovine transferrin is that with a single iron ion bound to the N-lobe, designated monoferric N-lobe transferrin.

1.2.2 Iron-binding proteins - bacterial

Whether the source of available iron for bacteria is free iron, transferrin-bound iron, haem or haemoglobin, there are several methods through which bacteria can acquire iron (Andrews, Robinson and Rodriguez-Quinones, 2003; Braun and Killmann, 1999; Guerinot, 1994). The most common method is through production of high affinity iron-scavenging molecules known as siderophores, which will be discussed later (Faraldo-Gomez and Sansom, 2003). A second method involves expression of specific outer membrane proteins which bind ferric iron, most often conjugated to a protein, directly for subsequent transport into the bacterium. These proteins are commonly known as iron-restricted/regulated/related proteins (IRPs). This method is commonly utilised by Gram-negative bacteria to acquire iron which is either bound to host transferrin (Andrews, Robinson and Rodriguez-Quinones, 2003) or in the form of haemoglobin (Andrews, Robinson and Rodriguez-Quinones, 2003; Genco and Dixon, 2001). The transport process involves 3 steps; first, iron or an iron-containing compound is bound to a specific outer membrane protein. Next, iron is passed to a periplasmic protein which shuttles it to a cytoplasmic membrane protein complex containing an ATPase, or ABC (ATP-binding cassette) type transporter, which, through hydrolysis of ATP, transports the iron into the cytoplasm of the cell (Andrews, Robinson and Rodriguez-Quinones, 2003). Similar ABC

transporters are involved in the transport of other small molecules, such as amino acids into bacteria and indeed mammalian cells (Jones and George, 2002; Schmitt and Tampe, 2002). Many such systems for iron transport have been identified in a range of bacterial species, with several of them sharing significant structural homology between species, suggesting a common ancestor. Expression of iron-binding proteins, as mentioned previously, must be tightly regulated to prevent intracellular iron levels becoming toxic; these mechanisms will be discussed subsequently (Andrews, Robinson and Rodriguez-Quinones, 2003; Braun and Killmann, 1999; Guerinot, 1994).

1.2.2.1 Transferrin and lactoferrin binding proteins

The Transferrin-binding proteins A/B (TbpAB) and Lactoferrin-binding proteins A/B (LbpAB) are outer membrane proteins found in a number of species including *Haemophilus influenzae* and *Neisseria* spp. and act together with a periplasmic iron transport system such as the Ferric-binding protein ABC (FbpABC) complex or the *Haemophilus* iron transport ABC (HitABC) complex to deliver iron to the bacterial cytoplasm (Clarke, Tari and Vogel, 2001). The energy for transport of iron across the outer membrane is provided by the Ton system (Moeck and Coulton, 1998), described later. Analysis has shown that the TbpA of *Neisseria meningitidis* shares homology with the Ferric enterobactin permease A (FepA) and Ferric hydroxamate uptake receptor A (FhuA) siderophore receptors of *E. coli*, and that it forms a narrow transmembrane pore through which iron can pass (Oakhill *et al*, 2005). A separate study has indicated that the TbpB receptor alone cannot sequester metal ions from transferrin and that successful removal of iron requires additional proteins

(Nemish *et al*, 2003). Evidence suggests that *P. multocida* possesses only a single transferrin-binding protein (Ogunnariwo and Schryvers, 2001), described later.

This thesis will focus on the acquisition of iron from bovine transferrin by *P. multocida*, via its outer membrane TbpA and periplasmic FbpABC system.

1.2.2.2 Haemin/haemoglobin-binding proteins

In mammalian hosts the ubiquity of haemoglobin presents a readily-available source of iron for invading bacteria (Finkelstein, Sciortino and McIntosh, 1983). Haem itself consists of an iron ion bound to a porphyrin ring and is, with very few exceptions, always found conjugated to an associated protein. This is due to the reactivity of haem, through oxidation/reduction, and its tendency to form potentially harmful ROS. In addition, mechanisms exist to sequester free haem, including chelation by albumin and haemopexin, whilst haemoglobin released through haemolysis is sequestered by haptoglobin; albumin, haemopexin and haptoglobin being abundant in serum. The term haemin indicates that the iron ion associated with the porphyrin ring is in its ferrous (Fe^{2+}) state, as opposed to haem which contains ferric (Fe^{3+}) iron (Balla *et al*, 2007).

A number of mechanisms of sequestering haem, bound either by haemoglobin or haemopexin, are employed by bacteria. These differing mechanisms result in 2 main classes of proteins involved in haem sequestration: haemin-binding proteins (HmBPs) and haemoglobin-binding proteins (HbBPs). A third class, the

haemopexin-binding proteins, has been identified in *Haemophilus influenzae* (Pidcock *et al*, 1988), but has not been found in any other species of bacteria to date.

The HmBPs are thought to be involved in the acquisition of haem from its associated protein, regardless of what that protein may be. Indeed, there is some evidence to suggest that the HmBPs of the gonococci and meningococci can bind haemoglobin and acquire haem from it (Lee, 1992; Rohde and Dyer, 2004).

The second class, the HbBPs, unlike the haemin-binding proteins, acquire haem only from haemoglobin. Evidence suggests that a single bacterium can possess several different distinct HbBPs, thus providing redundancy, whereby if one receptor is knocked out a second can function in its place. Studies of meningococcal HbBPs indicates that they may act in concert with a HmBP, with the HbBP involved in initial binding of haemoglobin, after which the haem is passed to the HmBP for transport through the outer membrane. It is thought that the transport of haem across the outer membrane is facilitated by the Ton system, described in the following section. Because of the reactivity of haem, a periplasmic binding protein is likely to shuttle the haem across the periplasmic space to the cytoplasmic membrane where the haem is then internalised by means of an ABC transporter. Regulation of all of these proteins is thought to be facilitated by the Fur protein (Lee, 1992; Stintzi *et al*, 2000).

1.2.2.3 Siderophores

Siderophores are iron-scavenging molecules which bind ferric iron with high affinity. Production of these small iron-specific molecules is inversely proportional to iron levels (Jurado, 1997). They are secreted by bacteria, bind iron and subsequently deliver it to specific outer membrane receptors for transport into the bacterium (Clarke, Tari and Vogel, 2001). The mechanism of siderophore uptake by the bacterium varies between Gram-positive and Gram-negative bacteria because of differences in membrane structure. In Gram-positive bacteria, siderophores are internalised by an ATP-binding cassette. However, in Gram-negative bacteria, due to the extra lipid bilayer the process is slightly different, with the iron-loaded siderophore being shuttled across the periplasmic space, aided by the TonB, ExbB, ExbD complex, or Ton system. This complex spanning the periplasmic space supplies energy to the outer membrane to facilitate transport. Energy is produced by the electrochemical gradient of the cytoplasmic membrane, known as proton-motive force (PMF) (Faraldo-Gomez and Sansom, 2003).

A large number of bacterial siderophores and siderophore receptors have been identified and characterised functionally, however, less information is available on the structures of these molecules. There are 2 broad groups into which siderophores can be placed on the basis of their structure: phenolate (catecholate) and hydroxamate (Faraldo-Gomez and Sansom, 2003). An example of a phenolate siderophore is the HasA of *Serratia marcecsens.* Interestingly, analysis of the HasR siderophore receptor of *S. marcescens* indicates that it can bind haem or haemoglobin either directly, or indirectly when haem or haemoglobin is bound to

the siderophore HasA, albeit with greater affinity. Structural analyses of 2 siderophore receptors of *Escherichia coli* reveals that they possess an outer domain involved in binding of iron-loaded siderophore and a barrel-like transmembrane structure for transport of the iron-siderophore complex into the periplasm. Energy for this transport is provided by the Ton system (Clarke, Tari and Vogel, 2001). The vital role played by siderophores was displayed in a study which created mutants lacking the capability to produce siderophores, the result of which was a total loss of virulence, whilst several others studies have related siderophore production directly to virulence (Bearden, Fetherston and Perry, 1997; Konopka, Bindereif and Neilands, 1982; Meyer *et al*, 1996).

1.2.2.4 The Ton system

Closely linked through function with a number of bacterial iron-binding proteins, the Ton system is a complex of 3 proteins: TonB, ExbB and ExbD; their function being to provide energy for the translocation of iron across the outer membrane (Faraldo-Gomez and Sansom, 2003). Whereas small molecules such as peptides can diffuse across the outer membrane, larger molecules (above ≈600 Da), in this case transferrin or siderophore-bound iron, require active transport to achieve this (Nikaido, 1994). Structural studies have indicated that ExbB and ExbD are located on the cytoplasmic membrane and are complexed to TonB which spans the whole bacterial membrane from cytoplasmic membrane to outer membrane. It is thought that the ExbB/ExbD complex utilises the cytoplasmic membrane PMF to change the conformation of TonB, allowing interaction with the outer membrane iron-binding proteins and providing the energy needed to transport iron to the periplasm (Faraldo-

Gomez and Sansom, 2003). Such iron-binding proteins utilising the Ton system are known as TonB-dependent receptors. Sequence analysis of a range of TonB-dependent receptors has revealed a short, conserved section of protein sequence near the N-terminal end, designated the Ton box. It is thought that the Ton box is involved in the interaction between the TonB-dependent receptors and TonB itself, and may register to TonB the presence of substrate bound to the receptor (Postle and Kadner, 2003).

It should be noted that this is only one of several proposed mechanisms by which the Ton system acts and that its exact mode of action is as yet unknown (Postle and Kadner, 2003). Furthermore, the majority of structural studies of the Ton system have been carried out in *E. coli* and one must be aware of potential inter-species variation in its mechanism (Postle, 1993; Skare *et al*, 1993).

Analyses of the composition of the TonB-ExbB-ExbD complex have enabled its stoichiometry to be estimated as 1TonB:2ExbB:7ExbD, resulting in a complex with a molecular mass of approximately 260 kDa (Higgs, Myers and Postle, 1998). However, Chang *et al* (2001) have shown that TonB can exist in a dimeric form which would double the above ratio to 2TonB:4ExbB:14ExbD and result in a molecular mass of approximately 520 kDa.

Recently, several studies have noted the presence of multiple Ton systems in some species of bacteria, leading to speculation that each Ton system may be dedicated to its own iron acquisition system and hence also a different source of iron (Beddek *et*

al, 2004). If correct, then this would be yet another example of the extensive redundancy in bacterial iron acquisition mechanisms.

1.2.2.5 The Fur protein

The process of iron acquisition is dependent upon a number of underlying factors one of which is gene regulation and expression. Intracellular levels of ferrous iron (Fe^{2+}) control expression of IRPs in a negative feedback process known as transcriptional metalloregulation (Escolar, Perez-Martin and de, V, 1999). In this case, expression of the proteins TbpA, TonB, ExbB and ExbD of *P. multocida* is regulated by the aforementioned process (Bosch *et al*, 2002a; Ogunnariwo and Schryvers, 2001). This metalloregulation is controlled by the Fur protein, first characterised in *Salmonella typhimurium* and encoded by the *fur* gene (Ernst, Bennett and Rothfield, 1978). The Fur protein recognises a target sequence in the promoter region of iron-regulated genes, known as the Fur box (Bagg and Neilands, 1987). In *E. coli*, this sequence has been identified as a 19 base pair sequence, 5'-GATAATGATAATCATTATC-3', and *fur* gene homologues have been identified in many other species (**Table 1.1**) (Braun *et al*, 1990; Escolar, Perez-Martin and de, V, 1999). Evidence shows that there may be several overlapping Fur-boxes present upstream of iron-regulated genes (Griggs and Konisky, 1989; Hunt, Pettis and McIntosh, 1994). The Fur protein has also been found to be an extremely abundant protein compared to other proteins with regulatory roles. When intracellular iron levels are high, ferrous iron binds to the Fur protein thus changing its conformation to allow it to bind to the Fur box on the target DNA. Once bound, the Fur protein prevents ribosomes from interacting with DNA and hence prevents mRNA

translation and subsequent protein expression. However, under low iron conditions the Fur protein cannot bind to the Fur box and the relevant protein is expressed. The pool of genes whose expression is regulated by Fur are known as the 'Fur regulon' (Escolar, Perez-Martin and de, V, 1999).

Species	Nucleotide sequence	Reference
Consensus	5'-NAT$^{(A}/_{T)}$AT NAT$^{(A}/_{T)}$AT NAT$^{(A}/_{T)}$AT-3'	(Escolar, Perez-Martin and de, V, 1998)
E. coli	5'-GATAATGATAATCATTATC-3'	(Escolar, Perez-Martin and de, V, 1999)
Campylobacter jejuni	5'-ATTTTGATAATTAATATTA-3'	(Palyada, Threadgill and Stintzi, 2004)
P. multocida	5'-TATTATCAATATTGATAAT-3'	(Bosch *et al*, 2002b)
Histophilus ovis	5'-AATTATAAGAACCATTCTC-3'	(Ekins and Niven, 2002)
Vibrio cholerae	5'-GATAATGATAATNATTATC-3'	(Mey *et al*, 2005)

Table 1.1: Published sequences of putative 'Fur boxes' from several species. Nucleotides matching the consensus sequence are shown in red.

In addition to its iron regulatory role, studies in *Yersinia pestis* have implicated that the iron-Fur complex can also regulate expression of non-iron related genes e.g. membrane proteins, ribonucleoside-diphosphate reductase, oxidative defence and electron transport genes. The same group also reported that, under iron-replete conditions, Fur may repress expression of a number of virulence-associated genes (Zhou *et al*, 2006), an interesting observation which may implicate low iron availability in an increase in bacterial virulence, a hypothesis shared by Ratledge and Dover (2000). Furthermore, of 56 genes found to be regulated by the iron-Fur complex, 48 were found to be upregulated whilst only 8 were downregulated both when iron availability was restricted by the iron chelator αα-dipyridyl, and also when the ability of the bacteria to synthesise the Fur protein was perturbed through mutation. Interestingly, the upregulated genes included *tonB*, *exbB* and *exbD* (Zhou *et al*, 2006). Studies in *Vibrio cholerae* have shown that Fur may also have a positive regulatory role in addition to its well characterised role as a negative regulator. Interestingly, amongst the genes shown to be repressed by Fur in iron-

restricted conditions were genes encoding non-essential proteins containing iron, perhaps an attempt to conserve available iron for incorporation into more vital enzymes and proteins (Mey *et al*, 2005).

1.2.2.6 Utilisation and storage of iron by bacteria

Zhou *et al* (2006) have shown, in the bacterium *Y. pestis*, that under conditions where iron uptake is high transcription levels of the genes which encode the iron storage protein bacterioferritin are upregulated, thus creating a reserve of iron to be utilised in times of iron deficit.

The work described in this thesis focuses on iron acquisition by *P. multocida* and begins with a description of this bacterium and what is known of its role in disease in cattle.

1.3 *Pasteurella multocida*

P. multocida serotype A3 is the leading cause of bovine pneumonic pasteurellosis which results in considerable economic burden (Dowling *et al*, 2004; Mosier, Confer and Panciera, 1989). Also, preliminary analysis of the recently published genome of *P. multocida* indicates that a significant proportion of the genome represents genes specifically associated with iron acquisition (May *et al*, 2001). This, coupled with the limited knowledge of the pathogenesis of this organism, suggests that investigation of iron acquisition mechanisms in *P. multocida* should provide new insight into both the pathogenesis of the disease and may also highlight future strategies for prophylaxis and treatment. The following section will describe

the organism; the disease, pneumonic pasteurellosis and its virulence factors, specifically the methods it uses to acquire iron.

1.3.1 General information and taxonomy

Within the Gram-negative bacteria there are many species which are grouped taxonomically based upon phenotypic and genotypic traits. The order gammaproteobacteria of the phylum proteobacteria are grouped according to 16S rRNA sequences and contains some 15 families.

The *Pasteurellaceae* is a family of non spore-forming, facultatively anaerobic coccobacilli and consists of 13 genera: the genus *Pasteurella* being subdivided into 22 species and 3 subspecies.

Originally, the *Pasteurellaceae* were characterised and grouped on the basis of their phenotypic traits including colony morphology, biochemical properties and host specificity. Towards the end of the 1980s there was a move away from this phenotypic characterisation to concentrate instead on genotypic methods. As a result the number of species in the family *Pasteurellaceae* rose from 29 in 1980 to over 50 species in 1990. Currently, taxonomy is in a state of flux with 38 species classified correctly plus a further 24 mis-classified species (Christensen and Bisgaard, 2008).

The Gram-negative pathogen *P. multocida* was discovered by Louis Pasteur over one hundred years ago and contributes to a number of diseases in both humans and animals, including: pneumonic pasteurellosis and haemorrhagic septicaemia in

cattle, atrophic rhinitis in pigs and fowl cholera in birds (May *et al*, 2001; Ogunnariwo and Schryvers, 2001).

1.3.2 Identification and characteristics of *P. multocida*

As mentioned previously, the *Pasteurellaceae* were classified previously by phenotypic methods, including biochemical properties. A number of biochemical properties can be determined by tests such as API (analytical profile index) strips, which test the ability of the bacterium to utilise a range of nutrients. Within the species *P. multocida* there is subspecies variation in biochemical properties (**Table 1.2**).

There are, at present, 5 recognised serogroups of *P. multocida*: A, B, D, E and F. These represent the capsular serotypes and they can be identified by a number of methods. Carter developed an indirect haemagglutination assay for capsular serotyping by screening a large number of isolates against immune sera. Immune sera were raised through prior knowledge of serotype by the precipitation method. These sera were then reacted with red blood cells and each serotype of *P. multocida* in turn. Haemagglutination was shown to correlate with the matching sera and serotypes. Although effective, this method of serotyping is time consuming and production of serotype-specific sera is lengthy (Carter, 1955). As seen in **Table 1.3**, diseases caused by *P. multocida* can be tentatively assigned to each of the 5 serogroups. Townsend *et al* (2001) reported a multiplex PCR developed to enable rapid and reliable serotyping of *P. multocida*. The assay relies upon variability of 'region 2' of the capsular biosynthetic genes, with unique primers developed for

each of the 5 serotypes. In conjunction with these 5 primers is a sixth primer which is specific for all serotypes and acts as a positive control for the presence of *P. multocida* (Townsend *et al*, 1998).

Test	*ssp. gallicida*	*ssp. multocida*	*ssp. septica*
Ornithine decarboxylase	+	ND	+
L-arabinose fermentation	+	ND	-
Urease production	-	ND	-
Maltose fermentation	-	-	-
Trehalose fermentation	-	v	+
Mannitol fermentation	+	+	+
Sorbitol fermentation	+	+	-
Ribitol fermentation	v	-	-
Indole production	+	+	+
Gas from glucose	-	-	-
Catalase	+	+	+
Cytochrome oxidase	+	+	+
Nitrate reduction	+	+	+
MacConkey growth	-	-	-
Xylose fermentation	v	v	+
Glucose fermentation	+	+	+
Saccharose fermentation	+	+	+

Table 1.2: *P. multocida* subspecies variation in response to a range of biochemical tests (ND = No Data available).

Serogroup	Associated disease/s
A	Fowl cholera, bovine pneumonic pasteurellosis
B	Haemorrhagic septicaemia in Asia - cattle, buffalo
D	Atrophic rhinitis in pigs
E	Haemorrhagic septicaemia in Africa - cattle
F	Fowl cholera

Table 1.3: Assignment of diseases to serogroups A-F of *P. multocida*

1.3.3 Bovine pneumonic pasteurellosis

1.3.3.1 Characteristics of bovine pneumonic pasteurellosis

Bovine respiratory disease has significant economic costs estimated at approximately £30 million in the UK and $1 billion in the US per annum in addition to significantly compromising the welfare of affected animals. Clinical signs of

pneumonic pasteurellosis disease include dullness, raised temperature, laboured breathing, nasal discharge and loss of appetite (Gibbs *et al*, 1984).

The disease process is still understood poorly, although the pathology associated with it has been described in some detail (Jubb, Kennedy and Palmer, 1963). A large proportion of otherwise healthy cattle carry *P. multocida* asymptomatically deep within the nasal passage. One survey recorded 61% of cattle from which *P. multocida* could be detected from nasal swabs (Jericho and Carter, 1985). In addition, a second survey found that *P. multocida* was one of the 2 most frequently isolated organisms from the lungs of feedlot cattle and found a significant correlation with morbidity (Allen *et al*, 1991). Initiation of pneumonic pasteurellosis is thought to result from one of several 'stressors' to the host. These can include stress induced when cattle are transported long distances (hence the name shipping fever), through underlying infection and hence immunosuppression, through calving and a number of other stressors. It is assumed that any one or a combination of these stressors may lead to a local proliferation of *P. multocida* within the nasopharynx and subsequent transit of the bacteria further down the respiratory tract. Additionally, aerosol spread of bacteria from the nasopharynx of one animal to other susceptible animals can occur (Weekley, Veit and Eyre, 1998). Several studies have linked development of pneumonic pasteurellosis with pre-existing infections such as infectious bovine rhinotracheitis (IBR), bovine respiratory syncitial virus (BRSV) and a number of other viral diseases (Allen *et al*, 1992a; Briggs and Frank, 1992; Weekley, Veit and Eyre, 1998). Indeed, in a bovine experimental challenge model, Jericho and Carter (1985) found that lung pathology was worsened when animals

were previously infected with bovine herpesvirus 1 before subsequent infection with *P. multocida*.

Infection can be confirmed through positive culture of *P. multocida* on nasal swabs or by a *P. multocida* specific PCR (mentioned previously). Disease is only confirmed post-mortem by bacteriology and histopathology. On examination of infected lungs, consolidation of the apical lung lobes predominantly, pleurisy and pleural lesions are observed. Histopathology reveals focussed areas of necrosis surrounded by large numbers of recruited macrophages and neutrophils which commonly result in abscess formation (Jubb, Kennedy and Palmer, 1963). There is considerable evidence linking high levels of acute phase protein production with the presence of pneumonic disease (Dowling *et al* 2002).

1.3.3.2 Treatment strategies

To date vaccination strategies against disease caused by *P. multocida* have had mixed results. One study in mice compared the efficacy of a single purified OMP vaccine, a total OMP vaccine, a formalin-killed bacterin and a commercial vaccine in stimulating antibody production and in protecting against a homologous challenge. The total OMP, formalin-killed bacterin and commercial vaccines all offered protection against a homologous challenge, whilst the single purified OMP vaccine offered no protection. The ability of sera from each vaccinate group to stimulate cell-mediated killing (CMK) of *P. multocida* was also studied. The sera from the total OMP and formalin-killed bacterin groups stimulated CMK, whilst sera from the single purified OMP and commercial vaccine groups did not

significantly stimulate CMK (Gatto *et al*, 2002). A second study, evaluating the effectiveness of a formalin-killed bacterin in protecting against a homologous intratracheal challenge with *P. multocida* in a cattle model found, somewhat counter-intuitively, that rather than conferring protection the bacterin resulted in more severe pathology in the lungs of challenge animals. Despite this their ability to clear bacterial infection did appear to be improved, perhaps consistent with the above study in mice and the finding that CMK was stimulated after vaccination with a formalin-killed bacterin (Dowling *et al*, 2004). Mathy *et al* (2002) found some protection was present after vaccination with a live bacterin of *P. multocida* and that induction of the acquired immune response was more rapid than in naïve animals.

Treatment of pneumonic pasteurellosis varies between the USA and UK. In the USA antibiotics are added prophylactically to both feed and water provided to cattle despite the increased risk of antibiotic resistance (Gibbs, 2001; Post, Cole and Raleigh, 1991). In the UK, antibiotics are given as a means of prophylaxis, but only in those cattle housed with infected cattle and therefore judged to be at risk of infection. In infected animals veterinarians recommend treatment with tulathromycin to rid them of infection (Robb *et al*, 2007).

The lack of a suitably protective vaccine against pneumonic pasteurellosis and the emergence of antibiotic resistant strains of *P. multocida* coupled with the severe morbidity of pneumonic pasteurellosis suggest that an effective non-antibiotic prophylactic therapy or treatment for the disease would be much sought after (Catry *et al*, 2006; Post, Cole and Raleigh, 1991).

1.3.4 Virulence factors of *P. multocida*

As described earlier, the array of virulence factors possessed by a bacterium is key to its success as a pathogen. Successful colonisation and spread within the host requires the invading bacterium both to overcome the host innate immune response and to acquire the nutrients which it requires for growth and survival. In their review of microbial iron acquisition, Finkelstein, Sciortino and McIntosh (1983) state that if the normal homeostasis of iron in the host is disrupted by stress, metabolic disorders or by infection opportunistic pathogens can proliferate. Knowing that *P. multocida* can reside in the nasopharynx of cattle without causing apparent symptoms and that there is likely a trigger resulting in the bacteria becoming virulent, perhaps this trigger is a disruption of the normal iron homeostasis in the host. Furthermore, studies in a number of bacteria have shown that restricting iron availability results in a dramatic increase in their virulence (Sussman, 1974). Hence, the host's attempts to limit available iron may, paradoxically, make the bacteria more virulent.

1.3.4.1 Iron acquisition by *Pasteurella multocida*

Despite much time devoted to its study, a detailed understanding of *P. multocida* virulence is still lacking, as is information on mechanisms of innate and acquired immunity and vaccine strategies in the host with respect to this organism. However, the published genome sequence of an avian strain of *Pasteurella multocida* serotype A:3 in which at least 2.5% of identified genes relate to iron acquisition and uptake (May *et al*, 2001) and the availability of reliable *in vivo* models of disease (May *et al*, 2001; Dowling *et al*, 2002) provide new opportunities for the study of the pathogenesis of *P. multocida*.

Iron-binding proteins and transferrin-binding proteins of *P. multocida*

As mentioned previously, host transferrin chelates free iron to withhold it from invading bacteria (Cornelissen, 2003). Despite this, bacteria can remove iron from transferrin by binding to specific membrane receptors. The process of binding the iron-transferrin complex occurs through binding to an outer membrane receptor present on *P. multocida*, Transferrin-binding protein A (TbpA). This protein is an 82 kDa protein encoded by the *tbpA* gene (Ogunnariwo and Schryvers, 2001). The presence of an 82 kDa receptor with transferrin-binding properties was noted first in 2 bovine pneumonic isolates of *P. multocida* by Ogunnariwo, Alcantara and Schryvers (1991) and was shown only to bind the bovine isoform of transferrin; whilst avian strains lacked both the 82 kDa receptor and transferrin-binding capabilities. Further evidence from studies of serotype B isolates of *P. multocida* from cases of haemorrhagic septicaemia (HS) indicates that transferrin-binding capabilities may even vary within serotypes; with B:2 and B:5 isolates able to bind transferrin, whilst B:3 and B:4 cannot (Veken *et al*, 1994). Ogunnariwo and Schryvers (2001) speculate that expression of the TbpA protein may be a disposing factor in bovine pneumonic pasteurellosis absent from other diseases caused by *P. multocida* A:3 . It was suggested recently that unlike other bacterial species and indeed other serotypes of *P. multocida*, A:3 possesses only one transferrin-binding protein rather than 2 (Ogunnariwo and Schryvers, 2001). Analysis of the TbpA of another member of the Pasteurellaceae, *H. ovis*, showed that it shared approximately 73% homology with the TbpA of *P. multocida* (Ekins and Niven, 2002). Once the N-lobe of the transferrin-iron complex is bound to TbpA a conformational change

occurs both in the transferrin molecule and the TbpA which releases the iron ion and allows it to pass through the now open pore of TbpA into the periplasmic space. The transport across the outer membrane is stabilised and driven by the TonB complex, consisting of the TonB, ExbB and ExbD proteins in the periplasmic space (Ogunnariwo and Schryvers, 2001).

On passing into the periplasmic space, the ferric iron ion is bound by a second iron-binding protein known as Ferric-binding protein A (FbpA). Due to the paucity of data on the mechanisms of ferric ion transport by FbpA in *P. multocida*, detailed mechanistic data on the FbpA of the closely related bacterium *Mannheimia haemolytica* will be assumed to represent a close approximation of the process in *P. multocida*. Basic Local Alignment Search Tool (BLAST) comparisons reveal that the FbpA of *P. multocida* shares 78% identity with its orthologue in *M. haemolytica*, whilst the *fbpA* gene encoding FbpA in *P. multocida* shares 89% identity with the *fbpA* gene of *M. haemolytica*. The mechanism of FbpA-mediated transport of Fe^{3+} is described herein, based upon X-ray crystallography studies in *M. haemolytica*. FbpA binds it synergistic anion HCO_3^-, thereby increasing the affinity of FbpA for ferric iron, although Khan *et al* (2006) suggest that FbpA may be able to bind Fe^{3+} without interaction with a synergistic anion, albeit with lower affinity (Cornelissen, 2003). With iron bound, the FbpA molecule then migrates across the periplasm where it binds to the inner membrane protein pore FbpB. Upon binding, FbpA releases HCO_3^- back into the periplasm and the ferric iron ion passes through the inner membrane into the cytosol. This passage across the membrane is driven by FbpC, an ATPase hydrolysing ATP to ADP. The 3 Ferric-binding proteins FbpA,

FbpB and FbpC act together as an ATP-binding cassette (ABC) type transporter (Shouldice *et al*, 2004). Despite this knowledge, the process has not yet been quantified or its efficiency assessed. The YfeABCD protein complex is structurally similar, and performs a similar role to that of FbpABC, transporting iron from the periplasmic space into the cytoplasm of the bacterium (Roehrig *et al*, 2006).

As discussed earlier, haem and haemoglobin provide major sources of iron for invading bacteria. Acquisition of iron from haem-containing compounds is achieved through high-affinity HmBPs or HbBPs on the bacterial outer membrane, a number of which have been identified in *P. multocida*. The haemoglobin-binding protein A (HgbA) of *P. multocida* was described first by Bosch *et al* (2002b), and was shown to be capable of binding haemoglobin directly. However, when mutants lacking the ability to express HgbA were created there was little effect on the strain's ability to bind haemoglobin suggesting redundancy and, by implication, additional haemoglobin-binding proteins. Indeed, Cox *et al* (2003) have characterised a second HbBP, Haemoglobin-binding protein B (HgbB). Again, mutant strains defective in expression of HgbB showed no loss of virulence or decreased ability to bind haemoglobin which is further evidence for multiple HbBPs expressed by *P. multocida*. The same study also noted a further putative HbBP, PM0336, based upon sequence analysis. In a study of a range of *P. multocida* isolates, varying both in serotype and host species, the genes encoding both HgbA and HgbB were shown to be present in a vast majority of isolates, perhaps confirming haem as a vital source of environmental iron for *P. multocida* (Ewers *et al*, 2006). A separate study identified a further 6 proteins demonstrating both haemin and haemoglobin-binding

activity and an additional 2 proteins, one of which bound haemin only and the other binding haemoglobin only, all of which stimulated production of antibodies in mice, although none was found to confer protective immunity (Bosch *et al*, 2004).

A recent study examining the virulome of *P. multocida* from a variety of sources revealed that only 70% of bovine strains tested possessed the gene encoding TbpA, with the figures for strains isolated from buffalo and sheep being 57.1% and 80% respectively. Additionally, it was noted that all strains tested from swine, rabbit, poultry, cat and dog lacked the TbpA gene completely (Ewers *et al*, 2006). Perhaps these findings result from the source of available iron at the site/s of infection in each host, with those strains lacking the ability to encode the TbpA protein utilising haemoglobin as an alternative iron source. Indeed, the fact that isolates of serogroup A of *P. multocida* can colonise both bovine and avian hosts, whilst only the bovine strains possess TbpA, raises an interesting question. Was TbpA lost from avian strains of *P. multocida* because it was no longer needed, or did the loss occur before *P. multocida* colonised avian hosts? This point may be key in the predilection of strains of serogroup A for either avian or bovine disease. Further work by Paustian *et al* (2002) indicates that genes upregulated under growth supplemented with haemoglobin were not upregulated when growth was supplemented with transferrin. Equally, those genes upregulated when growth was supplemented with transferrin were not upregulated when growth was supplemented with haemoglobin. This work, together with the finding that the expression of the product of the *hbpA* gene, a haemin-binding protein, in *P. multocida* is regulated by a *fur*-independent pathway in response to changes in iron levels (Garrido *et al*, 2003) could indicate the

existence of an additional regulator of expression of iron acquisition genes, in addition to Fur, as it seems that separate subsets of genes are activated in response to a paucity of either haem or ferrous iron.

The Ton system

The role of the Ton system in iron acquisition by *P. multocida* is interesting as it is also involved in siderophore-mediated iron uptake by Gram-negative bacteria. Coupled with the knowledge that the outer membrane siderophore receptor HasR of *S. marcescens* can bind haem or haemoglobin directly, when not bound to siderophore, there appears to be many similarities between iron uptake with or without siderophores (Clarke, Tari and Vogel, 2001). Perhaps siderophores act to enhance the efficiency of iron uptake as opposed to being essential for iron acquisition, and could suggest that those bacteria lacking siderophores have lost the ability to produce them by evolving more efficient methods for acquiring iron directly. Furthermore, perhaps host transferrin occupies a similar role to that of a siderophore, thus explaining the clear similarities between each mechanism of iron acquisition.

Bosch *et al* (2002a) have suggested that in *P. multocida*, the genes *exbB, exbD* and *tonB* encoding the Ton system are linked physically, but not transcribed as an operon. It was assumed previously that because of their products' activity as a complex that the 3 genes would be an operon, however, they suggest that the Ton genes are transcribed independently and each regulated by iron levels, with all 3 genes being necessary for virulence.

Whilst a vast majority of studies have concentrated on direct acquisition by *P. multocida* of iron from transferrin or haem, several studies have noted the presence of a siderophore in *P. multocida*, apparently unique to this species, known as multocidin (Choi-Kim *et al*, 1991; Hu *et al*, 1986; Reissbrodt, Erler and Winkelmann, 1994). This molecule was found to be secreted into the medium and enhanced *P. multocida* growth. It also reduced iron binding to transferrin suggesting high affinity. Multocidin is known to be neither a phenolate or hydroxamate siderophore (Hu *et al*, 1986).

Expression of these iron-binding proteins is upregulated greatly under iron restriction. Paustian, May and Kapur (2001) showed at least 20 genes involved in iron transport and binding that were upregulated by more than 2-fold under iron restriction, whilst Boyce *et al* (2002) identified 9 or more genes involved in iron uptake that were upregulated *in vivo* in a chicken infection model. In addition, there is evidence to suggest that iron acquisition genes may be constitutively expressed at low levels, with upregulation occurring when iron is in deficit (Boyce and Adler, 2006; Cox *et al*, 2003). One study has suggested that *P. multocida* IROMPs may play a role in providing cross-protective immunity in mice challenged intraperitoneally with *P. multocida*, and the authors hypothesise that antibodies directed against IROMPs may limit the bacterium's ability to take up iron by physically blocking its iron binding sites (Ruffolo, Jost and Adler, 1998). A number of studies have examined IRPs in bacteria and considered them to be potential

vaccine candidates (Adler *et al*, 1999; Ogunnariwo and Schryvers, 2001; Prado *et al*, 2006).

1.3.4.2 Capsule, fimbriae and other adhesins

As mentioned previously, the capsule of *P. multocida* can be used to assign strains capsular serotypes A, B, D, E and F. The role of the capsule in virulence is becoming clearer through comparison of capsular and acapsular strains. It seems that the capsule confers to the bacteria an increased resistance to both phagocytosis and complement-mediated lysis, both important components of the innate immune response (Harper, Boyce and Adler, 2006). Indeed, one study observed intracellular survival of *P. multocida in vitro* in phagocytic cells and attributed this to the protective nature of the hyaluronic acid capsule (Dowling *et al*, 2004).

The adhesins have been well characterised as a group of surface exposed proteins intimately involved in the attachment of bacteria to host cells, and as such are associated closely with virulence (Coutte *et al*, 2003). Two putative adhesin-coding genes, *pfhaB1* and *pfhaB1*, of *P. multocida* have been described and through comparison with *Haemophilus ducreyi* and *Bordetella pertussis*, are thought to encode filamentous-haemagglutinin-like proteins. It is of particular note that the filamentous haemagglutinin of *B. pertussis* has been shown to be involved directly in binding of the bacteria to the trachea and nasopharynx of the host (Fuller, Kennedy and Lowery, 2000).

Fimbriae (or pili), a subset of the adhesins, are found commonly in Gram-negative and rarely in Gram-positive bacteria and are proteinaceous hair-like structures involved in binding to host cells (Pizarro-Cerda and Cossart, 2006). In *P. multocida* several fimbriae have been identified thus far (Isaacson and Trigo, 1995; Ruffolo *et al*, 1997). Isaacson and Trigo (1995) discovered 2 distinct types of fimbriae in serogroup D isolates from cases of atrophic rhinitis in pigs. The first bore similarity to the type 1 fimbriae of enterbacteria, whilst the other appeared to share structural similarities with the "curli" pili of *E. coli*. Interestingly, binding assays revealed that neither of these fimbriae were involved in adhesion of *P. multocida* to host cells. Meanwhile, type IV fimbriae identified in serogroup A strains have been implicated in adhesion to mucosal epithelial cells (Ruffolo *et al*, 1997). Despite these findings, there has been, to date, no conclusive evidence to explain the role of fimbriae and other adhesins in the pathogenesis of *P. multocida* (Harper, Boyce and Adler, 2006).

Rationale for work and chosen approach

In cattle *P. multocida* is a significant cause of pneumonic pasteurellosis, a disease resulting in significant welfare problems and loss of revenue and productivity (VIDA UK data, 2005). A better understanding of bacterial factors that influence virulence, including metabolism, growth and gene expression, and how these factors interact with the host may lead to the identification of novel immunogens and development of novel therapeutic treatments against pneumonic pasteurellosis. One key to improving our knowledge of the disease process is attempting to understand what, if any, changes occur in bacteria when they become pathogenic. *P. multocida* is found in the nasopharynx of healthy cattle but causes disease only in some cases

(Allen *et al*, 1992b). It follows that there may be a trigger which initiates a pathogenic change in the bacterium whereby it can colonise the lung and cause infection. Undoubtedly, this pathogenic change in the bacterium will be elicited by the repertoire of virulence factors possessed by *P. multocida*, most likely in response to an environmental trigger. By focussing on iron acquisition, a process fundamental to the survival and proliferation of the bacteria, and hence virulence, it is hoped that a detailed understanding of the mechanisms involved and identification of crucial steps in the pathway will provide novel therapeutic targets and aid treatment of the disease in the future.

Bacterial infection is a complex interaction between host and bacterium dependent upon genes and gene regulation, expressed proteins and their regulation, and many other factors (Mims *et al*, 1998b). As iron acquisition is an essential process for the vast majority of bacteria (Andrews, Robinson and Rodriguez-Quinones, 2003), it would seem logical that the system may be highly conserved between bacterial species, as with housekeeping genes i.e. genes involved in cell maintenance whose transcription is relatively unaffected by environmental changes. Furthermore, there may be a core set of genes common to many species which probably consists predominantly of housekeeping genes. Comparison of whole genomes supports this and it also seems that horizontal transfer may be responsible for virulence genes which are shared between species which are evolutionarily distant (**Fig. 1.1**). However, despite these genetic similarities, a number of distinct methods of iron acquisition exist and a study of published material has provided detail on the process in *P. multocida*.

Here, the process of iron acquisition will be studied using 2 complementary approaches. The first, a theoretical approach, will construct a model of the iron acquisition process in *P. multocida* based upon published data on the biochemical reactions involved and will include complementary pathways vital to the process such as ATP production and final outcomes, for example, bacterial biomass. The second, an *in vitro* approach, will investigate the effects of changes in environmental parameters on gene expression, iron acquisition and growth rate using a range of culture conditions and analytical techniques.

These processes can be studied by focusing only on the pathway of interest, but in a complex biological system a more detailed understanding of the process can be gained by a systems approach. The field of systems biology aims to generate a large amount of data from a range of experimental methods to gain an overview of the entire process being studied rather than traditional methods of focusing on specific mechanisms of interest. This multidisciplinary approach exploits the fact that biological systems operate on a genomic and a proteomic level and thus to gain the best understanding of the system both genomic and proteomic analyses should be carried out (Kitano, 2002).

An integral part of a systems biology approach is the use of theoretical modelling, a tool employed increasingly in recent years for understanding a wide number of biological processes, including metabolic pathways (Edwards, Covert and Palsson, 2002). By breaking a metabolic pathway into its constituent parts, individual

reactions, the behaviour of the network being studied can be analysed. Specifically, the mechanism utilised by *P. multocida* to acquire iron from host transferrin will be analysed *in silico* to generate data for comparison with and refinement of *in vitro* experiments in an iterative process.

In tandem with this *in silico* modelling, *in vitro* studies of the iron acquisition mechanism in *P. multocida* will examine the effects of changes in environmental conditions on key iron acquisition genes' transcription, on the growth rate of the bacteria and on bacterial metabolism. These data will be used to refine the *in silico* model through comparison of measured *in vitro* fluxes and predicted fluxes.

With complementary theoretical and *in vitro* analyses of iron acquisition and related pathways in *P. multocida*, the systems approach employed should allow a better comparison with other bacterial species to elucidate similarities and indeed differences in the mechanisms employed to acquire iron.

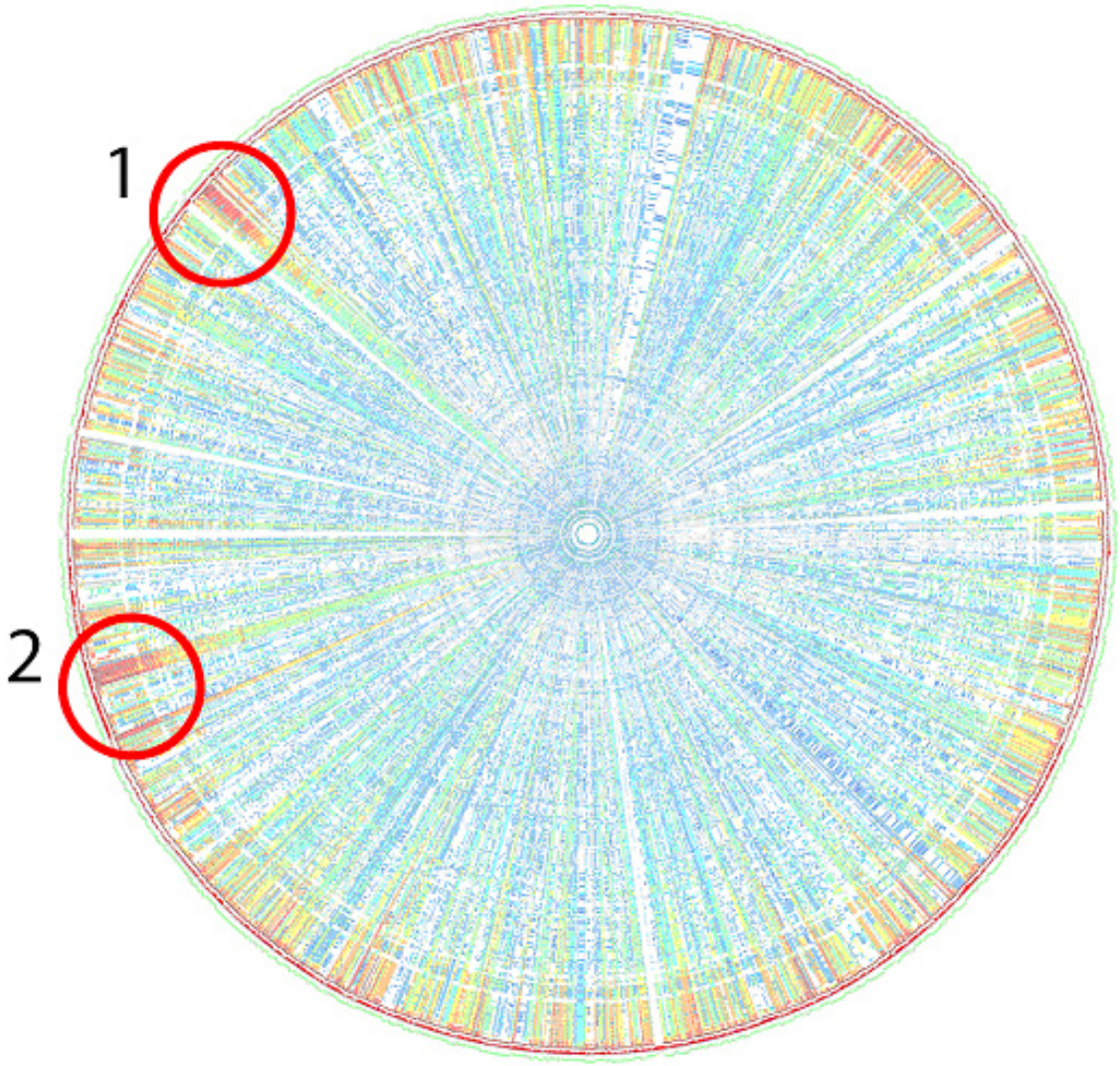

Fig. 1.1: GenomeDiagram comparison of *P. multocida* PM70 genome vs. 228 other bacterial genomes. PM70 coding sequences (CDSs) are represented in genome order on the outermost concentric ring of the diagram, whilst each successive ring depicts a single genome with reciprocal FASTA comparisons of orthologous CDSs coloured by 'heat' i.e. red = high similarity, blue = low similarity, white = no orthologue matched. Genomes are ordered from outermost to innermost concentric ring by similarity of the elongation factor-coding *tufA* gene to the *P.multocida* PM70 *tufA* gene, providing some gauge of evolutionary distance. Lone red spots towards centre of diagram may indicate genes acquired by horizontal transfer. (1) Region showing high similarity between several genomes, as shown by block of red colour. This region represents genes coding for several *rpL* genes coding for ribosomal proteins, and several *rpoB* and *rpoC* genes coding for RNA polymerase B and C subunits respectively. (2) Second region of high similarity, including *rpL* and *rpS* genes coding for ribosomal proteins and *tufA* and *fusA* genes coding for elongation factors.

1.4 Theoretical modelling

The field of metabolic modelling is one which began around 40 years ago (Garfinkel, 1963; Kerson, Garfinkel and Mildvan, 1967; Koga, Burg and Humphrey, 1967; Newton, 1965). With the current emphasis on a systems biology approach to disease investigation it is an area which will be brought to the fore in years to come. The power of theoretical modelling in this case is to allow key pathways in disease to be modelled and studied, providing a basis for both *in vitro* and *in vivo* experiments to be designed to study the disease process. The increasing use of theoretical modelling and its refinement may bring about a future reduction in animal experimentation. In recent years, 2 key methods have been adopted for metabolic pathway analyses; these are elementary flux modes and extreme pathways (Schilling, Letscher and Palsson, 2000; Schuster, Dandekar and Fell, 1999). Both techniques seek to provide insights into "meaningful routes" through reaction networks. In this case, elementary flux modes have been chosen as the preferred method for pathway analysis. An elementary flux mode is defined as a route through a reaction network which cannot be further decomposed, i.e. if any one reaction step in that route is removed then the whole route will not function (Schuster, Dandekar and Fell, 1999). By this definition, the method provides a set of elementary flux modes which should indicate key reaction steps which can be targeted for *in vitro* study and potential modifications to block that pathway. In addition, any thermodynamically feasible route through a network can be reconstructed by linear combination (or summation) of the appropriate elementary flux modes (Schuster, Dandekar and Fell, 1999).

An algorithm has been developed for computation of the complete set of elementary flux modes from a given set of reactions and has been incorporated into several software programs, the first of which was Metatool (Pfeiffer *et al*, 1999). Once computed, elementary flux modes can be subjected to a number of analyses to examine key network properties such as network redundancy/robustness, efficiency/flexibility of the network, output optimisation and flux estimation (Pfeiffer *et al*, 1999; Schuster, Dandekar and Fell, 1999; Stelling *et al*, 2002; Wilhelm, Behre and Schuster, 2004). To begin to perturb a cellular process effectively, one must first understand intimately both the reaction network driving that process, and the key properties of that network. Through selective pressure, biological systems have adapted to be resistant both to inherent malfunctions and environmental change, so as to maintain some level of homeostasis and as such to aid survival and proliferation. Robustness, as a property of a biological network, allows that network to continue to output when perturbations are made to reactions within the network. This is achieved through a network property known as redundancy, whereby 2 or more pathways function to serve the same output; hence, the more redundancy within a network, the more robust it becomes. Flexibility and efficiency of the network are 2 further closely-related properties. Flexibility dictates how the network adapts to changing environmental conditions via a set of redundant pathways, whilst efficiency states that for a given output the network will use a minimal set of constituent reactions. Stelling *et al* (2002) described a method of measuring both the flexibility and efficiency of a network through so-called ‘control effective fluxes’ which characterise the importance of a reaction for optimal functioning of a given network.

Elementary flux modes have been used to study a wide range of biological processes, although glucose metabolism in both yeast and *E. coli* dominate the field (Duarte, Herrgard and Palsson, 2004; Schuster, Fell and Dandekar, 2000; Stelling *et al*, 2002; Wilhelm, Behre and Schuster, 2004). To date, there has been no published study of an elementary flux modes analysis of iron acquisition in bacteria and as such this represents a completely novel investigation. In this case, the acquisition of iron by *P. multocida* and subsequent energy input will be modelled using this technique. A detailed description of the development of this model and contributing techniques will follow in **Chapter 3**.

An additional *in silico* method of analysis is flux balance analysis (FBA). Sharing similarities with elementary flux modes analysis, FBA allows the integration of experimentally-measured flux rates and subsequent estimation of un-measured fluxes based upon reaction stoichiometries. A key feature of this technique is that fluxes in the network are optimised for maximal output of a so-called objective function, in most cases maximal biomass (Varma and Palsson, 1994).

1.5 Aims

As mentioned in **Section 1.3**, the aim of this work is to understand better the key process of bacterial iron acquisition, in terms of its role in virulence, by the Gram-negative pathogen *P. multocida*. In cattle, pneumonic pasteurellosis caused by *P. multocida* is a source of considerable welfare concern and economic burden. It is hoped that a better understanding if the role of iron acquisition by this pathogen will

push forward attempts to develop novel therapies to combat pneumonic pasteurellosis, and also have relevance to disease mechanisms in other bacterial pathogens.

First, a theoretical model will describe in detail the key steps of iron acquisition by *P. multocida*, and structural analyses of the network will be made, focussing particularly on network robustness and elementary flux modes. Next, *in vitro* analyses will investigate the effect of varying environmental factors on *P. multocida*, with emphasis on the effects of iron restriction on bacterial growth and metabolism. Finally, data from both sets of analyses will be integrated to enable validation of both approaches and the relevance of findings to pathogenesis *in vivo* will be discussed.

Chapter 2. General materials and methods

2.1 Bacterial strains and growth media

Bacterial strains

Unless otherwise stated, cultures of *P. multocida* were inoculated with a starter culture of a bovine A:3 isolate 671/90, used as the standard challenge strain at Moredun and prepared as follows. A 1 ml aliquot of *P. multocida* isolate 671/90 from -70°C storage was added to 9 ml sterile TSB/YE growth medium and incubated for approximately 12 hours at 39°C, statically. Cultures of other isolates were prepared also from -70°C culture stocks in a similar method to isolate 671/90.

Growth media

Tryptic soy broth/yeast extract (TSB/YE) medium was prepared by addition of 30 g/l Bacto Tryptic Soy Broth (BD, Oxford, UK) plus 10 g/l Bacto Yeast Extract (BD, Oxford, UK) to deionised water, and sterilised by autoclaving for 20 minutes at 120°C. Brain heart infusion (BHI) broth was prepared by adding 37 g/l of Bacto Brain Heart Infusion to deionised water and autoclaving for 20 minutes at 120°C. Iron-restricted media were prepared by adding 20 ml/l of 10 mM filter-sterilised αα-dipyridyl (Sigma, Poole, UK) to culture media.

5% sheep blood agar (SBA) plates were prepared by adding 25 ml sterile sheep's blood to 500 ml molten sterile Blood Agar Base no. 2 (Oxoid, Basingstoke, UK) and pouring approximately 25 ml into sterile Petri dishes. Plates were stored at 4°C until use.

2.2 Bacterial counts

Live bacterial counts

Replicate live bacterial counts were performed after pipetting 25 μl of bacterial culture into 225 μl of phosphate buffered saline (PBS [137 mM NaCl, 10 mM PO_4^-, 2.7 mM KCl]) in a 96-well microtitre plate and mixing thoroughly. Serial 10-fold dilutions were carried out up to 10^{-6} dilution using a multichannel pipette, mixing thoroughly each dilution. Aliquots (20 μl) of each dilution was spotted by pipette in duplicate onto 5% SBA (v/v) plates and allowed to air dry. Plates were incubated for approximately 12 hours at 39°C and then examined for colony growth. A dilution with approximately 20 colonies was chosen and the number of colonies in each duplicate spot was recorded. Live bacterial counts in colony forming units per ml (CFU/ml) were calculated by multiplying the mean number of colonies counted by 50 and then by the dilution factor at which colonies were counted.

Estimated viable counts

Estimated viable counts (EVCs) were performed by pipetting 3 ml of bacterial culture into a plastic bijou and taking a McFarland reading using a Densimat (bioMérieux, Basingstoke, UK) densitometer. This reading was multiplied by 3×10^8 to give an estimated viable count in CFU/ml (Koch, 1970).

2.3 RNA extraction and qRT-PCR

RNA extraction

Bacteria in 1 ml of culture were pelleted by centrifugation at 3000xg for 20 minutes and total bacterial RNA extracted using an RNeasy Mini Kit (Qiagen, Crawley, UK) as per manufacturer's guidelines. RNA held on the columns was eluted using 50 µl ultrapure water and samples were stored at -20°C.

RNA concentrations were measured using a NanoDrop 1000 spectrophotometer (Thermo, Wilmington, DE, USA).

qRT-PCR

Quantitative Reverse Transcription-PCR (qRT-PCR) was carried out using a QuantiTect SYBR Green RT-PCR Kit (Qiagen, Crawley, UK) and a Chromo4 real-time detector system (Bio-Rad Laboratories Ltd, Hemel Hempstead, Hertfordshire). Primers were designed using Primer3 (http://biotools.umassmed.edu/bioapps/primer3_www.cgi; (Rozen and Skaletsky, 2000)) for 7 key *P. multocida* iron acquisition genes: *fur*, *tonB*, *fbpA*, *fbpB*, *fbpC*, *exbB* and *exbD*. A primer for the housekeeping gene *gyrB* was also designed to allow quantitative measurement of transcript levels. Primers were optimised for use in similar cycling conditions and primer sequences are listed (**Table 2.1**). Primers were also tested to ensure correct amplification, i.e. single products of correct molecular weight (data not shown).

Primer name	Sequence	Source
gyrB_for	5'-GCCCTTTCCGATAAATTGCAA-3'	All created for this project
gyrB_rev	5'-ATCGCGGCTAATGGTGCTT-3'	
fur_for	5'-GACTGTGTGTGGCTAATTCAATA-3'	
fur_rev	5'-CGGGGTTGAAAATCACCGAAC-3'	
tonB2_for	5'-TCATTGCTTTTTCACGCAAG-3'	
tonB2_rev	5'-TTGGTGGCTCAGGTTTTACC-3'	
tbpA2_for	5'-CGGATCATTTCTTGGCATTT-3'	
tbpA2_rev	5'-GCCAAACAGCAATCCATTTT-3'	
fbpA2_for	5'-TGCAAAAGATCGTGTGGGTA-3'	
fbpA2_rev	5'-CACTTGATCACGGTCACCAC-3'	
fbpB3_for	5'-ACATCTTTGGCAAACCGTTC-3'	
fbpB3_rev	5'-CCGGACCGGGATAATCTAAT-3'	
fbpC2_for	5'-GCCTTCGCTGATAAACTTGC-3'	
fbpC2_rev	5'-ACCAATCACCGAATTGAAGC-3'	
exbB2_for	5'-GGTACCGTCATTGGTATTCTCT-3'	
exbB2_rev	5'-CGTCCTAAACCGTTGTAACACA-3'	
exbD2_for	5'-GCGTTTCGTTCAGATGATTTAG-3'	
exbD2_rev	5'-TGCATCTACCTTCAAGGTGAC-3'	

Table 2.1: PCR primer names, sequences and sources.

Each 10 μl reaction contained the following: 5 μl of 2x QuantiTect SYBR Green RT-PCR Master Mix, 0.1 μl of QuantiTect RT mix, 0.2 μl of each primer (final concentration of 2 μM) and 4.5 μl template RNA plus ultrapure water (10 ng RNA per 10 μl reaction). Standards containing 10, 5, 2 and 1 ng pooled RNA were run, in triplicate, containing the *gyrB* primers to allow transcript levels for each of the other genes to be quantitatively estimated; these also acted as positive controls. Negative controls containing ultrapure water with no template RNA added were also run, in triplicate.

Cycling conditions were: a single reverse transcription step for 30 minutes at 50°C followed by a single initial activation step for 15 minutes at 95°C, and then 35 cycles of 15 seconds denaturation at 94°C, 30 seconds annealing at 50°C and 30 seconds

extension at 72°C, followed by a final extension step for 15 minutes at 72°C. A melting curve analysis was also carried out between 70°C and 95°C to test for single amplified products.

Agarose gels contained 1% agarose (w/v) in 1x Tris-EDTA buffer (TAE buffer; 40mM Tris-acetate, 1 mM EDTA; Sigma, Poole, UK) and 1x GelRed Nucleic Acid Stain (Biotium, Hayward, CA, USA). 10 µl PCR product containing 1x blue/orange loading dye (Promega, Southampton, UK) was loaded in each lane. 5 µl of 100 base pair ladder (Invitrogen, Paisley, UK) to allow estimation of size of amplified products was also loaded. Gels were run at 100 V for approximately 30 minutes in 1x TAE buffer. Products were visualised using a UV transilluminator.

2.4 Total bacterial protein assay

To measure the protein content of the bacterial pellet a modification of the well-established Lowry assay was used. Total protein incorporation was assayed during bacterial growth in the various culture conditions. A microplate-based colorimetric method using a DC Protein Assay kit (Bio-Rad, Hemel Hempstead, UK) was used to quantify the total protein content of bacterial pellets, performed with a slight modification of the manufacturer's protocol (Lowry *et al*, 1951). This assay measured both soluble and insoluble proteins, as boiling the pellets not only lysed the bacteria but also denatured all protein within the bacteria.

Bacteria were pelleted by centrifugation at 3000xg of 1 ml bacterial culture for 20 minutes, then washed twice in 500 µl ultrapure water and heated at 100°C for 5

minutes to lyse cells. Each sample was diluted 50-fold in ultrapure water, 20 µl of DC Assay Reagent 1 and 200 µl of DC Assay Reagent 2 added to 5 µl of diluted sample and the optical density (OD) measured at 562 nm in a 96-well microtitre plate. Protein standards (Protein Standard 1, bovine gamma globulin) of 2, 1, 0.5, 0.25 and 0.1 mg/ml were used. All samples were run in triplicate. Sample protein concentrations were calculated by comparison with protein standards.

2.5 Glucose oxidase assay

The decrease in glucose concentration in the culture medium was assayed as a measure of total glucose use by bacteria during growth under various culture conditions. Glucose concentrations in culture supernatants obtained after centrifuging 1 ml of culture at 3000xg for 20 minutes and diluting 100-fold in ultrapure water were measured in triplicate using a Glucose Oxidase Assay kit (Sigma, Poole, UK). Detection of glucose was via its oxidation by glucose oxidase to gluconic acid and hydrogen peroxide, the reaction of hydrogen peroxide with peroxidase and o-dianisidine, and finally the reaction of oxidised o-dianisidine with sulphuric acid. The manufacturer's method was modified by scaling down volumes of reagents 10-fold to allow measurement in a 96-well microtitre plate. At time 0, 200 µl of Assay Reagent was added to 100 µl of diluted sample, mixed thoroughly and incubated at 37ºC for 30 minutes. After 30 minutes, 200 µl of 6M sulphuric acid was added to stop the reaction. The OD of the pink-coloured product was measured at 562 nm and, through comparison with standards of 10, 50, 100, 150 and 200 µg/ml glucose (Sigma, Poole, UK) and ultrapure water blanks, the concentrations of glucose in culture supernatant were quantified.

2.6 Bacterial ATP assay

ATP can be detected and quantified using a bioluminescent method, relying upon the requirement of ATP in the production of light by recombinant firefly luciferase (**Fig. 2.1**). Two methods for measurement of intracellular bacterial ATP levels were trialled, both based upon the firefly luciferase luminometric assay. The first was the ATP Determination kit (Molecular Probes, Leiden, Netherlands), which involved extraction of ATP from pelleted *P. multocida* using boiling tris-EDTA buffer to prepare samples for luminometry. The second was the BacTiter Glo kit (Promega, Southampton, UK), an assay optimised specifically for use with un-processed aliquots of bacterial cultures with no ATP extraction step required. Both assays provided very good estimation of bacterial ATP levels, consistent with values quoted elsewhere, and highly replicable sets of standards. However, due to the ease of use the BacTiter Glo kit it was chosen for further experimental assays.

Bacteria were lysed to determine the amounts of ATP synthesised during different culture conditions. Bacterial ATP concentrations were measured using a BacTiter-Glo Kit (Promega, Southampton, UK). 100 µl of each culture sample was added to wells of an opaque-walled 96-well microtitre plate and 100 µl of BacTiter-Glo reagent was added automatically to each well using a Tropix TR717 Luminometer (Applied Biosystems, Warrington, UK); peak luminescence values were measured after incubation at 37ºC. Standards of 1, 0.1, 0.01, 0.001, 0.0001 µM ATP (ATP standard solution; Sigma, Poole, UK) diluted in TSB/YE media were run to allow quantification of ATP concentrations by comparison to a standard curve. TSB/YE medium blanks were also run to allow subtraction of background luminescence of

the media. Triplicate culture samples were run singly and ATP standards were run in triplicate.

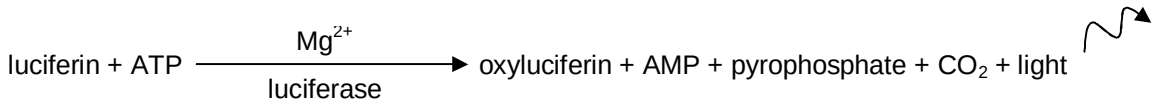

Fig. 2.1: Production of light through reaction of luciferin and ATP with luciferase.

2.7 Measurement of bacterial dry weights

Dry weights were assayed as a measure of bacterial mass generation during different culture conditions and included alive and dead cells. First, 1 ml of bacterial culture was pelleted by centrifugation at 3000xg for 20 minutes. Pellets were then resuspended in 1 ml PBS (137 mM NaCl, 10 mM PO_4^-, 2.7 mM KCl) and pelleted again by centrifugation at 3000xg for 20 minutes. Washed pellets were frozen at -20ºC, before lyophilisation in tared eppendorf tubes and bacterial dry weights measured in grams to 3 decimal places.

2.8 Growth of bacteria using a Bioscreen C

Bacteria were grown in a Bioscreen C bacterial growth curve analysis system (Thermo, Basingstoke, UK), allowing measurements of growth curves by OD readings. Starter cultures were prepared as per **Section 2.1** and 500 µl added to each well of a 100-well honeycomb plate (Thermo, Basingstoke, UK). Cultures were grown in triplicate with triplicate media blanks also run to allow subtraction of background OD readings. OD readings were recorded at wideband wavelength (420-580 nm) at 30 minute intervals, with 30 seconds shaking prior to OD measurement. All cultures were grown at 39ºC for 24 hours.

2.9 Growth of bacteria using a Biostat Q fermenter

Each of the 4 vessels of a Biostat Q fermenter (Sartorius, Epsom, UK) was prepared as follows. Oxygen and pH probes were calibrated according to manufacturer's recommendations. Culture medium (800 ml) plus 100 µl Antifoam A (Sigma, Poole, UK) was added to each vessel and sterilised by autoclaving for 30 minutes at 120ºC. Sterile solutions of 0.1 M sulphuric acid (Sigma, Poole, UK) and 0.1 M sodium hydroxide (Sigma, Poole, UK) were prepared for adjustment of vessel pH during culture. Each vessel was inoculated with 10 ml of *P. multocida* 671/90 starter culture, prepared as described in **Section 2.1**, by syringe through one of the vessel ports. Airflow and agitation were set to maximum, pH was set to 7.0 and temperature was set to 39ºC for each vessel. Cultures were grown for 7 or 8 hours, varying by experiment. At each sampling time, 3 ml of culture were extracted by syringe for analysis.

2.10 Growth of bacteria using a Microreactor fermenter

The Microreactor fermentation and cell culture device (Applikon, Tewkesbury, UK) used 24 wells plates with an optimum working volume of 3 ml per well and permitted growth of cultures in defined conditions. For all runs, TSB/YE was used as the growth medium. For iron-restricted conditions, 200µM αα-dipyridyl (Sigma, Poole, UK) was added to the TSB/YE medium. Plates were pre-warmed at 39ºC on the Microreactor for 1 hour prior to inoculation; this time also allowed stabilisation of dO_2 and pH. Each well was inoculated with 150 µl of *P. multocida* starter culture (prepared as described in **Section 2.1)** at time 0. Plates were sealed with breathable, sterile sealing tapes (Nunc, Roskilde, Denmark). All wells were set to maximum

aeration i.e. 100 mmol/l/hr or 45 ppm dO_2, and 500 rpm orbital shaking. Temperature and pH setpoints varied according to experiment, and can be found in **Section 5.2.2**. Vessel pH was controlled by CO_2 gas for lowering pH, and ammonia gas for raising pH. At each sampling time, the entire contents of 4 wells, 2 from each defined condition, were removed for analysis.

2.11 Growth of bacteria by shaking flask culture

P. multocida was grown in shaking flask culture as follows. Cultures were prepared in sterile 1 litre Duran bottles by adding 500 ml TSB/YE medium, either iron-replete or iron-restricted. Media were pre-warmed at 39ºC prior to inoculation with 10 ml starter culture of *P. multocida*, prepared as described in **Section 2.1**. Cultures were incubated at 39ºC for 8 hours on a flat-bed rotary shaker at 200 rpm. At various timepoints, 10 ml of each culture was extracted for analysis.

2.12 Optimisation of *in vitro* culture methods and assays

Before embarking on any *in vitro* analyses of iron acquisition and in order to ensure an accurate and effective set of assays to quantify key model parameters it was necessary to ascertain suitable culture conditions in which to study the effects of restricting available iron and other environmental changes on growth and metabolism of *P. multocida*.

2.12.1 Restriction of available iron in bacterial growth media

Two approaches could be taken when restricting the amount of iron in a bacterial culture medium. The first was to develop a chemically defined medium lacking iron

to which defined amounts of iron were added, thus creating low or high iron availability. The second was to use a chelator of divalent cations which, when added to the growth medium, chelated free iron thus rendering it unavailable for use by bacteria grown in the medium. A chemically-defined medium was developed based upon an existing commercially available cell culture medium, RPMI-1640 (Sigma, Poole, UK) which lacked iron. Two chelators of divalent cations were compared and doses of each were titrated to find a concentration which perturbed growth by only a small amount but would trigger an over-expression of iron-related outer membrane proteins. These chelators were ethylenediaminediacetic acid (EDDA; Sigma, Poole, UK) and 2,4 or αα-dipyridyl (Sigma, Poole, UK) and the concentrations used were 200, 250, 300, 350, 400 and 600 μM for both. Cultures were grown for 8 hours at 39°C, the approximate core body temperature of cattle.

These approaches were compared by growing *P. multocida* in the Bioscreen C, a high throughput growth analysis instrument that allowed up to 100 bacterial cultures to be grown simultaneously at a user-defined temperature in a microplate format, with or without shaking. Culture ODs were measured at user-defined intervals and growth curves generated for each well. The wavelength at which optical density measurements were taken could be altered according to the physical characteristics of the bacterium being studied. In the case of *P. multocida*, the 'wideband' setting was chosen, which measured optical density over a range of wavelength between 420 and 580 nm. This decision was based upon previous studies comparing each of the available wavelength settings and the accuracy of the growth curves generated. A detailed method for bacterial growth in the Bioscreen C can be found in **Section 2.8**.

The chemically-defined medium to which no iron was added showed a significant initial lag in the onset of log phase growth and a slower growth rate during log phase, although the final density of *P. multocida* was similar to cultures grown in TSB/YE (**Fig. 2.2**). When cultures were grown in TSB/YE with each of the chelators added, results indicated that of the 2 chelators tested, αα-dipyridyl was by far the most effective. In fact, EDDA did not appear to perturb growth to any extent when compared to iron replete conditions suggesting either an inability to chelate iron or that bacteria had the ability to remove iron bound to EDDA thus allowing its use for metabolism. In contrast, αα-dipyridyl exhibited effective perturbation of growth and hence chelation of iron in a dose-dependent manner, with a positive correlation between concentration of αα-dipyridyl and perturbation of growth (**Fig. 2.2**).

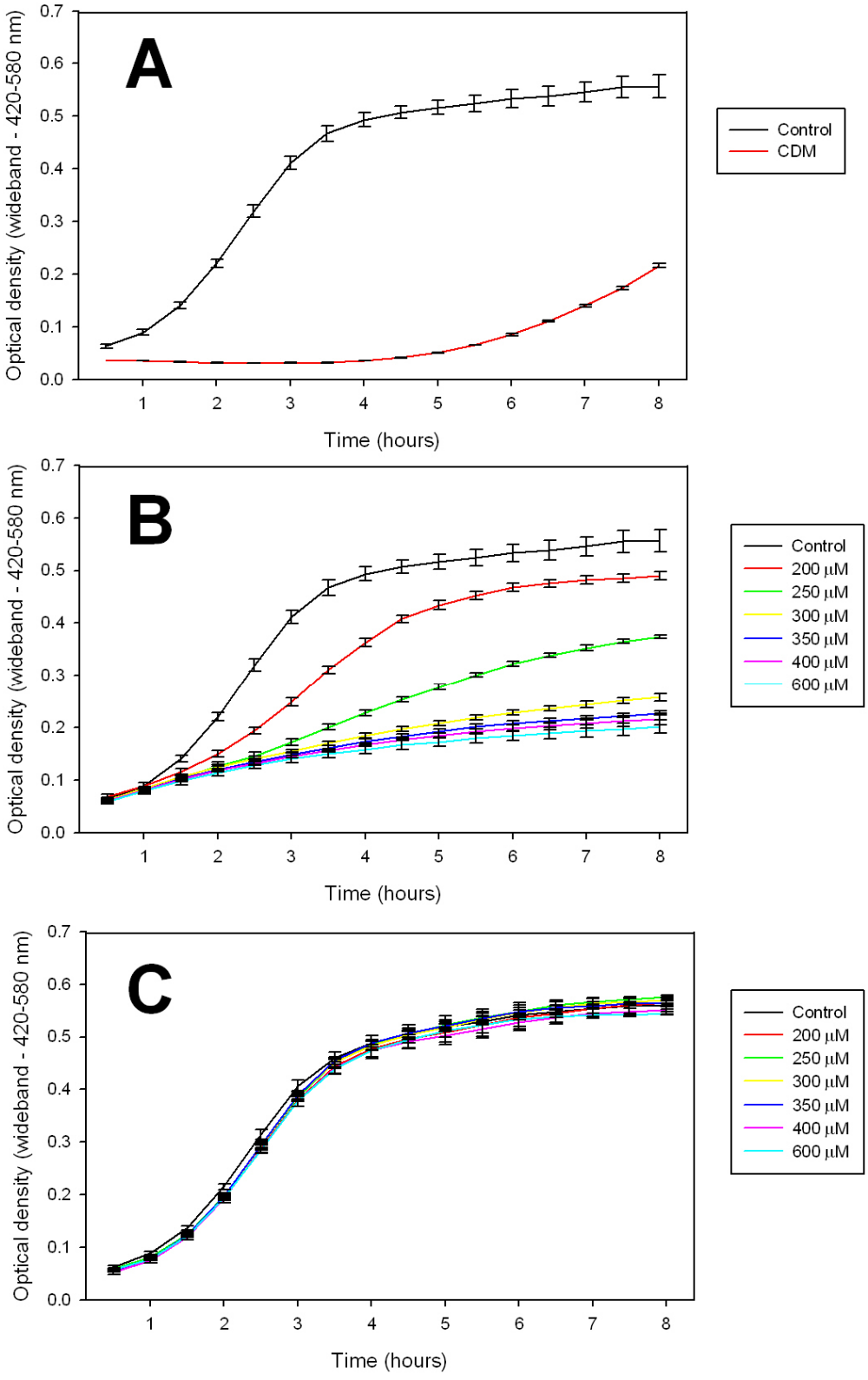

Fig. 2.2: Graphs showing effects of iron-restriction on growth of *P. multocida* 671/90. **A)** Growth in an iron-deficient chemically defined medium (CDM) versus growth in iron-replete TSB/YE media. **B)** Dose titration of αα-dipyridyl from 200 to 600 µM. **C)** Dose titration of EDDA from 200 to 600 µM. N.B. Each point shown here represents the mean value of three replicate wells, with background OD subtracted. Growth curves were generated by taking sequential measurements of optical density (OD) of cultures at 30 minute intervals. All cultures, with the exception of CDM were grown in TSB/YE media with or without an iron chelator.

Therefore, it was decided that αα-dipyridyl at a concentration of 200μM was suitable for iron-restriction of cultures in these studies. However, as a final screen, the effects of chelation in those conditions were compared across each of the serotypes of *P. multocida* to check consistency between strains (**Fig. 2.3**). Each of the *P. multocida* serotype A, B, D, E and F type strains (Rimler) were used for this comparison. Interestingly, it was evident that there were differences in the extent of perturbation between each of the 5 strains of *P. multocida* tested. Of the 5 serotypes grown in control conditions, serotype A had the most rapid progression to plateau, whilst serotype D had the slowest; serotype F had the highest final density. In iron-restricted conditions it was evident that the growth rates of serotypes D and F were perturbed to a much greater extent than the 3 other serotypes, whilst serotype A was affected least by iron-restriction.

Although there is only one published genome sequence for *P. multocida* serotype A:3, thus preventing accurate, detailed analyses of the heterogeneity between the genomes of each serotype, it is likely that significant between-serotype heterogeneity does exist. In addition to this heterogeneity, the differing environmental niches colonised by each serotype are likely to result in metabolic differences between serotypes and this may explain differences in the effects of iron restriction observed here. Heterogeneity will be explored further in **Chapter 5**, with analysis of the effects of iron restriction on growth and metabolism of a range of isolates of *P. multocida* A:3.

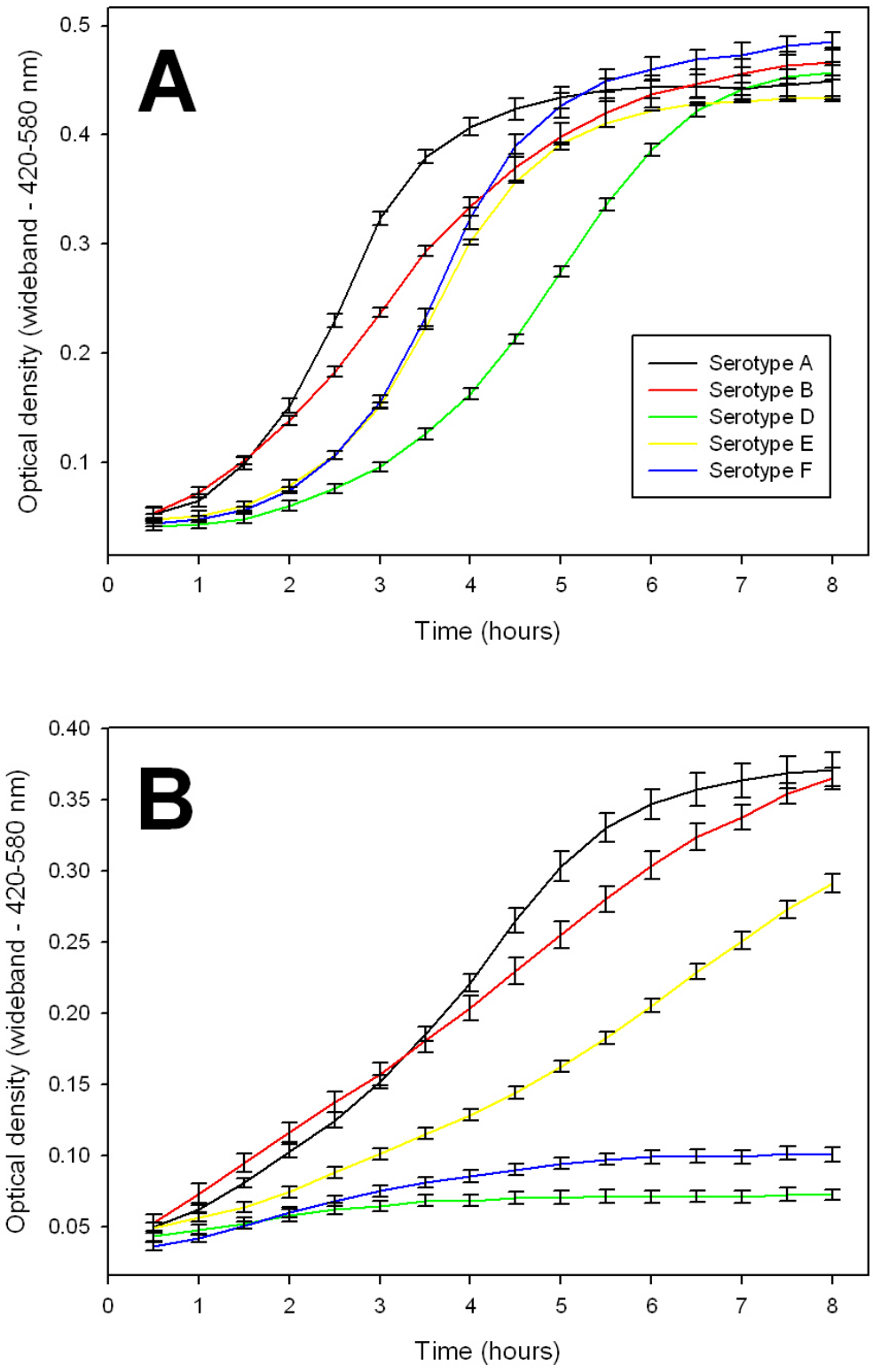

Fig. 2.3: Effect of iron-restriction using 200 µM αα-dipyridyl on growth of the type strains of each serotype of *P. multocida* and comparison to growth in iron-replete conditions. **A)** Serotype A, B, D. E and F type strains of *P. multocida* grown in iron-replete TSB/YE medium. **B)** Serotype A, B, D. E and F type strains of *P. multocida* grown in iron-restricted TSB/YE medium. N.B. Each point shown here represents the mean value of three replicate wells, with background OD subtracted. Growth curves were generated by taking sequential measurements of optical density (OD) of cultures at 30 minute intervals.

2.12.2 Comparison of growth in a non TSE-compliant medium versus a TSE-compliant medium

Due to potential future applications for vaccine development, it was decided that growth in a standard rich medium which was non-TSE compliant (BHI) should be compared with a TSE-compliant rich medium (TSB/YE) which would be suitable for use in vaccine development. As in the iron-restriction study, growth was assessed quantitatively using the Bioscreen C (Thermo, Basingstoke, UK). *P. multocida* strain 671/90 was used in this study and was grown for 12 hours at 39°C. Detailed methods for preparation of BHI and TSB/YE media can be found in **Section 2.1**.

Results indicated that there was little variation in the growth curves of *P. multocida* grown in non-TSE and TSE-compliant media, therefore the TSE-compliant medium (TSB/YE) was selected for use in future studies (**Fig. 2.4**).

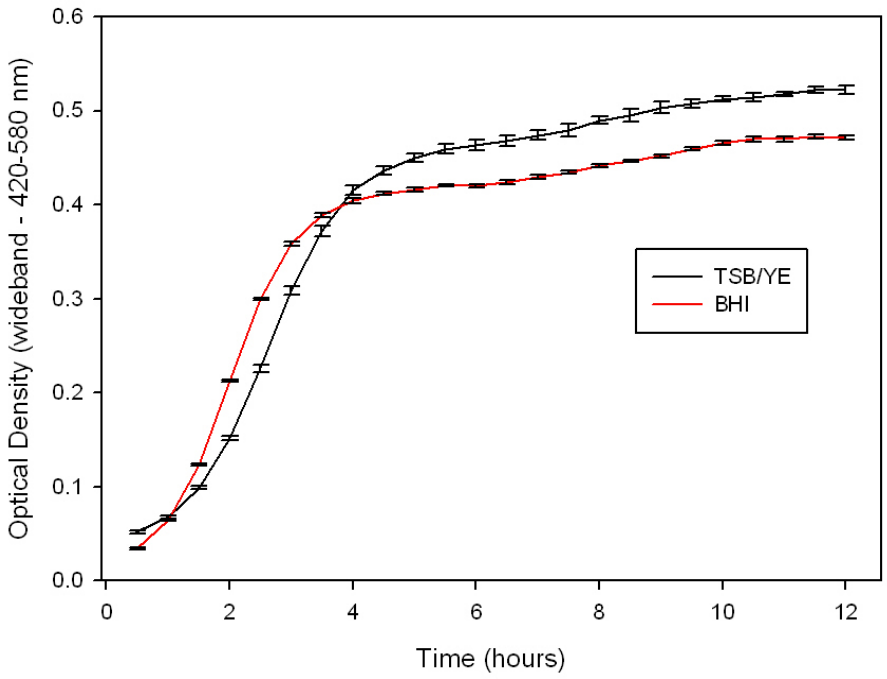

Fig. 2.4: Comparison of growth of *P. multocida* 671/90 in a TSE-compliant (TSB/YE) medium versus growth in a non-TSE-compliant (BHI) medium. Each point shown here represents the mean value of three replicate wells, with background OD subtracted. Growth curves were generated by taking sequential measurements of optical density (OD) of cultures at 30 minute intervals.

2.12.3 Reproducibility of growth of *P. multocida* in a bacterial fermenter

A 4-vessel bacterial fermenter (Biostat-Q, Sartorius, Epsom, UK) was used to study the growth *in vitro* of bacterial cultures in defined environmental conditions on a larger scale, with regulation of temperature, pH, aeration and stirring of cultures, in volumes of up to 1 litre. The fermenter allowed real-time monitoring of vessel pH, dissolved oxygen concentration and temperature. Samples could be drawn sequentially from the cultures through septum ports built into each vessel. Detailed methods for growth of bacteria in the Biostat Q fermenter can be found in **Section 2.9**.

Before studying the effect of iron restriction in the bacterial fermenter, it was decided that the amount of between-vessel variation during each run should be studied. All 4 vessels of the fermenter were prepared with identical cultures of *P. multocida* strain 671/90 in TSB/YE and were sampled sequentially at hourly intervals for 7 hours. Estimated viable counts were recorded to allow the growth rates of cultures in each vessel to be compared.

Replication between all vessels was shown to be good, most notably between vessels 2, 3 and 4 (**Fig. 2.5**). Slight deviation from the latter 3 vessels was evident in the growth of vessel 1, however this was most likely due to slight inconsistencies in the maintenance of constant environmental parameters, particularly pH control.

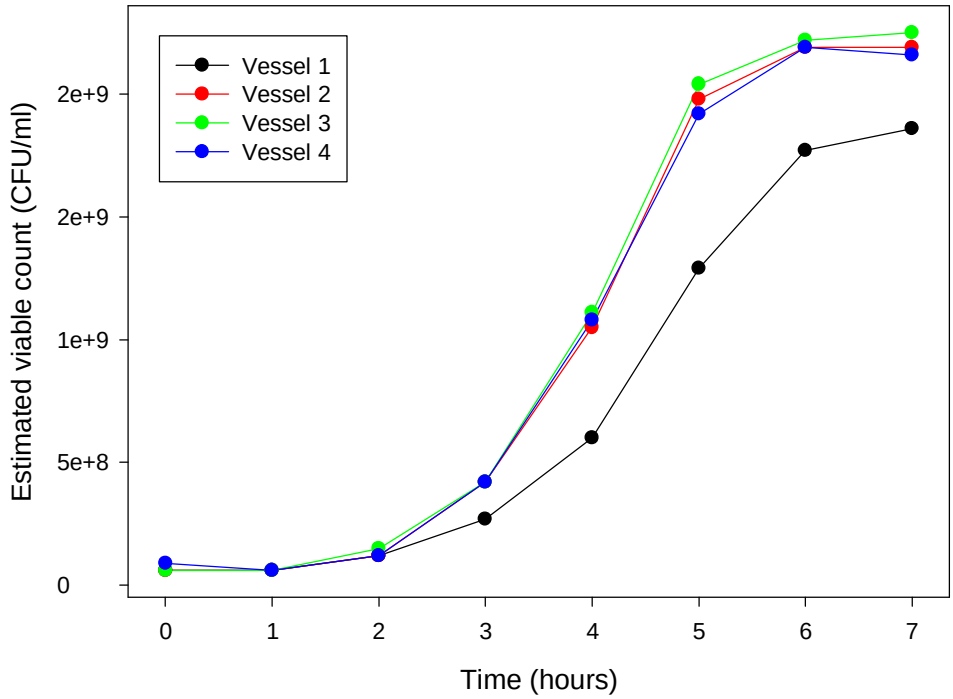

Fig. 2.5: Graph showing growth of *P. multocida* 671/90 over a 7 hour period in TSB/YE using the Biostat Q 4-vessel fermenter. Each of the 4 vessels contained identical cultures and each was grown in identical environmental conditions i.e. 39°C, pH 7.0, 100% aeration, 400 rpm stirring. No iron chelator was added, therefore conditions were assumed to be iron replete. Growth was estimated from the turbidity of culture using a densitometer (Densimat, BioMerieux)

Chapter 3. Development of a theoretical model describing iron acquisition by *P. multocida*

3.1 Introduction

Theoretical analysis of a reaction network can yield key information on the structural properties of the network, provide hypotheses for *in vitro* experiments and enable prediction of metabolic fluxes through the network. Subsequent integration of theoretical data with experimental data is a vital tool in systems biology, an emerging field seeking to increase our understanding of biological systems (Poolman, Fell and Raines, 2003; Schuster, Dandekar and Fell, 1999). Before theoretical analysis of a reaction network can take place, the network itself must be carefully described. Metabolic networks can be constructed on a whole genome scale (Cornish-Bowden and Hofmeyr, 2002; Duarte, Herrgard and Palsson, 2004; Schilling *et al*, 2002; Schilling and Palsson, 2000; Schuster, Fell and Dandekar, 2000), or alternatively can be based on a defined subsection of metabolism (Cornish-Bowden and Hofmeyr, 2002; Schuster, Fell and Dandekar, 2000), for example the process of iron acquisition. Therefore, the choice of which reactions are included in or excluded from the network is dictated by the biological function under investigation. With the addition of more reactions to a network, the analyses carried out on that network will become more accurate. However, this also increases the complexity of the network and consequently makes analysis more time-consuming and computer-intensive (Klamt and Stelling, 2002). As such, a balance must be struck between complexity of the network and the information sought.

As mentioned previously, the acquisition of iron by a bacterium is a prerequisite for its survival and proliferation in the host and is linked closely to virulence (Finkelstein, Sciortino and McIntosh, 1983). Transferrin and haemoglobin represent the two major sources of iron in the bovine lung and are bound by proteins in the outer membrane of invading bacteria and the iron removed and transported to the bacterial cytoplasm, either for storage or metabolism (Andrews, Robinson and Rodriguez-Quinones, 2003). This process requires energy, normally in the form of ATP provided from the metabolism of glucose through glycolysis, TCA cycle, pentose phosphate pathway and electron transfer, to drive the transport of the iron across the cytoplasmic membrane (Cornelissen, 2003; Ekins and Niven, 2002). Once internalised, iron is either stored in reserve, bound to an iron chelator such as bacterioferritin for use during times of iron deficit, or metabolised (Ratledge, 2007; Yariv *et al*, 1981). In the current work, details of biochemical pathways published from studies of the Pasteurellaceae have been used to reconstruct the transferrin and haemoglobin-based iron acquisition pathways in *P. multocida* and examined in the context of disease such as bovine pneumonic pasteurellosis caused by this organism.

To reconstruct and analyse a reaction network, a number of key steps were completed. The first of these was a systematic literature search to determine the components of the reaction network being studied. Once complete, the reaction network or networks were defined with specific system boundaries. From this network, stoichiometrically balanced equations were written for each reaction step in the network and those reactions catalogued in a database. These balanced equations provided the data from which elementary flux modes were calculated.

One key benefit of analysing a network using elementary flux modes is that it is an approach is based solely upon the reaction stoichiometries which exist in the network (Poolman, Fell and Raines, 2003; Schuster, Dandekar and Fell, 1999). Therefore, kinetic data is required only for validation of the model and not for analysis of it. As such, when defining the network, each reaction is balanced and the reversibility of each reaction stated.

Once complete, the metabolic network was analysed, in a separate study, to determine key information such as network robustness (Wilhelm, Behre and Schuster, 2004) and to identify key reactions within the network (Cakir *et al*, 2007; Cakir, Tacer and Ulgen, 2004).

Further analysis by flux balance analysis (FBA) (Schilling *et al*, 2000) allowed functional extension of the *in silico* model to incorporate experimentally-measured flux rates and estimation of un-measured flux rates and biomass. This technique is described in greater depth in **Chapter 6**.

3.2 Aims and methodology

The *P. multocida* iron acquisition network was described first in a simplified block diagram form (**Fig. 3.1**), showing each of the subnetworks contained within the whole network. Each of the subnetworks in turn was then described in detail, and balanced equations and elementary flux modes derived for each of them.

The modelling process must make clear the biological justification for which reactions are included in or excluded from the final model, that is to say they should be backed up by experimental data. Preliminary data indicated that growth rate and the rate of glucose uptake from the medium by *P. multocida* correlated closely. In addition, it appeared that when iron was restricted, growth rate and hence glucose uptake rate were also both lowered. This seemed a clear indicator that there was close interaction between iron availability and uptake, glucose uptake and eventual contribution to biomass and growth. It is known that to pump iron from the bacterial periplasm, through the cytoplasmic membrane, and into the bacterial cytoplasm requires energy in the form of ATP (Shouldice *et al*, 2004). One of the main sources of ATP for *P. multocida* is from metabolism of glucose, through the reactions of glycolysis, TCA cycle and the pentose phosphate pathway (Oberhofer, 1981). Accordingly, these two pathways were linked in the model. Although primarily an aerobic bacterium, *P. multocida* is also a facultative anaerobe, so the possibility of fermentative growth was also be considered, however, it was assumed that in the well-aerated bovine lung environment growth was largely aerobic (Lee, Kim and Kwon, 2007).

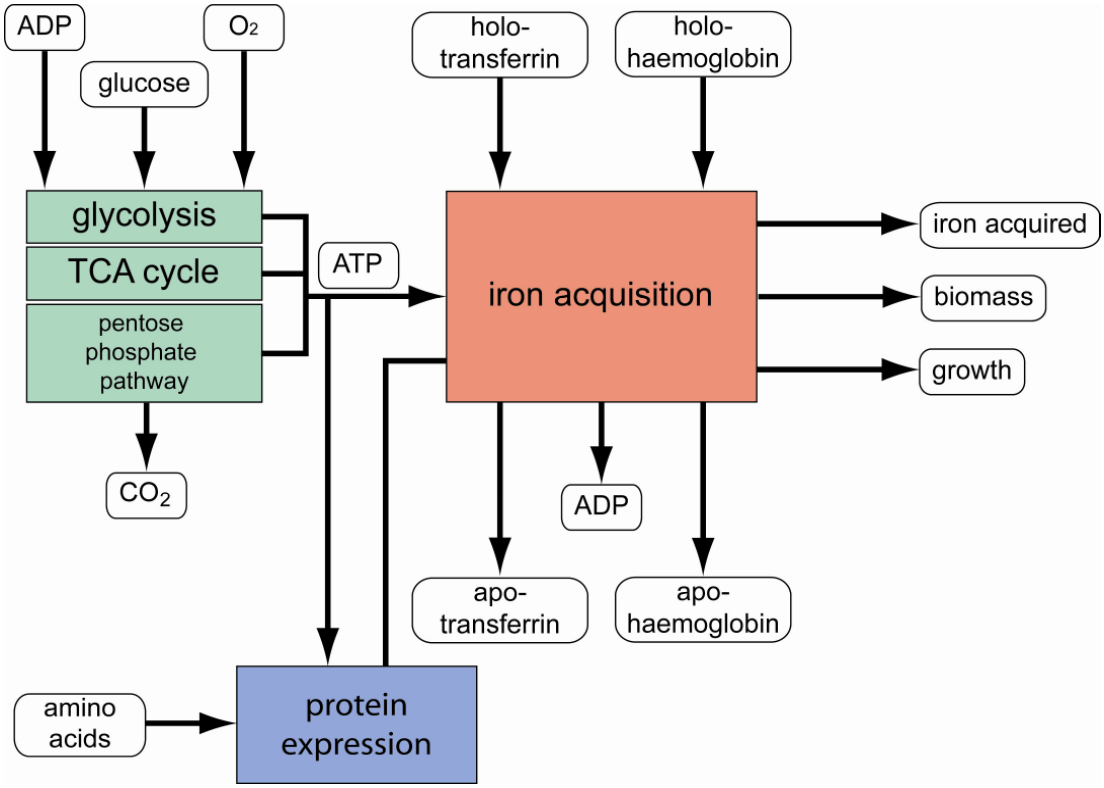

Fig. 3.1: Simplified diagram of the iron acquisition network of *P. multocida*. Highlighted in colour are the glucose metabolism (green), iron acquisition (red) and protein expression (blue) subnetworks. External metabolites as inputs/outputs to the network are shown in rounded rectangles.

Bacterial iron acquisition is a complex process and, as discussed earlier, several different pathways involving iron uptake by *P. multocida* are present. In the current model, pathways for uptake of iron from both transferrin and haemoglobin were included. Because several of the steps in the iron acquisition pathway involved only transfer of iron from one protein carrier to another, with the protein carrier remaining unchanged, this meant that the protein carriers were required to be specified as external metabolites to be included in the calculated elementary flux modes. However, inclusion of too great a number of external metabolites can limit the usefulness of data gained from the model. One method of changing the status of these metabolites from external to internal was to include a generic protein

expression subnetwork, as described by others (Allen and Palsson, 2003). This simplified network described the transcription of a gene by RNA polymerase, generating mRNA, and subsequent translation by tRNA to generate the expressed protein. Thus, the status of the proteins involved in the transmembrane transport of iron into the bacterial cytoplasm changed from external to internal.

3.2.1 Construction of a reaction database

Initially, reactions were catalogued using a Microsoft Access database, listing reaction number, a description of the reaction, balanced equation, relevant compartment and reference. However, with the availability of the YANA software (Schwarz *et al*, 2005), data from the Microsoft Access database was transferred to the YANA software as data storage was a built-in function of the program.

In order to ensure consistent notation of each reaction, reactants and products when compiling and cataloguing the reactions within a network, the following schema was used: each reaction in the whole network was given a unique number from 1 upwards and an alphabetical prefix to describe the pathway to which it belonged. The prefixes used were: FE for transmembrane iron transport; G for glycolysis; TCA for TCA cycle; PPP for pentose phosphate pathway; ET for electron transport; and P for protein synthesis. When analysing the network using elementary flux modes it was essential that all metabolites were correctly defined as internal or external. If the metabolite was a product of one of the component reactions of the network then it was defined as internal; in all other cases, it followed that that reactant must have been obtained from outwith the system and was, therefore, defined as external. In

addition, reversible reactions were differentiated from irreversible reactions by inclusion of a lower case letter ‘r’ as a suffix to the alphabetical prefix and reaction number.

3.2.2 Derivation of elementary flux modes – an example

As discussed earlier, elementary flux modes represent the most basic complete set of routes through a reaction network, none of which can be decomposed, or simplified, further. Their analysis provides information on the dynamic properties of a reaction network, and can be used both to suggest experimental hypotheses to be tested, and to compare with measured experimental fluxes (Schuster, Dandekar and Fell, 1999).

Once a set of balanced equations was listed from the reaction network, elementary flux modes were derived by converting the set of balanced equations into a numerical representation of the complete set of balanced equations, referred to as a stoichiometric matrix, from which elementary flux modes were calculated.

Each set of balanced equations was solved using linear algebra and the complete set of solutions to the full set of linear equations representing the metabolic network was termed the null space (Schilling *et al*, 1999). One important aspect of this approach is that determination of elementary flux modes assumes that the network is at steady state (Stelling *et al*, 2002). In the *in vitro* experimental section of this work in **Chapter 5**, batch cultures are used to investigate the process of iron acquisition in *P. multocida*. In such a closed system, nutrients become depleted whilst products build up, thus affecting bacterial metabolism and hence the steady state of the system.

However, if only log phase growth is considered then these effects can be minimised and the system can be assumed to be at a pseudo steady state (Kim *et al*, 2007). These concepts are explored further in **Chapters 5 and 6**.

The following example illustrates the mathematical basis for calculation of elementary flux modes for a simple pathway (**Fig. 3.2**).

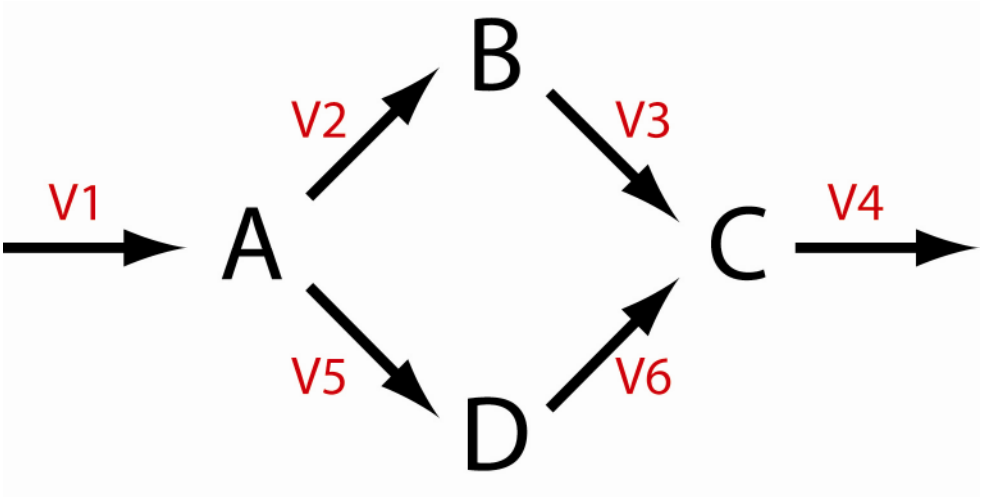

Fig. 3.2: Simple pathway. Metabolites A, B, C, D; and fluxes V1-6 (shown in red).

The reactions derived from this pathway are as follows:

$$V_1 = V_2 + V_5 \qquad V_2 = V_3 \qquad V_3 + V_6 = V_4 \qquad V_5 = V_6$$

OR

$$V_1 - V_2 - V_5 = 0 \qquad V_2 - V_3 = 0 \qquad V_3 - V_4 + V_6 = 0 \qquad V_5 - V_6 = 0$$

These linear algebraic equations can now be listed as a stoichiometric matrix, with each row of the matrix corresponding to a single reaction and each column showing the coefficients of each of the 6 fluxes in the pathway:

V_1	V_2	V_3	V_4	V_5	V_6
1	-1	0	0	-1	0
0	1	-1	0	0	0
0	0	1	-1	0	1
0	0	0	0	1	-1

The span of this matrix contains all the solutions to the set of linear algebraic equations (the null space) and can be written as:

$$NulS = Span\{b_1 ..... b_n\}$$

where $b_1 \ldots . b_n$ represent each of the vectors, or rows, within the matrix.

The above matrix can be written more correctly as:

$$\begin{bmatrix} 1 & -1 & 0 & 0 & -1 & 0 \\ 0 & 1 & -1 & 0 & 0 & 0 \\ 0 & 0 & 1 & -1 & 0 & 1 \\ 0 & 0 & 0 & 0 & 1 & -1 \end{bmatrix} \begin{bmatrix} V_1 \\ V_2 \\ V_3 \\ V_4 \\ V_5 \\ V_6 \end{bmatrix} = \begin{bmatrix} 0 \\ 0 \\ 0 \\ 0 \end{bmatrix}$$

Through simple Gaussian elimination, this system of linear equations can be solved in matrix form to give:

$$\begin{bmatrix} V_1 \\ V_2 \\ V_3 \\ V_4 \\ V_5 \\ V_6 \end{bmatrix} = \begin{bmatrix} V_4 \\ V_4 - V_6 \\ V_4 - V_6 \\ V_4 \\ V_6 \\ V_6 \end{bmatrix} = V_4 \begin{bmatrix} 1 \\ 1 \\ 1 \\ 1 \\ 0 \\ 0 \end{bmatrix} + V_6 \begin{bmatrix} 0 \\ -1 \\ -1 \\ 0 \\ 1 \\ 1 \end{bmatrix} = V_4 b_1 + V_6 b_2$$

In the above equation, b_1 and b_2 represent the basis vectors or solutions to the set of linear algebraic equations. These basis vectors can be converted back into linear equations:

$$V_1 + V_2 + V_3 + V_4 = 0$$
$$V_5 + V_6 - V_2 - V_3 = 0$$

Then the basis vectors (**Fig. 3.3**) can be mapped onto the pathway.

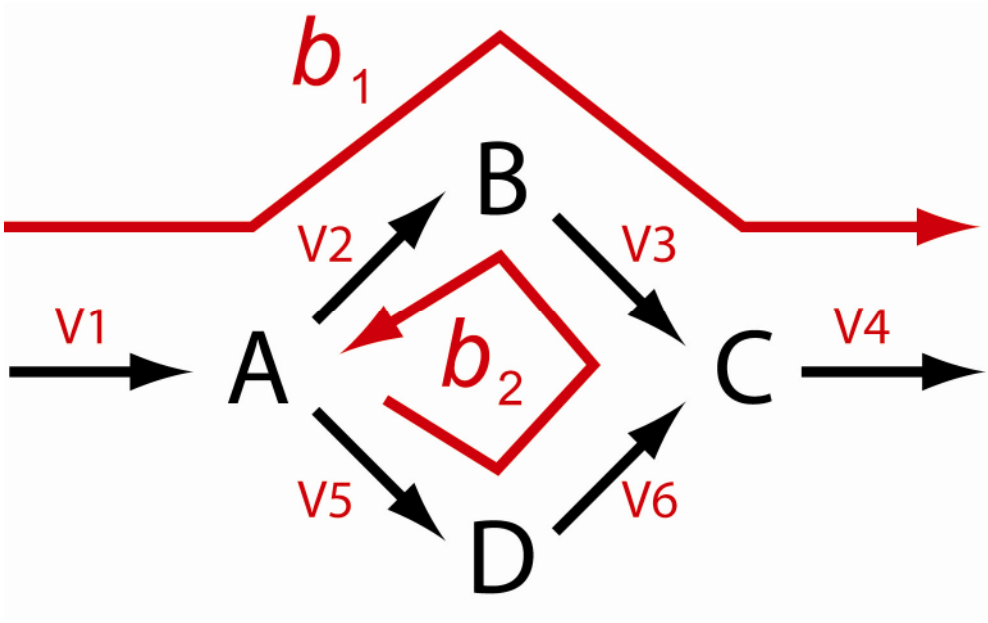

Fig. 3.3: Simple pathway. Metabolites A, B, C, D; and fluxes V1-6. Basis vectors b_1, b_2 indicated by red lines.

However, it can be seen that basis vector b_2 is not feasible thermodynamically as fluxes V_2 and V_3 can only proceed in a forwards direction. Therefore, to make the basis vectors feasible thermodynamically, basis transformation must be used to give all the coefficients positive values.

If the two basis vectors, designated B, are multiplied by the transformation matrix, designated T, then two new basis vectors, designated P, are generated, thus:

$$B \cdot T = P, \text{ where } T = \begin{bmatrix} 1 & 1 \\ 1 & 0 \end{bmatrix} \qquad B \cdot T = \begin{bmatrix} 1 & 0 \\ 1 & -1 \\ 1 & -1 \\ 1 & 0 \\ 0 & 1 \\ 0 & 1 \end{bmatrix} \begin{bmatrix} 1 & 1 \\ 1 & 0 \end{bmatrix} = \begin{bmatrix} 1 & 1 \\ 1 & 0 \\ 1 & 0 \\ 1 & 1 \\ 0 & 1 \\ 0 & 1 \end{bmatrix} = P$$

In simpler terms, this operation could be carried out as follows:

$$P = \{p1, p2\} = \{b1, b1 + b2\}$$

Both of these new basis vectors, p_1 and p_2, are feasible thermodynamically and can be mapped onto the pathway as follows (**Fig. 3.4**):

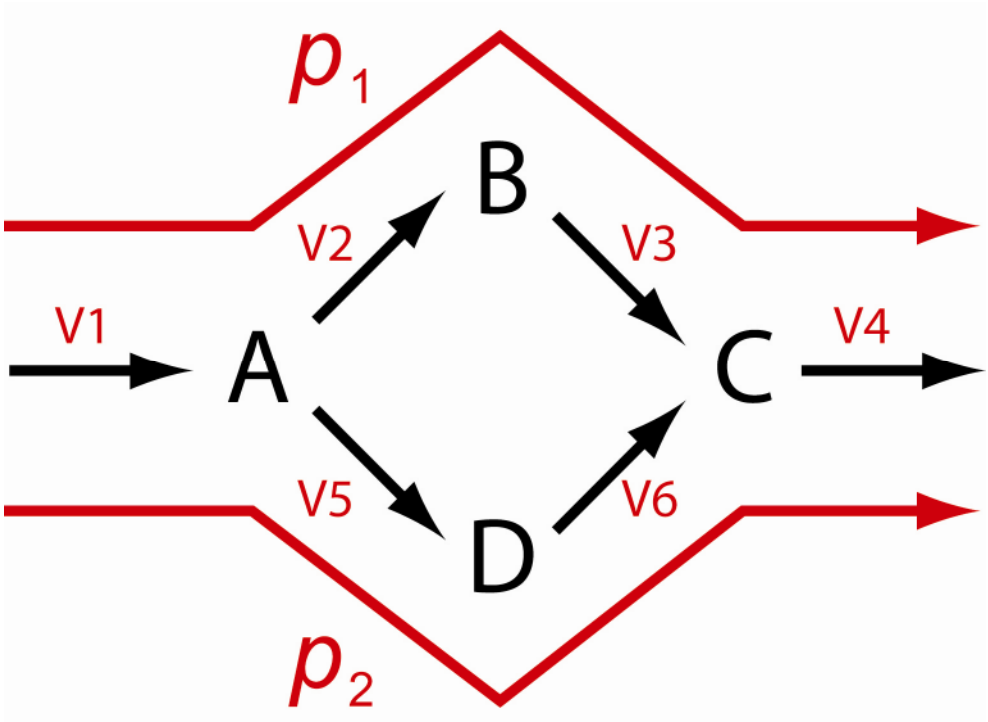

Fig. 3.4: Simple pathway. Metabolites A, B, C, D; and fluxes V1-6. Transformed basis vectors p_1, p_2 indicated by red lines.

In transforming the basis vectors into new thermodynamically feasible vectors, the null space has been constrained, and this transformation has been carried out through implementing inequality constraints, in this case, that all basis vectors must be positive. This set of basis vectors now represents the most basic set of routes through this simple pathway, also known as the **elementary flux modes**. In mathematical terms, this constrained null space, if plotted in 3-dimensional space, forms a convex polyhedral cone. In biological terms, any one point within this flux cone represents a unique flux distribution, and hence a unique combination of elementary flux modes. Furthermore, it means that the entire set of metabolic phenotypes, or physiological states, of the network is represented within that cone (Gagneur and Klamt, 2004). This enables the fitting of variables measured *in vitro* to the *in silico* data and

prediction of un-measured fluxes, as described further in **Chapters 5 and 6**. An extension of this is FBA (Edwards, Covert and Palsson, 2002), explored further in **Chapter 6**.

The derivation of elementary flux modes can be automated using a specific algorithm. However, it must be remembered that with increasing network size and complexity, the number of elementary flux modes, and therefore the time taken to compute these modes, will increase exponentially (Klamt and Stelling, 2002).

3.3 Results

3.3.1 Glucose metabolism subnetwork

Initially, the glucose network (**Fig. 3.5**) was reconstructed with reference to the scheme of Carlson and Srienc (2004) and the KEGG glycolysis and TCA cycle pathways for *P. multocida* (Kanehisa and Goto, 2000) to ensure that the appropriate enzymes were present in *P. multocida*. Component reactions were then listed for the network (**Table 3.1**).

Elementary flux modes were derived from this set of reactions using the YANA software (Schwarz *et al*, 2005).

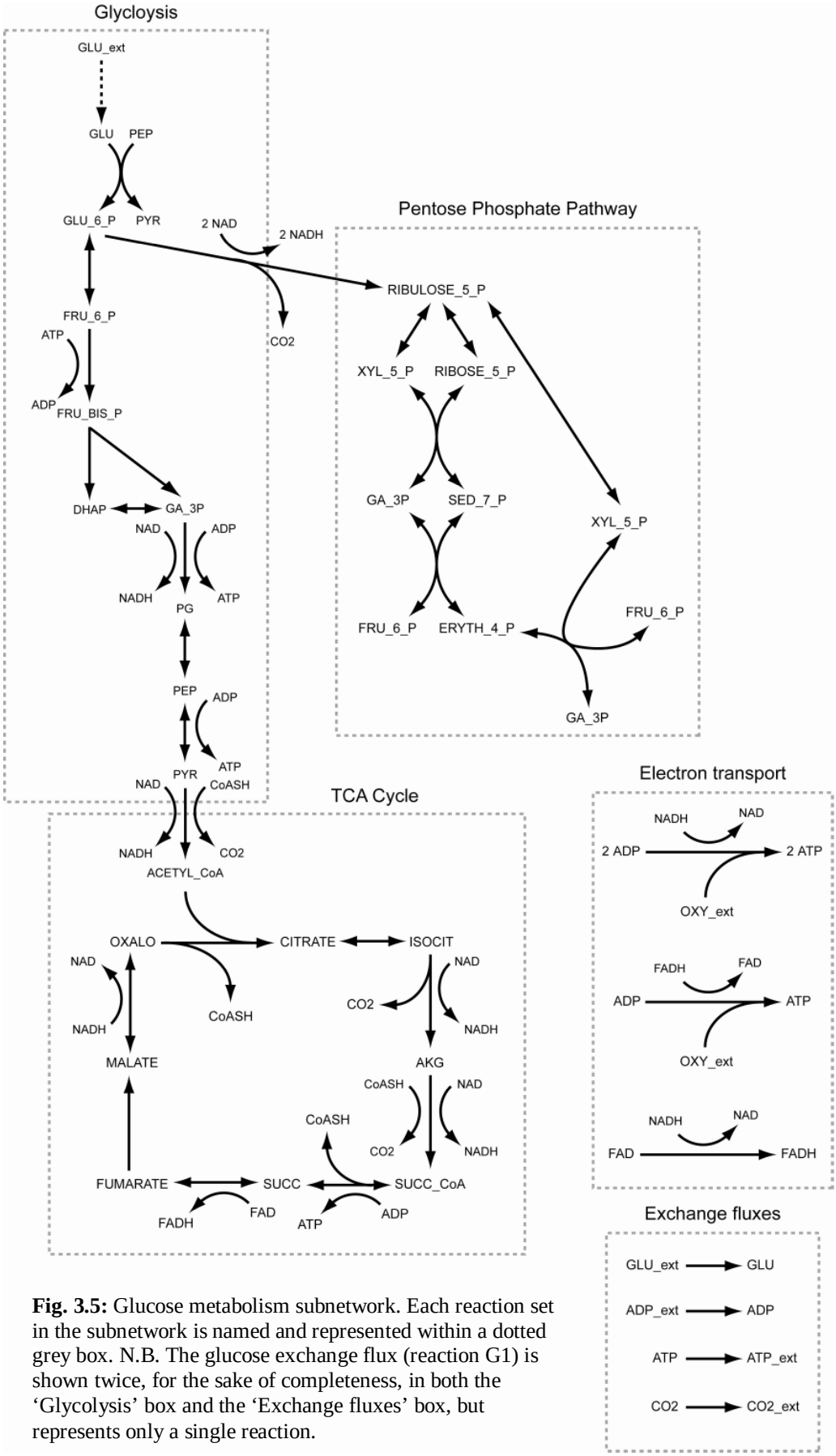

Fig. 3.5: Glucose metabolism subnetwork. Each reaction set in the subnetwork is named and represented within a dotted grey box. N.B. The glucose exchange flux (reaction G1) is shown twice, for the sake of completeness, in both the 'Glycolysis' box and the 'Exchange fluxes' box, but represents only a single reaction.

Reaction	Reaction equation	Reversibility
G1	GLU_ext ↔ GLU	irr
G2	GLU + PEP → GLU_6_P + PYR	irr
G3r	GLU_6_P ↔ FRU_6_P	rev
G4	ATP + FRU_6_P → ADP + FRU_BIS_P	irr
G5r	FRU_BIS_P ↔ DHAP + GA_3P	rev
G6r	GA_3P ↔ DHAP	rev
G7	ADP + GA_3P + NAD ↔ ATP + NADH + PG	irr
G8r	PG ↔ PEP	rev
G9r	ADP + PEP ↔ ATP + PYR	rev
PPP10	GLU_6_P + 2 NAD → CO2 + 2 NADH + RIBULOSE_5_P	irr
PPP11r	RIBULOSE_5_P ↔ XYL_5_P	rev
PPP12r	RIBULOSE_5_P ↔ RIBOSE_5_P	rev
PPP13r	RIBOSE_5_P + XYL_5_P ↔ GA_3P + SED_7_P	rev
PPP14r	GA_3P + SED_7_P ↔ ERYTH_4_P + FRU_6_P	rev
PPP15r	ERYTH_4_P + XYL_5_P ↔ FRU_6_P + GA_3P	rev
TCA16r	CO2 → CO2_ext	rev
TCA17	CoASH + NAD + PYR → ACETYL_CoA + CO2 + NADH	irr
TCA18	ACETYL_CoA + OXALO → CITRATE + CoASH	irr
TCA19r	CITRATE ↔ ISOCIT	rev
TCA20	ISOCIT + NAD → AKG + CO2 + NADH	irr
TCA21	AKG + CoASH + NAD → CO2 + NADH + SUCC_CoA	irr
TCA22r	ADP + SUCC_CoA ↔ ATP + CoASH + SUCC	rev
TCA23r	FAD + SUCC ↔ FADH + FUMARATE	rev
TCA24	FUMARATE ↔ MALATE	irr
TCA25r	MALATE + NAD ↔ NADH + OXALO	rev
ET26	2 ADP + NADH + OXY_ext → 2 ATP + NAD	irr
ET27	ADP + FADH + OXY_ext → ATP + FAD	irr
ET28	FAD + NADH → FADH + NAD	irr
ADP	ADP_ext ↔ ADP	irr
ATP	ATP ↔ ATP_ext	irr

Table 3.1: Component reactions of the glucose metabolism subnetwork. Each reaction name (left hand column), with the exception of the ADP and ATP reactions, has a prefix corresponding to the relevant part of the subnetwork: G = glycolysis, PPP = pentose phosphate pathway, TCA = TCA cycle, ET = electron transport. A lower case 'r' suffix in the reaction name indicates that a reaction is reversible. The reversibility of each reaction is also stated in the right hand column: rev = reversible, irr = irreversible.

Glucose metabolism subnetwork elementary flux modes

Six elementary flux modes were derived from the glucose metabolism subnetwork (**Fig. 3.6**), and represented 3 main routes through the subnetwork. The first route, represented in elementary modes (EM) 3 and 4, showed the flux of glucose through glycolysis and the TCA cycle. The differences between EM3 and EM4 were that in EM3, reaction ET26 was excluded from the electron transport reactions with only

reactions ET27 and ET28 functional, whilst in mode 4, reaction ET28 was excluded and reactions ET26 and ET27 were functional. This first route excluded all 6 reactions of the pentose phosphate pathway.

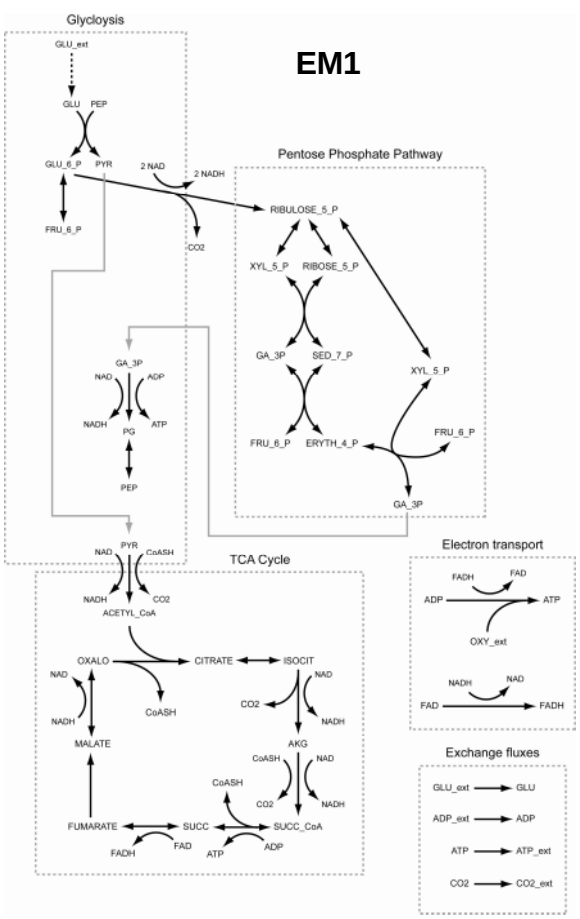
EM1
Glycolysis
Pentose Phosphate Pathway
TCA Cycle
Electron transport
Exchange fluxes
GLU_ext
GLU
PEP
GLU_6_P
PYR
2 NAD
2 NADH
FRU_6_P
CO2
RIBULOSE_5_P
XYL_5_P
RIBOSE_5_P
GA_3P
SED_7_P
FRU_6_P
ERYTH_4_P
XYL_5_P
FRU_6_P
GA_3P
NAD
ADP
NADH
ATP
PG
PEP
PYR
CoASH
NADH
CO2
ACETYL_CoA
OXALO
CITRATE
ISOCIT
NAD
CoASH
CO2
NADH
MALATE
AKG
CoASH
NAD
CoASH
CO2
NADH
FUMARATE
SUCC
SUCC_CoA
FADH
FAD
ATP
ADP
FADH
FAD
ADP
ATP
OXY_ext
NADH
NAD
FAD
FADH
GLU_ext
GLU
ADP_ext
ADP
ATP
ATP_ext
CO2
CO2_ext

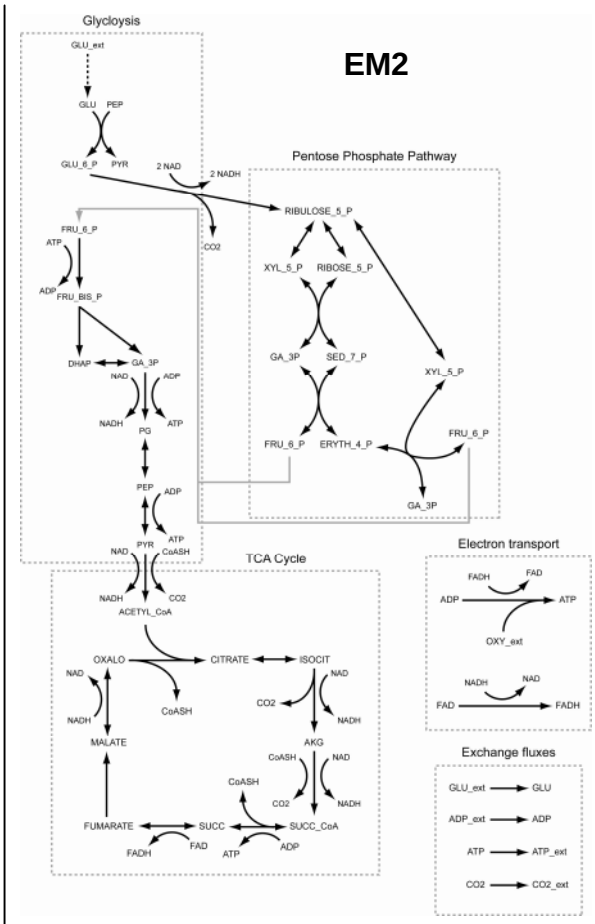
EM2
Glycolysis
Pentose Phosphate Pathway
TCA Cycle
Electron transport
Exchange fluxes
GLU_ext
GLU
PEP
GLU_6_P
PYR
2 NAD
2 NADH
FRU_6_P
ATP
ADP
FRU_BIS_P
CO2
RIBULOSE_5_P
XYL_5_P
RIBOSE_5_P
DHAP
GA_3P
SED_7_P
XYL_5_P
NAD
ADP
NADH
ATP
PG
FRU_6_P
ERYTH_4_P
FRU_6_P
PEP
ADP
ATP
GA_3P
NAD
PYR
CoASH
NADH
CO2
ACETYL_CoA
OXALO
CITRATE
ISOCIT
NAD
CoASH
CO2
NADH
MALATE
AKG
CoASH
NAD
CoASH
CO2
NADH
FUMARATE
SUCC
SUCC_CoA
FADH
FAD
ATP
ADP
FADH
FAD
ADP
ATP
OXY_ext
NADH
NAD
FAD
FADH
GLU_ext
GLU
ADP_ext
ADP
ATP
ATP_ext
CO2
CO2_ext

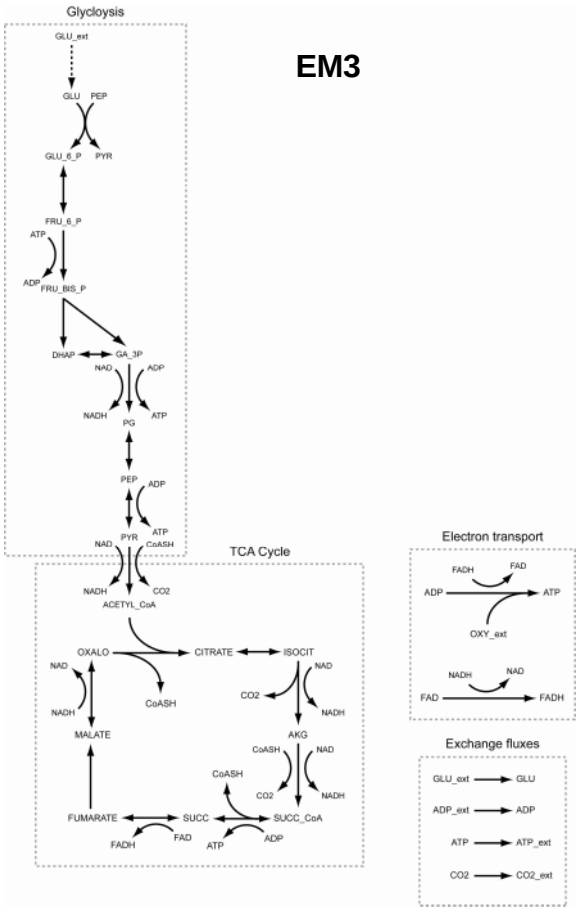
EM3
Glycolysis
TCA Cycle
Electron transport
Exchange fluxes
GLU_ext
GLU
PEP
GLU_6_P
PYR
FRU_6_P
ATP
ADP
FRU_BIS_P
DHAP
GA_3P
NAD
ADP
NADH
ATP
PG
PEP
ADP
ATP
NAD
PYR
CoASH
NADH
CO2
ACETYL_CoA
OXALO
CITRATE
ISOCIT
NAD
CoASH
CO2
NADH
MALATE
AKG
CoASH
NAD
CoASH
CO2
NADH
FUMARATE
SUCC
SUCC_CoA
FADH
FAD
ATP
ADP
FADH
FAD
ADP
ATP
OXY_ext
NADH
NAD
FAD
FADH
GLU_ext
GLU
ADP_ext
ADP
ATP
ATP_ext
CO2
CO2_ext

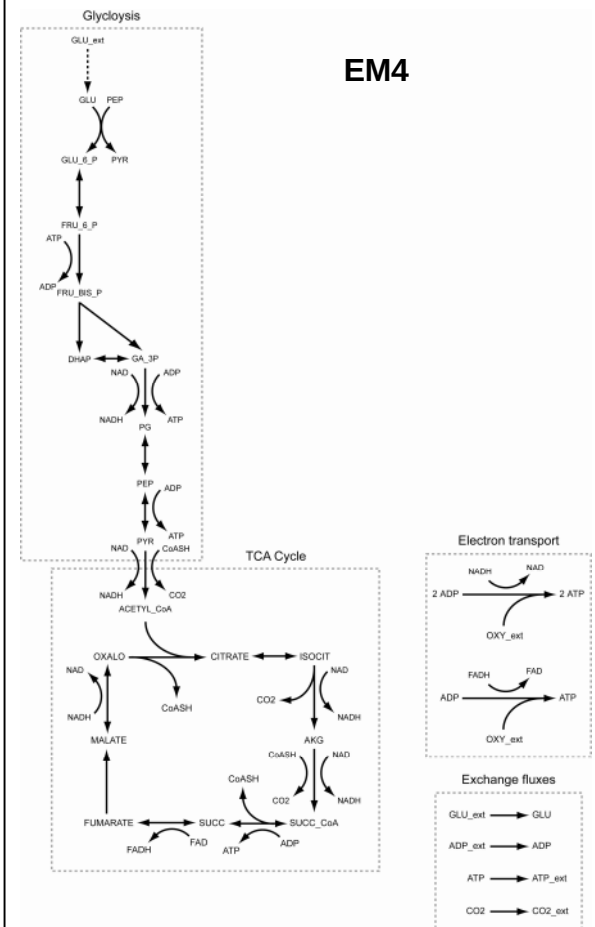
EM4
Glycolysis
TCA Cycle
Electron transport
Exchange fluxes
GLU_ext
GLU
PEP
GLU_6_P
PYR
FRU_6_P
ATP
ADP
FRU_BIS_P
DHAP
GA_3P
NAD
ADP
NADH
ATP
PG
PEP
ADP
ATP
NAD
PYR
CoASH
NADH
CO2
ACETYL_CoA
OXALO
CITRATE
ISOCIT
NAD
CoASH
CO2
NADH
MALATE
AKG
CoASH
NAD
CoASH
CO2
NADH
FUMARATE
SUCC
SUCC_CoA
FADH
FAD
ATP
ADP
NADH
NAD
2 ADP
2 ATP
OXY_ext
FADH
FAD
ADP
ATP
OXY_ext
GLU_ext
GLU
ADP_ext
ADP
ATP
ATP_ext
CO2
CO2_ext

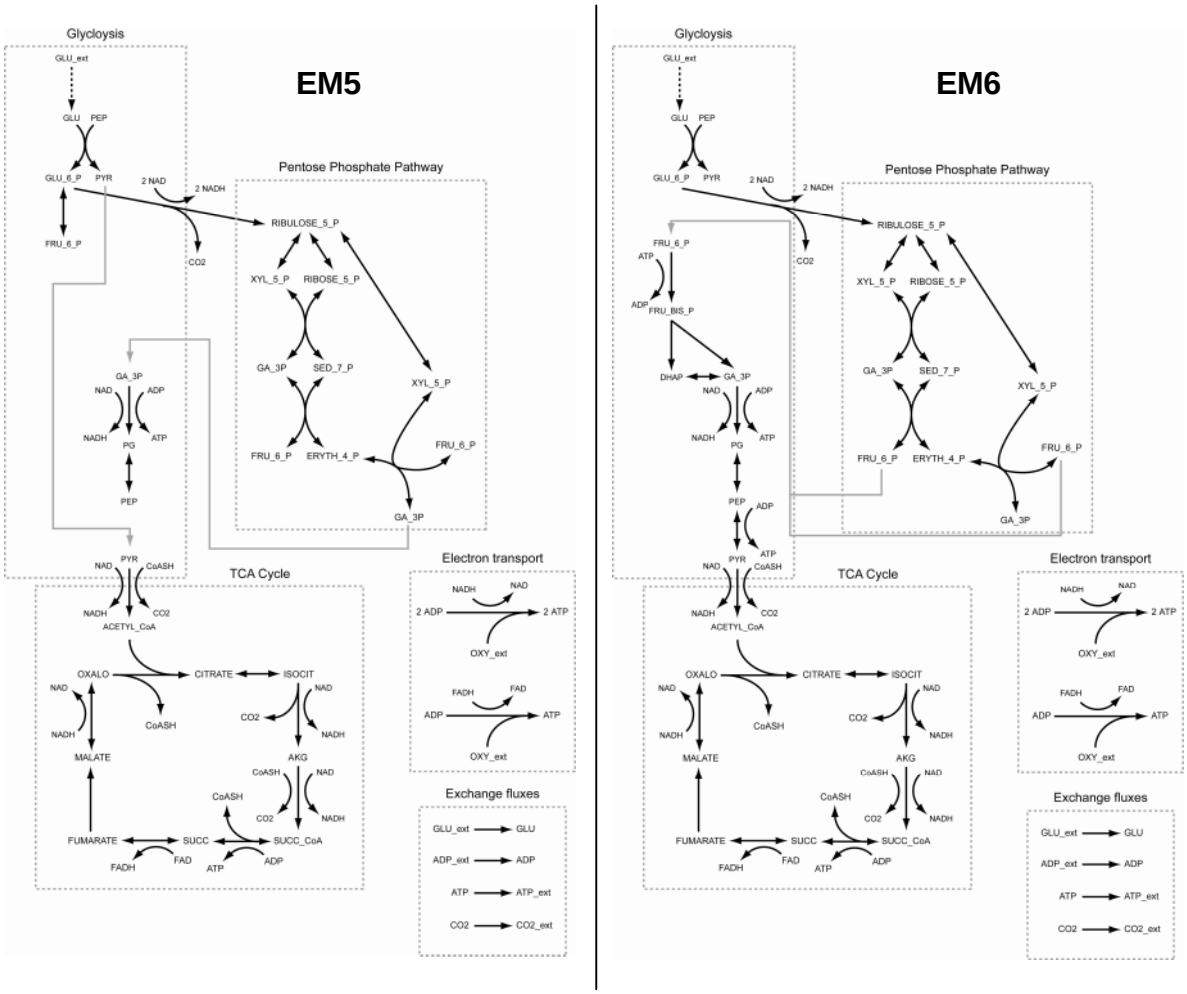

Fig. 3.6: Elementary flux modes of glucose metabolism subnetwork generated by YANA software. Elementary modes 1-6 are labelled EM1-EM6. Solid grey lines represent probable flux of metabolites.

A second route through the subnetwork was noted in which reactions G4, G5r, G6r and G9r were excluded (EM1 and EM5) (**Fig. 3.6**). As a result the pyruvate produced in reaction G2 became a substrate in reaction TCA17, whilst the glyceraldehyde-3-phosphate produced in reaction PPP15r became a substrate in reaction G7. In addition, fructose-6-phosphate produced from the pentose phosphate pathway was converted back into glucose-6-phosphate in reaction G3r, which was in turn cycled back through the pentose phosphate pathway to provide additional glyceraldehyde-6-phosphate and NADH. EM1 and EM5 differed in their electron transport reactions, with reaction ET26 taking no part in EM1 and reaction ET28 excluded from EM5.

A third route through the glucose metabolism subnetwork was seen in EM2 and EM6. The only reaction excluded from the glycolysis, TCA cycle and pentose phosphate pathway reactions in these modes was reaction G3r. Rather than being produced by reaction G3r, the fructose-6-phosphate was produced by reactions PPP14r and PPP15r, and became the substrate for reaction G4. Similar to the first and second routes described, EM2 and EM6 differed in their electron transport reactions, with EM2 lacking reaction ET26 and EM6 lacking reaction ET28.

The contribution of the glucose metabolism subnetwork to the overall iron acquisition process was the provision of ATP, both for active transport of iron across the bacterial cytoplasmic membrane and for synthesis of proteins taking part in the iron acquisition process. The net reactions of each elementary flux mode derived from the glucose metabolism subnetwork took the form:

$$aADPext + bGLUext + cOXYext \rightarrow dATPext + eCO2ext$$

From these balanced equations, the efficiency with which each elementary mode converted glucose into ATP was estimated by finding the glucose:ATP ratio. These ratios and the net reactions for each of the six elementary modes are shown in **Table 3.2** below.

EM no.	Net reaction	Gluc:ATP ratio
1	14ADP_ext + GLU_ext + 12OXY_ext → 14ATP_ext + 6CO2_ext	1:14
2	46ADP_ext + 3GLU_ext + 36OXY_ext → 46ATP_ext + 18CO2_ext	1:15.33
3	14ADP_ext + GLU_ext + 12OXY_ext → 14ATP_ext + 6CO2_ext	1:14
4	26ADP_ext + GLU_ext + 12OXY_ext → 26ATP_ext + 6CO2_ext	1:26
5	25ADP_ext + GLU_ext + 12OXY_ext → 25ATP_ext + 6CO2_ext	1:25
6	77ADP_ext + 3GLU_ext + 36OXY_ext → 77ATP_ext + 18CO2_ext	1:25.67

Table 3.2: Net reactions and glucose:ATP ratios of glucose metabolism subnetwork elementary flux modes 1-6.

From **Table 3.2**, it was seen that elementary modes 4, 5 and 6 had a glucose:ATP ratio almost twice that of modes 1, 2 and 3; mode 4 having the highest ratio and modes 1 and 3 having the lowest ratios. The balances of oxygen and CO_2 remained in constant ratio to that of glucose.

After calculation of elementary modes, as described in **Section 3.2.2**, each reaction in each elementary mode was assigned an integer value; these integers described the steady state for each elementary mode. As mentioned previously, any possible flux distribution, and hence metabolic phenotype, of the subnetwork could be calculated from a combination of the set of elementary flux modes. Percentage activities could be assigned to each elementary mode, and adjustment of the balance of these activities allowed possible phenotypes to be represented. This process is explored in greater detail in following chapters. However, when the activities of all 6 elementary modes of the glucose metabolism subnetwork were set to 100% and the integer values for each reaction across these 6 modes was summed, then the arbitrary contribution or importance of each reaction to the overall subnetwork could be estimated. These values are described here as flux contribution (FC) values, and are listed in **Table 3.3**.

Reaction	Reaction equation	FC value
ADP	ADP_ext ↔ ADP	204
ATP	ATP ↔ ATP_ext	204
ET27	ADP + FADH + OXY_ext → ATP + FAD	68
TCA16r	CO2 → CO2_ext	60
ET26	2 ADP + NADH + OXY_ext → 2 ATP + NAD	52
ET28	FAD + NADH → FADH + NAD	52
G7	ADP + GA_3P + NAD ↔ ATP + NADH + PG	16
G8r	PG ↔ PEP	16
TCA17	CoASH + NAD + PYR → ACETYL_CoA + CO2 + NADH	16
TCA18	ACETYL_CoA + OXALO → CITRATE + CoASH	16
TCA19r	CITRATE ↔ ISOCIT	16
TCA20	ISOCIT + NAD → AKG + CO2 + NADH	16
TCA21	AKG + CoASH + NAD → CO2 + NADH + SUCC_CoA	16
TCA22r	ADP + SUCC_CoA ↔ ATP + CoASH + SUCC	16
TCA23r	FAD + SUCC ↔ FADH + FUMARATE	16
TCA24	FUMARATE ↔ MALATE	16
TCA25r	MALATE + NAD ↔ NADH + OXALO	16
PPP10	GLU_6_P + 2 NAD → CO2 + 2 NADH + RIBULOSE_5_P	12
G1	GLU_ext ↔ GLU	10
G2	GLU + PEP → GLU_6_P + PYR	10
PPP11r	RIBULOSE_5_P ↔ XYL_5_P	8
G3r	GLU_6_P ↔ FRU_6_P	6
G4	ATP + FRU_6_P → ADP + FRU_BIS_P	6
G5r	FRU_BIS_P ↔ DHAP + GA_3P	6
G6r	GA_3P ↔ DHAP	6
G9r	ADP + PEP ↔ ATP + PYR	6
PPP12r	RIBULOSE_5_P ↔ RIBOSE_5_P	4
PPP13r	RIBOSE_5_P + XYL_5_P ↔ GA_3P + SED_7_P	4
PPP14r	GA_3P + SED_7_P ↔ ERYTH_4_P + FRU_6_P	4
PPP15r	ERYTH_4_P + XYL_5_P ↔ FRU_6_P + GA_3P	4

Table 3.3: FC values and balanced equations of the glucose metabolism subnetwork, in descending order of contribution to the overall subnetwork.

It was noted, after studying the FC values of each reaction in the subnetwork, that the 2 highest FC values were those representing ADP input and ATP output. In addition, the efflux of CO_2 from the system also showed a high FC value. The 3 electron transport reactions, producing ATP from NADH and FADH generated by the TCA cycle, also had high FC values. In contrast, the reactions of the pentose phosphate pathway generally had lower FC values.

3.3.2 Protein synthesis subnetwork

As mentioned previously, the inclusion of a protein synthesis subnetwork required many previously external metabolites to be re-classified as internal metabolites. The simplified network described here (**Fig. 3.7** and **Table 3.4**) was based upon a system that provided a generic set of reactions representing gene expression through transcription, translation and associated ATP and amino acid inputs (Allen and Palsson, 2003). The same scheme was used to represent synthesis of every protein involved in the transmembrane transport of iron. It should be noted that synthesis of complexes of two or more proteins, in this case the Ton system, FbpBC and YfeBCD complexes, were considered as a single protein; this was taken into account when comparing *in vitro* and *in silico* model outputs (**Chapter 6**).

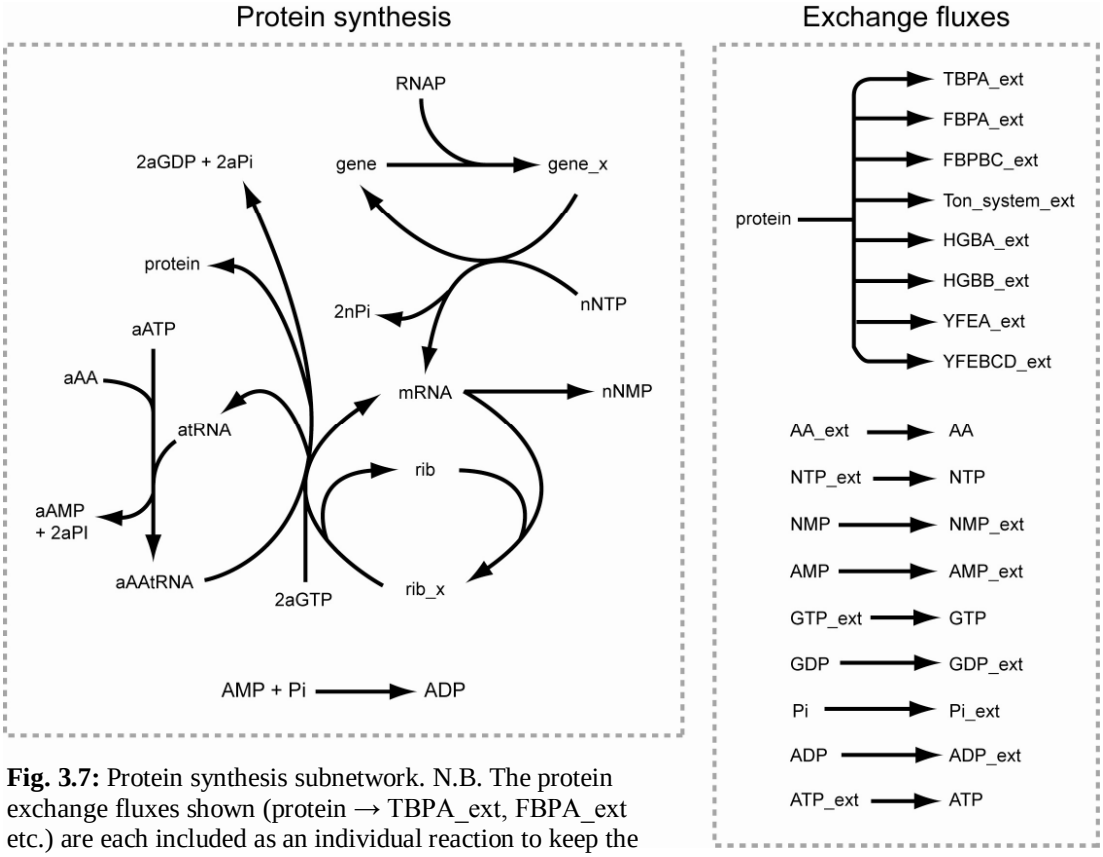

Fig. 3.7: Protein synthesis subnetwork. N.B. The protein exchange fluxes shown (protein → TBPA_ext, FBPA_ext etc.) are each included as an individual reaction to keep the stoichiometric balance of the subnetwork correct.

Reaction	Reaction equation	Reversibility
P81	RNAP + gene → gene_x	irr
P82	gene_x + nNTP → RNAP + gene + mRNA + 2 nPi	irr
P83	mRNA2 → nNMP	irr
P84	mRNA + rib → rib_x	irr
P85	aAAtRNA + 2 aGTP + rib_x → 2 aGDP + 2 aPi + atRNA + mRNA2 + protein + rib	irr
P86	AA + ATP + atRNA → AMP + 2 Pi + aAAtRNA	irr
P87	AA_ext → AA	irr
P88	NTP_ext → nNTP	irr
P89	nNMP → NMP_ext	irr
P90	AMP → AMP_ext	irr
P91	GTP_ext → aGTP	irr
P92	aGDP → GDP_ext	irr
P93	Pi → Pi_ext	irr
P94	aPi → Pi_ext	irr
P95	nPi → Pi_ext	irr
P96	AMP + Pi → ADP	irr
P97	protein → TBPA_ext	irr
P98	protein → FBPA_ext	irr
P99	protein → FBPBC_ext	irr
P100	protein → Ton_system_ext	irr
P101	protein → HGBA_ext	irr
P102	protein → HGBB_ext	irr
P103	protein → YFEA_ext	irr
P104	protein → YFEBCD_ext	irr
ADP	ADP → ADP_ext	irr
ATP	ATP_ext → ATP	irr

Table 3.4: Component reactions of the protein synthesis subnetwork. Each reaction name (left hand column) has a prefix 'P' denoting that it relates to the protein synthesis subnetwork. All reactions are irreversible (denoted by "irr" in right hand column).

It is important to note that in both **Fig. 3.7** and **Table 3.4** the lower case 'n' prefix in reactions P82, P83, P88, P89 and P95, and the lower case 'a' prefix in reactions P85, P86, P92 and P94 represent arbitrary integers and enabled the reactions to be balanced despite the exact number of molecules of each reactant being unknown. These values could be calculated from measurements of the concentrations of reactants and products.

Protein synthesis subnetwork elementary flux modes

When analysed using the YANA software, as in **Section 3.3.1**, 16 elementary flux modes were generated from the protein synthesis subnetwork (**Fig. 3.8, Table 3.5)**.

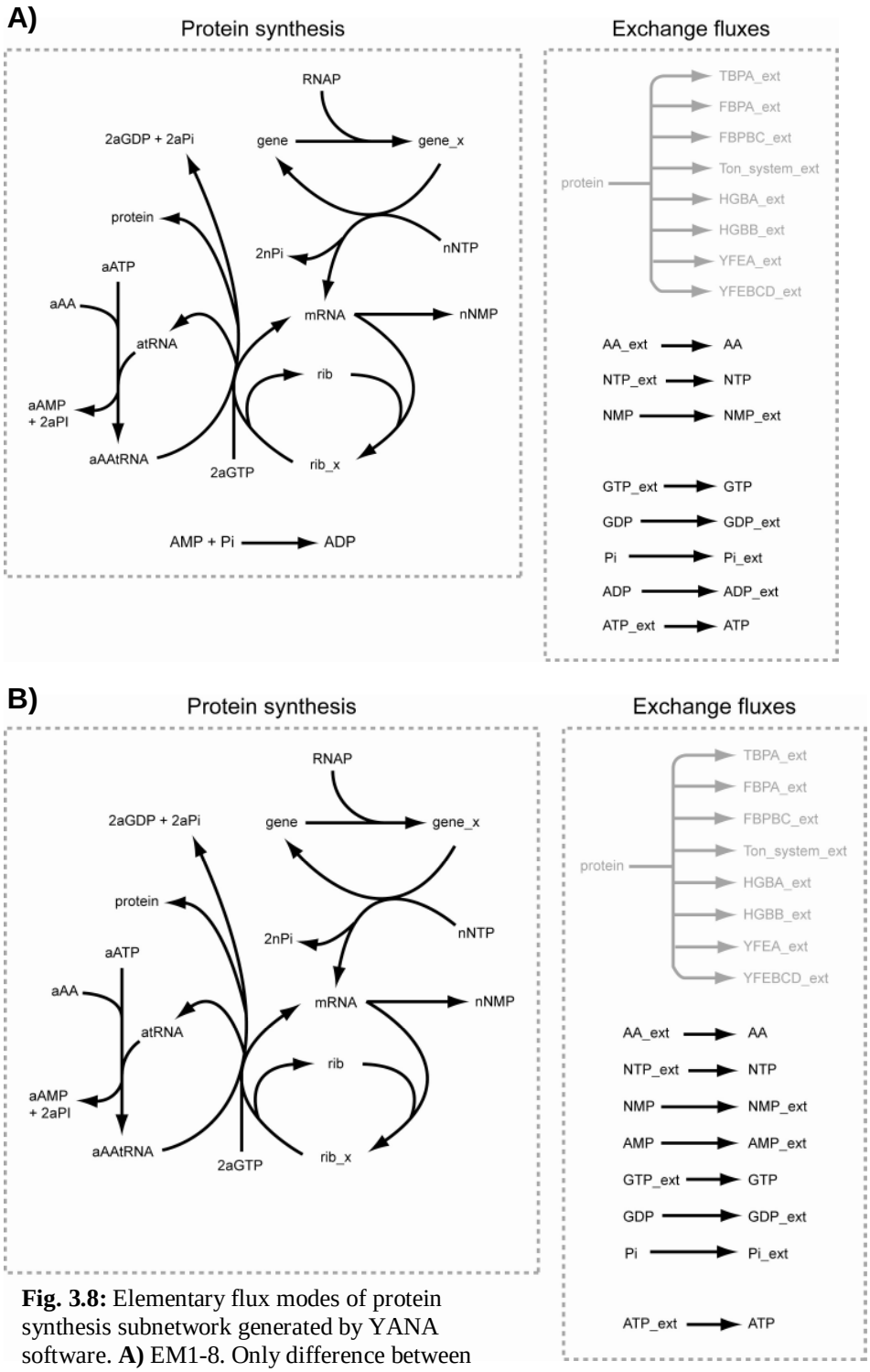

Fig. 3.8: Elementary flux modes of protein synthesis subnetwork generated by YANA software. **A)** EM1-8. Only difference between EM1-8 is final protein exchange flux. Each mode represents output of only one of the eight proteins/protein complexes. **B)** EM9-16. As in **A)**, EM9-16 represent output of only one protein/protein complex each.

ıEM no.	Net reaction
1	AA_ext + ATP_ext + 2GTP_ext + NTP_ext → ADP_ext + 2GDP_ext + NMP_ext + 5Pi_ext + TBPA_ext
2	AA_ext + ATP_ext + 2GTP_ext + NTP_ext → ADP_ext + 2GDP_ext + NMP_ext + 5Pi_ext + FBPA_ext
3	AA_ext + ATP_ext + 2GTP_ext + NTP_ext → ADP_ext + 2GDP_ext + NMP_ext + 5Pi_ext + FBPBC_ext
4	AA_ext + ATP_ext + 2GTP_ext + NTP_ext → ADP_ext + 2GDP_ext + NMP_ext + 5Pi_ext + Ton_system_ext
5	AA_ext + ATP_ext + 2GTP_ext + NTP_ext → ADP_ext + 2GDP_ext + NMP_ext + 5Pi_ext + HGBA_ext
6	AA_ext + ATP_ext + 2GTP_ext + NTP_ext → ADP_ext + 2GDP_ext + NMP_ext + 5Pi_ext + HGBB_ext
7	AA_ext + ATP_ext + 2GTP_ext + NTP_ext → ADP_ext + 2GDP_ext + NMP_ext + 5Pi_ext + YFEA_ext
8	AA_ext + ATP_ext + 2GTP_ext + NTP_ext → ADP_ext + 2GDP_ext + NMP_ext + 5Pi_ext + YFEBCD_ext
9	AA_ext + ATP_ext + 2GTP_ext + NTP_ext → AMP_ext + 2GDP_ext + NMP_ext + 6Pi_ext + TBPA_ext
10	AA_ext + ATP_ext + 2GTP_ext + NTP_ext → AMP_ext + 2GDP_ext + NMP_ext + 6Pi_ext + FBPA_ext
11	AA_ext + ATP_ext + 2GTP_ext + NTP_ext → AMP_ext + 2GDP_ext + NMP_ext + 6Pi_ext + FBPBC_ext
12	AA_ext + ATP_ext + 2GTP_ext + NTP_ext → AMP_ext + 2GDP_ext + NMP_ext + 6Pi_ext + Ton_system_ext
13	AA_ext + ATP_ext + 2GTP_ext + NTP_ext → AMP_ext + 2GDP_ext + NMP_ext + 6Pi_ext + HGBA_ext
14	AA_ext + ATP_ext + 2GTP_ext + NTP_ext → AMP_ext + 2GDP_ext + NMP_ext + 6Pi_ext + HGBB_ext
15	AA_ext + ATP_ext + 2GTP_ext + NTP_ext → AMP_ext + 2GDP_ext + NMP_ext + 6Pi_ext + YFEA_ext
16	AA_ext + ATP_ext + 2GTP_ext + NTP_ext → AMP_ext + 2GDP_ext + NMP_ext + 6Pi_ext + YFEBCD_ext

Table 3.5: Net reactions for each of the 16 elementary flux modes of the protein synthesis network. As seen in **Fig. 3.8**, elementary modes 1-8 comprise an identical set of reactions with the exception of the final protein exchange flux, with each mode contributing a single one of the eight synthesised proteins/protein complexes. These are: TbpA, FbpA, FbpBC complex, Ton System complex, HgbA, HgbB, YfeA and YfeBCD complex. Similarly, elementary modes 9-16 share an identical set of reactions with the exception of the final protein exchange flux.

As seen in both **Fig. 3.8** and **Table 3.5**, the 16 elementary modes fell into 2 clear sets of 8 similar routes. The difference between these 2 sets was the inclusion or exclusion of reactions P90, P96 and 'ADP'. In EM1-8, reactions 'ADP' and P96, representing the efflux of ADP from the system and the conversion of AMP to ADP respectively, were included. However, reaction P90, representing the efflux of AMP from the system, was excluded from these modes. Conversely, in EM9-16, reactions 'ADP' and P96 were excluded, whilst reaction P90 was included. In both sets of 8 modes, a single mode represented output of each of the 8 proteins or protein complexes being synthesised.

Reaction	Reaction equation	FC value
P91	GTP_ext → aGTP	32
P92	aGDP → GDP_ext	32
P94	aPi → Pi_ext	32
P95	nPi → Pi_ext	32
P93	Pi → Pi_ext	24
ATP	ATP_ext → ATP_protein	16
P81	RNAP + gene → gene_x	16
P82	gene_x + nNTP → RNAP + gene + mRNA + 2 nPi	16
P83	mRNA2 → nNMP	16
P84	mRNA + rib → rib_x	16
P85	aAAtRNA + 2 aGTP + rib_x → 2 aGDP + 2 aPi + atRNA + mRNA2 + protein + rib	16
P86	AA + ATP + atRNA → AMP + 2 Pi + aAAtRNA	16
P87	AA_ext → AA	16
P88	NTP_ext → nNTP	16
P89	nNMP → NMP_ext	16
ADP	ADP → ADP_ext	8
P90	AMP → AMP_ext	8
P96	AMP + Pi → ADP	8
P100	protein → Ton_system_ext	2
P101	protein → HGBA_ext	2
P102	protein → HGBB_ext	2
P103	protein → YFEA_ext	2
P104	protein → YFEBCD_ext	2
P97	protein → TBPA_ext	2
P98	protein → FBPA_ext	2
P99	protein → FBPBC_ext	2

Table 3.6: FC values and balanced equations of the protein synthesis subnetwork, in descending order of contribution to the overall subnetwork.

From **Table 3.6**, it was evident that the highest FC values in the protein synthesis subnetwork were from those reactions controlling the efflux and influx of inorganic phosphate (Pi), GDP/GTP and ATP, with these reactions representing the top 6 FC values within the subnetwork.

3.3.3 Transmembrane iron transport subnetwork

The transmembrane iron transport subnetwork was reconstructed based upon published data on the process in *P. multocida* and in closely related organisms. Two main systems were responsible for the transport of iron across the outer and cytoplasmic membranes and into the cytoplasm of *P. multocida*. The first was the acquisition of iron from host transferrin, an iron storage molecule which acts to bind freely available iron in the host, thus withholding it from any invading bacteria. The second system operated by removing iron from haemoglobin, a rich source of iron which is ubiquitous in mammalian systems. Both of these iron acquisition systems had a similar mode of action, relying first on a specific outer membrane receptor to bind the iron-containing molecule, and secondly on a series of iron-binding molecules in the periplasm and on the cytoplasmic membrane which transported the iron to the bacterial cytoplasm. Greater detail on both mechanisms is available in **Section 1.3.4.1**.

The integrated transmembrane iron transport subnetwork is shown in diagrammatic form in **Fig. 3.9** and the component reactions are listed in **Table 3.7**.

It should be noted that exchange fluxes representing input of the proteins associated with the transport process were excluded when the protein expression and transmembrane iron transport subnetworks were combined with each other, as expression of these proteins was represented within the protein expression subnetwork.

Also, although the TbpA of *P. multocida* removes a ferric ion only from the N-lobe of the transferrin molecule (see **Section 1.2.1**), different binding conformations of transferrin, representing a single ferric ion bound to either the C or N-lobe of the molecule (mono-ferric holo-transferrin), a ferric ion bound to both lobes (bi-ferric holo-transferrin) or no iron bound (apo-transferrin), were included for completeness and biological accuracy (reactions FE_37, 38, 40, 57 and 58; Fig. 3.9).

Further, it was assumed that the fate of iron entering a bacterium was either to be metabolised, or to be bound to an iron storage molecule such as ferritin for use in times of iron deficit. As such, reactions FE_63 and FE_64 represent the incorporation or storage of cytoplasmic iron respectively.

Reaction	Reaction equation	Reversibility
FE_29	FETRFE_TBPA + Ton_system_e → FE_PERI + TRFE_TBPA + Ton_system2	irr
FE_30	TRFE_TBPA → TBPA2 + TRFE	irr
FE_31	FBPA + HCO3 → FBPA_HCO3	irr
FE_32	FBPA_HCO3 + FE_PERI → FBPA_HCO3_FE	irr
FE_33	FBPA_HCO3_FE + FBPBC → FBPABC_HCO3_FE	irr
FE_34	ATP + FBPABC_HCO3_FE → ADP + FBPABC + FE_CYTO + HCO3	irr
FE_35	FBPABC → FBPA2 + FBPBC2	irr
FE_36	FE_ext → FE	irr
FE_37	2 FE + TR → FETRFE	irr
FE_38	FE + TRFE FETRFE	irr
FE_39	TR_ext → TR	irr
FE_40	FE + FETR → FETRFE	irr
FE_41	PMF + Ton_system → Ton_system_e	irr

FE_42	PMF_ext → PMF	irr
FE_43	HGBA + Hb_4HAEM → HGBA_Hb_4HAEM	irr
FE_44	HGBA_Hb_4HAEM + Ton_system_e HAEM_PERI + HGBA_Hb_3HAEM + Ton_system2	irr
FE_45	HGBA_Hb_3HAEM → HGBA2 + Hb_3HAEM	irr
FE_46	HGBB + Hb_4HAEM → HGBB_Hb_4HAEM	irr
FE_47	HGBB_Hb_4HAEM + Ton_system_e → HAEM_PERI + HGBB_Hb_3HAEM + Ton_system2	irr
FE_48	HGBB_Hb_3HAEM → HGBB2 + Hb_3HAEM	irr
FE_49	HAEM_PERI + YFEA → YFEA_HAEM	irr
FE_50	YFEA_HAEM + YFEBCD → YFEABCD_HAEM	irr
FE_51	ATP + YFEABCD_HAEM → ADP + HAEM_CYTO + YFEABCD	irr
FE_52	YFEABCD → YFEA2 + YFEBCD2	irr
FE_53	HAEM_CYTO → APO_HAEM_CYTO + 2 FE_CYTO	irr
FE_54	HAEM_HOST + Hb_3HAEM Hb_4HAEM	irr
FE_55r	Hb_4HAEM_ext ↔ Hb_4HAEM	rev
FE_56	APO_HAEM_CYTO APO_HAEM_CYTO_ext	irr
FE_57	FE + TR FETR	irr
FE_58	FE + TR → TRFE	irr
FE_59	FETR + TBPA FETR_TBPA	irr
FE_60	TR_TBPA → TBPA + TR	irr
FE_61	HAEM_HOST_ext → HAEM_HOST	irr
FE_62	FETRFE + TBPA FETRFE_TBPA	irr
FE_63	FE_CYTO FE_INCORP	irr
FE_64	FE_CYTO FE_STORED	irr
FE_65	TBPA2 TBPA_ext	irr
FE_66	Ton_system2 Ton_system_ext	irr
FE_67	FBPA2 → FBPA_ext	irr
FE_68	FBPBC2 → FBPBC_ext	irr
FE_69	HGBA2 HGBA_ext	irr
FE_70	HGBB2 → HGBB_ext	irr
FE_71	YFEA2 YFEA_ext	irr
FE_72	YFEBCD2 YFEBCD_ext	irr
FE_73	TBPA2 TBPA	irr
FE_74	Ton_system2 → Ton_system	irr
FE_75	FBPA2 → FBPA	irr
FE_76	FBPBC2 → FBPBC	irr
FE_77	HGBA2 → HGBA	irr
FE_78	HGBB2 → HGBB	irr
FE_79	YFEA2 → YFEA	irr
FE_80	YFEBCD2 YFEBCD	irr
ADP	ADP → ADP_ext	irr
ATP	ATP_ext → ATP	irr
FBPA	FBPA_ext → FBPA	irr
FBPBC	FBPBC_ext → FBPBC	irr
HGBA	HGBA_ext HGBA	irr
HGBB	HGBB_ext → HGBB	irr
TBPA	TBPA_ext → TBPA	irr
Ton_system	Ton_system_ext → Ton_system	irr
YFEA	YFEA_ext → YFEA	irr
YFEBCD	YFEBCD_ext → YFEBCD	irr

Table 3.7: Component reactions of the transmembrane iron transport subnetwork. Each reaction name (left hand column) has a prefix 'FE' denoting that it relates to the transmembrane iron transport subnetwork. Whether a reaction is reversible (rev) or irreversible (irr) is stated in the right hand column.The exchange fluxes ADP, ATP, FBPA, FBPBC, HGBA, HGBB, TBPA, Ton_system, YFEA and YFEBCD are not coded as these reactions are removed when all three subnetworks are combined.

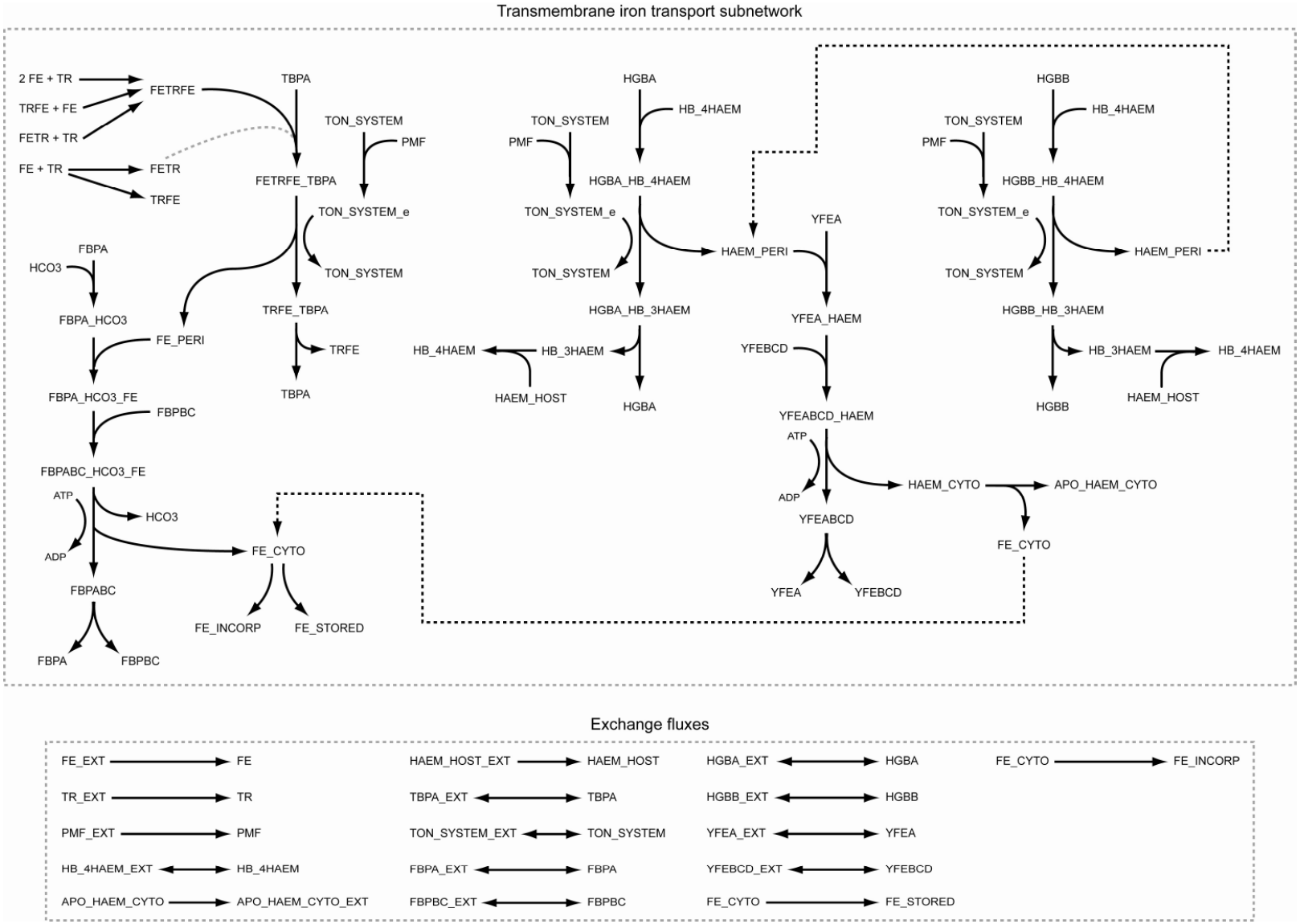

Fig. 3.9: Transmembrane iron transport subnetwork. Both transferrin-based and haemoglobin-based iron acquisition systems are shown.

Transmembrane iron transport subnetwork elementary flux modes

Ninety-six elementary flux modes were derived from the transmembrane iron transport subnetwork (shown in full in **Appendix 1**). Examination of the net reactions for each mode (see **Appendix 2**) showed that 32 elementary modes were identical and took the form: ATP_ext + HAEM_HOST_ext + PMF_ext → ADP_ext + APO_HAEM_CYTO_ext + 2 FE_STORED. A further 32 elementary modes were of the form: ATP_ext + HAEM_HOST_ext + PMF_ext → ADP_ext + APO_HAEM_CYTO_ext + 2 FE_INCORP. These 64 elementary modes involved the acquisition of iron from haemoglobin, whilst the remaining 32 modes concerned the acquisition of iron from host transferrin. Of these 32 elementary modes, 16 took the form: ATP_ext + FE_ext + PMF_ext → ADP_ext + FE_STORED, and 16 took the form: ATP_ext + FE_ext + PMF_ext → ADP_ext +FE_INCORP. Although many of the elementary modes shared similar net equations, when studied in greater detail, it was evident that the full pathways of these modes differed subtly from each other.

The path length of an elementary flux mode i.e. the number of reactions involved, correlated inversely with the biological activity of the process that is represented, in that the activity of processes represented by elementary flux modes with shorter path lengths is higher than those with longer path lengths (Fell and Wagner, 2000; Wagner and Fell, 2001). When the path lengths of the elementary flux modes derived from the transmembrane iron transport subnetwork were studied it was seen that the 2 elementary modes with the shortest path lengths were involved in iron acquisition from transferrin, whilst those with the longest path lengths were involved in iron acquisition from haemoglobin (see **Appendices 1, 2**).

FC values were derived from the set of elementary flux modes in order to rank the importance of each reaction in the overall function of the network. Analysis of the FC values of the transmembrane iron transport subnetwork revealed that the top 4 highest ranking FC values (FC value = 96) were those of the ATP and ADP exchange fluxes, and reactions FE_41 and FE_42 which described the input of energy into the Ton system using the proton motive force (PMF) of the cytoplasmic membrane, and the introduction of PMF into the system, respectively. The next 2 highest ranked FC values were those of reactions FE_63 and FE_64 (FC value = 80) representing the conversion of cytoplasmic iron to incorporated iron or stored iron, respectively. The core set of reactions, consisting of iron acquisition from transferrin and haemoglobin, had varying FC values, although they were clustered approximately according to which function they served. Accordingly, those reactions relating to transport of haem through the cytoplasmic membrane via the YfeABCD complex (FE_49-54, 56, 61) all shared a FC value of 64. Ranked next, with FC values of 48 were reactions relating to the influx and efflux of the Ton system (FE_66, 74, TON_SYSTEM). Reactions relating to transferrin-mediated iron uptake, haem uptake by HgbA and HgbB, and the influx and efflux of the YfeABCD complex (FE_29-36, 38, 43-48, 62, 71, 72, 79, 80, YFEA, YFEBCD) all had a FC value of 32. Reactions representing influx and efflux of TbpA, FbpA, FbpBC, HgbA and HgbB all had FC values of 16. Lastly, there were several reactions which had FC values of 0 (FE_37, 39, 40, 55r, 57-60) indicating that those reactions were not functional. Those reactions represented formation and/or influx of several of the possible conformations of iron-bound transferrin and the influx of Hb_4HAEM, that

is, haemoglobin with 4 haem moieties bound to it. This meant that the conformation of transferrin that was bound solely by TbpA was biferric transferrin imported directly into the system and hence not formed within the system boundary from either free transferrin or recycled monoferric transferrin. The zero flux of reaction FE_55r, representing influx of Hb_4HAEM into the system, indicated that Hb_4HAEM was provided from recycled Hb_3HAEM, to which an additional haem moiety was bound.

3.4 Discussion

The construction of a theoretical model allowed, in the first instance, the structural properties of the biological network to be investigated. An important aspect in the construction of such a model is the correct segmentation of the network; in the present work the complete network was divided into 3 smaller subnetworks representing glucose metabolism, protein synthesis and transmembrane iron transport. Although the focus was on iron acquisition, this allowed details of the source and provision of energy to drive the process to be included in the model. Analysis of these subnetworks allowed, through derivation of elementary flux modes, the identification of key reactions and pathways within each of the subnetworks. Furthermore, when combined, these subnetworks allow a number of simulations to be carried out. These include: the effect of glucose availability on ability to uptake iron; the difference in energy required to uptake iron from transferrin versus haemoglobin; or the effect of oxygen starvation on glucose metabolism, ATP production and iron uptake. The 3 subnetworks are combined and the properties of the complete network investigated in **Chapter 4**. Here, the salient

points from each subnetwork in turn are discussed with particular reference to their biological relevance.

3.4.1 Glucose metabolism subnetwork

The metabolism of glucose is a key process for the generation of energy in the form of ATP in many bacterial species to drive a number of processes (Morse and Hebeler, 1978; Nordkvist, Jensen and Villadsen, 2003; White, Steele and Pierce, Jr., 1955). In this case, ATP from glucose metabolism provides energy for synthesis of iron-related proteins in the membrane of *P. multocida*; these proteins in turn require ATP to facilitate uptake of host iron from transferrin or haemoglobin. The glucose metabolism subnetwork consists of both glycolysis and pentose phosphate pathway reactions leading to the TCA cycle and electron transport reactions. It was apparent from the 6 elementary flux modes generated that there were 3 distinct pathways from which glucose could be assimilated. The first, contained the full set of reactions of glycolysis and TCA cycle, but none of the pentose phosphate pathway reactions. The second and third distinct pathways involved reactions of the pentose pathway providing glyceraldehyde-3-phosphate and fructose-6-phosphate, respectively, in place of reactions in the glycolysis pathway. When the efficiency of ATP production from glucose in terms of maximal ATP per unit glucose was estimated it was found that elementary mode 4 (**Fig. 3.6**), involving only reactions from glycolysis and the TCA cycle, was the most efficient. However, 2 other elementary flux modes (elementary modes 5 and 6 – **Fig. 3.6**) had glucose:ATP ratios that were almost as efficient. This showed that inclusion of the pentose phosphate pathway reactions increased robustness of the glucose metabolism subnetwork. In fact, using the

number of elementary flux modes as an approximate measure of network robustness, i.e. greater number of EFMs = more robust, it was seen that inclusion of the pentose phosphate pathway increased robustness significantly, increasing the number of EFMs from 2, when pentose phosphate pathway reactions are excluded, to 6 when they are included (data not shown). The concept of robustness will be explored in greater detail in **Chapter 4**.

Of the set of 6 elementary flux modes, modes 4, 5 and 6 showed glucose:ATP ratios that were approximately twice as high as modes 1, 2 and 3. No single elementary mode included all 3 electron transport reactions, and it was noted that those modes with the highest glucose:ATP ratios (modes 4, 5 and 6) included both ATP-generating electron transport reactions (reactions ET26 and ET27). Furthermore, elementary modes 1, 2 and 3, which had lower glucose:ATP ratios, included only 1 ATP-generating reaction, ET27, and the FADH-generating reaction ET28. This FADH was then cycled through reaction ET27, producing a second ATP molecule, but at the expense of an additional NADH. Therefore, reactions ET26 and ET27 could produce 1 more ATP molecule (3 in total) than the 2 produced by reactions ET27 and ET28, with both reactions expending 1 NADH and 1 FADH.

When the FC values of the glucose metabolism subnetwork were studied (**Table 3.3**), it was seen that the reactions supplying ADP and exporting ATP from the network had by far the highest values (FC value = 204). The FC values for the 3 electron transport reactions, ET26, ET27 and ET28, were 52, 68 and 52 respectively, whilst the FC value for the CO_2 efflux reaction was 60. Taken together, these data

suggested that those reactions involved directly in production of ATP were, in terms of flux contribution, the most important to the glucose metabolism subnetwork.

In their study of biomass and energy producing elementary modes in *E. coli*, Carlson and Srienc (2004) presented a larger glucose metabolism network including the contribution of metabolised glucose to the biomass of the bacterium. This generated a substantially higher number of elementary flux modes (over 1000). It would have been possible to postulate which additional reactions may have been present within *P. multocida* and include them in the hope of obtaining more accurate predictions from the model. However, a more sensible approach seemed to be the use of a smaller set of reactions, all of which were known to take place within *P. multocida* (from KEGG data), which can be built upon as further biochemical data becomes available for the bacterium. As a result of this, the robustness of the subnetwork may be somewhat lower than in reality, and this is studied further in the next chapter.

3.4.2 Protein synthesis subnetwork

Inclusion of a protein synthesis subnetwork allowed expression of the proteins facilitating bacterial iron uptake to be modelled. The network included is a generic one, adapted from Allen and Palsson (2003), and has been modified to represent expression of the set of eight iron uptake proteins/complexes included in the transmembrane iron uptake subnetwork from a basic set of substrates. Addition of this subnetwork will also allowed a number of exchange fluxes and hence external metabolites from the transmembrane iron transport subnetwork to become internal

metabolites when the complete network was assembled in the following chapter.

The 16 elementary flux modes generated from the protein synthesis subnetwork (**Fig. 3.8**, **Table 3.5**) all shared the full set of central protein synthesis reactions and differ only in their AMP/ADP efflux and final protein expression reactions. This showed a lack of robustness in the network, and hence that these central reactions were absolutely vital to the process of protein expression. The process of protein expression *in vivo* would involve many more reactions than the simplified network shown here. Each protein expressed requires a different combination and number of amino acids, and will have a different primary, secondary, tertiary and quaternary structure. Furthermore, the expression of a particular protein is likely to be regulated by a number of global and specific regulators. These factors were not included in the current model because of a lack of biochemical data and to reduce computational burden, however, it is postulated that addition of these reactions would add robustness to the network and increase the reliability and accuracy of results gained from modelling.

Despite the simplified nature of the protein synthesis subnetwork, useful data was gained from analysis of the set of elementary flux modes generated. Examination of the FC values (**Table 3.6**) revealed that supply and removal of GTP/GDP (FC value = 32) and Pi (FC values = 32,24), and, crucially, that the supply of ATP (FC value = 16) were all vital for function of the network.

In the study in which they present their protein synthesis network, Allen and Palsson (2003) note that if both the half-life of a particular mRNA and the promoter strength are known, then the concentration of mRNA can be calculated. In terms of expression of protein, both the amino acid availability and number of available ribosomes will be limiting factors in the amount of expressed protein. As these data are not readily available for the majority of genes or proteins, particularly in the case of the iron acquisition proteins being studied here, Allen and Palsson (2003) explain that these data may be re-calculated from gene expression data, either from qRT-PCR or microarray data (Tao *et al*, 1999). Thus, for a more accurate approximation of the actual *in vitro* fluxes, the amino acid availability, promoter strengths, mRNA half-lives and mRNA concentrations for each of the studied genes/proteins should be added to the data generated from the current model.

3.4.3 Transmembrane iron transport subnetwork

A much larger number of elementary flux modes were generated from the transmembrane iron transport subnetwork than from either of the other subnetworks (96 versus 16 for protein subnetwork and 6 for glucose subnetwork). This was a consequence both of the greater number of reactions within the subnetwork and of the presence of 3 (partly) redundant iron acquisition pathways. The more detailed nature of this subnetwork reflected also the better availability of structural and biochemical data on the acquisition of iron by *P. multocida*.

From analysis of the 96 elementary flux modes generated, it was found that there was clear segmentation of those elementary flux modes which involved iron acquisition

from transferrin and those which acquired iron from haemoglobin. Based upon analysis of path lengths of the elementary flux modes current dogma would indicate that those reactions involving transferrin were more likely to occur than those involving haemoglobin. However, this hypothesis was contradicted when the FC values of the transferrin and haemoglobin-related reactions were compared, with the haemoglobin-related reactions having, in general, higher FC values than the transferrin-related ones. This may have been influenced by the greater number of haemoglobin-related reactions in the subnetwork compared to transferrin-related reactions, conferring higher FC values for haemoglobin-related reactions. Alternatively, this may have been a novel finding which indicated that flux through haemoglobin-related pathways was higher than that of the transferrin-related pathways. This finding is investigated further through comparison of *in vitro* and *in silico* data in **Chapter 6**. In the calf lung environment, it is expected that serum transferrin will be a more readily accessible source of iron than haemoglobin, although as the disease progresses and necrosis and haemorrhage worsen, increasing amounts of haemoglobin may infiltrate the lungs.

It was clear from the FC values that the contribution of ATP and the transduction of energy from the Ton system to the iron acquisition proteins were vital for effective operation of the iron subnetwork. In addition, a very interesting finding was the preference for biferric holo-transferrin over all of the other included isoforms of transferrin, and the preference for haemoglobin generated by recycling of already-processed haemoglobin over directly imported haemoglobin. In biological terms, this finding would not have been predicted from the observations of Ogunnariwo and

Schryvers (1990) which stated that the principal isoform of bovine transferrin available in circulation was monoferric N-lobe holo-transferrin. However, perhaps the results here simply represent a preference for the most energy efficient form of transferrin, or that which is bound with highest affinity by the bacterium. This could be explored further by *in vitro* radiolabelling and competitive-binding studies (Baumrucker, Gibson and Schanbacher, 2003; Modun, Kendall and Williams, 1994).

3.5 Conclusions

The analysis of the 3 presented subnetworks has both substantiated current knowledge and revealed a number of interesting new findings. Most importantly, the subnetworks were all thermodynamically feasible and when combined it is anticipated will form a network which can be exploited both in the design of *in vitro* experiments and in the generation of theoretical fluxes which can be combined and compared with *in vitro* data.

In all 3 subnetworks, the involvement of ATP was found to be crucial for effective operation of the pathways within. As preliminary experimental data suggests that growth rate and glucose consumption are correlated linearly, and that the bacterium's growth rate is also dependent on the availability of sufficient iron, it becomes clear that the role of ATP in the overall function of the network is a vital one.

Despite the subnetworks presented here being thermodynamically feasible, the model can only be validated through comparison with experimental data. As such, **Chapter 5** describes *in vitro* experiments designed to investigate the effects of iron-restriction

on the growth rate and metabolism of *P. multocida*, which in turn provides data to compare with and validate the theoretical model in **Chapter 6**.

Chapter 4. Elementary flux modes analysis of a theoretical model describing iron acquisition by *P. multocida*

4.1 Introduction

In the previous chapter, 3 subnetworks representing transmembrane iron transport, glucose metabolism and protein synthesis were reconstructed based upon current knowledge from published data. Each of these subnetworks was analysed in turn, with elementary flux modes being generated for each and key reactions within each subnetwork were identified. ATP was found to play a vital role in the efficient operation of all 3 subnetworks.

Preliminary experiments carried out as part of this study have shown there to be close links between glucose metabolism, protein synthesis and transmembrane transport of iron in *P. multocida*. In this chapter, the 3 subnetworks were combined and a detailed analysis of the complete network was carried out. This involved, as in the previous chapter, generation of elementary flux modes for the full network and subsequent analysis of these modes by studying flux contribution (FC) values and path lengths.

In addition, the robustness of each of the subnetworks and then the complete network was calculated. Robustness is a key structural property of biological networks, particularly in bacteria, providing stability against genetic mutations, metabolic deficiencies and changes in environmental parameters (Wilhelm, Behre and Schuster, 2004). Closely linked with the robustness of a biological network is a second

property known as redundancy, referring to pathways that convert the same set of substrates to the same set of products but use differing sets of intermediate reactions to achieve this (Price, Papin and Palsson, 2002). These are referred to as redundant pathways and the greater the number of redundant pathways present, the more robust the biological network is. As mentioned in the previous chapter, examples of pathways which increased robustness of the current network included: the pentose phosphate pathway in the glucose metabolism subnetwork and the haemoglobin-mediated iron uptake pathway in the transmembrane iron uptake subnetwork. The pentose phosphate pathway provides an alternative route for glycolysis thus also protecting against gene knockout or mutation whilst the haemoglobin-mediated iron uptake pathway provides flexibility against changes in available external substrates or gene knockouts or mutations.

Robustness and redundancy in biological networks can be identified visually; however, quantifying robustness allows one to estimate the network's ability to withstand external perturbations. There are several methods of quantifying robustness and these methods are explained in the following sections.

4.2 Aims and methodology

4.2.1 Elementary flux modes analysis

Initially, the glucose metabolism, protein synthesis and transmembrane iron transport subnetworks were combined. On combining the subnetworks, several of the exchange fluxes in each subnetwork were removed as the status of the substrates involved changed from external to internal. For instance, ATP utilised in the

transmembrane iron transport subnetwork was provided subsequently by the glucose metabolism subnetwork.

Once combined, elementary flux modes were derived by the YANA software as described previously in **Section 3.2.2**. Through analysis of the elementary modes, FC values for each reaction were calculated (described in **Section 3.3.1**) and important reactions identified. Pathlengths of elementary flux modes were analysed also to pinpoint the most biologically active modes.

Flux sum analysis

In addition to the FC values of individual reactions, the flux sum of each elementary flux mode was calculated using a method similar to the calculation of FC values. The activity of each elementary flux mode was set to 100% in the YANA software and the integers assigned to each reaction within each individual mode were summed. This value was the flux sum of each elementary flux mode.

Glucose:iron ratios

To study the efficiency with which each elementary flux mode utilised glucose as a means of providing energy to transport iron across the bacterial membrane a glucose:iron ratio was calculated as follows. From the net reactions of each elementary flux mode, as calculated by the YANA software and assuming 100% activity, the coefficient for GLU_ext was divided by the coefficient for either

FE_STORED or FE_INCORPORATED to give the glucose:iron ratio, as shown in the following example:

$$GLU\_ext + 14\,HAEM\_HOST + 12\,OXY\_ext + 14\,PMF\_ext \rightarrow 14\,APO\_HAEM\_CYTO\_ext + 6\,CO2\_ext + 28\,FE\_STORED$$

$$\text{therefore,} \quad glucose:iron\,ratio = 1/28 = \underline{0.036}$$

Statistical analysis of flux sum vs path length data

In **Section 4.3.1**, to assess whether there was any correlation between the flux sum of an elementary flux mode and its path length, the data were first adjusted and then subjected to a regression analysis in Microsoft Excel to assess the significance of any correlation observed. First, data were sorted by path length and then by flux sum within each group of similar path lengths. Next, the mean of groups of elementary flux modes with only one or two differences in their component reactions, with identical path length and closely matching flux sums was taken. This allowed the quality of the data set to be improved by removing overlapping and closely matching values and a line of best fit to be plotted.

4.2.2 Measures of network robustness

Robustness of biological networks can be quantified using 4 simple measures (Wilhelm, Behre and Schuster, 2004).

Measure 1

In its simplest terms, robustness of a biological network can be estimated by the number of elementary flux modes derived from that network (Stelling *et al*, 2002).

Since an elementary flux mode represents a unique route through the network, the more elementary flux modes that are derived from a network, the greater the number of unique routes there are through that network, and hence the higher the robustness of the network in question. An example network containing 8 reactions and 4 elementary flux modes is shown in **Fig. 4.1**. The robustness of this network would be 4, although this measure in itself carried no information as to whether the network was of high or low robustness – this could be assessed only by comparison with other networks. Furthermore, this first measure did not factor in the effect of knocking out individual reactions on operation of the complete network (Wilhelm, Behre and Schuster, 2004). A more satisfactory measure would have been one which quantified robustness absolutely and allowed the effect of reaction knockouts to be factored in.

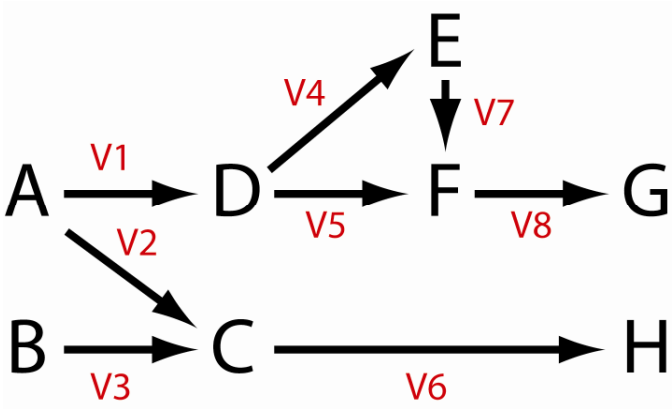

Fig. 4.1: Simple network with metabolites A-H and fluxes V1-8 (shown in red). N.B. Metabolites A, B, G and H are external metabolites.

Measure 2

The second measure of robustness took into account the effect of reaction knockouts on operation of the complete network. First, each of the reaction fluxes in turn was removed and the number of elementary modes remaining after knockout was listed. The sum of these values was divided by the number of elementary flux modes in the

unperturbed network multiplied by the number of reactions in the network. So in the case of **Fig. 4.1**, the calculation was as follows:

$$\frac{2+3+3+3+3+2+3+2}{4\times 8}=\frac{21}{32}=0.66$$

Therefore, the robustness of the example network was calculated to be 0.66, where 0 was equal to no robustness and 1 is completely robust, although in reality robustness could never reach 1. In practical terms, a robustness value of 0.66 indicated that if one reaction was knocked out, two-thirds of the elementary modes in the network were still operative.

Although more accurate, this measure did not differentiate between reactions within the network which contributed to essential products and those which contribute to non-essential products.

Measure 3

The third measure of robustness focussed on reactions within a network that contributed only to essential products. Essential products were identified and the robustness of each subsection of the network leading to the production of each of the essential products was calculated. Assuming that all essential products must be produced for the organism to operate efficiently, the minimal robustness value was taken as the robustness of the complete network. Again using the example network from **Fig. 4.1**, and defining metabolites G and H as essential products, it can be seen

in **Fig. 4.2** that the subsections of the network contributing to production of each of the essential products can be isolated.

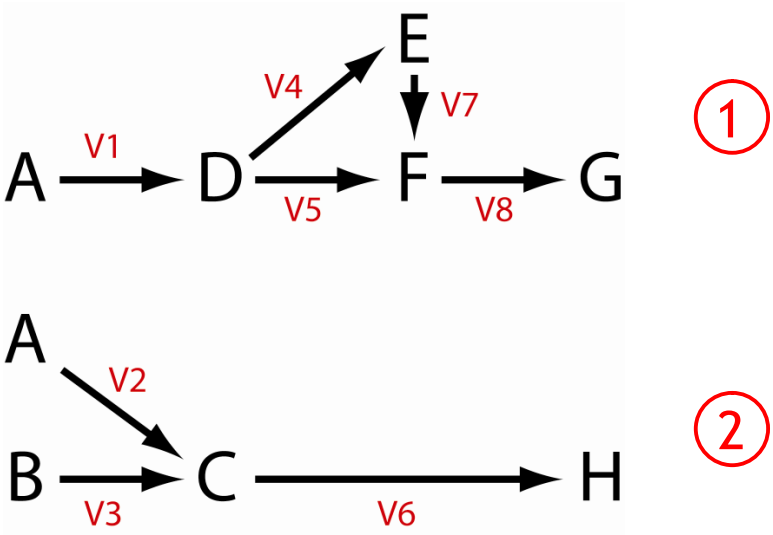

Fig. 4.2: Subsections of network (labelled 1 and 2, in red) contributing to essential products G and H. Fluxes V1-8 (shown in red). N.B. Metabolites A, B, G and H are external metabolites.

Next, the robustness of each of these subsections is calculated as for **Measure 2**.

$$\text{Robustness of subsection 1} = \frac{0+1+1+1+0}{5\times 2} = \frac{3}{10} = 0.30$$

$$\text{Robustness of subsection 2} = \frac{1+1+0}{3\times 2} = \frac{2}{6} = 0.33$$

Therefore, the robustness of the complete network was equal to the minimal robustness value of those calculated for each of the essential products, in this case 0.30, the robustness of subsection 1 of the example network.

Measure 4

A fourth measure of robustness was derived by calculating the arithmetic mean of all the essential product robustness values derived by Measure 3. This was deemed a better approximation of robustness because although one essential product had the

lowest robustness, random mutations may have been more likely to take place within pathways leading to other essential products. **Measure 3** took no account of this, as the robustness of pathways leading to only the essential product with the minimum robustness value was considered.

From the robustness values derived for each of the essential products in the example network, the robustness according to **Measure 4** was calculated as follows:

$$\frac{\text{robustness EP1} + \text{robustness EP2}}{2} = \frac{0.30 + 0.33}{2} = 0.32$$

Where EP = essential product

In the following analysis, the robustness of each of the subnetworks described in **Chapter 3**, and then the complete network, was derived using each of the above 4 measures of robustness above.

4.3 Results

4.3.1 Elementary flux modes of complete network

When the glucose metabolism, protein synthesis and transmembrane iron transport subnetworks were combined some reactants became internal metabolites and it was possible to refine the model by removing the associated exchange fluxes for ADP, ATP, FBPA, FBPBC, HGBA, HGBB, TBPA, Ton_system, YFEA and YFEBCD.

In total, 576 elementary flux modes were derived from the complete network. The strategy adopted for mining useful data from such a large number of elementary

modes was to study the FC values of each reaction within the complete network. FC values approximately quantify the contribution of each reaction to operation of the complete network, and are described in **Section 3.3.1**. When the FC values for the network were studied, it was apparent immediately that the reactions of the protein synthesis subnetwork were of particular importance. In fact, the 15 reactions with the highest FC values, with values ranging between 33504 and 67008, were all reactions belonging to the protein synthesis subnetwork, and these reactions accounted for 60% of all protein synthesis reactions. Additionally, the "ATP_protein" reaction, providing ATP from glucose metabolism to drive reactions of the protein synthesis network had an FC value of 33504, considerably higher than that of the "ATP_iron" reaction with a value of 5640.

When the reactions of the transmembrane iron transport subnetwork were considered, it was noted that in general, reactions involved in transport of haem had statistically higher FC values than those involved in transport of transferrin ($P = 0.004$). Of all the transmembrane iron transport reactions, the two reactions representing the conversion of the Ton system into its energised form, reactions FE_41 and FE_42, had the highest FC values, both 16920. Also high were the FC values of the final iron efflux reactions, FE_63 and FE_64. In fact, when compared with the analysis of elementary flux modes of the transmembrane iron transport network alone (**Section 3.3.3)**, it was noted that the ranking of the reactions in both cases was the same.

FC values of the reactions of the glucose metabolism subnetwork covered a wide range: from 14808 to 984. The highest of these was the reaction TCA16r representing the efflux of carbon dioxide from the TCA cycle, with a value of 14808. The ATP-producing electron transport reactions also showed high FC values. FC values of the other reactions of the glucose metabolism subnetwork grouped approximately according to which section of the subnetwork they were located in. For instance, the remaining 9 reactions of the TCA cycle (excluding reaction TCA16r) all had FC values of 3816. Furthermore, 4 out of 5 of the pentose phosphate pathway reactions had FC values of 984, the exception being reaction PPP10 which had an FC value of 2952. The 9 reactions of glycolysis had FC values between 1416 and 3816.

After listing the flux sums of each of the 576 elementary flux modes from highest to lowest, two distinct features were evident from the data. First, those elementary flux modes that included no protein synthesis reactions and thus drew upon iron transport proteins either 'recycled' or expressed previously had, in general, shorter path lengths and a smaller range of lower flux sums than those elementary flux modes which synthesised iron transport proteins *de novo*. Secondly, the path lengths of elementary flux modes were, in general, directly proportional to their flux sums: i.e. those elementary flux modes with high flux sums had longer path lengths and *vice versa* (**Fig. 4.3B**).

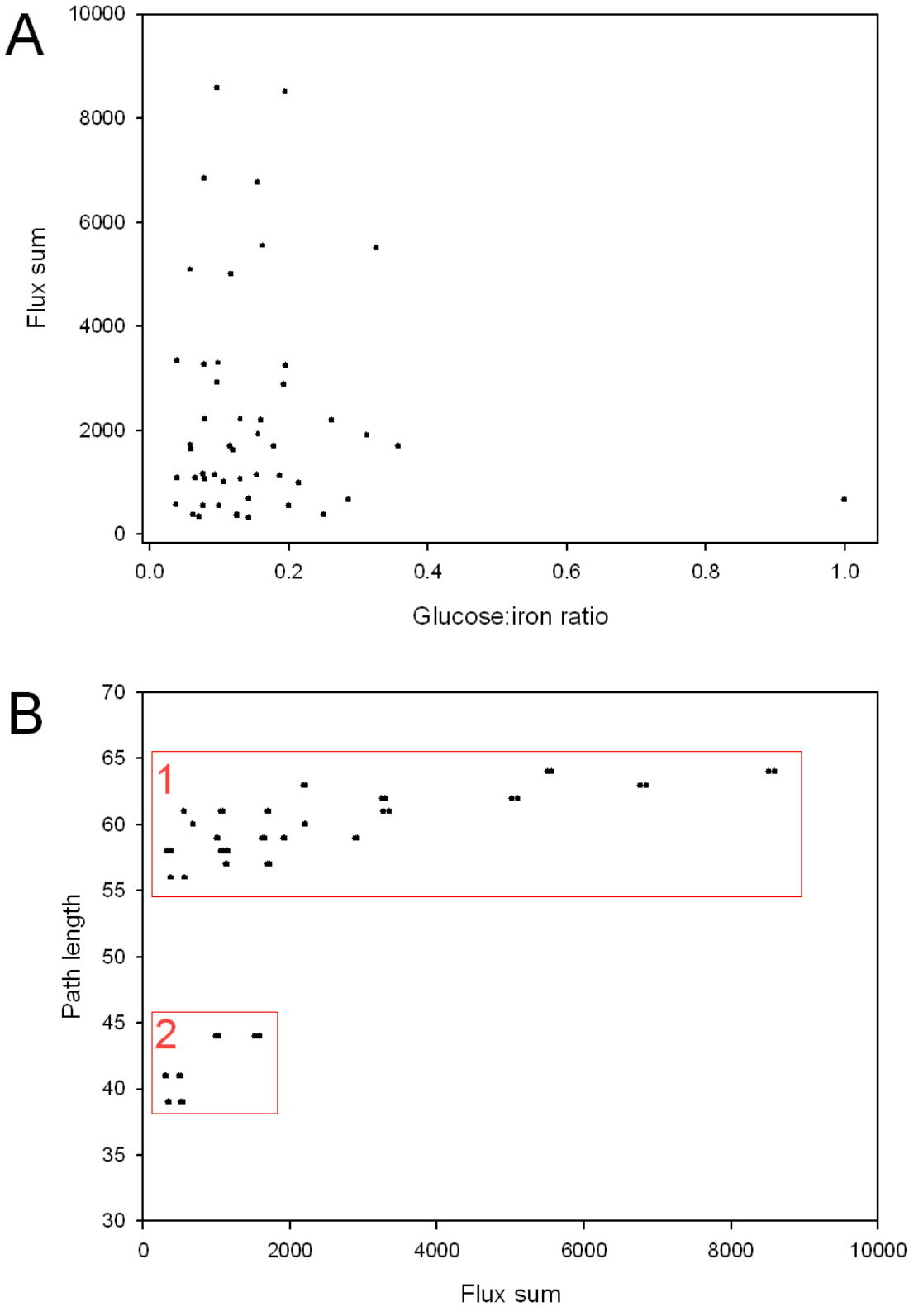

Fig. 4.3: A) Graph of flux sum versus glucose:iron ratios for all 576 elementary flux modes of the complete metabolic network representing iron acquistion by *P. multocida*. **B)** Graph of path length versus flux sum for all 576 elementary flux modes of the complete metabolic network representing iron acquisition by *P. multocida*. The red boxes, marked 1 and 2, show the two distinct groupings of values, box 1 containing those elementary flux modes involving protein synthesis and box 2 containing those elementary flux modes which exclude protein synthesis reactions. It should be noted that many points overlay each other.

A graph of the glucose:iron ratios for all 576 elementary flux modes against their respective flux sum values showed (**Fig. 4.3A**) that over 90% of the elementary flux modes had glucose:iron ratios of 0.2 or below (mean glucose:iron ratio 0.11; median value 0.09). In addition, the majority of the elementary flux modes had relatively low flux sums with approximately 80% below 3000 (range 369-8591), despite the range reaching as high as 8591, the mean value being 1973 and the median value being 1160. When the path lengths of the elementary flux modes were graphed against their respective flux sum values, 2 distinct groupings of the data were noted (**Fig. 4.3B**). The largest of these groups, representing approximately 94% of the total data, comprised those elementary flux modes which included protein synthesis reactions. The second group, representing the remaining 6% of the total elementary flux modes, depicted those modes which did not include protein synthesis reactions and therefore utilised iron transport proteins which had been previously expressed. This second grouping had, without exception, shorter path lengths than those modes that included protein synthesis reactions. This will be explored further in **Section 4.4**. It should also be noted that in **Fig.s. 4.3A**, **4.3B** and **4.4** there are often several data points that overlie each other.

Furthermore, when the flux sums of those elementary flux modes from the first group only (**Fig. 4.3B**) were graphed against their respective path lengths, therefore selecting only those modes which included protein synthesis reactions, there was a positive correlation ($P = <0.001$) between the flux sum of an elementary flux mode and its path length (**Fig. 4.4**).

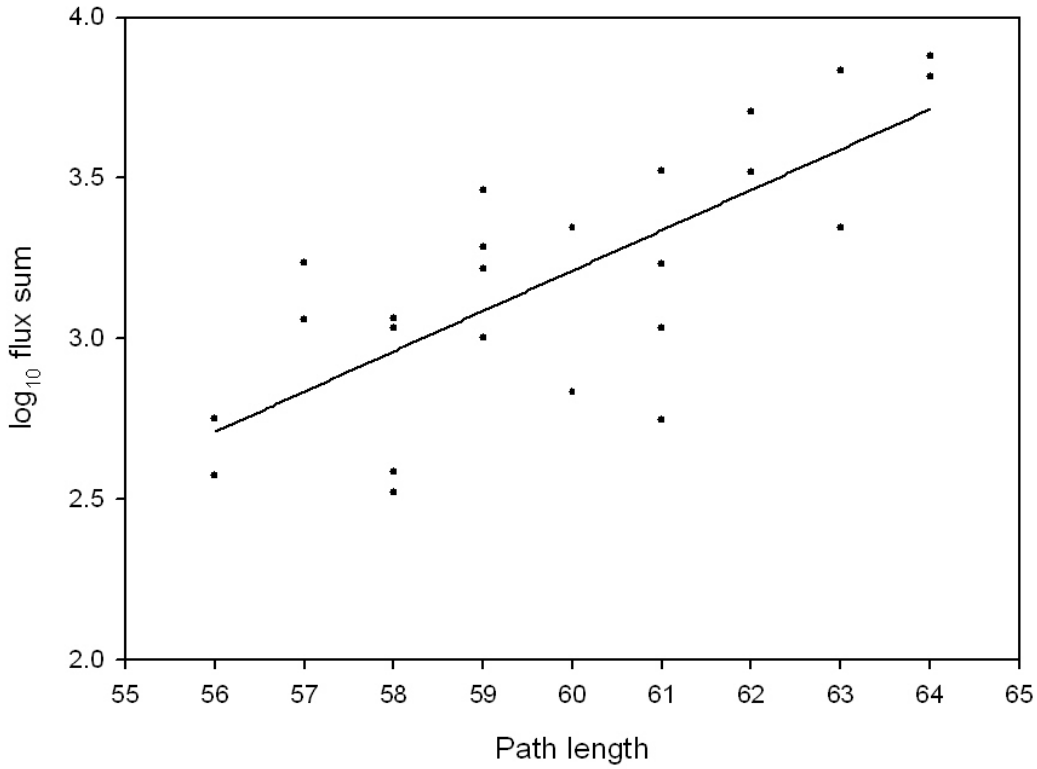

Fig. 4.4: Graph of $\log_{10}$ flux sum versus path length for those elementary flux modes including protein synthesis reactions. Line of best fit (in black) shows positive correlation (P = <0.001) between flux sum and path length. *(statistical analysis described in **Section 4.2.1**)*

4.3.2 Robustness of subnetworks and complete network

Robustness values, calculated as described in **Section 4.2.2**, for the subnetworks representing glucose metabolism, protein synthesis and transmembrane iron transport are shown in **Table 4.1**.

Subnetwork	Measure 1	Measure 2	Measure 3	Measure 4
Glucose metabolism	6	0.16	0.16	0.16
Glucose metabolism excluding PPP	2	0.04	0.04	0.04
Protein synthesis	16	0.33	0.08	0.08
Transmembrane iron transport	96	0.65	0.65	0.65

Table 4.1: Robustness values of each subnetwork, including glucose metabolism minus pentose phosphate pathway (PPP) reactions. Measure 1 is the number of elementary flux modes, Measure 2 is the robustness of the subnetwork, Measure 3 is the minimal value of the essential product robustness values and Measure 4 is the mean of the essential product robustness values. Measures 2, 3 and 4 assume that 0 = no robustness, and 1 = maximally robust.

From these data it was seen that the transmembrane iron transport subnetwork was the most robust by all 4 measures. The glucose metabolism subnetwork was the next most robust, if it is assumed that measures 3 and 4 are more accurate measures of robustness than measures 1 and 2. Lastly, the protein synthesis subnetwork was the least robust of the three subnetworks. Measures 2, 3 and 4 could be approximated as an estimation of how many elementary flux modes would remain if a single reaction was knocked out in the subnetwork. For example, the robustness of the transmembrane iron transport subnetwork, by measures 2, 3 and 4 was 0.65; therefore if a single reaction was knocked out, approximately 65% of the elementary flux modes remained intact. It should be noted that in the cases of the subnetworks representing glucose metabolism and transmembrane iron transport, robustness measures 2, 3 and 4 were all equal. For the glucose metabolism subnetwork, this was because there is only 1 essential product and therefore the minimal essential product value for measure 3 was the same as the overall robustness calculated in measure 2. Furthermore, because there was only 1 essential product, the mean essential product robustness and the values calculated by measures 2 and 3 were the same. In the case of the transmembrane iron transport subnetwork, there were two essential products: FE_STORED and FE_INCORPORATED. However, apart from the final conversion of cytoplasmic iron (FE_CYTO) to either stored or incorporated iron, all the reactions leading to this point were identical. Therefore, both the minimal essential product robustness and mean minimal essential product robustness values (measures 3 and 4 respectively) were equal to the overall robustness of the subnetwork as calculated by measure 2. However, for the protein synthesis network, measures 3 and 4 differed from measure 2 due to there being 8 essential products and resulted in a

much lower value of 0.08 for measures 3 and 4, compared to a robustness value of 0.33 for the whole subnetwork.

Interestingly, the impact of the inclusion of the pentose phosphate pathway reactions on the robustness of the glucose metabolism subnetwork was seen when the 4 robustness measures were calculated for the subnetwork excluding pentose phosphate pathway reactions (**Table 4.1**). The number of elementary flux modes generated for the subnetwork was reduced from 6 to 2, whilst robustness measures 2, 3 and 4 dropped substantially from 0.16 to 0.04.

When the 3 subnetworks were combined and the robustness of the complete network quantified, the mean robustness value calculated by measure 1 was 576 (equal to the number of elementary flux modes). Means calculated using measures 2, 3 and 4 were all equal to 0.45 because all of the reactions contributing to the final iron fate (either FE_INCORP or FE_STORED) were the same in both cases.

4.4 Discussion

In the previous chapter, 3 metabolic subnetworks representing the processes of transmembrane iron transport, glucose metabolism and protein synthesis were constructed. From those 3 subnetworks were derived elementary flux modes, which were analysed to identify crucial reactions for effective operation of the network and to understand better the structural properties of the network. These subnetworks were combined and elementary flux modes were derived for the complete network. Similar analyses were carried out to study FC values and path lengths, efficiency of

energy transfer from metabolised glucose to the iron uptake process and flux sums of elementary flux modes.

As an aid to gaining a fuller understanding of the structural properties of the network, the robustness of each of the 3 subnetworks and of the complete network was estimated in turn. This provided an opportunity to pinpoint reactions or pathways within the network that might be more vulnerable to perturbation as a possible means of developing novel control methods.

These analyses are explored and discussed with particular emphasis on their relevance to later comparisons with both *in vitro* and *in vivo* systems in **Chapters 5** and **6**.

4.4.1 Elementary flux modes of complete network

It is well documented that the number of elementary flux modes in any metabolic network increases exponentially as the number of reactions within that network increases (Klamt and Stelling, 2002). In the previous chapter, elementary flux modes were derived for the transmembrane iron transport, glucose metabolism and protein synthesis subnetworks and numbered 96, 6 and 16 respectively. However, when elementary flux modes were derived for the complete network the number of modes increased to 576. This substantial rise reflected an increase in the number of unique feasible routes through the network and as a consequence enhanced both the accuracy and reliability of any analyses or simulations carried out.

Analysis of FC values for each of the reactions in the complete network revealed that 60% of the protein synthesis reactions comprised the top 15 highest FC values, confirming the fundamental role of protein synthesis in the bacterial iron acquisition process. When the interactions between the 3 subnetworks were considered, and looking back at **Fig. 3.1** it was seen that the glucose metabolism subnetwork provided energy in the form of ATP first to the protein synthesis subnetwork to facilitate expression of outer membrane iron transport proteins, and then to the transmembrane iron transport network to facilitate iron uptake. When the FC values of the reactions supplying ATP to both of these subnetworks were compared, it was found that the FC value of the reaction supplying ATP to the protein synthesis network (ATP_protein) was substantially higher than the reaction supplying ATP to the transmembrane iron transport subnetwork (ATP_iron), their values being 33504 versus 5860 respectively.

When the elementary flux modes were ranked according to their flux sums, that is the comparative flux through each mode, it was apparent that the majority of the modes had relatively low flux sums, with 80% having flux sums in the lower third of the range of values **(Fig. 4.4**). Because of the statistically significant correlation between flux sum and path length of an elementary flux mode, it followed that this majority of modes with relatively low flux sums must also have shorter path lengths. In addition, when these values were plotted against each other, 2 clear groupings of the data points were seen. The smaller of these groups (6% of total modes)

comprised those elementary flux modes that did not synthesise iron transport proteins *de novo***.**

Calculation of glucose:iron ratios, measuring the energy efficiency of each elementary flux mode, revealed that 90% of the modes had ratios in the bottom 20% of the range of values (**Fig. 4.3**).This indicated a high efficiency of glucose use by a majority of modes to power transmembrane iron transport.

From a physiological point of view, these analyses of the elementary flux modes raised a number of interesting points. First, these data suggested that the bacterium mainly utilises short pathways with relatively low fluxes which take up iron with high energy efficiency. This supports the knowledge that pathways with shorter path lengths are the most biologically active (Fell and Wagner, 2000; Wagner and Fell, 2001), as discussed previously in **Section 3.3.3**. Secondly, in terms of bacterial metabolism *in vivo*, these short, energy efficient pathways with low flux may perform a housekeeping role, providing low-level constant flux of iron into the bacteria when sufficient iron is available. Only when extracellular iron is in deficit are the longer, less energy efficient pathways with higher flux utilised to increase both synthesis of iron transport proteins and influx of iron into the bacteria. These hypotheses are explored further in the following 2 chapters.

4.4.2 Robustness of subnetworks and complete network

As mentioned in **Section 4.2.2**, the number of elementary flux modes gives an approximation of the robustness of a metabolic network and therefore it was assumed that, having 576 elementary flux modes, the complete network was substantially more robust than any of the individual subnetworks. However, the 3 more accurate, quantitative measures of robustness revealed the robustness of the complete network to be 0.45, less than the robustness of the transmembrane iron transport subnetwork alone. Although, when it is considered that the robustness values of the other 2 subnetworks were substantially lower than that of the transmembrane iron transport subnetwork, then it seemed reasonable to assume that the robustness of the complete network would be somewhere between the robustness values for the 3 subnetworks. This substantiates the earlier claim that the number of elementary flux modes gives only a crude measure of the robustness of a network, and takes little consideration of the structural properties of the network and no consideration of the effect of reaction knockouts on robustness (Stelling *et al*, 2002). Furthermore, the 3 quantitative measures of robustness operate on a finite scale between 0 and 1, whilst the number of elementary modes increases exponentially with increasing network size and therefore is not scalar and cannot be used as a quantitative measure of robustness.

As noted by Wilhelm, Behre and Schuster (2004), organisms, particularly micro-organisms, are able to withstand external perturbation and gene mutations remarkably well, and this is key to maintaining a level of homeostasis. This is in no small part due to extensive redundancy in their metabolic pathways. As the current model is not a whole genome scale model and as such is a significant simplification

of the complete metabolism of *P. multocida*, any measure of robustness taken here will likely be lower than that of the whole genome. However, for each of the subnetworks studied here, their individual robustness values should be a reasonably close approximation of the true value. Despite this, it should be remembered that because of the close interplay between each of the separate pathways or subnetworks comprising a bacterium's complete metabolism, those pathways not included in a model are likely to still impact slightly upon the true robustness value. Evidence of this was seen in the 4-fold increase in robustness of the glucose metabolism subnetwork after inclusion of the reactions of the pentose phosphate pathway. Whilst the transmembrane iron transport subnetwork is assumed to be as accurate a description of the iron acquisition process in *P. multocida* as published data allows, it is acknowledged, from comparison with studies in other bacterial species, that both the glucose metabolism and protein synthesis networks are likely to be significantly more complex in reality than described here. Therefore, the robustness values quoted here are likely to be slight under-estimations.

Although the 3 measures of robustness proposed by Wilhelm, Behre and Schuster (2004) gave a much more accurate quantification of the robustness of a network, they did not give any measure of the effects of multiple reaction knockouts; instead they assumed only single knockouts. To take multiple reaction knockouts into account would allow more accurate estimation of robustness (Behre *et al*, 2008; Klamt and Gilles, 2004), although the methods for these more accurate calculations are much more complex than those presented by Wilhelm, Behre and Schuster (2004). In this case, it was felt that the simplified nature of the network under study negated the

need for more accurate measures of robustness, although if the network was expanded to a whole genome scale then it would certainly be of value.

4.4.3 Limitations imposed by the current data

As mentioned already, the data here imposed certain limitations upon the output of any analyses of the network. The caveats associated with robustness measures have been discussed in the previous section. However, the accuracy and reliability of any theoretical model is dependent on both the quality of the available biochemical data and the number of reactions within the network being studied. As a conservative estimate, the network being studied here was perhaps only a tenth the size of the full metabolic network of *P. multocida*. When the flux sums and path lengths of the elementary flux modes were studied in **Section 4.3.1**, it was noted that many of the modes shared identical or very similar flux sums or path lengths. This was attributed to the limited size of the reaction network and it was assumed that if a network with a greater number of reactions was used, then the data would spread further and not cluster as seen in **Fig. 4.4**.

Despite the limited size of the reaction network under study here, much useful data can be gained from it. Assuming suitable *in vitro* experiments are formulated to validate the *in silico* data generated, then the reliability of estimated fluxes and model outputs can be tested and if necessary the model can be refined. This is explored in greater detail in **Chapters 5** and **6**.

4.5 Conclusions

In combining the 3 subnetworks, reconstructed in the previous chapter, 576 elementary flux modes were generated and subsequently analysed to reveal key features of the complete *P. multocida* iron acquisition network. In addition, the robustness of each subnetwork in turn, followed by the complete network, was quantified.

Analysis of the elementary flux modes of the complete network revealed a number of interesting findings. Firstly, the importance of the reactions synthesising the membrane-associated iron transport proteins was established by the high FC values of the protein synthesis reactions. However, a number of elementary flux modes were found to utilise iron transport proteins that had already been expressed, in effect recycled proteins. These unique pathways also had the shortest path lengths of all of the elementary flux modes. When the fluxes through each of the modes of the complete network were studied it was apparent that the majority (approximately 80%) had both low flux and highly efficient transfer of energy from the glucose metabolism subnetwork to the transmembrane iron transport subnetwork. In view of this dearth of pathways with low flux and high energy efficiency, it is tempting to speculate that these pathways may provide a constant low-level influx of iron into the bacteria. Consequently, longer, less energy efficient pathways albeit with higher flux may only become operational when iron availability is low.

The data presented in this chapter is utilised in the 2 following chapters for comparison with *in vitro* data on iron acquisition by *P. multocida* and to allow *in silico* simulations of iron acquisition to be carried out.

Chapter 5. Effect of varying culture conditions *in vitro* on key metabolic processes of different *P. multocida* isolates

5.1 Introduction

Thus far, a general *in silico* model, based upon published data on the metabolic pathways of iron acquisition in *P. multocida* supplemented with information on mechanisms in closely-related bacterial species, has been developed. This chapter describes *in vitro* work measuring bacterial growth, biomass, protein content, rate of glucose uptake, bacterial ATP levels and transcription of key iron acquisition genes. These are key components of the *in silico* model of *P. multocida* iron acquisition presented in **Chapters 3** and **4**. Glucose, for example, has a central role in the *in silico* model as a key energy source for *P. multocida*, providing ATP for transmembrane iron transport. Experimental measurement of these variables under different culture conditions with a number of different *P. multocida* isolates provides data with which to test and refine the model and a comparison of *in silico* model outputs and predictions with *in vitro* data presented in this chapter is presented in **Chapter 6**. Integrating these observations with the effects of other culture variables provides also a greater understanding of the processes underpinning iron acquisition by *P. multocida*.

With the publication of the annotated genome sequence of *P. multocida* PM70, an avian serotype A strain, a great deal more information on the iron acquisition genes possessed by the organism became available (May *et al*, 2001). However, the usefulness of information gained from a genome sequence is dependent on the

quality of its annotation and, in the case of the PM70 genome sequence, many hypothetical iron-related genes still exist. Also, the *tbpA* gene encoding the transferrin binding protein A, one of the key iron acquisition proteins from the *in silico* model, is not present in the published avian genome sequence and its presence appears to vary significantly between serotypes of *P. multocida* and even between isolates of the same serotype, although the TbpA of *P. multocida* serotype A has been characterised and sequenced by several other groups (Ogunnariwo and Schryvers, 2001; Veken *et al*, 1994).

Many studies have investigated the effect of restricting the availability of iron upon expression of iron-regulated outer membrane proteins and have found that transcription of the genes encoding these proteins increases as availability of iron decreases (Litwin and Calderwood, 1993; Palyada, Threadgill and Stintzi, 2004; Paustian, May and Kapur, 2001; Roehrig *et al*, 2006; Zhou *et al*, 2006). However, there have been no quantitative studies of the effect of iron-restriction on key metabolic processes analysed here such as glucose uptake, bacterial ATP levels, protein content and biomass, during bacterial adaptation and growth under these conditions.

In restricting the availability of iron to *P. multocida*, the aim was to replicate the low levels of circulating iron observed within the diseased bovine host (Muller, Edwards and Smith, 1983; Weinberg, 1984). In that regard, *in vitro* growth media are commonly rich in nutrients (MacFaddin, 1985) and consequently are not reflective of the *in vivo* disease environment. Therefore, a number of strategies were adopted

to restrict iron availability and also to replicate other aspects of the diseased host more accurately. These strategies will be described in depth in this chapter.

5.2 Aims and methodology

Three different methods of bacterial culture were used to analyse the effect of iron-restriction on the growth rate, metabolism and gene expression of *P. multocida*. In addition, methods for the measurement of key metabolites and a qRT-PCR analysis of gene transcript levels were developed and refined in the course of these 3 studies. A description of the development and optimisation of these assays and of the culture methods can be found in **Section 2.12**.

5.2.1 Growth of *P. multocida* using a Biostat Q 4-vessel bacterial fermenter and qRT-PCR analysis of key iron acquisition gene transcription levels

The Biostat Q 4-vessel fermenter (Sartorius Ltd., Epsom, UK) was used to study the growth *in vitro* of bacterial cultures in defined environmental conditions, with regulation of temperature, pH, aeration and stirring of the culture, in volumes of up to 1 litre. The Biostat Q also allowed real-time monitoring of vessel pH, dissolved oxygen concentration and temperature and the large volume allowed samples to be drawn sequentially from each of the cultures (through septum ports built into each vessel) without altering significantly the culture conditions or composition. Between-vessel variation of growth rate was determined using identical cultures, and the variation in growth rate was shown to be minimal (results described in detail

in **Section 2.12.3**). A detailed method for growth of *P. multocida* in the Biostat Q fermenter can be found in **Section 2.9**.

Once reproducibility of the bacterial fermenter had been confirmed, the effect of iron-restriction on the growth of *P. multocida* 671/90 was investigated. Three vessels contained TSB/YE broth with 200 μM ∝∝-dipyridyl added to restrict available iron, whilst the fourth, a control vessel, contained TSB/YE broth alone and therefore was deemed iron-replete. Serial culture samples were extracted at 2-hourly intervals from each of the 4 vessels and estimated viable counts were calculated based upon densitometer measurements of culture turbidity. In addition, RNA was extracted from each of these samples for subsequent qRT-PCR analysis of the transcript levels of key iron acquisition genes. Detailed methods for calculation of estimated viable counts and RNA extraction/qRT-PCR analysis can be found in **Section 2.2** and **2.3** respectively.

5.2.2 Effects of changes in environmental conditions on growth rate, metabolism and gene transcription of *P. multocida* isolates

The Microreactor (Applikon Biotechnology, Tewkesbury, UK) allowed growth of 24 x 3 ml bacterial cultures with individual regulation of pH, temperature and aeration of each vessel. The large number of wells on a single disposable plate allowed greater opportunity for multiple variables to be studied and sufficient replicates to be included to allow an analysis of statistical significance. In addition, continuous readouts of temperature, pH and dissolved oxygen concentration of each

of the 24 vessels were logged automatically throughout each experiment, and these data allowed the efficiency of the homeostasis of each vessel to be assessed. A detailed method for growth of *P. multocida* in the Microreactor can be found in **Section 2.10**.

One aim here was to gain data suitable for calculation of glucose uptake rates by *P. multocida* in defined environmental conditions. Being a key energy source for *P. multocida* by providing ATP for transmembrane iron transport, and due to its central role in the *in silico* model, quantifying the uptake of glucose was vital (detailed method for glucose uptake assay can be found in **Section 2.5**). There has been much speculation as to the trigger or triggers resulting in *P. multocida* changing from a commensal to a pathogenic organism (Steenbergen *et al*, 2005). The possibility that this may result from a change in environmental conditions, most likely a change in temperature, pH or concentration of host iron will be investigated. Eight experiments were designed to allow 2 separate environmental conditions to be studied. These comprised:

A) Four runs to study the effects of iron-restriction on 4 isolates of *P. multocida* in simulated physiological conditions. The isolates used were: the current Moredun Research Institute *P. multocida* challenge strain (671/90), a North American *P. multocida* virulent isolate (45/04); and 2 commensal isolates (200038/A and 501249/A) isolated from nasal swabs of clinically healthy cattle. After a study of the literature, physiological conditions for a normal bovine lung were taken to be 39°C, pH 7.5 and 100% aeration.

B) Four runs to study the effects of changes in pH, temperature and iron-restriction on isolate 671/90.

Each run of the Microreactor lasted 8 hours with serial samples taken for analyses at 0, 2, 4, 6 and 8 hours. Growth conditions for each of the 8 separate experiments are detailed in **Table 5.1**. Estimated viable counts and live counts of bacterial growth were measured, as were protein content of bacterial pellets and bacterial glucose uptake rates for each of the 8 experiments (detailed method for live counts and protein assay can be found in **Section 2.2** and **Section 2.4** respectively). Being key components of the *in silico* model of *P. multocida* iron acquisition presented in **Chapters 3** and **4**, these *in vitro* data would allow validation of *in silico* model outputs and of predictions made based upon the model.

Run no.	Condition	Isolate used	Temperature	pH	Iron-replete	Iron-restricted
1	a	671/90	39	7.5	✓	
	b	671/90	39	7.5		✓
2	a	45/04	39	7.5	✓	
	b	45/04	39	7.5		✓
3	a	200038/A	39	7.5	✓	
	b	200038/A	39	7.5		✓
4	a	501249/A	39	7.5	✓	
	b	501249/A	39	7.5		✓
5	a	671/90	37	7.0	✓	
	b	671/90	37	7.0		✓
6	a	671/90	37	7.0	✓	
	b	671/90	39	7.0	✓	
7	a	671/90	37	6.0	✓	
	b	671/90	37	8.0	✓	
8	a	671/90	30	6.0	✓	
	b	671/90	30	8.0	✓	

Table 5.1: Conditions for each of 8 Microreactor runs. Note that runs 1-4 allowed a comparison of each of the 4 isolates in similar environmental conditions, whilst runs 5-8 allowed the effect of variations in environmental factors on isolate 671/90 to be studied.

5.2.3 *In vitro* culture of *P. multocida* 671/90 in iron-replete and iron-restricted conditions with key analyses providing data for integration with the *in silico* model of iron acquisition

Previous sections developed and optimised a number of assays to measure growth rate, total bacterial protein, bacterial glucose uptake and ATP levels, providing key data on metabolism of *P.* multocida in iron-replete and iron-restricted conditions (see **Section 2.6** for detailed ATP assay method). However to provide data suitable for comparison and integration with the *in silico* model of iron acquisition described in **Chapters 3 and 4**, accurate information on the changes in biomass, measured here as dry weight of bacteria was needed. This was to allow calculation of metabolite flux rates as millimoles per gram dry weight (bacteria) per hour, the standards units used in similar studies in the literature. These flux rates were calculated using data from log phase growth only, based on the assumption that the network is at pseudo-steady state during this phase (Maldonado *et al*, 2002).

This particular experiment involved growth of *P. multocida* 671/90 in iron-replete and iron-restricted conditions in TSB/YE medium on a rotary shaker at 39°C (see **Section 2.11** for detailed method). Three iron-replete and 3 iron-restricted cultures were grown over an 8-hour period with serial samples taken hourly from time 0. Estimated viable and live bacterial counts were recorded, as was dry weight of bacterial pellets after lyophilisation (see **Section 2.7** for detailed dry weight method). ATP content of bacteria was measured using the BacTiter Glo kit (Promega, Southampton, UK).

5.3 Results

5.3.1 Growth of *P. multocida* using a Biostat Q 4-vessel bacterial fermenter

The effect of iron-restriction on the growth rate of *P. multocida* 671/90 grown in the Biostat-Q 4-vessel fermenter was investigated. The growth rate of *P. multocida* under iron-replete conditions (vessel 4) was consistent with results obtained previously in similar conditions, as described in **Section 2.12.3**, whilst 2 of the 3 iron-restricted cultures (vessels 1 and 3) showed lower densities during log phase and a lower final plateau than the iron-replete vessel (**Fig. 5.1**). However, it was evident that growth of one of the iron-restricted cultures (vessel 2) was severely perturbed, to a much greater degree than either of the other iron-restricted cultures, with a final density more than 10-fold lower than either of the other iron-restricted cultures.

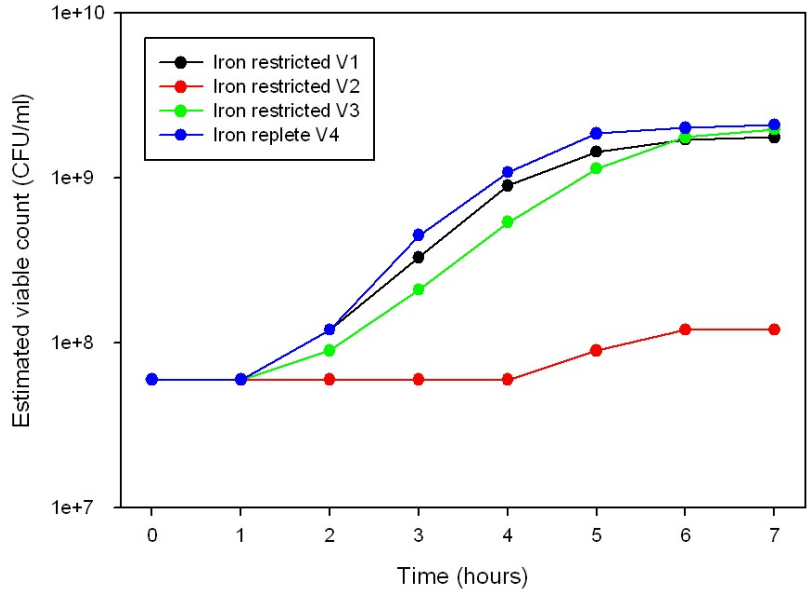

Fig. 5.1: Graph showing growth of *P. multocida* 671/90 over a 7-hour period in TSB/YE using the Biostat Q 4-vessel fermenter. Vessels 1, 2 and 3 contained TSB/YE medium with 200 µM αα-dipyridyl added to restrict available iron, whilst vessel 4 contained TSB/YE with no chelator added. All 4 vessels were grown in identical environmental conditions i.e. 39°C, pH 7.0, 100% aeration, 400 rpm stirring. Growth was estimated from the turbidity of culture using a densitometer (Densimat, Biomerieux). V1, V2, V3, V4 = vessel 1, 2, 3, 4.

5.3.1.1 qRT-PCR analysis of transcript levels of key *P. multocida* iron acquisition genes in iron-replete and iron-restricted conditions

There were no significant differences in the transcript levels of key iron acquisition genes of *P. multocida* 671/90 grown in either iron-replete or iron-restricted conditions as determined by qRT-PCR analysis.

5.3.2 Effects of changes in environmental conditions on growth rate and metabolism of *P. multocida* isolates

The Microreactor was used to analyse several aspects of growth by a number of isolates of *P. multocida*, and permitted tight control of environmental conditions and a greater number of replicates than in the Biostat-Q 4-vessel fermenter.

5.3.2.1 A comparison of the effect of iron-restriction on the growth rate of 4 different isolates of *P. multocida* A:3

The first set of experiments studied the effect of iron-restriction on growth rate, protein content of the bacterial pellet and glucose uptake of 4 isolates of *P. multocida*: UK isolate 671/90, USA isolate 45/04 and 2 commensal isolates, 20038/A and 501249/A, isolated from nasal swabs of clinically healthy cattle. The growth rates of each of the 4 isolates differed significantly from each other in both iron-replete and iron-restricted conditions (**Fig. 5.2**). Other than iron-restriction, all isolates were grown in identical conditions chosen to mimic physiological growth conditions in cattle: 39°C, pH 7.5, 100% aeration. Comparing iron-replete growth

for the 4 isolates, commensal isolate 20038/A (**Fig. 5.2C**) had the highest final density of approximately 9 x 10^{10} cfu/ml, USA isolate 45/04 (**Fig. 5.2B**) had a final density of approximately 7 x 10^{10} cfu/ml, UK isolate 671/90 (**Fig. 5.2A**) had a final density of approximately 3 x 10^{10} cfu/ml and commensal isolate 501249/A (**Fig. 5.2D**) had a final density of approximately 1 x 10^{10} cfu/ml (final density after 7 hours). There was a marked reduction in growth rate and final density of all 4 isolates under iron-restriction, however there seemed to be an association between the final density of isolates in iron-replete conditions and their final density in iron-restricted conditions. In other words, the 2 isolates with the highest final densities in iron-replete conditions, 20038/A and 45/04, had higher final densities in iron-restricted conditions than the isolates 671/90 and 501249/A. Final densities for isolates 20038/A, 45/04, 671/90 and 501249/A grown in iron-restricted conditions were 7 x 10^9 cfu/ml, 7.5 x 10^9 cfu/ml, 1.8 x 10^9 cfu/ml and 5.5 x 10^9 cfu/ml respectively.

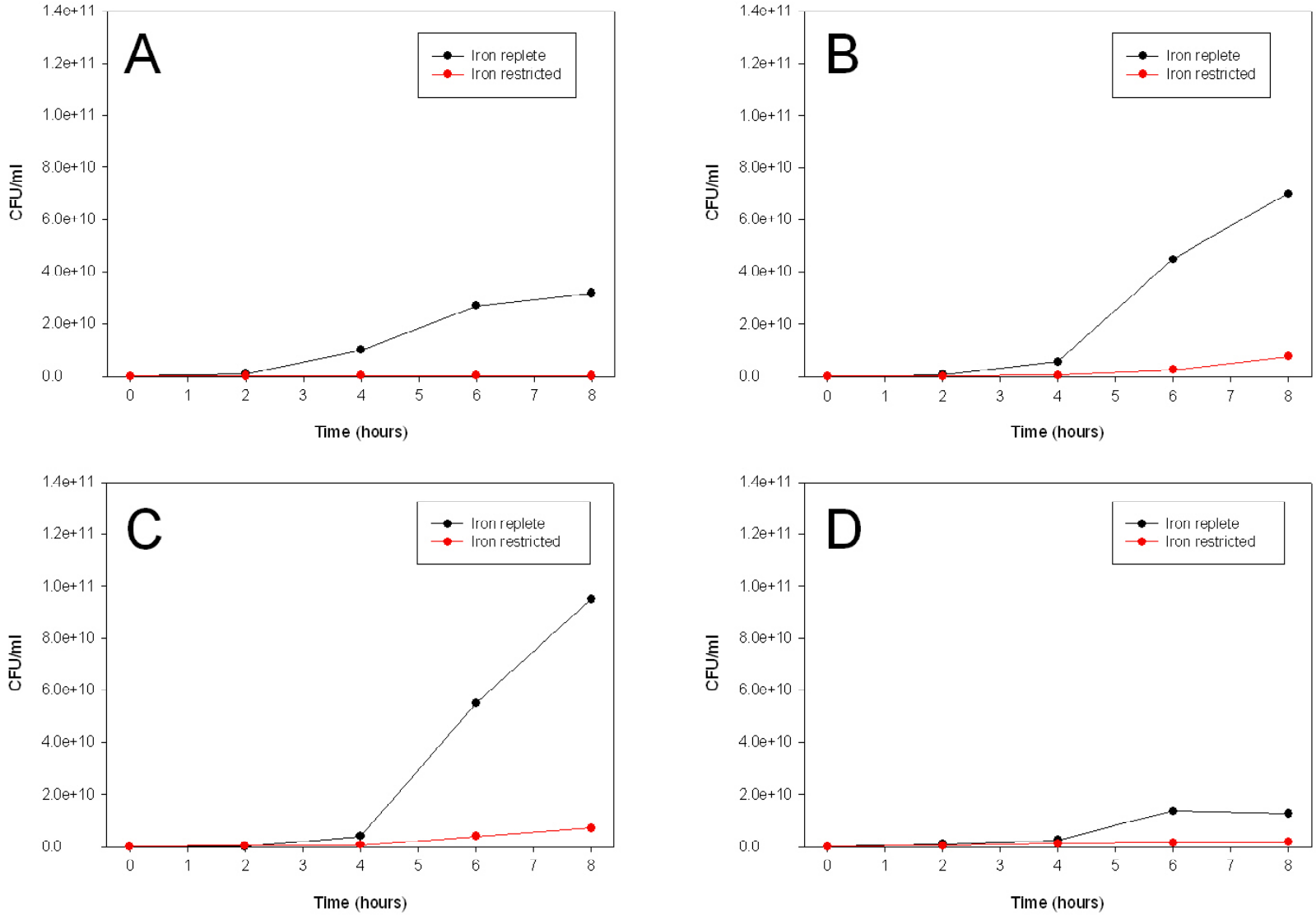

Fig. 5.2: Graphs showing changes in EVC with time (growth rates) of 4 isolates of *P. multocida* grown in the Applikon Mircoreactor under iron-replete and iron-restricted conditions over an 8-hour period with 2-hourly sampling. EVCs were calculated from optical densities of cultures measured using a densitometer (Densimat, Biomerieux). All 4 strains were grown in identical conditions (except iron availability) – temperature 39°C, pH 7.5, 100% aeration. **A)** *P. multocida* strain 671/90. **B)** *P. multocida* strain 45/04. **C)** *P. multocida* strain 200038A. **D)** *P. multocida* strain 501249A. See also **Appendix 3** for table of raw data.

5.3.2.2 A comparison of the effect of iron-restriction during culture on total protein content of 4 isolates of *P. multocida* A:3

For the most part, total protein content of the bacterial pellets showed a positive correlation with growth rates of each strain in both iron-replete and iron-restricted conditions (**Fig. 5.3**). Some differences were apparent, notably that, in iron-replete conditions, the total protein content of isolate 671/90 (**Fig. 5.3A**) was higher than that of isolate 200038/A (**Fig. 5.3C**) despite the growth rate of 671/90 being lower than that of 200038/A. In addition, the total protein content of isolate 501249/A (**Fig. 5.3D**) in both iron-replete and iron-restricted conditions appeared disproportionately high given the growth rates in either condition compared with other isolates.

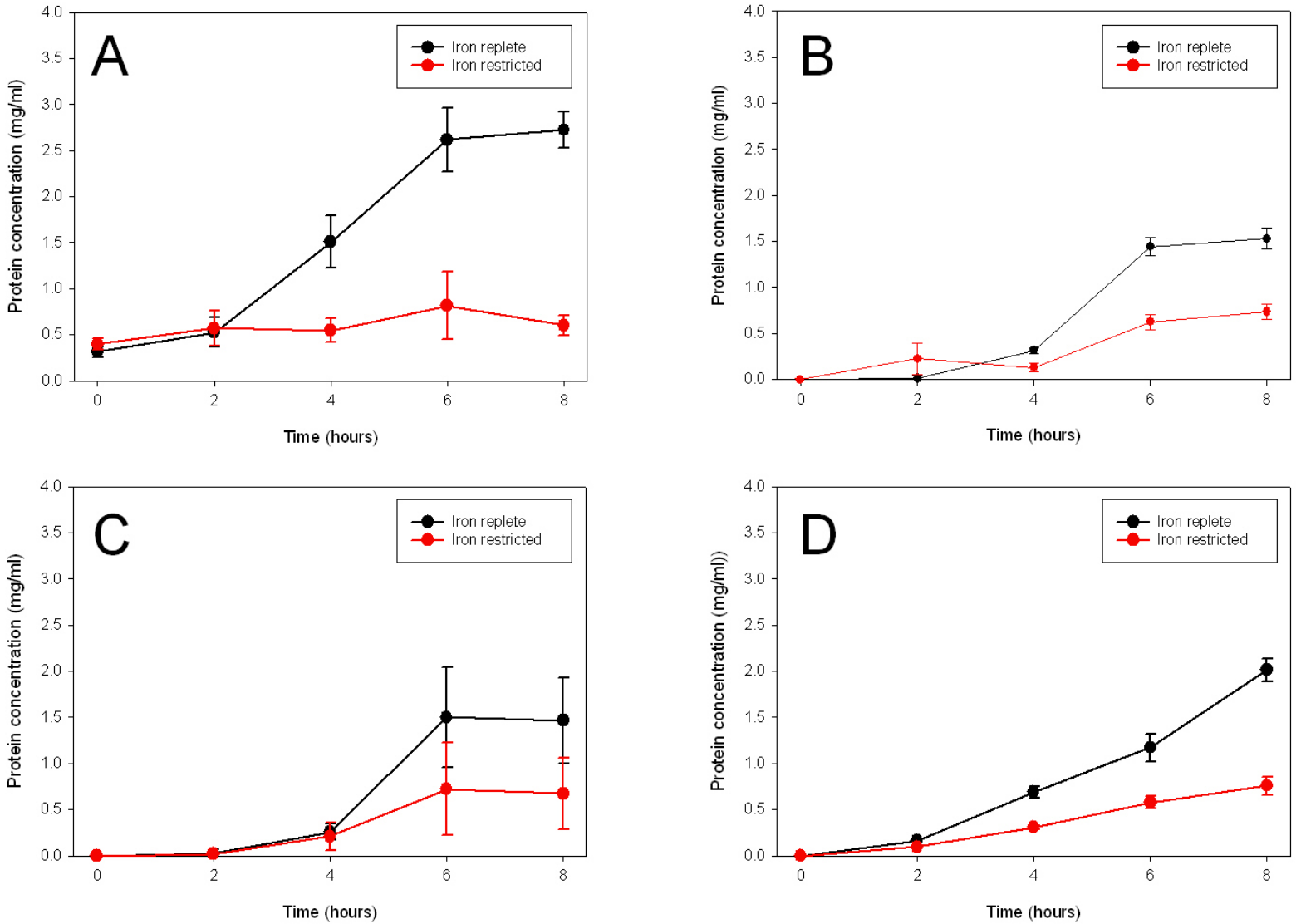

Fig. 5.3: Graphs showing total protein content of the pellets of 4 isolates of *P. multocida* grown in the Applikon Mircoreactor under iron-replete and iron-restricted conditions over an 8-hour period with 2-hourly sampling. Protein content was measured using a modification of the Lowry assay. All 4 strains were grown in identical conditions (except iron availability) – temperature 39°C, pH 7.5, 100% aeration. **A)** *P. multocida* strain 671/90. **B)** *P. multocida* strain 45/04. **C)** *P. multocida* strain 200038A. **D)** *P. multocida* strain 501249A. See also **Appendix 3** for table of raw data.

5.3.2.3 A comparison of the effect of iron-restriction during culture on glucose uptake of 4 isolates of *P. multocida* A:3

As glucose is the main energy source for *P. multocida* grown *in vitro* and drives bacterial protein synthesis and transport of iron across the bacterial cytoplasmic membrane (Oberhofer, 1981; Shouldice *et al*, 2004), glucose uptake rates were measured for the same set of isolates as in the previous two sections (**Sections 5.3.5.2 and 5.3.5.1)**. Similar to the protein content of the bacterial pellet, glucose uptake rates (**Fig. 5.4**) mirrored growth rates approximately. However, there appeared to be less variation between glucose uptake rates of all 4 isolates in both iron-replete and iron-restricted conditions than there was between the growth rates of the same isolates. It should be noted that standard errors for iron-restricted cultures 200038/A (**Fig. 5.4C**) and 501249/A (**Fig. 5.4D**) at the 6-hour time points were particularly high. A significant finding was the sharp increase in glucose uptake of iron-restricted isolate 45/04 (**Fig. 5.4B**) between 4 and 8 hours.

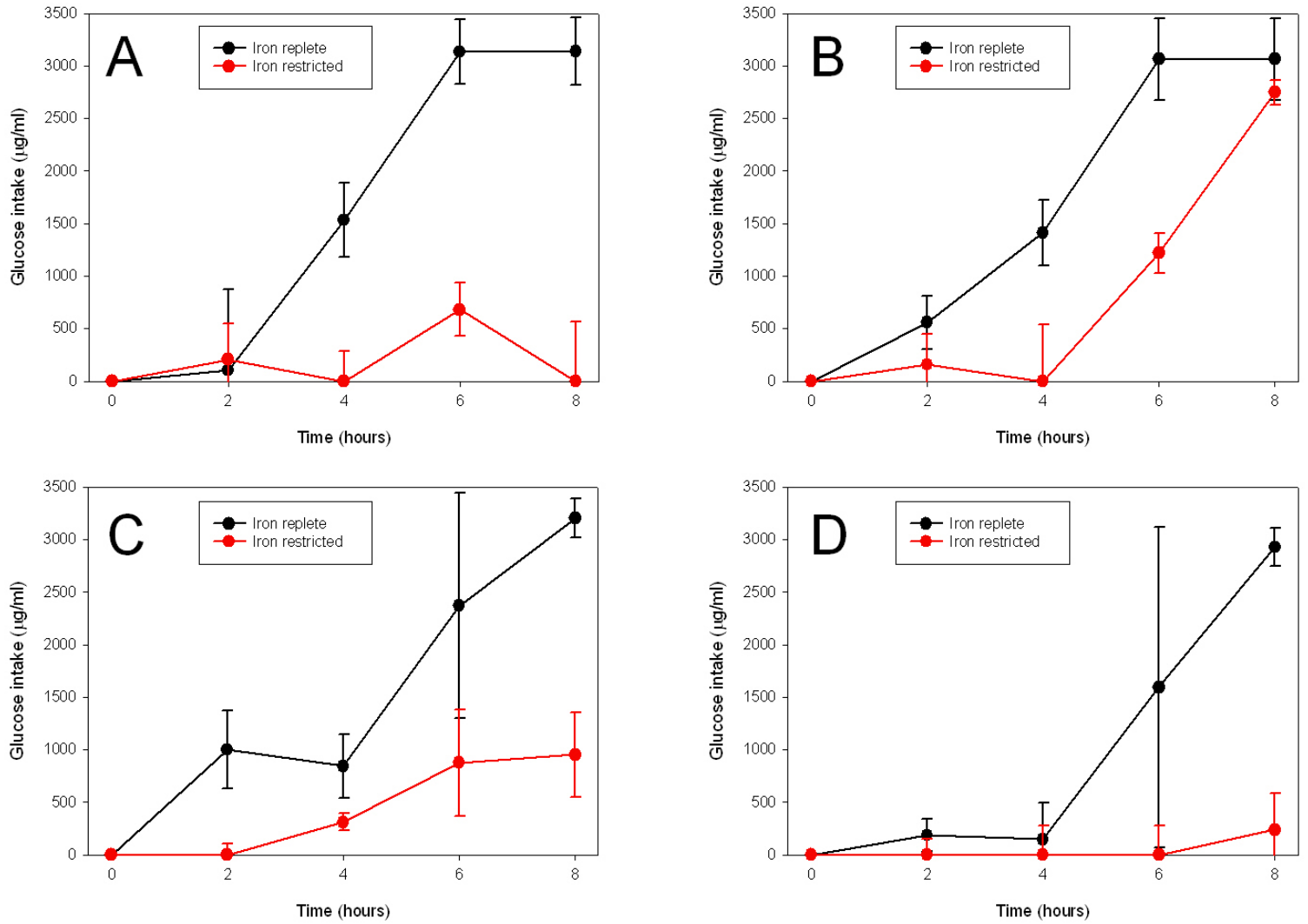

Fig. 5.4: Graphs showing glucose taken up by 4 isolates of *P. multocida* grown in the Applikon Mircoreactor under iron-replete and iron-restricted conditions over an 8-hour period with 2-hourly sampling. Glucose uptake was estimated by measuring the depletion of glucose from the bacterial growth medium using a glucose oxidase assay. All 4 strains were grown in identical conditions (except iron availability) – temperature 39°C, pH 7.5, 100% aeration. **A)** *P. multocida* strain 671/90. **B)** *P. multocida* strain 45/04. **C)** *P. multocida* strain 200038A. **D)** *P. multocida* strain 501249A. See also **Appendix 3** for table of raw data.

5.3.2.4 Effect of iron-restriction on growth rate, total protein content and glucose uptake of *P. multocida* 671/90

A second set of experiments studied the effects of changes in environmental conditions, namely temperature, pH and iron-restriction on the growth rate, protein content of bacterial pellet and glucose uptake of isolate 671/90. *P. multocida* isolate 671/90 is used routinely in pneumonic challenge experiments at Moredun Research Institute and has been shown to be particularly virulent *in vivo*. Therefore, a study of the effects of environmental changes on growth rate, total protein content and glucose uptake of this isolate was of particular interest.

Similar to the experiments described in **Sections 5.3.2.1** to **5.3.2.3**, isolate 671/90 was grown in the Microreactor for an 8-hour period and sequential samples were taken for analyses at 2-hourly intervals. Initially, the effect of iron-restriction on growth rate, total protein content and glucose uptake of isolate 671/90 was investigated. In this case, standard laboratory culture conditions (37°C, pH 7.0 and 100% aeration) were used, with addition of 200μM αα-dipyridyl to iron-restricted vessels.

Comparing growth rates in iron-replete and iron-restricted conditions it was evident that iron-restriction severely perturbed growth of isolate 671/90 (**Fig. 5.5**). The iron-restricted cultures did not enter log phase growth, whilst the iron-replete cultures showed an exponential increase in growth from 4 hours onwards and a final density of 1.2×10^{11} CFU/ml, as compared a final density of 5.5×10^{9} in iron-

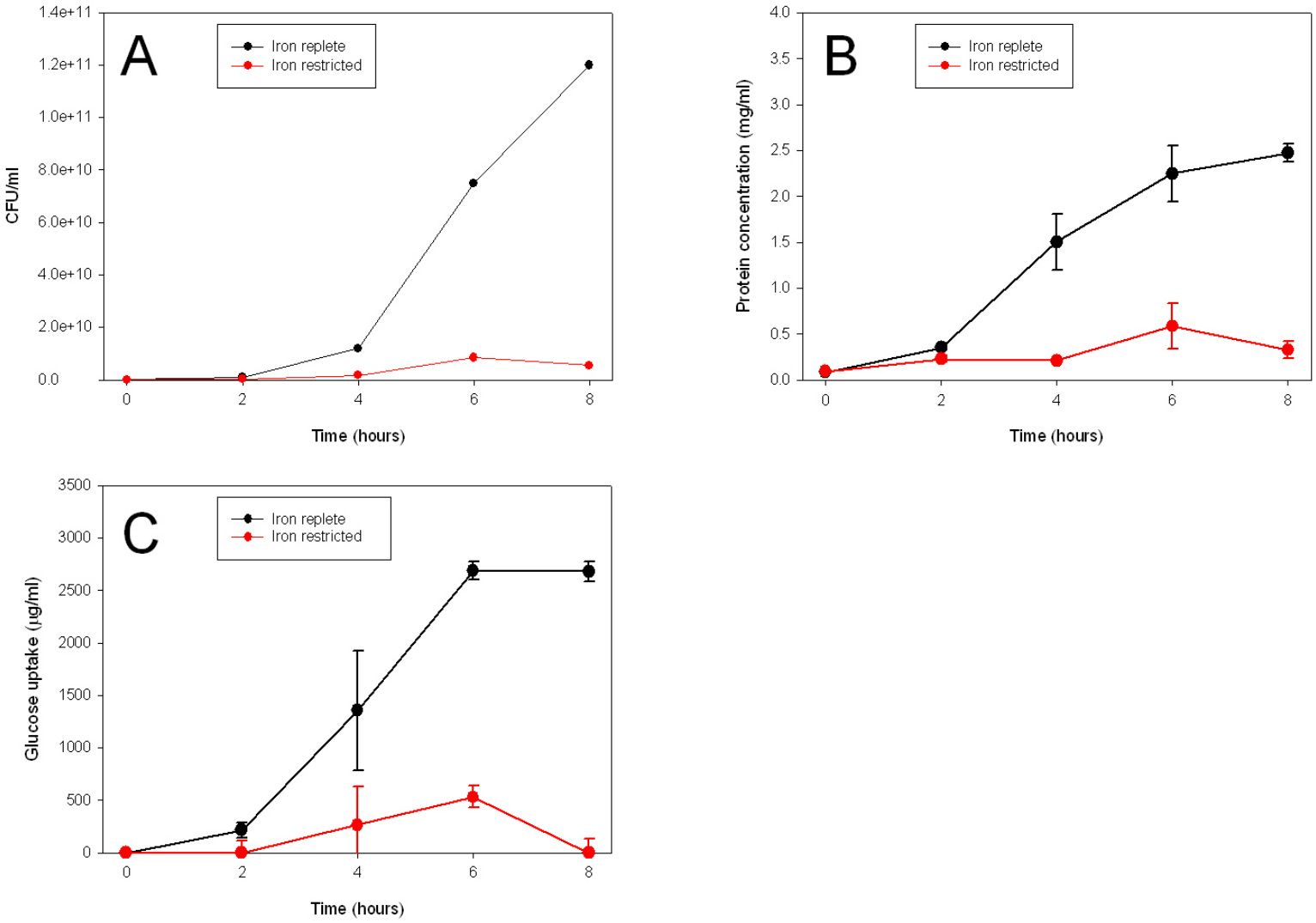

Fig. 5.5: Graphs showing of the effect of iron-restriction on growth rate **(**measured by EVC; **A)**, total protein content **(B)** and glucose intake **(C)** of *P. multocida* isolate 671/90 grown in the Applikon Mircoreactor over an 8-hour period with 2-hourly sampling. Cultures were grown in identical conditions (except iron availability) – temperature 37°C, pH 7.0, 100% aeration. EVCs were calculated from optical densities of cultures measured using a densitometer (Densimat, Biomerieux). See also **Appendix 4** for table of raw data.

restricted conditions. Both total protein content (**Fig. 5.5B**) of the bacterial pellet and bacterial glucose uptake (**Fig. 5.5C**) mirrored closely growth rates of isolate 671/90 in both iron-replete and iron-restricted conditions.

5.3.2.5 A comparison of growth of *P. multocida* 671/90 at 37°C versus 39°C and resultant effects on growth rate, total protein content and glucose uptake

The effects of growing *P. multocida* isolate 671/90 at 39°C, the core temperature of cattle and consequently the temperature at which isolate 671/90 causes significant pathology during respiratory challenge experiments (Dowling *et al*, 2002), were compared to those seen when the same isolate was grown at the standard laboratory culture temperature of 37°C. As in previous sections, isolate 671/90 was grown in the Microreactor for an 8-hour period and sequential samples were taken for analyses at 2-hourly intervals. Twelve cultures were grown at 37°C whilst the remaining 12 were grown at 39°C. All 24 cultures were maintained at pH 7.0, 100% aeration in iron-replete TSB/YE medium.

When growth rates were compared it was noted that cultures grown at 37°C entered log phase growth at around 4 hours and had a final density of 5.0×10^{10} CFU/ml (**Fig. 5.6**). Cultures grown at 39°C did not enter log phase growth and had a final density of 8.0×10^{9}. In contrast to previous experiments, total protein content of the bacterial pellet (**Fig. 5.6B**) and bacterial glucose uptake (**Fig. 5.6C**) did not mirror growth rates closely in either condition. Whilst the total protein and glucose intake of cultures grown at 37°C correlated with the associated growth curve, the

correlation at 39°C was less significant. In fact, total protein and glucose intake did not vary significantly between cultures grown at 37°C and at 39°C.

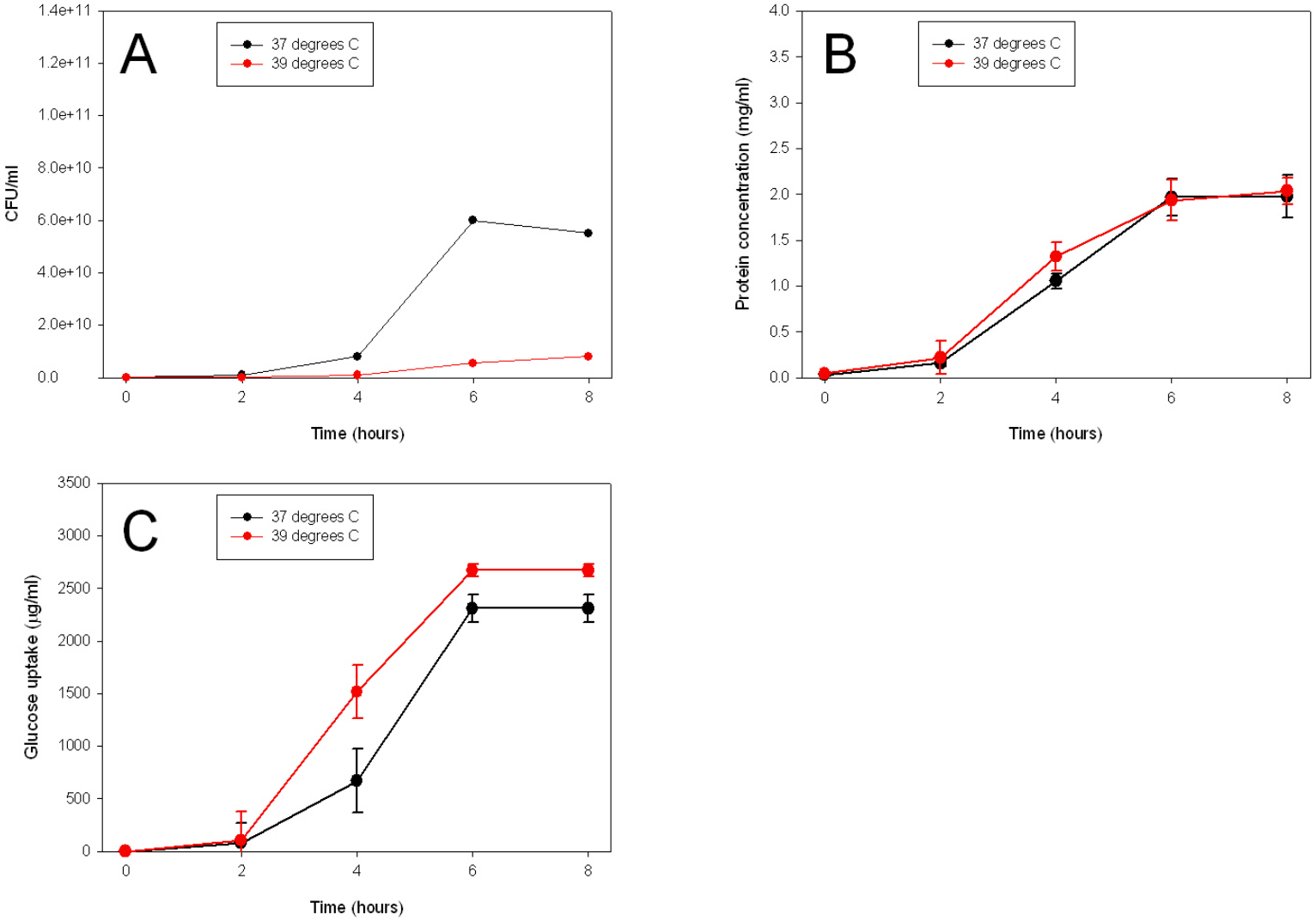

Fig. 5.6: Graphs comparing growth of *P. multocida* isolate 671/90 at 37°C versus 39°C and resultant effects on growth rate **(**measured by EVC; **A)**, total protein content **(B)** and glucose intake **(C)**. Cultures were grown in the Applikon Mircoreactor over an 8-hour period with 2-hourly sampling in iron-replete TSB/YE medium at pH 7.0 and with 100% aeration. EVCs were calculated from optical densities of cultures measured using a densitometer (Densimat, Biomerieux). See also **Appendix 4** for table of raw data.

5.3.2.6 A comparison of growth of *P. multocida* 671/90 at pH 6.0 versus pH 8.0 and resultant effects on growth rate, total protein content and glucose uptake

In comparison to standard laboratory culture conditions, the bovine respiratory tract constitutes a much harsher environment in which *P. multocida* must survive and proliferate. However, evidence in the literature suggests that virulence increases when bacteria are exposed to harsher conditions (Robledo, Serrano and Domingue, 1990; Rodriguez and Smith, 2003); for example when they are grown in iron-restricted conditions, or when temperature or pH is adjusted beyond standard limits. In **Chapter 1**, the link between iron-restriction and increased expression of immunogenic bacterial outer membrane proteins was described in detail. Therefore, it was decided that the effects of growing *P. multocida* 671/90 at pH 6.0 and a pH 8.0 at both 30°C and 37°C may give new insight into the behaviour of *P. multocida* in biologically harsh conditions and provide evidence to back up hypotheses suggested by the *in silico* model presented in **Chapters 3** and **4**.

When the growth rates of *P. multocida* 671/90 cultured at pH 6.0 and pH 8.0 and at 37°C were compared (**Fig. 5.7**) it could be seen that those cultures grown at pH 8.0 grew better than those grown at pH 6.0. Cultures grown at pH 8.0 entered log phase growth between 2 and 4 hours and had a final density of 9.0×10^{10} CFU/ml. However, cultures grown at pH 6.0 did not appear to enter log phase growth during the 8-hour period and had a final density of 1.6×10^{10} CFU/ml, almost 6-fold lower than those cultures grown at pH 8.0. Total protein content of the bacterial pellets

(**Fig. 5.7B**) correlated well with growth in both conditions, although values were slightly lower than expected at the 6 and 8-hour time points of the pH

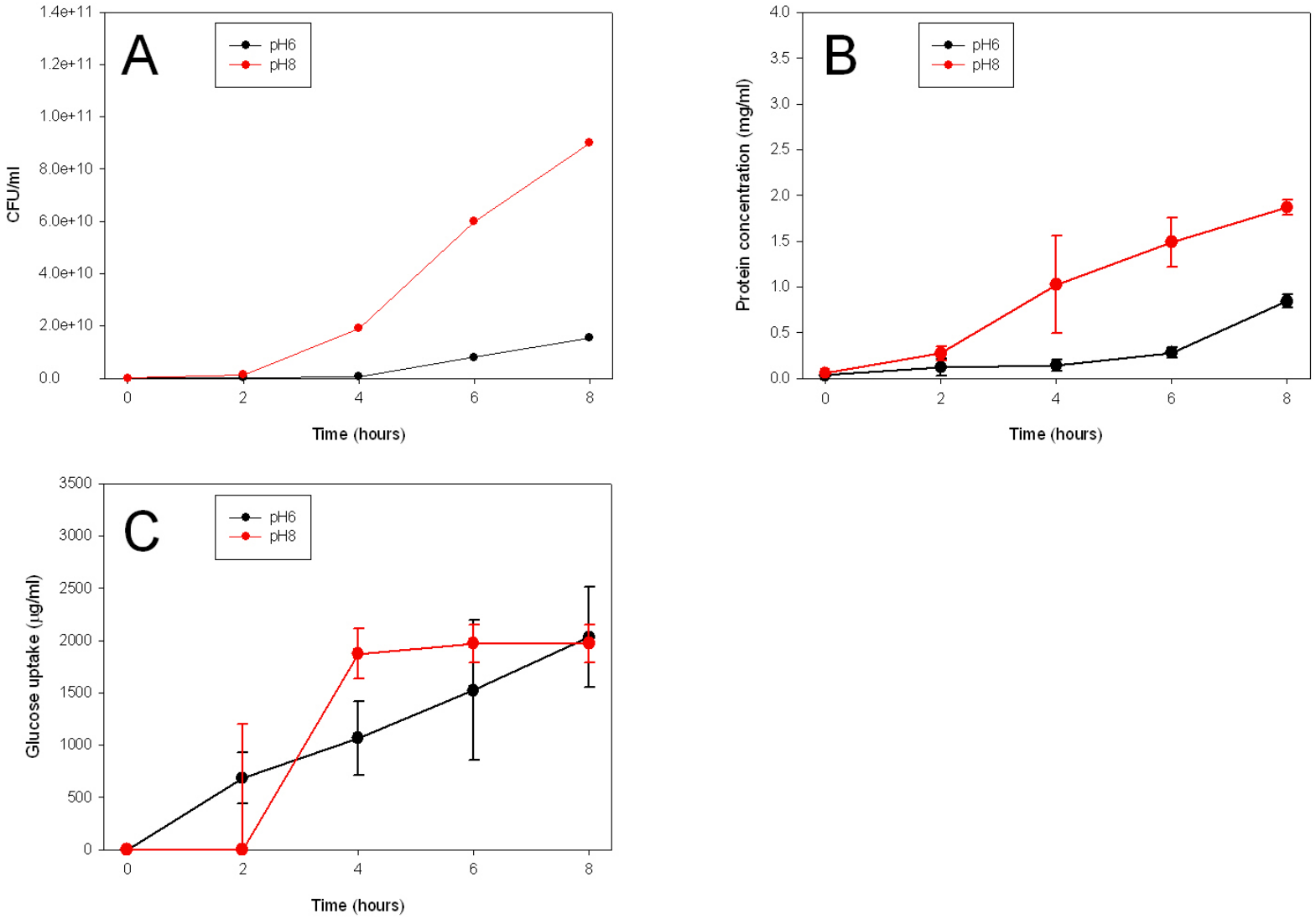

Fig. 5.7: Graphs comparing growth of *P. multocida* isolate 671/90 at pH 6.0 versus pH 8.0 and 37°C and resultant effects on growth rate **(**measured by EVC; **A)**, total protein content **(B)** and glucose intake **(C)**. Cultures were grown in the Applikon Mircoreactor over an 8-hour period with 2-hourly sampling in iron-replete TSB/YE medium and with 100% aeration. EVCs were calculated from optical densities of cultures measured using a densitometer (Densimat, Biomerieux). See also **Appendix 4** for table of raw data.

8.0 cultures. However, the glucose uptake rate (**Fig. 5.7C**) of those cultures grown at pH 6.0 was higher than expected given the close correlation noted previously between glucose uptake rate and growth rate. At the end of the 8-hour growth period, cultures grown at pH 6.0 and at pH 8.0 had similar values in terms of glucose taken up from the growth medium (2031 μg/ml vs. 1973 μg/ml respectively) despite an almost 6-fold difference in final bacterial density, although the standard deviations for the 4, 6 and 8-hour time points of the pH 6.0 cultures were relatively large. Glucose uptake rates for cultures grown at pH 8.0 showed a sharp increase between 2 and 4 hours, although the standard deviation for the 2-hour time point was large.

A separate experiment repeated the comparison of growth rate and metabolism at pH 6.0 versus pH 8.0, but cultures were grown at 30°C rather than 37°C (**Fig. 5.8**). When growth rates of these cultures were compared, similar growth curves to those seen at 37°C were observed. The final densities were 9.0×10^9 CFU/ml and 6.5×10^{10} CFU/ml for cultures grown at pH 6.0 and pH 8.0 respectively. Both protein concentration of the bacterial pellet (**Fig. 5.8B**) and glucose uptake rates (**Fig. 5.8C**) correlated closely with respective growth rates of cultures at pH 6.0 and pH 8.0.

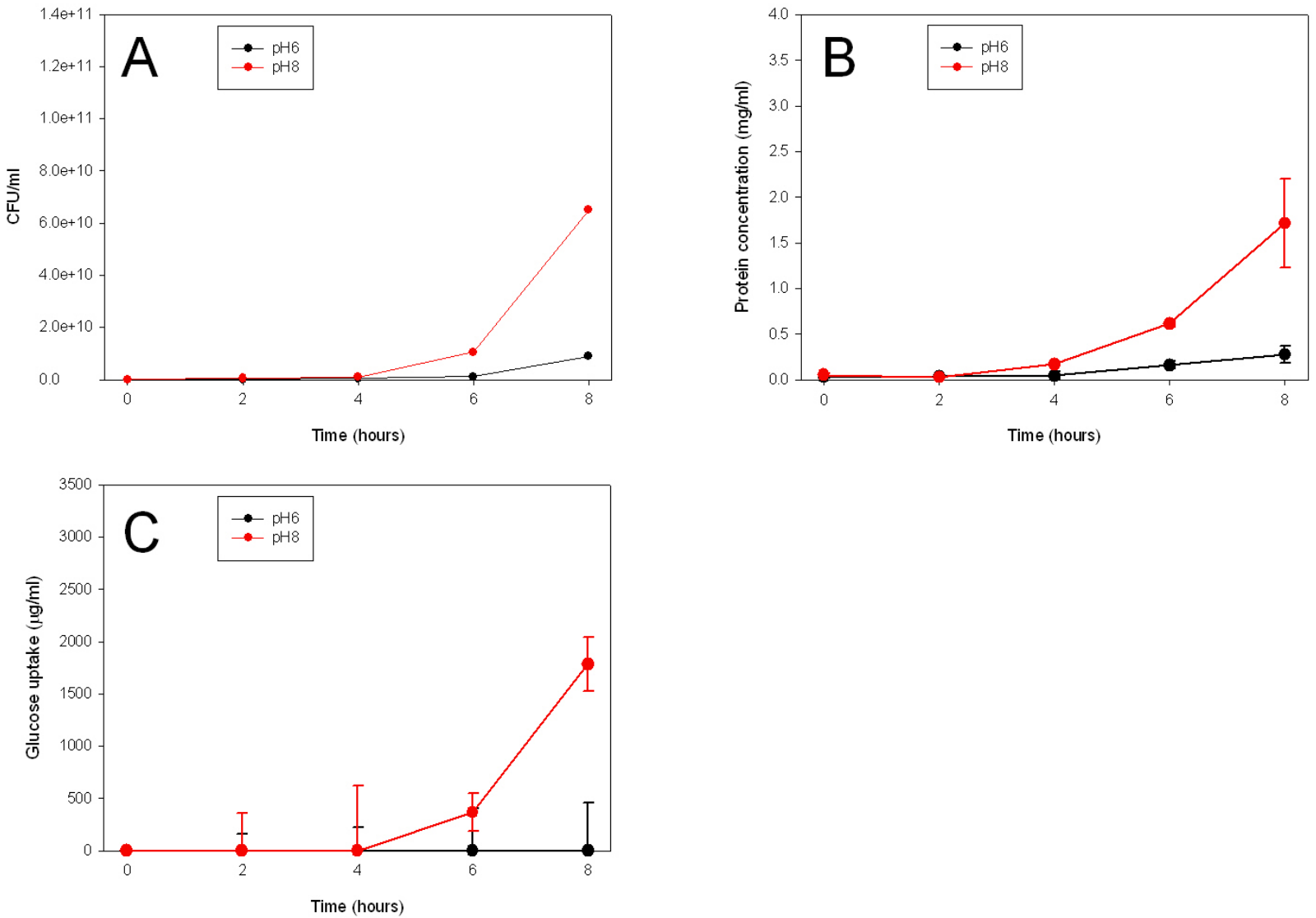

Fig. 5.8: Graphs comparing growth of *P. multocida* isolate 671/90 at pH 6.0 versus pH 8.0 and 30°C and resultant effects on growth rate **(**measured by EVC; **A)**, total protein content **(B)** and glucose intake **(C)**. Cultures were grown in the Applikon Mircoreactor over an 8-hour period with 2-hourly sampling in iron-replete TSB/YE medium and with 100% aeration. EVCs were calculated from optical densities of cultures measured using a densitometer (Densimat, Biomerieux). See also **Appendix 4** for table of raw data.

5.3.3 *In vitro* culture of *P. multocida* 671/90 in iron-replete and iron-restricted conditions with key analyses providing data for integration with the *in silico* model of iron acquisition

ATP hydrolysis plays a central role in the mechanism of iron uptake in *P. multocida* (Shouldice *et al*, 2004). This experiment measured bacterial ATP concentrations, growth rate and dry weight of cultures of *P. multocida* 671/90 grown in iron-replete and iron-restricted conditions in order to provide key parameters for integration with the *in silico* model of iron acquisition described previously.

Growth rates were estimated first by McFarland reading. Estimated viable counts were calculated by multiplying McFarland readings by 3×10^8 (Koch, 1970; Linde *et al*, 2001).This figure was then corrected by multiplying by a correction factor determined empirically by comparison with live counts. For a given optical density during log phase when it was assumed that a majority of bacteria were live, estimated viable counts deviated from live counts according to bacterial size. For example, a correction factor of greater than 1 indicated that bacteria were smaller in size, whereas a correction factor of less than 1 indicated that bacteria were larger in size. However, towards culture plateau, the number of dead bacteria may have increased and consequently the correction factor may have decreased.

When growth rates determined by live count were compared in iron-replete versus iron-restricted conditions (**Fig. 5.9A**), similar results were observed as in previous experiments comparing iron-replete and iron-restricted growth. More specifically, cultures grown in iron-restricted conditions showed severely perturbed growth in

comparison to those cultures grown in iron-replete conditions. Iron-replete cultures entered exponential phase growth after approximately 3 hours and began to plateau after approximately 6 hours; iron-restricted cultures did not enter exponential phase growth. The mean final density of the iron-replete cultures was 7.67×10^9 CFU/ml compared with a mean final density of 4.58×10^7 CFU/ml for the iron-restricted cultures (mean starting densities were 1.13×10^7 CFU/ml and 1.03×10^7 CFU/ml respectively). Compared with growth rates of *P. multocida* 671/90 grown in similar conditions in earlier experiments (**Section 5.3.2**), growth rates in iron-replete and iron-restricted conditions here were both at least 10-fold lower.

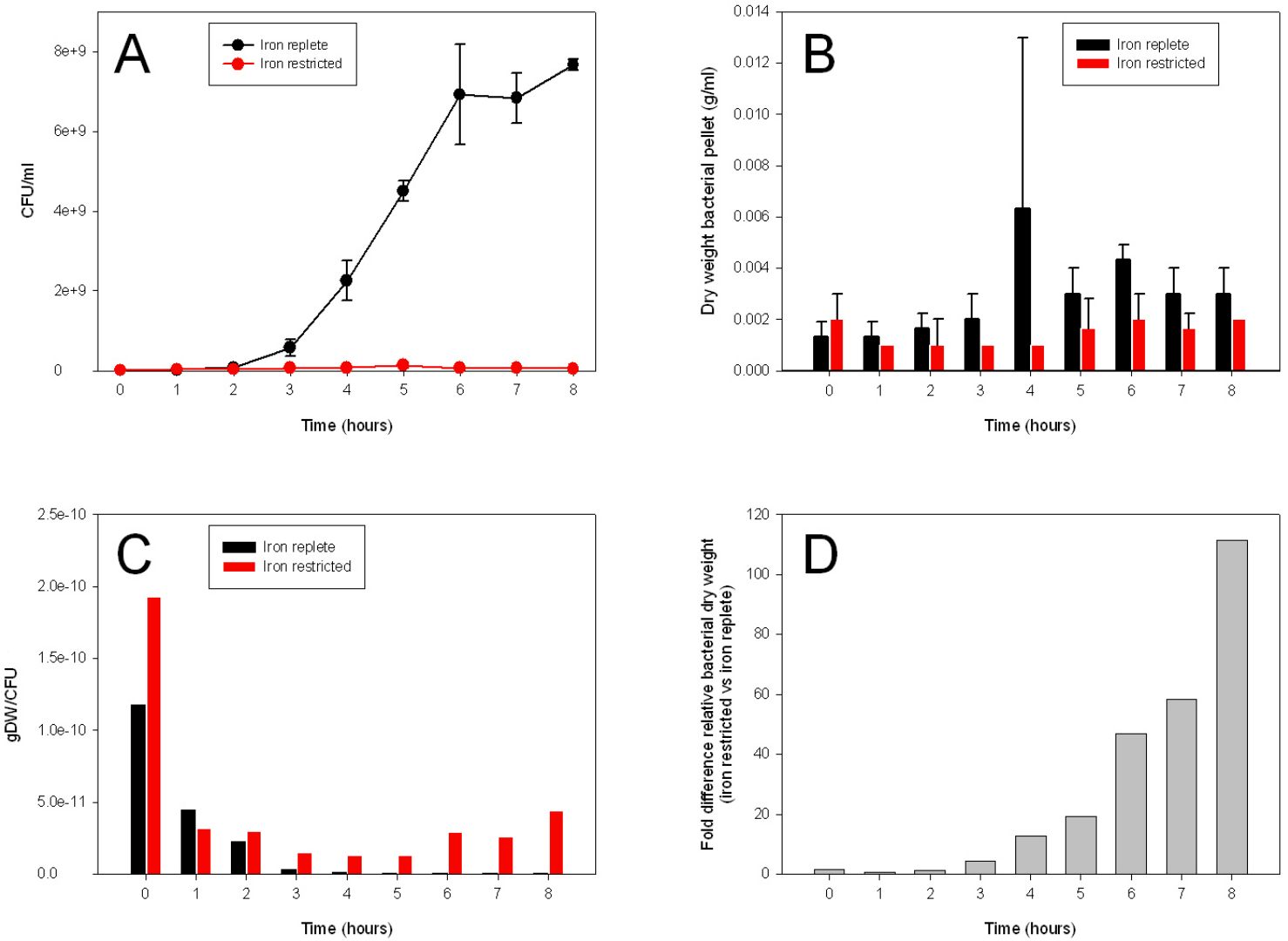

Fig. 5.9: Graphs showing growth rates and dry weights of *P. multocida* isolate 671/90 grown in iron-replete and iron-restricted conditions. **A)** Mean live bacterial counts (CFU/ml) of iron-replete and iron-restricted cultures. **B)** Mean dry weights of bacterial pellets from 1 ml of iron-replete and iron-restricted cultures. **C)** Mean relative dry weights per CFU of iron-replete and iron-restricted cultures. **D)** Fold difference in relative bacterial dry weights per CFU between iron-restricted and iron-replete cultures. Cultures were grown in shaking flask culture over an 8-hour period with hourly sampling in iron-replete TSB/YE medium and iron-restricted TSB/YE medium (with 200μM αα-dipyridyl added).

Dry weight of bacteria was measured after lyophilisation of 1ml of culture at each time point from both iron-replete and iron-restricted cultures. Mean dry weights (**Fig. 5.9B**) of iron-replete cultures showed a moderate increase over the 8-hour time course from approximately 1 mg to approximately 3 mg. Mean dry weights of iron-restricted cultures fluctuated between 1 mg and 2 mg throughout the 8-hour time course with no significant relation to their respective growth curve. Mean dry weights were also normalised according to the number of CFU/ml (live counts) at each time point (**Fig. 5.9C**), thus giving an approximate estimate of relative bacterial mass. These data indicated that iron-restricted bacteria had a higher relative mass than those cultured in iron-replete conditions at every time point with the exception of the 1-hour time point. Furthermore the difference in relative bacterial mass between iron-restricted and iron-replete bacteria increased from less than 2-fold at time 0 to greater than 100-fold after 8 hours (**Fig. 5.9D**).

Bacterial ATP levels were measured by luminometry of sequential samples of cultures grown in iron-replete and iron-restricted conditions. When millimolar concentrations of ATP from both conditions (**Fig. 5.10A**) were compared with growth rates of the same cultures, a positive correlation between growth rate and ATP concentration was observed ($r = 0.97$ and 0.64 for iron-replete and iron-restricted conditions respectively; Pearson correlation coefficient). In iron-replete conditions, bacterial ATP concentration increased sharply between 3 and 5 hours and reached a plateau from 6 hours onwards, reaching a maximum ATP concentration of 4.39×10^{-4} mM. In comparison, in iron-restricted conditions, bacterial ATP concentrations remained low, increasing from 1.12×10^{-6} mM at time

0 to a maximum concentration of 7.07 x 10^{-6} mM after 8 hours. ATP concentrations were also normalised against both dry weight and CFUs. In terms of millimoles ATP per gram dry weight (**Fig. 5.10B**), iron-replete cultures showed an approximate 10-fold increase from 5 hours onwards whilst values for iron-restricted cultures remained low throughout the 8-hour culture. When ATP concentrations were normalised against CFUs a differing pattern was observed (**Fig. 5.10C**). In general, there was less difference between ATP levels in iron-replete vs. iron-restricted conditions compared to ATP per gram dry weight values. However, at the 6, 7 and 8-hour time points millimoles of ATP per CFU of iron-restricted cultures exceeded those of iron-replete cultures by approximately 2-fold.

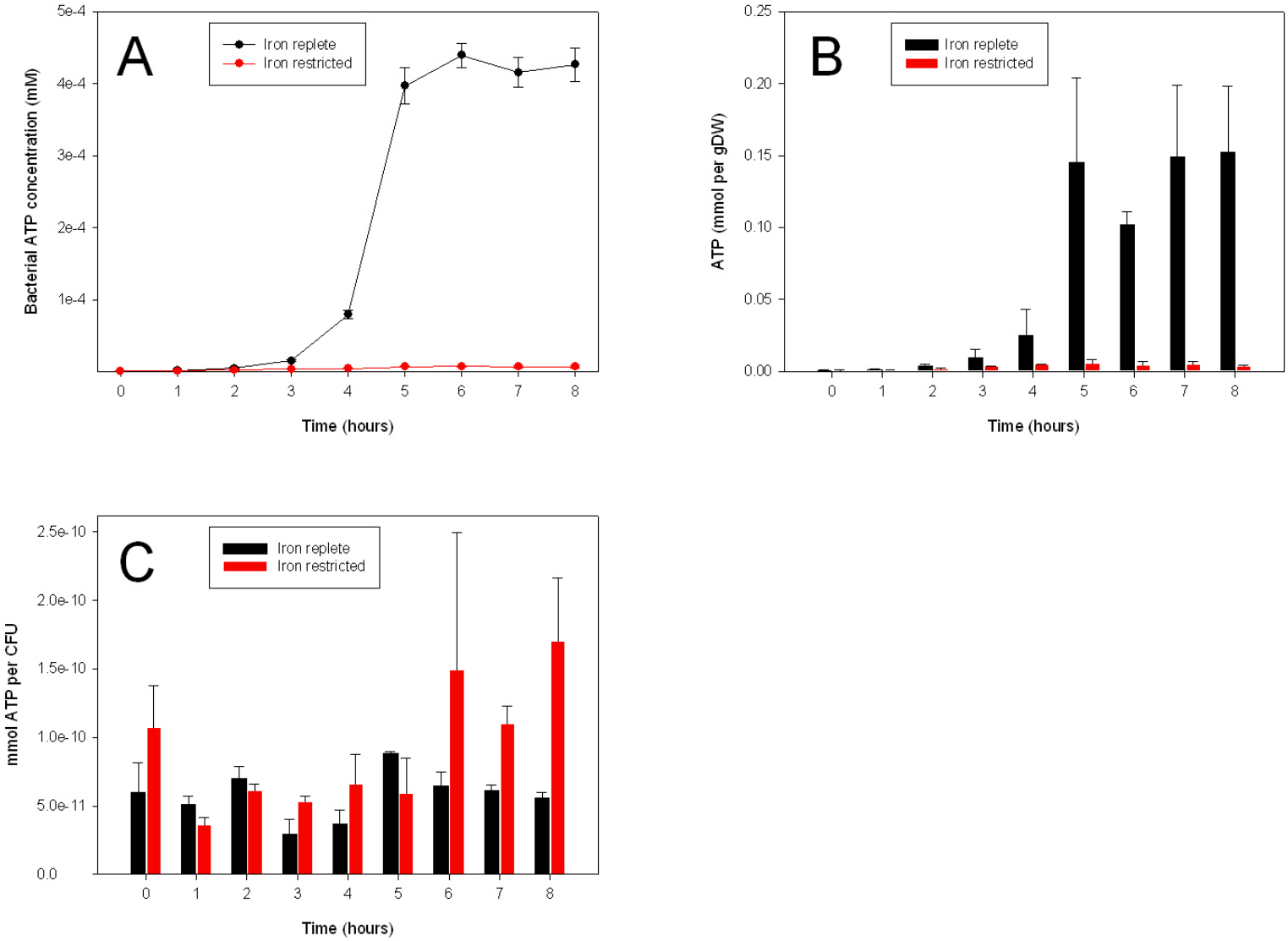

Fig. 5.10: Graphs showing bacterial ATP levels of *P. multocida* isolate 671/90 grown in iron-replete and iron-restricted conditions. **A)** Bacterial ATP concentrations (mM) of iron-replete and iron-restricted cultures. **B)** ATP (millimoles) per gram dry weight. **C)** ATP concentration (mM) per CFU (CFU measured by live bacterial counts). Cultures were grown in shaking flask culture over an 8-hour period with hourly sampling in iron-replete TSB/YE medium and iron-restricted TSB/YE medium (with 200μM αα-dipyridyl added).

5.4 Discussion

5.4.1 Growth of *P. multocida* using a Biostat Q 4-vessel bacterial fermenter

Growth of *P. multocida* 671/90 in a bacterial fermenter allowed the effect of iron restriction on growth rate and on transcription of key iron acquisition genes to be studied. Only 1 of the 3 iron-restricted cultures showed a significant perturbation of growth rate, whilst the growth rates of the other 2 cultures did not vary significantly from that of the iron-replete culture. Based upon analyses of iron-restricted growth rates in similar conditions (**Section 5.3.2.4**), significant perturbation of growth rates should have been observed in all 3 iron-restricted vessels. The pH of each culture was maintained at 7.0 by automated addition of alkali (sodium hydroxide) and acid (hydrochloric acid), and it was noted that large volumes of alkali were added to the iron-restricted cultures (data not shown). Even with this addition, pH was not maintained at 7.0 later in the 8 hour growth period and dropped sharply. This drop in vessel pH despite the addition of significant volumes of alkali may have indicated anaerobic growth due to contamination although live bacterial counts showed no evidence of this.

When transcript levels of 7 key iron acquisition genes of *P. multocida* were assayed by qRT-PCR, no significant up or down-regulation was seen in iron-restricted versus iron-replete conditions. This was most likely due to inefficient maintenance of the level of iron-restriction and of pH in the iron-restricted cultures.

5.4.2 Effects of changes in environmental conditions on growth rate and metabolism of *P. multocida* isolates

An initial comparison of the effects of iron restriction on the growth rate, total bacterial protein and glucose uptake on 4 different isolates of *P. multocida* serotype A provided some interesting insight into the metabolic diversity of isolates within this single serotype. Growth of these isolates in the Microreactor 24-well fermenter enabled environmental parameters to be tightly controlled, and these parameters were selected specifically to replicate the bovine lung environment.

Differences in growth rates between isolates in iron-replete conditions suggested phenotypic variations between the isolates and indeed when growth rates were compared in iron-restricted conditions, an approximate 10-fold decrease in growth rate was seen for each isolate. One hypothesis which will be explored further is that isolates with slower growth rates are more virulent *in vivo*. Indeed, isolate 671/90, previously shown to be a particularly pathogenic strain, had a slower growth rate in iron-replete and iron-restricted conditions than did isolate 45/04, previously shown to cause more limited pathology *in vivo* (data not shown).

For the most part, total protein content and glucose uptake of each of the isolates correlated well with growth rates, although there were some interesting differences. With respect to total protein content, isolate 671/90 had a higher content than isolates 45/04 and 200038/A despite its lower growth rate. Perhaps this resulted from increased expression of IROMPs and other virulence-associated proteins by 671/90 and in turn, this may also explain the lower growth rates seen for 671/90 due

to re-routing of energy from cell replication to protein synthesis and expression. In addition, glucose uptake for isolate 671/90 was high, given the relatively low growth rate. Isolate 45/04 showed a sharp increase in glucose uptake rate between 4 and 8 hours in iron-restricted conditions which coincided with an increase in growth rate during the same period, however, total protein content was lower than that of 671/90 and approximately the same as 200038/A, suggesting that the energy derived from this high glucose uptake was used for cell replication rather than for an up-regulation of protein expression.

A detailed analysis of the effects of altering a number of environmental parameters on the growth and metabolism of isolate 671/90 yielded some interesting data. Comparing culture of 671/90 at 37°C versus 39°C, growth rate at 39°C was severely perturbed in comparison with growth rate at 37°C. However, total protein content and glucose uptake rates in both conditions were similar. Again, these data suggested a diversion of energy derived from glucose uptake and metabolism to power protein synthesis and expression rather than for cell replication when cultures were grown at 39°C. Given that 39°C is within the normal core temperature range of the bovine host (Iqbal and Hunter, 1995), this slow growth rate, rapid glucose uptake and high protein expression may reflect what is happening in the lung *in vivo*. A comparison of culture at pH 6.0 vs pH 8.0 at 37°C revealed higher growth rates at pH 8.0 compared with pH 6.0, and interestingly when the comparison was repeated at 30°C values for growth rate and total protein content were similar to those seen at 37°C. This would suggest that *P. multocida* 671/90 can grow almost as effectively at 30°C as at 37°C and may be related to the ability of *P. multocida* to

persist in the nasal passages of cattle where the temperature is likely to be lower than core body temperature.

The measurement of bacterial ATP levels, dry weights and live counts from *P. multocida* grown in iron-replete and iron-restricted conditions provided important data for validation of the *in silico* model of iron acquisition developed in **Chapters 3** and **4**. Previous cultures grown in the Biostat-Q and the Microreactor were aerated, however, cultures grown in this experiment were grown in shaking flasks and as such were not aerated. This resulted in slower growth rates both in iron-replete and iron-restricted conditions compared with similar experiments carried out in the Microreactor.

With respect to dry weight, iron-replete cultures showed higher dry weights per ml culture than did iron-restricted cultures, as expected due to the higher growth rate of the former. However, when dry weight per CFU was calculated, it was observed that during log phase and plateau, the dry weight per CFU decreased substantially both in iron-replete and iron-restricted conditions. This is most likely due to high cell turnover and rapid replication during log phase, and in plateau the depletion of nutrients preventing any increase in relative biomass. However, comparatively, iron-restricted cultures showed higher dry weight per CFU than iron-replete cultures. This is probably a consequence of the lower growth rate and lack of log phase growth in the iron-restricted cultures, but could also be attributed to increased expression of IROMPs resulting in a higher relative biomass for iron-restricted bacteria.

Measurement of bacterial ATP concentrations revealed higher concentrations in iron-replete cultures in log phase and plateau than iron-restricted cultures. However, iron-restricted bacteria had a higher dry weight per CFU than iron-replete bacteria and indeed when ATP concentration was normalised it was observed that iron-restricted cultures had a higher concentration of ATP per CFU than iron-replete cultures. One suggestion could be that this higher ATP concentration in iron-restricted cultures is needed for increased IROMP expression and active transport of iron, both processes facilitated by ATP hydrolysis (Shouldice *et al*, 2004). This hypothesis is supported by the earlier observation, based on the *in silico* reconstruction of *P. multocida* iron acquisition, that ATP plays a crucial role in both protein synthesis and iron acquisition.

5.5 Conclusions

The *in vitro* analyses of several *P. multocida* strains presented here provided a number of important findings. Most importantly, these data could be used directly for validation of the *in silico* model of *P. multocida* iron acquisition, and this work is described in detail in the following chapter. However, a number of predictions related to the virulence of *P. multocida in vivo* were also made. The first was that the growth rate of virulent strains *in vivo* is predicted to be slow, and that there is a high level of protein expression driven by rapid glucose uptake and metabolism. Directly related to this was the observation that iron-restricted bacteria, characteristic of the *in vivo* environment, had relatively high levels of ATP per bacterium, presumed to be generated from metabolised glucose and driving protein

expression. Second was the observation that *P. multocida* could grow successfully at 30°C; a finding with implications for survival and growth of *P. multocida* within the bovine nasal cavity and also in the environment.

Taken together, these findings suggest a novel model for *in vivo* pathogenesis of *P. multocida* causing pneumonic pasteurellosis in cattle, as follows. Growth rate of *P. multocida* in the bovine lung is slow initially due to a diversion of ATP generated by glucose uptake and metabolism towards expression of IROMPs and other virulence-associated proteins rather than to drive cell replication. Expression of IROMPs and other virulence factors triggers an immune response from the host resulting in host cell damage, through neutrophil recruitment and degranulation. Inadvertent damage to host tissue may then lead to release of nutrients. These nutrients may be utilised directly by *P. multocida* enabling a down-regulation of expression of IROMPs and other transporters and the diversion of ATP to drive increased cell replication, resulting in an exponential increase in numbers of bacteria. These data are supported by the finding of Palyada, Threadgill and Stintzi (2004) that in *Campylobacter jejuni* addition of iron to iron-restricted cultures results in down-regulation of iron acquisition-related genes and up-regulation of protein synthesis-associated genes. Therefore, it is proposed that the harsher an environment in which a bacterium is grown, the more virulent it becomes; a direct consequence of low nutrient availability resulting in expression of virulence-associated factors initiating a series of events exacerbating pathogenesis of *P. multocida*.

Chapter 6. Functional extension and *in vitro* validation of the *in silico* model of iron acquisition in *P. multocida*

6.1 Introduction

In **Chapters 3** and **4**, an *in silico* framework of iron acquisition by *P. multocida* was described based upon the structural properties of the metabolic network. In **Chapter 5**, a series of *in vitro* experiments studied the effects of varying culture conditions on key metabolic processes of *P. multocida*, with particular emphasis on measurement of metabolites relevant to the *in silico* model. In this chapter, functionality was added to the structural model and validated based upon *in vitro* measurements of bacterial growth, glucose uptake, total protein and ATP concentration using *P. multocida* 671/90 grown in iron-replete and iron-restricted conditions.

Analyses in **Chapter 3** described mainly the structural properties of the network and here FBA allowed the integration of experimental data as a means of validating the *in silico* model. An extension of elementary modes analysis, FBA allowed the inclusion of so-called constraints for each reaction based upon experimental measurements of reaction fluxes. The network was then optimised to maximise output of a chosen objective coefficient, in this case maximal biomass, although the objective coefficient could also have been maximal production of a given product. This method of analysis has been employed in many studies, most recently for analysis of an *in silico* model of human metabolism (Mo, Jamshidi and Palsson, 2007), and formerly to analyse many whole-genome scale models of bacterial

metabolism (Lee *et al*, 2008; Nookaew *et al*, 2008; Oberhardt *et al*, 2008; Schilling *et al*, 2002).

The aim here was to derive flux rates from experimental measurements made in **Chapter 5** and to include these as constraints in a FBA model of *P. multocida* iron acquisition based upon the earlier elementary modes-based model. Integration of these data would test the validity of the model and, if necessary, guide any alterations of the model to fit the experimental data.

6.2 Aims and methodology

6.2.1 Construction of an *in silico* model of *P. multocida* iron acquisition suitable for FBA analysis

Most *in silico* metabolic models are constructed to conform to the Systems Biology Markup Language (SBML) format (Hucka *et al*, 2003). This standard is compatible with a majority of software packages designed for analysis of metabolic models and allows inclusion of flux constraints. As such, it was desirable that the current model should conform to this standard. The *in silico* model described previously in **Chapters 3** and **4** was curated in the YANA elementary modes analysis software and this program allowed export of the model as an SBML-compatible file (Schwarz *et al*, 2005). It was necessary to add manually the constraints data to this file before a FBA could be carried out. In this case, the units used for constraints were millimoles of metabolite per gram dry weight of bacteria per hour (mmol/gDW/hr).

As the measurement of every flux in the model was not feasible, constraints could not be defined accurately for every reaction. However, an advantage of constraints-based modelling was that constraints could be set as upper and lower bounds (Price *et al*, 2003). Thus, if experimentally measured flux data were not available for a reaction, then the upper bound was set to an arbitrarily large value, in this case 1 x 10^{30} mmol/gDW/hr. If a reaction was irreversible the lower bound was set to 0 and if a reaction was specified as reversible the lower bound was set to -1 x 10^{30} mmol/gDW/hr. In this way, reversibility of each reaction could be specified in the SBML file. Where *in vitro* data were available quantifying flux rates, for example protein production, glucose uptake and ATP production, these data were used as upper constraints for the corresponding reactions in the model.

As mentioned, a FBA model allows optimisation of a given objective of the model, in most cases maximal biomass. This is specified in the model as a biomass reaction, called here vGROWTH and denoted in the SBML file as "VGRO". As the biomass reaction is optimised during the FBA, for the analysis to give a positive increase in biomass, all metabolites included as reactants in the biomass reaction must be able to be produced by the network. In a whole genome scale metabolic model, the biomass reaction would include all metabolites needed to produce a viable bacterium, however, these data had not been measured experimentally for *P. multocida* and the current model was not of a whole genome scale. As a result, metabolites selected for inclusion in the VGRO reaction were based upon their necessity in the current limited model (**Fig. 3.1**). These biomass reactants were: "FE_INCORP", "FE_STORED", "protein", "Ton_system", "HGBA", "HGBB", "YFEA",

"YFEBCD", "TBPA", "FBPA" and "FBPBC" (**Fig. 3.9**). The sole product of the VGRO reaction was named "BIOMASS". As all reactions in the model were required to be stoichiometrically-balanced, stoichiometries had to be specified in the VGRO reaction. As these were not experimentally measured as part of the current work, arbitrary values were chosen based upon the approximate number of proteins expressed by *P. multocida* (2015) and the amount of protein per gram dry weight during log phase growth in iron-replete conditions. Stoichiometries for "FE_INCORP" and "FE_STORED" (0.1125 and 0.1125 respectively) were derived from the data of Yamamoto *et al* (2004), which stated that the average concentration of intracellular iron in wild type *Streptococcus mutans* is approximately 225 μM.

6.2.2 Calculation of metabolic flux rates for protein production, glucose uptake and ATP production in iron-replete and iron-restricted *P. multocida* 671/90 cultures

Flux rates were derived from data on bacterial growth rates, dry weight and ATP concentration from **Section 5.3.3** and from data on glucose uptake and protein concentration in **Section 5.3.2** (iron-replete and iron-restricted conditions, 39°C). These values were calculated as mmol/gDW/hour.

As discussed previously, elementary modes and FBA models assume that the system studied is at a steady state (Stelling *et al*, 2002), allowing the assumption that inputs to the system correlate exactly with outputs. In this case, in iron-replete conditions, data from log phase growth were taken to represent a pseudo-steady state and were used for calculation of flux rates.

6.2.3 FBA analysis and validation of model

Experimentally-derived constraints were imposed on the model and an FBA optimisation performed using the COBRA Toolbox (Becker *et al*, 2007) and MatLab (The Mathworks). The objective coefficient for the VGRO reaction was set to 1.0 (i.e. maximal biomass).

Initially, 2 scenarios were simulated using the model. The first was iron-replete growth, based upon experimentally-derived constraints for *P. multocida* 671/90. The second was iron-restricted growth of the same isolate with constraints derived from the same experimental data.

Next, a number of scenarios suggested by the structural studies in **Chapters 3** and **4** were simulated. These were:

1. The effect of glucose availability on iron uptake
2. The effect of oxygen starvation on iron uptake, glucose uptake, ATP production and total protein
3. Biomass output for iron uptake from haemoglobin versus transferrin

These scenarios were simulated by: 1) imposing a series of 10-fold increases and decreases on the glucose uptake constraint and recording the biomass output; 2) setting the upper bound for oxygen uptake to 0 and observing effects on the model; and 3) Setting the upper bound to 0 for haemoglobin uptake and transferrin uptake in turn and observing the effect on biomass output.

6.3 Results

6.3.1 Construction of an *in silico* model of *P. multocida* iron acquisition suitable for FBA analysis

The previously developed model of *P. multocida* iron acquisition (**Fig. 3.1**) was modified to allow simulations to be carried out using FBA. As part of this modification it was necessary to add 3 intermediate ATP transfer reactions named "ATP_trans1", "ATP_trans2" and "ATP_trans3", as follows:

ATP_trans1: $ATP \rightarrow ATP2$

ATP_trans2: $ATP2 \rightarrow ATP\_iron$

ATP_trans3: $ATP2 \rightarrow ATP\_protein$

Inclusion of these 3 reactions allowed a constraint to be added to the "ATP_trans1" reaction based upon experimental measurements of ATP production described in **Section 5.3.3**. Calculation of this constraint is described in **Section 6.3.2**.

As mentioned in **Section 6.2.1**, stoichiometries of the 8 outer membrane iron acquisition components in the biomass reaction were calculated based approximately upon the number of expressed proteins in *P. multocida* (2015) and mmol/gDW/hr of protein during log phase growth of *P. multocida* isolate 671/90 in iron-replete conditions. It should be noted that these stoichiometries are arbitrary values only and accurate values would require experimental quantification of each protein *in vitro*. The complete list of biomass stoichiometries in shown below in **Table 6.1**.

Metabolites	Stoichiometry
Reactants	
FE_INCORP	0.1125
FE_STORED	0.1125
Protein	2.8×10^{-6} (1.9×10^{-11} for iron res.)
Ton_system	4.17×10^{-9}
HGBA	1.39×10^{-9}
HGBB	1.39×10^{-9}
YFEA	1.39×10^{-9}
YFEBCD	4.17×10^{-9}
TBPA	1.39×10^{-9}
FBPA	1.39×10^{-9}
FBPBC	2.78×10^{-9}
Products	
Biomass	1.0

Table 6.1: Stoichiometries of metabolites in the biomass reaction "VGRO" of the FBA model of *P. multocida* iron acquisition. Note the lower protein stoichiometry for iron restricted conditions.

6.3.2 Calculation of metabolic flux rates for protein production, glucose uptake and ATP production in iron-replete and iron-restricted *P. multocida* 671/90 cultures

Dry weights, ATP concentrations and growth rates of *P. multocida* 671/90 cultured in iron-replete and iron-restricted conditions were detailed in **Section 5.3.3** whilst total protein and ATP concentrations were measured in **Section 5.2.2**. Log phase growth of iron-replete cultures occurred between 3 and 6 hours, and data within this period were used for calculations of flux rates. Standard units for flux rates in *in silico* models are mmol/gDW/hr and as such, concentrations of protein, glucose and ATP measured in mg/ml, μg/ml and nanomoles respectively had first to be converted to millimolar concentrations and second normalised according to dry weight. Calculated values for protein, glucose and ATP flux rates in iron-replete conditions were 2.8×10^{-6}, 1.3 and 3.9×10^{-2} mmol/gDW/hr respectively. Data from the same period were used for calculation of iron-restricted flux rates, although it should be

noted that these cultures did not enter log phase during the 8-hour culture. Values for protein, glucose and ATP flux rates in iron-restricted conditions were and 1.9×10^{-11}, 0.9 and 7.0×10^{-4} mmol/gDW/hr respectively.

These data were used as constraints in the *in silico* model and used to simulate iron-replete and iron-restricted conditions, the results of which are described in the following section. Constraints were set for reactions "P85" (**Table 3.6**), "G1" (**Table 3.1**) and "ATP_trans2" (see **Section 6.3.1**) to constrain protein production, glucose uptake and ATP production respectively.

6.3.3 FBA analysis and validation of model

Iron-replete growth

Constraints were added based upon data described in the previous section. Biomass output for growth in these conditions was 0.3467 mmol/gDW/hr.

Iron-restricted growth

Constraints were added based upon data described in the previous section. Biomass output for growth in these conditions was 0.0062 mmol/gDW/hr.

The effect of glucose availability on biomass

The constraint value for the "G1" glucose uptake reaction of 1.3 mmol/gDW/hr was multiplied in 10-fold steps between 0.00013 to 1300 in iron-replete conditions. In iron-restricted conditions the rate for the same reaction was multiplied in 10-fold

steps between 0.00009 and 900. The effects on the biomass outputs of the network in both cases were recorded and graphed (**Fig. 6.1**).

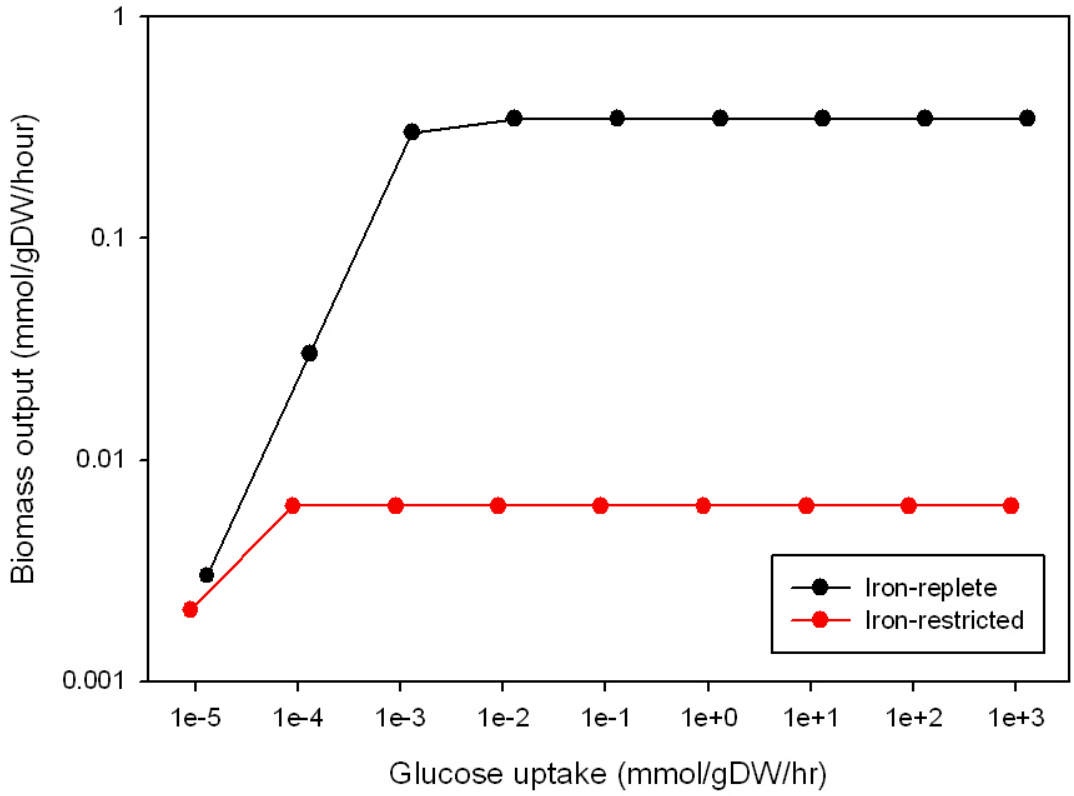

Fig. 6.1: Graph showing the effect of 10-fold increases or decreases in glucose uptake constraint on biomass in iron-replete and iron-restricted conditions.

The effect of oxygen starvation on biomass

This scenario was simulated by setting the upper bound constraint of the oxygen uptake reaction "UP_OXY" to 0 and then observing the effect on biomass of the system. When this simulation was modelled there was no biomass output.

Biomass output for iron uptake from haemoglobin versus transferrin

These 2 scenarios were modelled by setting upper bound constraints for transferrin and haemoglobin uptake reactions to 0 respectively and then observing the effect on

biomass output in iron-replete and iron-restricted conditions. When haemoglobin was the sole source of iron for the system the biomass output was 0.3467 in iron-replete conditions and 0 in iron-restricted conditions. When transferrin was the sole source of iron the biomass output was 0.1733 in iron-replete conditions and 0 in iron-restricted conditions.

6.4 Discussion

Functional extension of the existing structural model of iron acquisition by *P. multocida* 671/90 allowed a number of simulations to be carried out based on *in vitro* measurements made in **Chapter 5** and the feasibility of these data to be assessed.

When constraints were added based upon data from iron-replete and iron-restricted conditions, biomass output was approximately 56 times lower in iron-restricted conditions than in iron-replete conditions. When these figures were compared to growth rates from iron-replete and iron-restricted bacteria grown *in vitro* (**Section 5.3.3**) it was found that growth rate (live counts, CFU/ml/hour) in iron-restricted conditions was approximately 58 times lower than in iron-replete conditions for the period between 4 and 6 hours in both cases. This represents an error of only 5% in between the predicted *in silico* biomass and *in vitro* measurements - a remarkable similarity.

Data in **Fig. 6.1** observing the effects of 10-fold increases or decreases in glucose uptake rates on biomass seemed to suggest that iron-restricted bacteria were more tolerant to a reduction in glucose uptake rate compared with iron-replete bacteria.

However, increasing glucose uptake rate by 3 orders of magnitude had no effect on biomass in either condition indicating that the original glucose uptake rates provided sufficient glucose to generate the required biomass. The tolerance of iron-restricted bacteria to a decrease in glucose uptake rate fits with the observation of low biomass in iron-restricted cultures *in vitro*.

The observation that oxygen starvation resulted in an inability to generate biomass may have implications *in vivo*. Preliminary data indicate that growth of *P. multocida* in microaerophilic conditions, that is with low oxygen availability, may favour biofilm formation. It is known that bacteria within biofilms are almost static in terms of growth and metabolism (Kobayashi, 2005; Merritt, Kadouri and O'Toole, 2005), reflected here by an inability to generate biomass when oxygen is limited. The role of biofilms in *P. multocida* infection *in vivo* will be discussed in detail in **Chapter 7**.

Finally, an analysis of the effect of providing either haemoglobin or transferrin alone as the sole source of iron in iron-replete or iron-restricted conditions revealed two key points. First, was the possibility of a role for transferrin in early colonisation when biomass is low and haemoglobin availability is limited. Only when the host immune response results in release of nutrients including haemoglobin, does biomass increase, driven by the ability of haemoglobin to generate greater biomass than transferrin.

6.5 Conclusions

The adaptation of the existing structural model of *P. multocida* iron acquisition allowed FBA simulations to be carried out and revealed a remarkably close fit between *in silico* and *in vitro* data.

When *in vitro* and *in silico* data were compared a number of key hypotheses were suggested, all of which gave strength to the proposed model of *P. multocida* pathogenesis presented in **Section 5.5**. A strength of this set of experiments was that integration of *in silico* and *in vitro* data allowed pertinent observations to be made relating to disease caused by *P. multocida in vivo*. Furthermore, these findings offer promising insight into the previously ambiguous role of iron acquisition as a bacterial virulence factor and have implications for potentially novel disease treatment strategies. These implications will be discussed at length in **Chapter 7**.

Chapter 7. General discussion

7.1 Construction of an *in silico* model of iron acquisition by *P. multocida*

An increasing number of studies are utilising *in silico* metabolic models as part of systems biology approaches to study not only bacterial systems (Lee *et al*, 2008; Nookaew *et al*, 2008), but also systems of higher organisms, for example humans (Mo, Jamshidi and Palsson, 2007) and insects (Feala *et al*, 2007). These models allow predictions to be made with minimal prior *in vitro* data and provide a source of hypotheses for validation *in vitro*. A majority of these models are of a whole genome scale, however a number of factors made *P. multocida* intractable to study on a whole genome scale. First, preliminary data suggests that the published genome of *P. multocida* PM70 may be of significantly smaller size than some other strains of *P. multocida* A:3. Therefore any attempt to build a whole genome scale model of *P. multocida* may result in a significant number of metabolic reactions being excluded, resulting in an inaccurate model. Second, the manual annotation of a whole genome scale model is a time-consuming exercise and in this case it was felt that the construction of such a model for a limited *in vitro* study would be impractical.

Despite the limited size of the model presented here, predictions made based upon the model fitted the *in vitro* data closely and revealed a number of noteworthy observations. Structural analyses revealed that the network was robust against perturbation and that the values presented for robustness may even have been underestimated. This robustness highlighted redundancy in the iron uptake

mechanisms, likely due to the vital role of iron in bacterial survival and replication. However, the Ton system was revealed to be crucial for the normal function of both the transferrin and haemoglobin-based iron uptake pathways, as evidenced by the high FC values of Ton system-related reactions. As such, the Ton system may represent a potential target for perturbation of iron uptake by *P. multocida* and hence control of infection *in vivo*.

Analysis of FC values proved a useful means of identifying potentially novel hypotheses with relevance to *P. multocida in vitro* and *in vivo*. One such finding was high FC values of reactions related to iron uptake from haemoglobin indicating high flux through those reactions. These results were strengthened further by FBA simulations which suggested that with haemoglobin as its sole iron source, *P. multocida* could generate greater biomass than with transferrin as the sole source of iron. Taken together with *in vitro* data suggesting slower growth rate and hence increase in biomass when *P. multocida* is grown in harsh environmental conditions, these data may suggest that the source iron *in vivo* in these conditions is transferrin. Only when the host immune response to *P. multocida* results in release of nutrients including haemoglobin, as evidenced by significant haemorrhage in *P. multocida* infected lungs (Dowling *et al*, 2002), does growth rate and hence biomass of *P. multocida* increase significantly.

Investigations of path lengths of elementary modes in relation to flux through them, indicated that elementary modes of short path length, low flux and high energy efficiency may play a housekeeping role in iron acquisition providing constant low

level flux of iron into bacteria when sufficient iron is available in the environment. Only in times of iron deficit in the environment were less efficient, longer pathways with higher flux favoured. This finding fitted directly with the observation *in vitro* that energy in the form of ATP was likely diverted from its role in cell replication to power expression of proteins involved in iron uptake when *P. multocida* was grown in iron-restricted conditions. Conversely, in iron-replete conditions lower protein expression was seen and it was postulated that energy in the form of ATP was used mostly for cell replication. These findings were consistent with the work of Palyada, Threadgill and Stintzi (2004) which suggested that on addition of iron to iron-restricted cultures of *C. jejuni* iron-acquisition-related genes were down-regulated and protein synthesis-associated genes were up-regulated.

7.2 Investigations *in vitro* of key metabolic process of *P. multocida*

It is noteworthy that few studies have examined in detail the role of metabolic changes in relation to bacterial virulence and pathogenesis, although a number of studies by Smith (Smith, 2000a; Smith, 2000b; Smith *et al*, 2001) address the metabolic interactions between host and pathogen. As such, this thesis represents one of the few detailed studies of key metabolic processes of a bacterium in relation to their interaction with the host, and particularly with relevance to iron acquisition.

The study *in vitro* of effects on metabolism when different environmental conditions were imposed on *P. multocida* culminated in a detailed study of the effect of iron-restriction on key metabolic factors of *P. multocida*. As a whole, data in the chapter

suggested a novel finding that growth of *P. multocida* in harsh environmental conditions may enhance virulence of the organism through increased expression of potentially immunogenic proteins. These hostile conditions were elicited by imposing a series of environmental stressors on *P. multocida* including iron-restriction and extremes of both pH and temperature; all characteristics likely to be found *in vivo*.

It was noted that dry weight of bacteria grown in iron-restriction was higher relative to dry weight of bacteria grown in iron-replete conditions. This poses a paradox in relation to what might have been expected. However, when the deviations between estimated viable counts and live counts of *P. multocida* grown in iron-replete and iron-restricted conditions were examined this paradox could be resolved. An increase in the ratio of live count:estimated viable count suggested a decrease in size of bacteria during log phase growth. However, during iron-restricted growth this ratio first increased and then decreased towards the end of the culture period. As bacteria in these conditions did not enter log phase, it was hypothesised that rather than an increase in relative bacterial size this represented an increase in the number of dead bacteria as a result of the nutritionally-limited conditions imposed. Furthermore, the decrease in bacterial size in the initial period of iron-restricted growth may have implications *in vivo* in relation to biofilm formation.

Biofilms have been shown to be formed by a number of bacterial species (Longhi *et al*, 2008; Petrelli *et al*, 2008; Sausville *et al*, 2008). These isolated communities of bacteria form in response to defined environmental conditions resulting in increased

expression of adhesins and matrix proteins and a slowing of metabolism and replication (Kobayashi, 2005; Merritt, Kadouri and O'Toole, 2005). The formation of biofilms has also been shown to make bacteria particularly resistant to antimicrobial clearance (Kobayashi, 2005). Preliminary data from this laboratory suggest a possible role of *P. multocida* biofilm formation *in vivo*, particularly in the nasopharynx where commensal carriage is known to occur in approximately 17% of clinically-healthy cattle (also preliminary data). In a closely-related organism, *M. haemolytica*, iron-restricted conditions were found to favour microcolony formation (Rowe, Poxton and Donachie, 2001), a factor also thought to be involved in biofilm formation. The initial decrease in size of *P. multocida* grown in iron-restricted conditions may reflect this phenomenon. In addition, slower growth rates and increased protein expression seen in iron-restricted cultures of *P. multocida* may suggest phenomena indicative of biofilm formation.

7.3 Functional extension and *in vitro* validation of the *in silico* model of iron acquisition in *P. multocida*

Modification of the structural model of *P. multocida* iron acquisition allowed FBA and simulations of key scenarios to be carried out. These analyses showed *in silico* predictions of biomass of *P. multocida* in iron-replete and iron-restricted conditions to be extremely close to values measured *in vitro*. Indeed, there was a less than 5% discrepancy in the predicted value for biomass of *P. multocida* in iron-restricted conditions compared with biomass in iron-replete conditions.

The 3 simulations of *in vivo* scenarios all produced interesting findings. First, the observation that glucose uptake could be reduced several orders of magnitude with no effect on biomass in both iron-replete and iron-restricted conditions may reflect the limited size of the model. As many metabolic pathways were not included in the current model, this apparent excess of glucose may represent glucose normally metabolised through these missing pathways.

Next, it was noted that starving the system of oxygen resulted in a failure to increase biomass. Although *P. multocida* is known to be a facultative anaerobe, and the current model did not include any anaerobic respiratory pathways, it is likely that a reduction in environmental oxygen availability would result in a significant decrease in biomass. It is known that microaerophilic conditions favour formation of bacterial biofilms (Mehrotra, 2007), and preliminary data have shown this to be the case for *P. multocida in vitro*. Perhaps this low environmental oxygen availability results in a decrease in biomass and resultant slowing of metabolism. This may in turn trigger key factors, such as increased adhesin and matrix protein expression that culminate in the formation of a *P. multocida* biofilm.

The final simulation resulted in another hypothesis linked to the model of *P. multocida* colonisation and disease progression proposed in **Section 5.5**. This was that the provision of transferrin as the sole iron source for *P. multocida* resulted in a significantly (approximately 50%) lower biomass in iron-restricted conditions than when haemoglobin was also provided. When this analysis was repeated in iron-restricted conditions, there was a complete failure to increase biomass. In contrast,

when haemoglobin was provided as the sole iron source there was no change in biomass compared to wild type in iron-replete conditions, and again a failure to produce biomass in iron-restricted conditions. This suggests that transferrin is a less efficient source of iron for *P. multocida* resulting in lower potential biomass and a potentially lower iron uptake in iron-restricted conditions than set in the biomass equation. Again, this finding fits with the proposal that haemoglobin released as a result of tissue damage in the latter stages of infection results in a dramatic increase in the biomass of *P. multocida in vivo*.

7.4 Relevance to *P. multocida* infection *in vivo* in cases of pneumonic pasteurellosis

Currently, there are few effective prophylactic or therapeutic strategies for treating pneumonic pasteurellosis caused by *P. multocida*. This is, in part, due to a lack of knowledge of key *P. multocida* virulence factors and of the pathogenesis of the organism *in vivo*. Despite initially being a study of *P. multocida* iron acquisition, the *in silico* and *in vitro* analyses and their comparison have presented a number of new hypotheses related to biofilm formation, energy provision and a proposed model of colonisation and disease progression.

The modern age of disease therapeutics and vaccine design is based upon detailed knowledge of pathogen lifestyles *in vivo* and key elements of the disease process (Cheminay and Hensel, 2008). Systems biology is proving a useful study method in this field (Braga-Neto and Marques, Jr., 2006), and large-scale analyses are uncovering key findings missed previously in more focussed studies. The insights

provided by the *in silico* and *in vitro* approaches described here suggest two opportunities for potential therapies. The central role of the Ton system in iron acquisition by *P. multocida* from both haemoglobin and transferrin indicates that a Ton system-deficient mutant may be significantly attenuated in terms of virulence and such a mutant may be a potential live attenuated vaccine candidate. Second is the observation that growth of *P. multocida* in environmentally-harsh conditions may result in an increase in virulence and in expression of potentially immunogenic proteins. A similar finding was exploited in the production of a vaccine against pneumonic pasteurellosis caused by *M. haemolytica*, which involved growth of the organism in iron-restricted conditions and inoculation with isolated outer membrane proteins (Gilmour *et al*, 1991). The suggestion here is that inclusion of additional stressors such as lower temperature, lower pH or glucose limitation may result in increased expression of immunogenic proteins which could be used either as a subunit vaccine or killed bacterin.

7.5 Proposed model of *P. multocida* pathogenesis

The diagram below (**Fig. 7.1**) presents the proposed model for *P. multocida* pathogenesis, suggested by the *in silico* and *in vitro* analyses presented here.

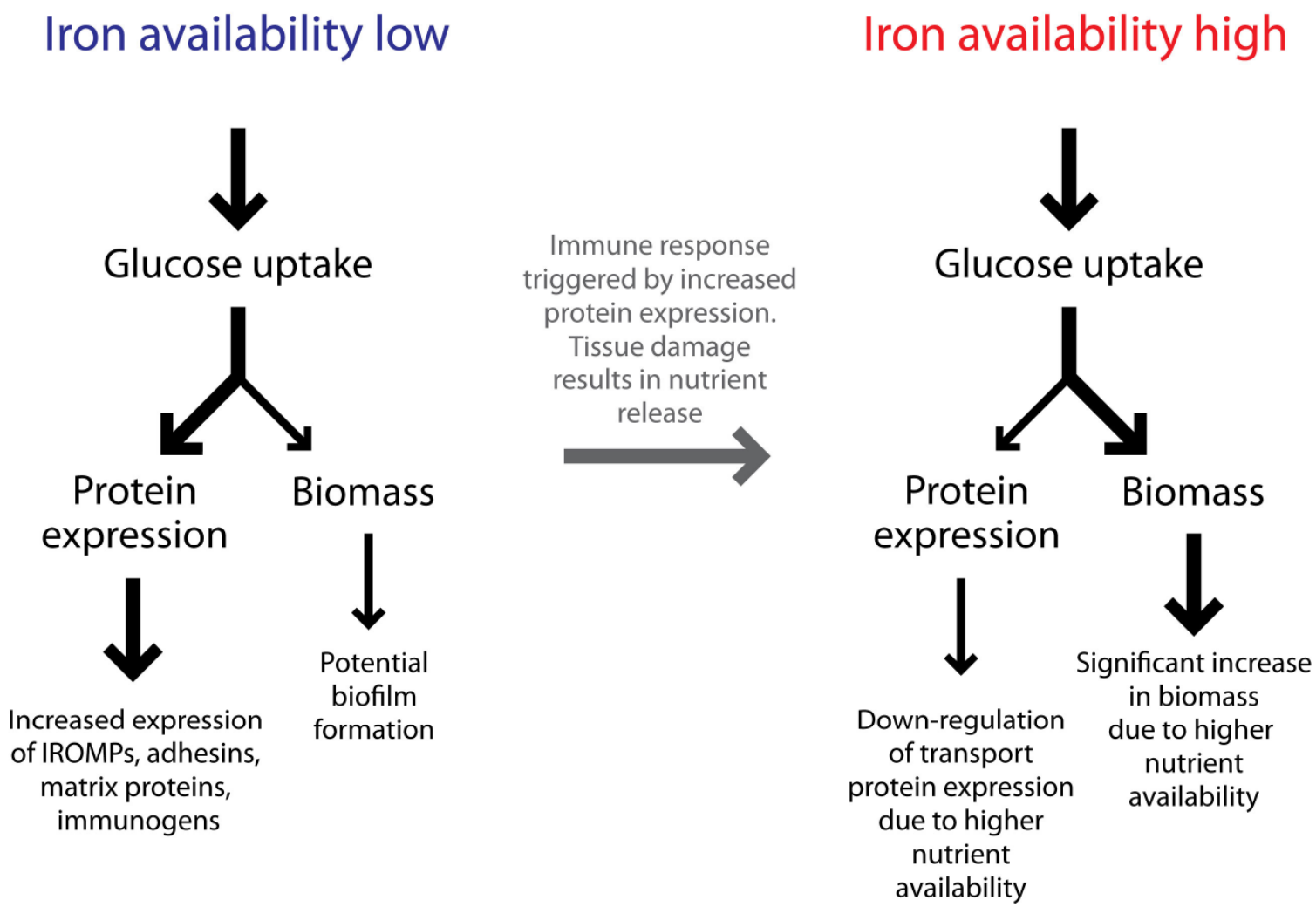

Fig. 7.1: Schematic diagram showing proposed mechanism of *P. multocida* pathogenesis based on *in silico* and *in vitro* data (thickness of arrows represents relative flux).

7.6 Conclusions and future opportunities

The *in silico* and *in vitro* data presented here suggest a novel mechanism for pathogenesis of *P. multocida in vivo*, and several insights have been offered as to the role of iron acquisition; in particular the effects of iron-restriction on virulence. Two potential therapeutic strategies have been identified that may offer promise in the treatment of pneumonic pasteurellosis caused by *P. multocida*, a disease of significant economic cost and welfare significance (Dowling *et al*, 2004; Mosier, Confer and Panciera, 1989).

Key to these findings was the development of an *in silico* reconstruction of iron acquisition by *P. multocida*, although the model was of limited scale as time did not permit construction of a whole genome scale model. No doubt the construction of such a model would offer additional insight into this fascinating area.

In addition, it would be interesting to apply the *in vitro* metabolic assays developed here to samples *in vivo* from disease cases and to compare with *in vitro* and *in silico* data presented here. Doing so would provide confirmation of the model hypothesis of *P. multocida* pathogenesis proposed (**Fig. 7.1**).

To conclude, the data presented here have offered fresh insight into an area where many questions lay unanswered. They have allowed the identification of potentially novel control strategies which may have applications in treatment of other diseases, and as a whole the study highlights the key role of systems approaches in the future of biology.

References

Adler B, Bulach D, Chung J *et al.* Candidate vaccine antigens and genes in *Pasteurella multocida*. *J Biotechnol* 1999; 73: 83-90.

Allen JW, Viel L, Bateman KG, Nagy E, Rosendal S, Shewen PE. Serological titers to bovine herpesvirus 1, bovine viral diarrhea virus, parainfluenza 3 virus, bovine respiratory syncytial virus and *Pasteurella haemolytica* in feedlot calves with respiratory disease: associations with bacteriological and pulmonary cytological variables. *Can J Vet Res* 1992a; 56: 281-288.

Allen JW, Viel L, Bateman KG, Rosendal S. Changes in the bacterial flora of the upper and lower respiratory tracts and bronchoalveolar lavage differential cell counts in feedlot calves treated for respiratory diseases. *Can J Vet Res* 1992b; 56: 177-183.

Allen JW, Viel L, Bateman KG, Rosendal S, Shewen PE, Physick-Sheard P. The microbial flora of the respiratory tract in feedlot calves: associations between nasopharyngeal and bronchoalveolar lavage cultures. *Can J Vet Res* 1991; 55: 341-346.

Allen TE, Palsson BO. Sequence-based analysis of metabolic demands for protein synthesis in prokaryotes. *J Theor Biol* 2003; 220: 1-18.

Andrews SC, Robinson AK, Rodriguez-Quinones F. Bacterial iron homeostasis. *FEMS Microbiol Rev* 2003; 27: 215-237.

Bagg A, Neilands JB. Molecular mechanism of regulation of siderophore-mediated iron assimilation. *Microbiol Rev* 1987; 51: 509-518.

Balla G, Jacob HS, Balla J *et al.* Ferritin: a cytoprotective antioxidant strategem of endothelium. *J Biol Chem* 1992; 267: 18148-18153.

Balla J, Balla G, Lakatos B, Jeney V, Szentmihalyi K. [Heme-iron in the human body]. *Orv Hetil* 2007; 148: 1699-1706.

Balla J, Nath KA, Balla G, Juckett MB, Jacob HS, Vercellotti GM. Endothelial cell heme oxygenase and ferritin induction in rat lung by hemoglobin *in vivo*. *Am J Physiol* 1995; 268: L321-L327.

Baumrucker CR, Gibson CA, Schanbacher FL. Bovine lactoferrin binds to insulin-like growth factor-binding protein-3. *Domest Anim Endocrinol* 2003; 24: 287-303.

Bearden SW, Fetherston JD, Perry RD. Genetic organization of the yersiniabactin biosynthetic region and construction of avirulent mutants in *Yersinia pestis*. *Infect Immun* 1997; 65: 1659-1668.

Becker SA, Feist AM, Mo ML, Hannum G, Palsson BO, Herrgard MJ. Quantitative prediction of cellular metabolism with constraint-based models: the COBRA Toolbox. *Nat Protoc* 2007; 2: 727-738.

Beddek AJ, Sheehan BJ, Bosse JT, Rycroft AN, Kroll JS, Langford PR. Two TonB systems in *Actinobacillus pleuropneumoniae*: their roles in iron acquisition and virulence. *Infect Immun* 2004; 72: 701-708.

Behre J, Wilhelm T, von Kamp A, Ruppin E, Schuster S. Structural robustness of metabolic networks with respect to multiple knockouts. *J Theor Biol* 2008; 252: 433-441.

Bosch M, Garrido E, Llagostera M, Perez de Rozas AM, Badiola I, Barbe J. *Pasteurella multocida exbB, exbD* and *tonB* genes are physically linked but independently transcribed. *FEMS Microbiol Lett* 2002a; 210: 201-208.

Bosch M, Garrido ME, Llagostera M, Perez de Rozas AM, Badiola I, Barbe J. Characterization of the *Pasteurella multocida hgbA* gene encoding a hemoglobin-binding protein. *Infect Immun* 2002b; 70: 5955-5964.

Bosch M, Garrido ME, Perez de Rozas AM, Badiola I, Barbe J, Llagostera M. *Pasteurella multocida* contains multiple immunogenic haemin- and haemoglobin-binding proteins. *Vet Microbiol* 2004; 99: 103-112.

Boyce JD, Adler B. How does *Pasteurella multocida* respond to the host environment? *Curr Opin Microbiol* 2006; 9: 117-122.

Boyce JD, Wilkie I, Harper M, Paustian ML, Kapur V, Adler B. Genomic scale analysis of *Pasteurella multocida* gene expression during growth within the natural chicken host. *Infect Immun* 2002; 70: 6871-6879.

Braga-Neto UM, Marques ET, Jr. From functional genomics to functional immunomics: new challenges, old problems, big rewards. *PLoS Comput Biol* 2006; 2: e81.

Braun V, Killmann H. Bacterial solutions to the iron-supply problem. *Trends Biochem Sci* 1999; 24: 104-109.

Braun V, Schaffer S, Hantke K, Troger W. Regulation of gene expression by iron. Colloquim Mosbach 1990. The molecular basis of bacterial metabolism. Berlin, Germany, Springer-Verlag. 1990.

Briggs RE, Frank GH. Increased elastase activity in nasal mucus associated with nasal colonization by *Pasteurella haemolytica* in infectious bovine rhinotracheitis virus-infected calves. *Am J Vet Res* 1992; 53: 631-635.

Bullen JJ, Rogers HJ, Spalding PB, Ward CG. Iron and infection: the heart of the matter. *FEMS Immunol Med Microbiol* 2005; 43: 325-330.

Cakir T, Kirdar B, Onsan ZI, Ulgen KO, Nielsen J. Effect of carbon source perturbations on transcriptional regulation of metabolic fluxes in *Saccharomyces cerevisiae*. *BMC Syst Biol* 2007; 1: 18.

Cakir T, Tacer CS, Ulgen KO. Metabolic pathway analysis of enzyme-deficient human red blood cells. *Biosystems* 2004; 78: 49-67.

Carlson R, Srienc F. Fundamental *Escherichia coli* biochemical pathways for biomass and energy production: creation of overall flux states. *Biotechnol Bioeng* 2004; 86: 149-162.

Carter GR. Studies on Pasteurella multocida. I. A hemagglutination test for the identification of serological types. *Am J Vet Res* 1955; 16: 481-484.

Catry B, Decostere A, Schwarz S, Kehrenberg C, de KA, Haesebrouck F. Detection of tetracycline-resistant and susceptible pasteurellaceae in the nasopharynx of loose group-housed calves. *Vet Res Commun* 2006; 30: 707-715.

Chang C, Mooser A, Pluckthun A, Wlodawer A. Crystal structure of the dimeric C-terminal domain of TonB reveals a novel fold. *J Biol Chem* 2001; 276: 27535-27540.

Cheminay C, Hensel M. Rational design of *Salmonella* recombinant vaccines. *Int J Med Microbiol* 2008; 298: 87-98.

Choi-Kim K, Maheswaran SK, Felice LJ, Molitor TW. Relationship between the iron regulated outer membrane proteins and the outer membrane proteins of in vivo grown *Pasteurella multocida*. *Vet Microbiol* 1991; 28: 75-92.

Christensen H, Bisgaard M. Taxonomy and biodiversity of members of Pasteurellaceae. In: Kunhert P, Christensen H (eds) Pasteurellaceae; Biology, Genomics and Molecular Aspects. Norfolk, UK, Caister Academic Press. 2008: 1-26.

Clarke TE, Tari LW, Vogel HJ. Structural biology of bacterial iron uptake systems. *Curr Top Med Chem* 2001; 1: 7-30.

Cornelissen CN. Transferrin-iron uptake by Gram-negative bacteria. *Front Biosci* 2003; 8: d836-d847.

Cornish-Bowden A, Hofmeyr JH. The role of stoichiometric analysis in studies of metabolism: an example. *J Theor Biol* 2002; 216: 179-191.

Coutte L, Alonso S, Reveneau N *et al.* Role of adhesin release for mucosal colonization by a bacterial pathogen. *J Exp Med* 2003; 197: 735-742.

Cox AJ, Hunt ML, Boyce JD, Adler B. Functional characterization of HgbB, a new hemoglobin binding protein of *Pasteurella multocida*. *Microb Pathog* 2003; 34: 287-296.

Cozzi A, Santambrogio P, Levi S, Arosio P. Iron detoxifying activity of ferritin. Effects of H and L human apoferritins on lipid peroxidation *in vitro*. *FEBS Lett* 1990; 277: 119-122.

Davis JC, Petrov DA. Preferential duplication of conserved proteins in eukaryotic genomes. *PLoS Biol* 2004; 2: E55.

Dinarello CA. Interleukin-1 and the pathogenesis of the acute-phase response. *N Engl J Med* 1984; 311: 1413-1418.

Dowling A, Hodgson JC, Dagleish MP, Eckersall PD, Sales J. Pathophysiological and immune cell responses in calves prior to and following lung challenge with formalin-killed *Pasteurella multocida* biotype A:3 and protection studies involving

subsequent homologous live challenge. *Vet Immunol Immunopathol* 2004; 100: 197-207.

Dowling A, Hodgson JC, Schock A, Donachie W, Eckersall PD, Mckendrick IJ. Experimental induction of pneumonic pasteurellosis in calves by intratracheal infection with *Pasteurella multocida* biotype A:3. *Res Vet Sci* 2002; 73: 37-44.

Duarte NC, Herrgard MJ, Palsson BO. Reconstruction and validation of *Saccharomyces cerevisiae* iND750, a fully compartmentalized genome-scale metabolic model. *Genome Res* 2004; 14: 1298-1309.

Edwards JS, Covert M, Palsson B. Metabolic modelling of microbes: the flux-balance approach. *Environ Microbiol* 2002; 4: 133-140.

Ekins A, Niven DF. Identification of *fur* and *fldA* homologs and a *Pasteurella multocida tbpA* homolog in *Histophilus ovis* and effects of iron availability on their transcription. *J Bacteriol* 2002; 184: 2539-2542.

Ernst JF, Bennett RL, Rothfield LI. Constitutive expression of the iron-enterochelin and ferrichrome uptake systems in a mutant strain of *Salmonella typhimurium*. *J Bacteriol* 1978; 135: 928-934.

Escolar L, Perez-Martin J, de L, V. Binding of the *fur* (ferric uptake regulator) repressor of *Escherichia coli* to arrays of the GATAAT sequence. *J Mol Biol* 1998; 283: 537-547.

Escolar L, Perez-Martin J, de L, V. Opening the iron box: transcriptional metalloregulation by the Fur protein. *J Bacteriol* 1999; 181: 6223-6229.

Ewers C, Lubke-Becker A, Bethe A, Kiebling S, Filter M, Wieler LH. Virulence genotype of *Pasteurella multocida* strains isolated from different hosts with various disease status. *Vet Microbiol* 2006; 114: 304-317.

Faraldo-Gomez JD, Sansom MS. Acquisition of siderophores in gram-negative bacteria. *Nat Rev Mol Cell Biol* 2003; 4: 105-116.

Feala JD, Coquin L, McCulloch AD, Paternostro G. Flexibility in energy metabolism supports hypoxia tolerance in *Drosophila* flight muscle: metabolomic and computational systems analysis. *Mol Syst Biol* 2007; 3: 99.

Fell DA, Wagner A. The small world of metabolism. *Nat Biotechnol* 2000; 18: 1121-1122.

Finkelstein RA, Sciortino CV, McIntosh MA. Role of iron in microbe-host interactions. *Rev Infect Dis* 1983; 5 Suppl 4: S759-S777.

Fuller TE, Kennedy MJ, Lowery DE. Identification of *Pasteurella multocida* virulence genes in a septicemic mouse model using signature-tagged mutagenesis. *Microb Pathog* 2000; 29: 25-38.

Gagneur J, Klamt S. Computation of elementary modes: a unifying framework and the new binary approach. *BMC Bioinformatics* 2004; 5: 175.

Garfinkel D. Digital computer simulation of systems apparently compartmented at the cellular level. *Ann N Y Acad Sci* 1963; 108: 293-304.

Garrido ME, Bosch M, Medina R *et al*. *fur*-independent regulation of the *Pasteurella multocida hbpA* gene encoding a haemin-binding protein. *Microbiology* 2003; 149: 2273-2281.

Gatto NT, Dabo SM, Hancock RE, Confer AW. Characterization of, and immune responses of mice to, the purified OmpA-equivalent outer membrane protein of *Pasteurella multocida* serotype A:3 (Omp28). *Vet Microbiol* 2002; 87: 221-235.

Genco CA, Dixon DW. Emerging strategies in microbial haem capture. *Mol Microbiol* 2001; 39: 1-11.

Ghio AJ, Turi JL, Yang F, Garrick LM, Garrick MD. Iron homeostasis in the lung. *Biol Res* 2006; 39: 67-77.

Gibbs HA. Practical approach to the control of pneumonia in housed calves. *In Practice* 2001; 23: 32-39.

Gibbs HA, Allan EM, Wiseman A, Selman IE. Experimental production of bovine pneumonic pasteurellosis. *Res Vet Sci* 1984; 37: 154-166.

Gilmour NJ, Donachie W, Sutherland AD, Gilmour JS, Jones GE, Quirie M. Vaccine containing iron-regulated proteins of *Pasteurella haemolytica* A2 enhances protection against experimental pasteurellosis in lambs. *Vaccine* 1991; 9: 137-140.

Griggs DW, Konisky J. Mechanism for iron-regulated transcription of the *Escherichia coli cir* gene: metal-dependent binding of Fur protein to the promoters. *J Bacteriol* 1989; 171: 1048-1054.

Guerinot ML. Microbial iron transport. *Annu Rev Microbiol* 1994; 48: 743-772.

Harper M, Boyce JD, Adler B. *Pasteurella multocida* pathogenesis: 125 years after Pasteur. *FEMS Microbiol Lett* 2006; 265: 1-10.

Higgs PI, Myers PS, Postle K. Interactions in the TonB-dependent energy transduction complex: ExbB and ExbD form homomultimers. *J Bacteriol* 1998; 180: 6031-6038.

Hu SP, Felice LJ, Sivanandan V, Maheswaran SK. Siderophore production by *Pasteurella multocida*. *Infect Immun* 1986; 54: 804-810.

Hucka M, Finney A, Sauro HM *et al.* The systems biology markup language (SBML): a medium for representation and exchange of biochemical network models. *Bioinformatics* 2003; 19: 524-531.

Hunt MD, Pettis GS, McIntosh MA. Promoter and operator determinants for *fur*-mediated iron regulation in the bidirectional *fepA-fes* control region of the *Escherichia coli* enterobactin gene system. *J Bacteriol* 1994; 176: 3944-3955.

Iqbal N, Hunter AG. Comparison of bovine sperm capacitation systems for ability of sperm to penetrate zona-free hamster oocytes and bovine oocytes matured *in vitro*. *J Dairy Sci* 1995; 78: 77-83.

Isaacson RE, Trigo E. Pili of *Pasteurella multocida* of porcine origin. *FEMS Microbiol Lett* 1995; 132: 247-251.

Jericho KW, Carter GR. Pneumonia in calves produced with aerosols of *Pasteurella multocida* alone and in combination with bovine herpesvirus 1. *Can J Comp Med* 1985; 49: 138-144.

Jones PM, George AM. Mechanism of ABC transporters: a molecular dynamics simulation of a well characterized nucleotide-binding subunit. *Proc Natl Acad Sci U S A* 2002; 99: 12639-12644.

Jubb KVF, Kennedy PC, Palmer N. The Respiratory System. Pathology of Domestic Animals. London, Academic Press Ltd. 1963: 539-699.

Kanehisa M, Goto S. KEGG: Kyoto Encyclopedia of Genes and Genomes. *Nucleic Acids Res* 2000; 28: 27-30.

Kerson LA, Garfinkel D, Mildvan AS. Computer simulation studies of mammalian pyruvate kinase. *J Biol Chem* 1967; 242: 2124-2133.

Khan AG, Shouldice SS, Tari LW, Schryvers AB. The role of the synergistic phosphate anion in iron transport by the periplasmic iron binding protein from *Haemophilus influenzae*. *Biochem J* 2006.

Kim PJ, Lee DY, Kim TY *et al.* Metabolite essentiality elucidates robustness of *Escherichia coli* metabolism. *Proc Natl Acad Sci U S A* 2007; 104: 13638-13642.

Kitano H. Looking beyond the details: a rise in system-oriented approaches in genetics and molecular biology. *Curr Genet* 2002; 41: 1-10.

Klamt S, Gilles ED. Minimal cut sets in biochemical reaction networks. *Bioinformatics* 2004; 20: 226-234.

Klamt S, Stelling J. Combinatorial complexity of pathway analysis in metabolic networks. *Mol Biol Rep* 2002; 29: 233-236.

Klamt S, Stelling J. Two approaches for metabolic pathway analysis? *Trends Biotechnol* 2003; 21: 64-69.

Kobayashi H. Airway biofilms: implications for pathogenesis and therapy of respiratory tract infections. *Treat Respir Med* 2005; 4: 241-253.

Koch AL. Turbidity measurements of bacterial cultures in some available commercial instruments. *Anal Biochem* 1970; 38: 252-259.

Koga S, Burg CR, Humphrey AE. Computer simulation of fermentation systems. *Appl Microbiol* 1967; 15: 683-689.

Konopka K, Bindereif A, Neilands JB. Aerobactin-mediated utilization of transferrin iron. *Biochemistry* 1982; 21: 6503-6508.

Lambert LA, Perri H, Meehan TJ. Evolution of duplications in the transferrin family of proteins. *Comp Biochem Physiol B Biochem Mol Biol* 2005; 140: 11-25.

Lee BC. Isolation of haemin-binding proteins of *Neisseria gonorrhoeae*. *J Med Microbiol* 1992; 36: 121-127.

Lee J, Kim YB, Kwon M. Outer membrane protein H for protective immunity against *Pasteurella multocida*. *J Microbiol* 2007; 45: 179-184.

Lee J, Yun H, Feist AM, Palsson BO, Lee SY. Genome-scale reconstruction and *in silico* analysis of the *Clostridium acetobutylicum* ATCC 824 metabolic network. *Appl Microbiol Biotechnol* 2008; 80: 849-862.

Linde CM, Hoffner SE, Refai E, Andersson M. *In vitro* activity of PR-39, a proline-arginine-rich peptide, against susceptible and multi-drug-resistant *Mycobacterium tuberculosis*. *J Antimicrob Chemother* 2001; 47: 575-580.

Litwin CM, Calderwood SB. Role of iron in regulation of virulence genes. *Clin Microbiol Rev* 1993; 6: 137-149.

Longhi C, Cossu A, Iebba V *et al*. Virulence traits in *Escherichia* coli strains isolated from outpatients with urinary tract infections. *Int J Immunopathol Pharmacol* 2008; 21: 715-724.

MacFaddin JF. Media for the isolation-cultivation-identification-maintenance of medial bacteria. Baltimore, Willliams & Wilkins. 1985.

Maldonado MT, Hughes MP, Rue EL, Wells ML. The Effect of Fe and Cu on Growth and Domoic Acid Production by *Pseudo-nitzschia multiseries* and *Pseudo-nitzschia australis*. *Limnology and Oceanography* 2002; 47: 515-526.

Mathy NL, Mathy JP, Lee RP, Walker J, Lofthouse S, Meeusen EN. Pathological and immunological changes after challenge infection with *Pasteurella multocida* in naive and immunized calves. *Vet Immunol Immunopathol* 2002; 85: 179-188.

May BJ, Zhang Q, Li LL, Paustian ML, Whittam TS, Kapur V. Complete genomic sequence of *Pasteurella multocida*, Pm70. *Proc Natl Acad Sci U S A* 2001; 98: 3460-3465.

Mehrotra A. Bacterial Biofilms. *Pediatric Asthma, Allergy & Immunology* 2007; 20: 191-195.

Merritt JH, Kadouri DE, O'Toole GA. Growing and analyzing static biofilms. *Curr Protoc Microbiol* 2005; Chapter 1: Unit.

Mey AR, Wyckoff EE, Kanukurthy V, Fisher CR, Payne SM. Iron and *fur* regulation in *Vibrio cholerae* and the role of *fur* in virulence. *Infect Immun* 2005; 73: 8167-8178.

Meyer JM, Neely A, Stintzi A, Georges C, Holder IA. Pyoverdin is essential for virulence of *Pseudomonas aeruginosa*. *Infect Immun* 1996; 64: 518-523.

Mims C, Playfair J, Roitt I, Wakelin D, Williams R. Events occurring immediately after the entry of the microorganism. In: Crowe L (ed) Medical Microbiology. London, Mosby. 1998a: 67-83.

Mims C, Playfair J, Roitt I, Wakelin D, Williams R. General Principles. In: Crowe L (ed) Medical Microbiology. London, Mosby. 1998b: 1-9.

Mo ML, Jamshidi N, Palsson BO. A genome-scale, constraint-based approach to systems biology of human metabolism. *Mol Biosyst* 2007; 3: 598-603.

Modun B, Kendall D, Williams P. Staphylococci express a receptor for human transferrin: identification of a 42-kilodalton cell wall transferrin-binding protein. *Infect Immun* 1994; 62: 3850-3858.

Moeck GS, Coulton JW. TonB-dependent iron acquisition: mechanisms of siderophore-mediated active transport. *Mol Microbiol* 1998; 28: 675-681.

Morse SA, Hebeler BH. Effect of pH on the growth and glucose metabolism of *Neisseria gonorrhoeae*. *Infect Immun* 1978; 21: 87-95.

Mosier DA, Confer AW, Panciera RJ. The evolution of vaccines for bovine pneumonic pasteurellosis. *Res Vet Sci* 1989; 47: 1-10.

Muller D, Edwards ML, Smith DW. Changes in iron and transferrin levels and body temperature in experimental airborne legionellosis. *J Infect Dis* 1983; 147: 302-307.

Nemish U, Yu RH, Tari LW, Krewulak K, Schryvers AB. The bacterial receptor protein, transferrin-binding protein B, does not independently facilitate the release of metal ion from human transferrin. *Biochem Cell Biol* 2003; 81: 275-283.

Newton CM. Computer simulation of stem-cell kinetics. *Bull Math Biophys* 1965; 27: Suppl-90.

Nikaido H. Porins and specific diffusion channels in bacterial outer membranes. *J Biol Chem* 1994; 269: 3905-3908.

Nookaew I, Jewett MC, Meechai A *et al.* The genome-scale metabolic model iIN800 of *Saccharomyces cerevisiae* and its validation: a scaffold to query lipid metabolism. *BMC Syst Biol* 2008; 2: 71.

Nordkvist M, Jensen NB, Villadsen J. Glucose metabolism in *Lactococcus lactis* MG1363 under different aeration conditions: requirement of acetate to sustain growth under microaerobic conditions. *Appl Environ Microbiol* 2003; 69: 3462-3468.

Oakhill JS, Sutton BJ, Gorringe AR, Evans RW. Homology modelling of transferrin-binding protein A from *Neisseria meningitidis*. *Protein Eng Des Sel* 2005; 18: 221-228.

Oberhardt MA, Puchalka J, Fryer KE, Martins dS, V, Papin JA. Genome-scale metabolic network analysis of the opportunistic pathogen *Pseudomonas aeruginosa* PAO1. *J Bacteriol* 2008; 190: 2790-2803.

Oberhofer TR. Characteristics and biotypes of *Pasteurella multocida* isolated from humans. *J Clin Microbiol* 1981; 13: 566-571.

Ogunnariwo JA, Alcantara J, Schryvers AB. Evidence for non-siderophore-mediated acquisition of transferrin-bound iron by *Pasteurella multocida*. *Microb Pathog* 1991; 11: 47-56.

Ogunnariwo JA, Schryvers AB. Iron acquisition in *Pasteurella haemolytica*: expression and identification of a bovine-specific transferrin receptor. *Infect Immun* 1990; 58: 2091-2097.

Ogunnariwo JA, Schryvers AB. Characterization of a novel transferrin receptor in bovine strains of *Pasteurella multocida*. *J Bacteriol* 2001; 183: 890-896.

Palyada K, Threadgill D, Stintzi A. Iron acquisition and regulation in *Campylobacter jejuni*. *J Bacteriol* 2004; 186: 4714-4729.

Park I, Schaeffer E, Sidoli A, Baralle FE, Cohen GN, Zakin MM. Organization of the human transferrin gene: direct evidence that it originated by gene duplication. *Proc Natl Acad Sci U S A* 1985; 82: 3149-3153.

Paustian ML, May BJ, Cao D, Boley D, Kapur V. Transcriptional response of *Pasteurella multocida* to defined iron sources. *J Bacteriol* 2002; 184: 6714-6720.

Paustian ML, May BJ, Kapur V. *Pasteurella multocida* gene expression in response to iron limitation. *Infect Immun* 2001; 69: 4109-4115.

Petrelli D, Repetto A, Di Luca MC *et al.* Characterization of a *Staphylococcus aureus* strain showing high levels of biofilm formation isolated from a vascular graft: case report. *Int J Immunopathol Pharmacol* 2008; 21: 745-750.

Pfeiffer T, Sanchez-Valdenebro I, Nuno JC, Montero F, Schuster S. METATOOL: for studying metabolic networks. *Bioinformatics* 1999; 15: 251-257.

Pidcock KA, Wooten JA, Daley BA, Stull TL. Iron acquisition by *Haemophilus influenzae*. *Infect Immun* 1988; 56: 721-725.

Pizarro-Cerda J, Cossart P. Bacterial adhesion and entry into host cells. *Cell* 2006; 124: 715-727.

Poolman MG, Fell DA, Raines CA. Elementary modes analysis of photosynthate metabolism in the chloroplast stroma. *Eur J Biochem* 2003; 270: 430-439.

Post KW, Cole NA, Raleigh RH. *In vitro* antimicrobial susceptibility of *Pasteurella haemolytica* and *Pasteurella multocida* recovered from cattle with bovine respiratory disease complex. *J Vet Diagn Invest* 1991; 3: 124-126.

Postle K. TonB protein and energy transduction between membranes. *J Bioenerg Biomembr* 1993; 25: 591-601.

Postle K, Kadner RJ. Touch and go: tying TonB to transport. *Mol Microbiol* 2003; 49: 869-882.

Prado ME, Prado TM, Payton M, Confer AW. Maternally and naturally acquired antibodies to *Mannheimia haemolytica* and *Pasteurella multocida* in beef calves. *Vet Immunol Immunopathol* 2006; 111: 301-307.

Price ND, Papin JA, Palsson BO. Determination of redundancy and systems properties of the metabolic network of *Helicobacter pylori* using genome-scale extreme pathway analysis. *Genome Res* 2002; 12: 760-769.

Price ND, Papin JA, Schilling CH, Palsson BO. Genome-scale microbial *in silico* models: the constraints-based approach. *Trends Biotechnol* 2003; 21: 162-169.

Ratledge C. Iron metabolism and infection. *Food Nutr Bull* 2007; 28: S515-S523.

Ratledge C, Dover LG. Iron metabolism in pathogenic bacteria. *Annu Rev Microbiol* 2000; 54: 881-941.

Reissbrodt R, Erler W, Winkelmann G. Iron supply of *Pasteurella multocida* and *Pasteurella haemolytica*. *J Basic Microbiol* 1994; 34: 61-63.

Robb EJ, Tucker CM, Corley L *et al.* Efficacy of tulathromycin or enrofloxacin for initial treatment of naturally occurring bovine respiratory disease in feeder calves. *Vet Ther* 2007; 8: 127-135.

Robledo JA, Serrano A, Domingue GJ. Outer membrane proteins of *E. coli* in the host-pathogen interaction in urinary tract infection. *J Urol* 1990; 143: 386-391.

Rodriguez GM, Smith I. Mechanisms of iron regulation in mycobacteria: role in physiology and virulence. *Mol Microbiol* 2003; 47: 1485-1494.

Roehrig SC, Tran HQ, Spehr V, Gunkel N, Selzer PM, Ullrich HJ. The response of *Mannheimia haemolytica* to iron limitation: Implications for the acquisition of iron in the bovine lung. *Vet Microbiol* 2006.

Rohde KH, Dyer DW. Analysis of haptoglobin and hemoglobin-haptoglobin interactions with the *Neisseria meningitidis* TonB-dependent receptor HpuAB by flow cytometry. *Infect Immun* 2004; 72: 2494-2506.

Rowe HA, Poxton IR, Donachie W. Survival of *Mannheimia* (*Pasteurella*) *haemolytica* in tracheobronchial washings of sheep and cattle. *Vet Microbiol* 2001; 81: 305-314.

Rozen S, Skaletsky H. Primer3 on the WWW for general users and for biologist programmers. *Methods Mol Biol* 2000; 132: 365-386.

Ruffolo CG, Jost BH, Adler B. Iron-regulated outer membrane proteins of *Pasteurella multocida* and their role in immunity. *Vet Microbiol* 1998; 59: 123-137.

Ruffolo CG, Tennent JM, Michalski WP, Adler B. Identification, purification, and characterization of the type 4 fimbriae of *Pasteurella multocida*. *Infect Immun* 1997; 65: 339-343.

Sausville J, Gupta G, Forrest G, Chai T. Salmonella Infection of a Penile Prosthesis. *J Sex Med* 2008.

Schilling CH, Covert MW, Famili I, Church GM, Edwards JS, Palsson BO. Genome-scale metabolic model of *Helicobacter pylori* 26695. *J Bacteriol* 2002; 184: 4582-4593.

Schilling CH, Edwards JS, Letscher D, Palsson BO. Combining pathway analysis with flux balance analysis for the comprehensive study of metabolic systems. *Biotechnol Bioeng* 2000; 71: 286-306.

Schilling CH, Letscher D, Palsson BO. Theory for the systemic definition of metabolic pathways and their use in interpreting metabolic function from a pathway-oriented perspective. *J Theor Biol* 2000; 203: 229-248.

Schilling CH, Palsson BO. Assessment of the metabolic capabilities of *Haemophilus influenzae* Rd through a genome-scale pathway analysis. *J Theor Biol* 2000; 203: 249-283.

Schilling CH, Schuster S, Palsson BO, Heinrich R. Metabolic pathway analysis: basic concepts and scientific applications in the post-genomic era. *Biotechnol Prog* 1999; 15: 296-303.

Schlabach MR, Bates GW. The synergistic binding of anions and Fe3+ by transferrin. Implications for the interlocking sites hypothesis. *J Biol Chem* 1975; 250: 2182-2188.

Schmitt L, Tampe R. Structure and mechanism of ABC transporters. *Curr Opin Struct Biol* 2002; 12: 754-760.

Schuster S, Dandekar T, Fell DA. Detection of elementary flux modes in biochemical networks: a promising tool for pathway analysis and metabolic engineering. *Trends Biotechnol* 1999; 17: 53-60.

Schuster S, Fell DA, Dandekar T. A general definition of metabolic pathways useful for systematic organization and analysis of complex metabolic networks. *Nat Biotechnol* 2000; 18: 326-332.

Schwarz R, Musch P, von KA *et al.* YANA - a software tool for analyzing flux modes, gene-expression and enzyme activities. *BMC Bioinformatics* 2005; 6: 135.

Shouldice SR, Skene RJ, Dougan DR *et al.* Structural basis for iron binding and release by a novel class of periplasmic iron-binding proteins found in gram-negative pathogens. *J Bacteriol* 2004; 186: 3903-3910.

Skare JT, Ahmer BM, Seachord CL, Darveau RP, Postle K. Energy transduction between membranes. TonB, a cytoplasmic membrane protein, can be chemically cross-linked in vivo to the outer membrane receptor FepA. *J Biol Chem* 1993; 268: 16302-16308.

Smith H. Host factors that influence the behaviour of bacterial pathogens *in vivo*. *Int J Med Microbiol* 2000a; 290: 207-213.

Smith H. Questions about the behaviour of bacterial pathogens *in vivo*. *Philos Trans R Soc Lond B Biol Sci* 2000b; 355: 551-564.

Smith H, Yates EA, Cole JA, Parsons NJ. Lactate stimulation of gonococcal metabolism in media containing glucose: mechanism, impact on pathogenicity, and wider implications for other pathogens. *Infect Immun* 2001; 69: 6565-6572.

Sparling PF. Bacterial virulence and pathogenesis: an overview. *Rev Infect Dis* 1983; 5 Suppl 4: S637-S646.

Steenbergen SM, Lichtensteiger CA, Caughlan R, Garfinkle J, Fuller TE, Vimr ER. Sialic Acid metabolism and systemic pasteurellosis. *Infect Immun* 2005; 73: 1284-1294.

Stelling J, Klamt S, Bettenbrock K, Schuster S, Gilles ED. Metabolic network structure determines key aspects of functionality and regulation. *Nature* 2002; 420: 190-193.

Stintzi A, Barnes C, Xu J, Raymond KN. Microbial iron transport via a siderophore shuttle: a membrane ion transport paradigm. *Proc Natl Acad Sci U S A* 2000; 97: 10691-10696.

Stohs SJ, Bagchi D. Oxidative mechanisms in the toxicity of metal ions. *Free Radic Biol Med* 1995; 18: 321-336.

Sussman M. Iron and infection. In: Jacobs A, Worwood M (eds) Iron in biochemistry and medicine. New York, Academic Press. 1974: 649-679.

Tao H, Bausch C, Richmond C, Blattner FR, Conway T. Functional genomics: expression analysis of *Escherichia coli* growing on minimal and rich media. *J Bacteriol* 1999; 181: 6425-6440.

Townsend KM, Boyce JD, Chung JY, Frost AJ, Adler B. Genetic organization of *Pasteurella multocida* cap Loci and development of a multiplex capsular PCR typing system. *J Clin Microbiol* 2001; 39: 924-929.

Townsend KM, Frost AJ, Lee CW, Papadimitriou JM, Dawkins HJ. Development of PCR assays for species- and type-specific identification of *Pasteurella multocida* isolates. *J Clin Microbiol* 1998; 36: 1096-1100.

Varma A, Palsson BO. Predictions for oxygen supply control to enhance population stability of engineered production strains. *Biotechnol Bioeng* 1994; 43: 275-285.

Veken JW, Oudega B, Luirink J, de Graaf FK. Binding of bovine transferrin by *Pasteurella multocida* serotype B:2,5, a strain which causes haemorrhagic septicaemia in buffalo and cattle. *FEMS Microbiol Lett* 1994; 115: 253-257.

Wagner A, Fell DA. The small world inside large metabolic networks. *Proc Biol Sci* 2001; 268: 1803-1810.

Wandersman C, Delepelaire P. Bacterial iron sources: from siderophores to hemophores. *Annu Rev Microbiol* 2004; 58: 611-647.

Ward CG, Bullen JJ, Rogers HJ. Iron and infection: new developments and their implications. *J Trauma* 1996; 41: 356-364.

Weekley LB, Veit HP, Eyre P. Bovine pneumonic pasteurellosis. Part I. Pathophysiology. *Comp Cont Educ Pract Vet* 1998; 20: S33-S45.

Weinberg ED. Iron withholding: a defense against infection and neoplasia. *Physiol Rev* 1984; 64: 65-102.

White AG, Steele RH, Pierce WA, Jr. The effect of pH on the fermentation of glucose and galactose by Streptococcus pyogenes. *J Bacteriol* 1955; 70: 82-86.

Wilhelm T, Behre J, Schuster S. Analysis of structural robustness of metabolic networks. *Syst Biol (Stevenage)* 2004; 1: 114-120.

Williams, J., Evans, R. W. & Moreton, K. The iron-binding properties of hen ovotransferrin. *Biochem J* 1978; 173: 533-539.

Yamamoto Y, Fukui K, Koujin N, Ohya H, Kimura K, Kamio Y. Regulation of the intracellular free iron pool by Dpr provides oxygen tolerance to *Streptococcus mutans*. *J Bacteriol* 2004; 186: 5997-6002.

Yariv J, Kalb AJ, Sperling R, Bauminger ER, Cohen SG, Ofer S. The composition and the structure of bacterioferritin of *Escherichia coli*. *Biochem J* 1981; 197: 171-175.

Zhou D, Qin L, Han Y *et al.* Global analysis of iron assimilation and *fur* regulation in *Yersinia pestis*. *FEMS Microbiol Lett* 2006; 258: 9-17.

Appendix 1 - Elementary flux modes of transmembrane iron transport subnetwork

EFM	Reactions
1	(1 ADP) (1 ATP) (1 FE_41) (1 FE_42) (1 FE_43) (1 FE_44) (1 FE_45) (1 FE_49) (1 FE_50) (1 FE_51) (1 FE_52) (1 FE_53) (1 FE_54) (1 FE_56) (1 FE_61) (2 FE_63) (1 FE_74) (1 FE_77) (1 FE_79) (1 FE_80)
2	(1 ADP) (1 ATP) (1 FE_41) (1 FE_42) (1 FE_43) (1 FE_44) (1 FE_45) (1 FE_49) (1 FE_50) (1 FE_51) (1 FE_52) (1 FE_53) (1 FE_54) (1 FE_56) (1 FE_61) (2 FE_64) (1 FE_74) (1 FE_77) (1 FE_79) (1 FE_80)
3	(1 ADP) (1 ATP) (1 FE_41) (1 FE_42) (1 FE_43) (1 FE_44) (1 FE_45) (1 FE_49) (1 FE_50) (1 FE_51) (1 FE_52) (1 FE_53) (1 FE_54) (1 FE_56) (1 FE_61) (2 FE_63) (1 FE_69) (1 FE_74) (1 FE_79) (1 FE_80) (1 HgbA)
4	(1 ADP) (1 ATP) (1 FE_41) (1 FE_42) (1 FE_43) (1 FE_44) (1 FE_45) (1 FE_49) (1 FE_50) (1 FE_51) (1 FE_52) (1 FE_53) (1 FE_54) (1 FE_56) (1 FE_61) (2 FE_64) (1 FE_69) (1 FE_74) (1 FE_79) (1 FE_80) (1 HgbA)
5	(1 ADP) (1 ATP) (1 FE_41) (1 FE_42) (1 FE_46) (1 FE_47) (1 FE_48) (1 FE_49) (1 FE_50) (1 FE_51) (1 FE_52) (1 FE_53) (1 FE_54) (1 FE_56) (1 FE_61) (2 FE_63) (1 FE_74) (1 FE_78) (1 FE_79) (1 FE_80)
6	(1 ADP) (1 ATP) (1 FE_41) (1 FE_42) (1 FE_46) (1 FE_47) (1 FE_48) (1 FE_49) (1 FE_50) (1 FE_51) (1 FE_52) (1 FE_53) (1 FE_54) (1 FE_56) (1 FE_61) (2 FE_64) (1 FE_74) (1 FE_78) (1 FE_79) (1 FE_80)
7	(1 ADP) (1 ATP) (1 FE_41) (1 FE_42) (1 FE_46) (1 FE_47) (1 FE_48) (1 FE_49) (1 FE_50) (1 FE_51) (1 FE_52) (1 FE_53) (1 FE_54) (1 FE_56) (1 FE_61) (2 FE_63) (1 FE_70) (1 FE_74) (1 FE_79) (1 FE_80) (1 HgbB)
8	(1 ADP) (1 ATP) (1 FE_41) (1 FE_42) (1 FE_46) (1 FE_47) (1 FE_48) (1 FE_49) (1 FE_50) (1 FE_51) (1 FE_52) (1 FE_53) (1 FE_54) (1 FE_56) (1 FE_61) (2 FE_64) (1 FE_70) (1 FE_74) (1 FE_79) (1 FE_80) (1 HgbB)
9	(1 ADP) (1 ATP) (1 FE_41) (1 FE_42) (1 FE_43) (1 FE_44) (1 FE_45) (1 FE_49) (1 FE_50) (1 FE_51) (1 FE_52) (1 FE_53) (1 FE_54) (1 FE_56) (1 FE_61) (2 FE_63) (1 FE_71) (1 FE_74) (1 FE_77) (1 FE_80) (1 YfeA)
10	(1 ADP) (1 ATP) (1 FE_41) (1 FE_42) (1 FE_43) (1 FE_44) (1 FE_45) (1 FE_49) (1 FE_50) (1 FE_51) (1 FE_52) (1 FE_53) (1 FE_54) (1 FE_56) (1 FE_61) (2 FE_64) (1 FE_71) (1 FE_74) (1 FE_77) (1 FE_80) (1 YfeA)
11	(1 ADP) (1 ATP) (1 FE_41) (1 FE_42) (1 FE_43) (1 FE_44) (1 FE_45) (1 FE_49) (1 FE_50) (1 FE_51) (1 FE_52) (1 FE_53) (1 FE_54) (1 FE_56) (1 FE_61) (2 FE_63) (1 FE_69) (1 FE_71) (1 FE_74) (1 FE_80) (1 HgbA) (1 YfeA)
12	(1 ADP) (1 ATP) (1 FE_41) (1 FE_42) (1 FE_43) (1 FE_44) (1 FE_45) (1 FE_49) (1 FE_50) (1 FE_51) (1 FE_52) (1 FE_53) (1 FE_54) (1 FE_56) (1 FE_61) (2 FE_64) (1 FE_69) (1 FE_71) (1 FE_74) (1 FE_80) (1 HgbA) (1 YfeA)
13	(1 ADP) (1 ATP) (1 FE_41) (1 FE_42) (1 FE_46) (1 FE_47) (1 FE_48) (1 FE_49) (1 FE_50) (1 FE_51) (1 FE_52) (1 FE_53) (1 FE_54) (1 FE_56) (1 FE_61) (2 FE_63) (1 FE_71) (1 FE_74) (1 FE_78) (1 FE_80) (1 YfeA)
14	(1 ADP) (1 ATP) (1 FE_41) (1 FE_42) (1 FE_46) (1 FE_47) (1 FE_48) (1 FE_49) (1 FE_50) (1 FE_51) (1 FE_52) (1 FE_53) (1 FE_54) (1 FE_56) (1 FE_61) (2 FE_64) (1 FE_71) (1 FE_74) (1 FE_78) (1 FE_80) (1 YfeA)
15	(1 ADP) (1 ATP) (1 FE_41) (1 FE_42) (1 FE_46) (1 FE_47) (1 FE_48) (1 FE_49) (1 FE_50) (1 FE_51) (1 FE_52) (1 FE_53) (1 FE_54) (1 FE_56) (1 FE_61) (2 FE_63) (1 FE_70) (1 FE_71) (1 FE_74) (1 FE_80) (1 HgbB) (1 YfeA)
16	(1 ADP) (1 ATP) (1 FE_41) (1 FE_42) (1 FE_46) (1 FE_47) (1 FE_48) (1 FE_49) (1 FE_50) (1 FE_51) (1 FE_52) (1 FE_53) (1 FE_54)

	(1 FE_56) (1 FE_61) (2 FE_64) (1 FE_70) (1 FE_71) (1 FE_74) (1 FE_80) (1 HgbB) (1 YfeA)
17	(1 ADP) (1 ATP) (1 FE_41) (1 FE_42) (1 FE_43) (1 FE_44) (1 FE_45) (1 FE_49) (1 FE_50) (1 FE_51) (1 FE_52) (1 FE_53) (1 FE_54) (1 FE_56) (1 FE_61) (2 FE_63) (1 FE_72) (1 FE_74) (1 FE_77) (1 FE_79) (1 YfeBCD)
18	(1 ADP) (1 ATP) (1 FE_41) (1 FE_42) (1 FE_43) (1 FE_44) (1 FE_45) (1 FE_49) (1 FE_50) (1 FE_51) (1 FE_52) (1 FE_53) (1 FE_54) (1 FE_56) (1 FE_61) (2 FE_64) (1 FE_72) (1 FE_74) (1 FE_77) (1 FE_79) (1 YfeBCD)
19	(1 ADP) (1 ATP) (1 FE_41) (1 FE_42) (1 FE_43) (1 FE_44) (1 FE_45) (1 FE_49) (1 FE_50) (1 FE_51) (1 FE_52) (1 FE_53) (1 FE_54) (1 FE_56) (1 FE_61) (2 FE_63) (1 FE_69) (1 FE_72) (1 FE_74) (1 FE_79) (1 HgbA) (1 YfeBCD)
20	(1 ADP) (1 ATP) (1 FE_41) (1 FE_42) (1 FE_43) (1 FE_44) (1 FE_45) (1 FE_49) (1 FE_50) (1 FE_51) (1 FE_52) (1 FE_53) (1 FE_54) (1 FE_56) (1 FE_61) (2 FE_64) (1 FE_69) (1 FE_72) (1 FE_74) (1 FE_79) (1 HgbA) (1 YfeBCD)
21	(1 ADP) (1 ATP) (1 FE_41) (1 FE_42) (1 FE_46) (1 FE_47) (1 FE_48) (1 FE_49) (1 FE_50) (1 FE_51) (1 FE_52) (1 FE_53) (1 FE_54) (1 FE_56) (1 FE_61) (2 FE_63) (1 FE_72) (1 FE_74) (1 FE_78) (1 FE_79) (1 YfeBCD)
22	(1 ADP) (1 ATP) (1 FE_41) (1 FE_42) (1 FE_46) (1 FE_47) (1 FE_48) (1 FE_49) (1 FE_50) (1 FE_51) (1 FE_52) (1 FE_53) (1 FE_54) (1 FE_56) (1 FE_61) (2 FE_64) (1 FE_72) (1 FE_74) (1 FE_78) (1 FE_79) (1 YfeBCD)
23	(1 ADP) (1 ATP) (1 FE_41) (1 FE_42) (1 FE_46) (1 FE_47) (1 FE_48) (1 FE_49) (1 FE_50) (1 FE_51) (1 FE_52) (1 FE_53) (1 FE_54) (1 FE_56) (1 FE_61) (2 FE_63) (1 FE_70) (1 FE_72) (1 FE_74) (1 FE_79) (1 HgbB) (1 YfeBCD)
24	(1 ADP) (1 ATP) (1 FE_41) (1 FE_42) (1 FE_46) (1 FE_47) (1 FE_48) (1 FE_49) (1 FE_50) (1 FE_51) (1 FE_52) (1 FE_53) (1 FE_54) (1 FE_56) (1 FE_61) (2 FE_64) (1 FE_70) (1 FE_72) (1 FE_74) (1 FE_79) (1 HgbB) (1 YfeBCD)
25	(1 ADP) (1 ATP) (1 FE_41) (1 FE_42) (1 FE_43) (1 FE_44) (1 FE_45) (1 FE_49) (1 FE_50) (1 FE_51) (1 FE_52) (1 FE_53) (1 FE_54) (1 FE_56) (1 FE_61) (2 FE_63) (1 FE_71) (1 FE_72) (1 FE_74) (1 FE_77) (1 YfeA) (1 YfeBCD)
26	(1 ADP) (1 ATP) (1 FE_41) (1 FE_42) (1 FE_43) (1 FE_44) (1 FE_45) (1 FE_49) (1 FE_50) (1 FE_51) (1 FE_52) (1 FE_53) (1 FE_54) (1 FE_56) (1 FE_61) (2 FE_64) (1 FE_71) (1 FE_72) (1 FE_74) (1 FE_77) (1 YfeA) (1 YfeBCD)
27	(1 ADP) (1 ATP) (1 FE_41) (1 FE_42) (1 FE_43) (1 FE_44) (1 FE_45) (1 FE_49) (1 FE_50) (1 FE_51) (1 FE_52) (1 FE_53) (1 FE_54) (1 FE_56) (1 FE_61) (2 FE_63) (1 FE_69) (1 FE_71) (1 FE_72) (1 FE_74) (1 HgbA) (1 YfeA) (1 YfeBCD)
28	(1 ADP) (1 ATP) (1 FE_41) (1 FE_42) (1 FE_43) (1 FE_44) (1 FE_45) (1 FE_49) (1 FE_50) (1 FE_51) (1 FE_52) (1 FE_53) (1 FE_54) (1 FE_56) (1 FE_61) (2 FE_64) (1 FE_69) (1 FE_71) (1 FE_72) (1 FE_74) (1 HgbA) (1 YfeA) (1 YfeBCD)
29	(1 ADP) (1 ATP) (1 FE_41) (1 FE_42) (1 FE_46) (1 FE_47) (1 FE_48) (1 FE_49) (1 FE_50) (1 FE_51) (1 FE_52) (1 FE_53) (1 FE_54) (1 FE_56) (1 FE_61) (2 FE_63) (1 FE_71) (1 FE_72) (1 FE_74) (1 FE_78) (1 YfeA) (1 YfeBCD)
30	(1 ADP) (1 ATP) (1 FE_41) (1 FE_42) (1 FE_46) (1 FE_47) (1 FE_48) (1 FE_49) (1 FE_50) (1 FE_51) (1 FE_52) (1 FE_53) (1 FE_54) (1 FE_56) (1 FE_61) (2 FE_64) (1 FE_71) (1 FE_72) (1 FE_74) (1 FE_78) (1 YfeA) (1 YfeBCD)
31	(1 ADP) (1 ATP) (1 FE_41) (1 FE_42) (1 FE_46) (1 FE_47) (1 FE_48) (1 FE_49) (1 FE_50) (1 FE_51) (1 FE_52) (1 FE_53) (1 FE_54) (1 FE_56) (1 FE_61) (2 FE_63) (1 FE_70) (1 FE_71) (1 FE_72) (1 FE_74) (1 HgbB) (1 YfeA) (1 YfeBCD)
32	(1 ADP) (1 ATP) (1 FE_41) (1 FE_42) (1 FE_46) (1 FE_47) (1 FE_48) (1 FE_49) (1 FE_50) (1 FE_51) (1 FE_52) (1 FE_53) (1 FE_54) (1 FE_56) (1 FE_61) (2 FE_64) (1 FE_70) (1 FE_71) (1 FE_72) (1 FE_74) (1 HgbB) (1 YfeA) (1 YfeBCD)
33	(1 ADP) (1 ATP) (1 FE_41) (1 FE_42) (1 FE_43) (1 FE_44) (1 FE_45) (1 FE_49) (1 FE_50) (1 FE_51) (1 FE_52) (1 FE_53) (1 FE_54)

	(1 FE_56) (1 FE_61) (2 FE_63) (1 FE_66) (1 FE_77) (1 FE_79) (1 FE_80) (1 Ton_system)
34	(1 ADP) (1 ATP) (1 FE_41) (1 FE_42) (1 FE_43) (1 FE_44) (1 FE_45) (1 FE_49) (1 FE_50) (1 FE_51) (1 FE_52) (1 FE_53) (1 FE_54) (1 FE_56) (1 FE_61) (2 FE_64) (1 FE_66) (1 FE_77) (1 FE_79) (1 FE_80) (1 Ton_system)
35	(1 ADP) (1 ATP) (1 FE_41) (1 FE_42) (1 FE_43) (1 FE_44) (1 FE_45) (1 FE_49) (1 FE_50) (1 FE_51) (1 FE_52) (1 FE_53) (1 FE_54) (1 FE_56) (1 FE_61) (2 FE_63) (1 FE_66) (1 FE_69) (1 FE_79) (1 FE_80) (1 HgbA) (1 Ton_system)
36	(1 ADP) (1 ATP) (1 FE_41) (1 FE_42) (1 FE_43) (1 FE_44) (1 FE_45) (1 FE_49) (1 FE_50) (1 FE_51) (1 FE_52) (1 FE_53) (1 FE_54) (1 FE_56) (1 FE_61) (2 FE_64) (1 FE_66) (1 FE_69) (1 FE_79) (1 FE_80) (1 HgbA) (1 Ton_system)
37	(1 ADP) (1 ATP) (1 FE_41) (1 FE_42) (1 FE_46) (1 FE_47) (1 FE_48) (1 FE_49) (1 FE_50) (1 FE_51) (1 FE_52) (1 FE_53) (1 FE_54) (1 FE_56) (1 FE_61) (2 FE_63) (1 FE_66) (1 FE_78) (1 FE_79) (1 FE_80) (1 Ton_system)
38	(1 ADP) (1 ATP) (1 FE_41) (1 FE_42) (1 FE_46) (1 FE_47) (1 FE_48) (1 FE_49) (1 FE_50) (1 FE_51) (1 FE_52) (1 FE_53) (1 FE_54) (1 FE_56) (1 FE_61) (2 FE_64) (1 FE_66) (1 FE_78) (1 FE_79) (1 FE_80) (1 Ton_system)
39	(1 ADP) (1 ATP) (1 FE_41) (1 FE_42) (1 FE_46) (1 FE_47) (1 FE_48) (1 FE_49) (1 FE_50) (1 FE_51) (1 FE_52) (1 FE_53) (1 FE_54) (1 FE_56) (1 FE_61) (2 FE_63) (1 FE_66) (1 FE_70) (1 FE_79) (1 FE_80) (1 HgbB) (1 Ton_system)
40	(1 ADP) (1 ATP) (1 FE_41) (1 FE_42) (1 FE_46) (1 FE_47) (1 FE_48) (1 FE_49) (1 FE_50) (1 FE_51) (1 FE_52) (1 FE_53) (1 FE_54) (1 FE_56) (1 FE_61) (2 FE_64) (1 FE_66) (1 FE_70) (1 FE_79) (1 FE_80) (1 HgbB) (1 Ton_system)
41	(1 ADP) (1 ATP) (1 FE_41) (1 FE_42) (1 FE_43) (1 FE_44) (1 FE_45) (1 FE_49) (1 FE_50) (1 FE_51) (1 FE_52) (1 FE_53) (1 FE_54) (1 FE_56) (1 FE_61) (2 FE_63) (1 FE_66) (1 FE_71) (1 FE_77) (1 FE_80) (1 Ton_system) (1 YfeA)
42	(1 ADP) (1 ATP) (1 FE_41) (1 FE_42) (1 FE_43) (1 FE_44) (1 FE_45) (1 FE_49) (1 FE_50) (1 FE_51) (1 FE_52) (1 FE_53) (1 FE_54) (1 FE_56) (1 FE_61) (2 FE_64) (1 FE_66) (1 FE_71) (1 FE_77) (1 FE_80) (1 Ton_system) (1 YfeA)
43	(1 ADP) (1 ATP) (1 FE_41) (1 FE_42) (1 FE_43) (1 FE_44) (1 FE_45) (1 FE_49) (1 FE_50) (1 FE_51) (1 FE_52) (1 FE_53) (1 FE_54) (1 FE_56) (1 FE_61) (2 FE_63) (1 FE_66) (1 FE_69) (1 FE_71) (1 FE_80) (1 HgbA) (1 Ton_system) (1 YfeA)
44	(1 ADP) (1 ATP) (1 FE_41) (1 FE_42) (1 FE_43) (1 FE_44) (1 FE_45) (1 FE_49) (1 FE_50) (1 FE_51) (1 FE_52) (1 FE_53) (1 FE_54) (1 FE_56) (1 FE_61) (2 FE_64) (1 FE_66) (1 FE_69) (1 FE_71) (1 FE_80) (1 HgbA) (1 Ton_system) (1 YfeA)
45	(1 ADP) (1 ATP) (1 FE_41) (1 FE_42) (1 FE_46) (1 FE_47) (1 FE_48) (1 FE_49) (1 FE_50) (1 FE_51) (1 FE_52) (1 FE_53) (1 FE_54) (1 FE_56) (1 FE_61) (2 FE_63) (1 FE_66) (1 FE_71) (1 FE_78) (1 FE_80) (1 Ton_system) (1 YfeA)
46	(1 ADP) (1 ATP) (1 FE_41) (1 FE_42) (1 FE_46) (1 FE_47) (1 FE_48) (1 FE_49) (1 FE_50) (1 FE_51) (1 FE_52) (1 FE_53) (1 FE_54) (1 FE_56) (1 FE_61) (2 FE_64) (1 FE_66) (1 FE_71) (1 FE_78) (1 FE_80) (1 Ton_system) (1 YfeA)
47	(1 ADP) (1 ATP) (1 FE_41) (1 FE_42) (1 FE_46) (1 FE_47) (1 FE_48) (1 FE_49) (1 FE_50) (1 FE_51) (1 FE_52) (1 FE_53) (1 FE_54) (1 FE_56) (1 FE_61) (2 FE_63) (1 FE_66) (1 FE_70) (1 FE_71) (1 FE_80) (1 HgbB) (1 Ton_system) (1 YfeA)
48	(1 ADP) (1 ATP) (1 FE_41) (1 FE_42) (1 FE_46) (1 FE_47) (1 FE_48) (1 FE_49) (1 FE_50) (1 FE_51) (1 FE_52) (1 FE_53) (1 FE_54) (1 FE_56) (1 FE_61) (2 FE_64) (1 FE_66) (1 FE_70) (1 FE_71) (1 FE_80) (1 HgbB) (1 Ton_system) (1 YfeA)
49	(1 ADP) (1 ATP) (1 FE_41) (1 FE_42) (1 FE_43) (1 FE_44) (1 FE_45) (1 FE_49) (1 FE_50) (1 FE_51) (1 FE_52) (1 FE_53) (1 FE_54) (1 FE_56) (1 FE_61) (2 FE_63) (1 FE_66) (1 FE_72) (1 FE_77) (1 FE_79) (1 Ton_system) (1 YfeBCD)
50	(1 ADP) (1 ATP) (1 FE_41) (1 FE_42) (1 FE_43) (1 FE_44) (1 FE_45) (1 FE_49) (1 FE_50) (1 FE_51) (1 FE_52) (1 FE_53) (1 FE_54)

	(1 FE_56) (1 FE_61) (2 FE_64) (1 FE_66) (1 FE_72) (1 FE_77) (1 FE_79) (1 Ton_system) (1 YfeBCD)
51	(1 ADP) (1 ATP) (1 FE_41) (1 FE_42) (1 FE_43) (1 FE_44) (1 FE_45) (1 FE_49) (1 FE_50) (1 FE_51) (1 FE_52) (1 FE_53) (1 FE_54) (1 FE_56) (1 FE_61) (2 FE_63) (1 FE_66) (1 FE_69) (1 FE_72) (1 FE_79) (1 HgbA) (1 Ton_system) (1 YfeBCD)
52	(1 ADP) (1 ATP) (1 FE_41) (1 FE_42) (1 FE_43) (1 FE_44) (1 FE_45) (1 FE_49) (1 FE_50) (1 FE_51) (1 FE_52) (1 FE_53) (1 FE_54) (1 FE_56) (1 FE_61) (2 FE_64) (1 FE_66) (1 FE_69) (1 FE_72) (1 FE_79) (1 HgbA) (1 Ton_system) (1 YfeBCD)
53	(1 ADP) (1 ATP) (1 FE_41) (1 FE_42) (1 FE_46) (1 FE_47) (1 FE_48) (1 FE_49) (1 FE_50) (1 FE_51) (1 FE_52) (1 FE_53) (1 FE_54) (1 FE_56) (1 FE_61) (2 FE_63) (1 FE_66) (1 FE_72) (1 FE_78) (1 FE_79) (1 Ton_system) (1 YfeBCD)
54	(1 ADP) (1 ATP) (1 FE_41) (1 FE_42) (1 FE_46) (1 FE_47) (1 FE_48) (1 FE_49) (1 FE_50) (1 FE_51) (1 FE_52) (1 FE_53) (1 FE_54) (1 FE_56) (1 FE_61) (2 FE_64) (1 FE_66) (1 FE_72) (1 FE_78) (1 FE_79) (1 Ton_system) (1 YfeBCD)
55	(1 ADP) (1 ATP) (1 FE_41) (1 FE_42) (1 FE_46) (1 FE_47) (1 FE_48) (1 FE_49) (1 FE_50) (1 FE_51) (1 FE_52) (1 FE_53) (1 FE_54) (1 FE_56) (1 FE_61) (2 FE_63) (1 FE_66) (1 FE_70) (1 FE_72) (1 FE_79) (1 HgbB) (1 Ton_system) (1 YfeBCD)
56	(1 ADP) (1 ATP) (1 FE_41) (1 FE_42) (1 FE_46) (1 FE_47) (1 FE_48) (1 FE_49) (1 FE_50) (1 FE_51) (1 FE_52) (1 FE_53) (1 FE_54) (1 FE_56) (1 FE_61) (2 FE_64) (1 FE_66) (1 FE_70) (1 FE_72) (1 FE_79) (1 HgbB) (1 Ton_system) (1 YfeBCD)
57	(1 ADP) (1 ATP) (1 FE_41) (1 FE_42) (1 FE_43) (1 FE_44) (1 FE_45) (1 FE_49) (1 FE_50) (1 FE_51) (1 FE_52) (1 FE_53) (1 FE_54) (1 FE_56) (1 FE_61) (2 FE_63) (1 FE_66) (1 FE_71) (1 FE_72) (1 FE_77) (1 Ton_system) (1 YfeA) (1 YfeBCD)
58	(1 ADP) (1 ATP) (1 FE_41) (1 FE_42) (1 FE_43) (1 FE_44) (1 FE_45) (1 FE_49) (1 FE_50) (1 FE_51) (1 FE_52) (1 FE_53) (1 FE_54) (1 FE_56) (1 FE_61) (2 FE_64) (1 FE_66) (1 FE_71) (1 FE_72) (1 FE_77) (1 Ton_system) (1 YfeA) (1 YfeBCD)
59	(1 ADP) (1 ATP) (1 FE_41) (1 FE_42) (1 FE_43) (1 FE_44) (1 FE_45) (1 FE_49) (1 FE_50) (1 FE_51) (1 FE_52) (1 FE_53) (1 FE_54) (1 FE_56) (1 FE_61) (2 FE_63) (1 FE_66) (1 FE_69) (1 FE_71) (1 FE_72) (1 HgbA) (1 Ton_system) (1 YfeA) (1 YfeBCD)
60	(1 ADP) (1 ATP) (1 FE_41) (1 FE_42) (1 FE_43) (1 FE_44) (1 FE_45) (1 FE_49) (1 FE_50) (1 FE_51) (1 FE_52) (1 FE_53) (1 FE_54) (1 FE_56) (1 FE_61) (2 FE_64) (1 FE_66) (1 FE_69) (1 FE_71) (1 FE_72) (1 HgbA) (1 Ton_system) (1 YfeA) (1 YfeBCD)
61	(1 ADP) (1 ATP) (1 FE_41) (1 FE_42) (1 FE_46) (1 FE_47) (1 FE_48) (1 FE_49) (1 FE_50) (1 FE_51) (1 FE_52) (1 FE_53) (1 FE_54) (1 FE_56) (1 FE_61) (2 FE_63) (1 FE_66) (1 FE_71) (1 FE_72) (1 FE_78) (1 Ton_system) (1 YfeA) (1 YfeBCD)
62	(1 ADP) (1 ATP) (1 FE_41) (1 FE_42) (1 FE_46) (1 FE_47) (1 FE_48) (1 FE_49) (1 FE_50) (1 FE_51) (1 FE_52) (1 FE_53) (1 FE_54) (1 FE_56) (1 FE_61) (2 FE_64) (1 FE_66) (1 FE_71) (1 FE_72) (1 FE_78) (1 Ton_system) (1 YfeA) (1 YfeBCD)
63	(1 ADP) (1 ATP) (1 FE_41) (1 FE_42) (1 FE_46) (1 FE_47) (1 FE_48) (1 FE_49) (1 FE_50) (1 FE_51) (1 FE_52) (1 FE_53) (1 FE_54) (1 FE_56) (1 FE_61) (2 FE_63) (1 FE_66) (1 FE_70) (1 FE_71) (1 FE_72) (1 HgbB) (1 Ton_system) (1 YfeA) (1 YfeBCD)
64	(1 ADP) (1 ATP) (1 FE_41) (1 FE_42) (1 FE_46) (1 FE_47) (1 FE_48) (1 FE_49) (1 FE_50) (1 FE_51) (1 FE_52) (1 FE_53) (1 FE_54) (1 FE_56) (1 FE_61) (2 FE_64) (1 FE_66) (1 FE_70) (1 FE_71) (1 FE_72) (1 HgbB) (1 Ton_system) (1 YfeA) (1 YfeBCD)
65	(1 ADP) (1 ATP) (1 FE_29) (1 FE_30) (1 FE_31) (1 FE_32) (1 FE_33) (1 FE_34) (1 FE_35) (1 FE_36) (1 FE_38) (1 FE_41) (1 FE_42) (1 FE_62) (1 FE_63) (1 FE_73) (1 FE_74) (1 FE_75) (1 FE_76)
66	(1 ADP) (1 ATP) (1 FE_29) (1 FE_30) (1 FE_31) (1 FE_32) (1 FE_33) (1 FE_34) (1 FE_35) (1 FE_36) (1 FE_38) (1 FE_41) (1 FE_42) (1 FE_62) (1 FE_64) (1 FE_73) (1 FE_74) (1 FE_75) (1 FE_76)
67	(1 ADP) (1 ATP) (1 FbpA) (1 FE_29) (1 FE_30) (1 FE_31) (1 FE_32) (1 FE_33) (1 FE_34) (1 FE_35) (1 FE_36) (1 FE_38) (1 FE_41)

	(1 FE_42) (1 FE_62) (1 FE_63) (1 FE_67) (1 FE_73) (1 FE_74) (1 FE_76)
68	(1 ADP) (1 ATP) (1 FbpA) (1 FE_29) (1 FE_30) (1 FE_31) (1 FE_32) (1 FE_33) (1 FE_34) (1 FE_35) (1 FE_36) (1 FE_38) (1 FE_41) (1 FE_42) (1 FE_62) (1 FE_64) (1 FE_67) (1 FE_73) (1 FE_74) (1 FE_76)
69	(1 ADP) (1 ATP) (1 FbpBC) (1 FE_29) (1 FE_30) (1 FE_31) (1 FE_32) (1 FE_33) (1 FE_34) (1 FE_35) (1 FE_36) (1 FE_38) (1 FE_41) (1 FE_42) (1 FE_62) (1 FE_63) (1 FE_68) (1 FE_73) (1 FE_74) (1 FE_75)
70	(1 ADP) (1 ATP) (1 FbpBC) (1 FE_29) (1 FE_30) (1 FE_31) (1 FE_32) (1 FE_33) (1 FE_34) (1 FE_35) (1 FE_36) (1 FE_38) (1 FE_41) (1 FE_42) (1 FE_62) (1 FE_64) (1 FE_68) (1 FE_73) (1 FE_74) (1 FE_75)
71	(1 ADP) (1 ATP) (1 FbpA) (1 FbpBC) (1 FE_29) (1 FE_30) (1 FE_31) (1 FE_32) (1 FE_33) (1 FE_34) (1 FE_35) (1 FE_36) (1 FE_38) (1 FE_41) (1 FE_42) (1 FE_62) (1 FE_63) (1 FE_67) (1 FE_68) (1 FE_73) (1 FE_74)
72	(1 ADP) (1 ATP) (1 FbpA) (1 FbpBC) (1 FE_29) (1 FE_30) (1 FE_31) (1 FE_32) (1 FE_33) (1 FE_34) (1 FE_35) (1 FE_36) (1 FE_38) (1 FE_41) (1 FE_42) (1 FE_62) (1 FE_64) (1 FE_67) (1 FE_68) (1 FE_73) (1 FE_74)
73	(1 ADP) (1 ATP) (1 FE_29) (1 FE_30) (1 FE_31) (1 FE_32) (1 FE_33) (1 FE_34) (1 FE_35) (1 FE_36) (1 FE_38) (1 FE_41) (1 FE_42) (1 FE_62) (1 FE_63) (1 FE_65) (1 FE_74) (1 FE_75) (1 FE_76) (1 TbpA)
74	(1 ADP) (1 ATP) (1 FE_29) (1 FE_30) (1 FE_31) (1 FE_32) (1 FE_33) (1 FE_34) (1 FE_35) (1 FE_36) (1 FE_38) (1 FE_41) (1 FE_42) (1 FE_62) (1 FE_64) (1 FE_65) (1 FE_74) (1 FE_75) (1 FE_76) (1 TbpA)
75	(1 ADP) (1 ATP) (1 FbpA) (1 FE_29) (1 FE_30) (1 FE_31) (1 FE_32) (1 FE_33) (1 FE_34) (1 FE_35) (1 FE_36) (1 FE_38) (1 FE_41) (1 FE_42) (1 FE_62) (1 FE_63) (1 FE_65) (1 FE_67) (1 FE_74) (1 FE_76) (1 TbpA)
76	(1 ADP) (1 ATP) (1 FbpA) (1 FE_29) (1 FE_30) (1 FE_31) (1 FE_32) (1 FE_33) (1 FE_34) (1 FE_35) (1 FE_36) (1 FE_38) (1 FE_41) (1 FE_42) (1 FE_62) (1 FE_64) (1 FE_65) (1 FE_67) (1 FE_74) (1 FE_76) (1 TbpA)
77	(1 ADP) (1 ATP) (1 FbpBC) (1 FE_29) (1 FE_30) (1 FE_31) (1 FE_32) (1 FE_33) (1 FE_34) (1 FE_35) (1 FE_36) (1 FE_38) (1 FE_41) (1 FE_42) (1 FE_62) (1 FE_63) (1 FE_65) (1 FE_68) (1 FE_74) (1 FE_75) (1 TbpA)
78	(1 ADP) (1 ATP) (1 FbpBC) (1 FE_29) (1 FE_30) (1 FE_31) (1 FE_32) (1 FE_33) (1 FE_34) (1 FE_35) (1 FE_36) (1 FE_38) (1 FE_41) (1 FE_42) (1 FE_62) (1 FE_64) (1 FE_65) (1 FE_68) (1 FE_74) (1 FE_75) (1 TbpA)
79	(1 ADP) (1 ATP) (1 FbpA) (1 FbpBC) (1 FE_29) (1 FE_30) (1 FE_31) (1 FE_32) (1 FE_33) (1 FE_34) (1 FE_35) (1 FE_36) (1 FE_38) (1 FE_41) (1 FE_42) (1 FE_62) (1 FE_63) (1 FE_65) (1 FE_67) (1 FE_68) (1 FE_74) (1 TbpA)
80	(1 ADP) (1 ATP) (1 FbpA) (1 FbpBC) (1 FE_29) (1 FE_30) (1 FE_31) (1 FE_32) (1 FE_33) (1 FE_34) (1 FE_35) (1 FE_36) (1 FE_38) (1 FE_41) (1 FE_42) (1 FE_62) (1 FE_64) (1 FE_65) (1 FE_67) (1 FE_68) (1 FE_74) (1 TbpA)
81	(1 ADP) (1 ATP) (1 FE_29) (1 FE_30) (1 FE_31) (1 FE_32) (1 FE_33) (1 FE_34) (1 FE_35) (1 FE_36) (1 FE_38) (1 FE_41) (1 FE_42) (1 FE_62) (1 FE_63) (1 FE_66) (1 FE_73) (1 FE_75) (1 FE_76) (1 Ton_system)
82	(1 ADP) (1 ATP) (1 FE_29) (1 FE_30) (1 FE_31) (1 FE_32) (1 FE_33) (1 FE_34) (1 FE_35) (1 FE_36) (1 FE_38) (1 FE_41) (1 FE_42) (1 FE_62) (1 FE_64) (1 FE_66) (1 FE_73) (1 FE_75) (1 FE_76) (1 Ton_system)
83	(1 ADP) (1 ATP) (1 FbpA) (1 FE_29) (1 FE_30) (1 FE_31) (1 FE_32) (1 FE_33) (1 FE_34) (1 FE_35) (1 FE_36) (1 FE_38) (1 FE_41) (1 FE_42) (1 FE_62) (1 FE_63) (1 FE_66) (1 FE_67) (1 FE_73) (1 FE_76) (1 Ton_system)
84	(1 ADP) (1 ATP) (1 FbpA) (1 FE_29) (1 FE_30) (1 FE_31) (1 FE_32) (1 FE_33) (1 FE_34) (1 FE_35) (1 FE_36) (1 FE_38) (1 FE_41)

	(1 FE_42) (1 FE_62) (1 FE_64) (1 FE_66) (1 FE_67) (1 FE_73) (1 FE_76) (1 Ton_system)
85	(1 ADP) (1 ATP) (1 FbpBC) (1 FE_29) (1 FE_30) (1 FE_31) (1 FE_32) (1 FE_33) (1 FE_34) (1 FE_35) (1 FE_36) (1 FE_38) (1 FE_41) (1 FE_42) (1 FE_62) (1 FE_63) (1 FE_66) (1 FE_68) (1 FE_73) (1 FE_75) (1 Ton_system)
86	(1 ADP) (1 ATP) (1 FbpBC) (1 FE_29) (1 FE_30) (1 FE_31) (1 FE_32) (1 FE_33) (1 FE_34) (1 FE_35) (1 FE_36) (1 FE_38) (1 FE_41) (1 FE_42) (1 FE_62) (1 FE_64) (1 FE_66) (1 FE_68) (1 FE_73) (1 FE_75) (1 Ton_system)
87	(1 ADP) (1 ATP) (1 FbpA) (1 FbpBC) (1 FE_29) (1 FE_30) (1 FE_31) (1 FE_32) (1 FE_33) (1 FE_34) (1 FE_35) (1 FE_36) (1 FE_38) (1 FE_41) (1 FE_42) (1 FE_62) (1 FE_63) (1 FE_66) (1 FE_67) (1 FE_68) (1 FE_73) (1 Ton_system)
88	(1 ADP) (1 ATP) (1 FbpA) (1 FbpBC) (1 FE_29) (1 FE_30) (1 FE_31) (1 FE_32) (1 FE_33) (1 FE_34) (1 FE_35) (1 FE_36) (1 FE_38) (1 FE_41) (1 FE_42) (1 FE_62) (1 FE_64) (1 FE_66) (1 FE_67) (1 FE_68) (1 FE_73) (1 Ton_system)
89	(1 ADP) (1 ATP) (1 FE_29) (1 FE_30) (1 FE_31) (1 FE_32) (1 FE_33) (1 FE_34) (1 FE_35) (1 FE_36) (1 FE_38) (1 FE_41) (1 FE_42) (1 FE_62) (1 FE_63) (1 FE_65) (1 FE_66) (1 FE_75) (1 FE_76) (1 TbpA) (1 Ton_system)
90	(1 ADP) (1 ATP) (1 FE_29) (1 FE_30) (1 FE_31) (1 FE_32) (1 FE_33) (1 FE_34) (1 FE_35) (1 FE_36) (1 FE_38) (1 FE_41) (1 FE_42) (1 FE_62) (1 FE_64) (1 FE_65) (1 FE_66) (1 FE_75) (1 FE_76) (1 TbpA) (1 Ton_system)
91	(1 ADP) (1 ATP) (1 FbpA) (1 FE_29) (1 FE_30) (1 FE_31) (1 FE_32) (1 FE_33) (1 FE_34) (1 FE_35) (1 FE_36) (1 FE_38) (1 FE_41) (1 FE_42) (1 FE_62) (1 FE_63) (1 FE_65) (1 FE_66) (1 FE_67) (1 FE_76) (1 TbpA) (1 Ton_system)
92	(1 ADP) (1 ATP) (1 FbpA) (1 FE_29) (1 FE_30) (1 FE_31) (1 FE_32) (1 FE_33) (1 FE_34) (1 FE_35) (1 FE_36) (1 FE_38) (1 FE_41) (1 FE_42) (1 FE_62) (1 FE_64) (1 FE_65) (1 FE_66) (1 FE_67) (1 FE_76) (1 TbpA) (1 Ton_system)
93	(1 ADP) (1 ATP) (1 FbpBC) (1 FE_29) (1 FE_30) (1 FE_31) (1 FE_32) (1 FE_33) (1 FE_34) (1 FE_35) (1 FE_36) (1 FE_38) (1 FE_41) (1 FE_42) (1 FE_62) (1 FE_63) (1 FE_65) (1 FE_66) (1 FE_68) (1 FE_75) (1 TbpA) (1 Ton_system)
94	(1 ADP) (1 ATP) (1 FbpBC) (1 FE_29) (1 FE_30) (1 FE_31) (1 FE_32) (1 FE_33) (1 FE_34) (1 FE_35) (1 FE_36) (1 FE_38) (1 FE_41) (1 FE_42) (1 FE_62) (1 FE_64) (1 FE_65) (1 FE_66) (1 FE_68) (1 FE_75) (1 TbpA) (1 Ton_system)
95	(1 ADP) (1 ATP) (1 FbpA) (1 FbpBC) (1 FE_29) (1 FE_30) (1 FE_31) (1 FE_32) (1 FE_33) (1 FE_34) (1 FE_35) (1 FE_36) (1 FE_38) (1 FE_41) (1 FE_42) (1 FE_62) (1 FE_63) (1 FE_65) (1 FE_66) (1 FE_67) (1 FE_68) (1 TbpA) (1 Ton_system)
96	(1 ADP) (1 ATP) (1 FbpA) (1 FbpBC) (1 FE_29) (1 FE_30) (1 FE_31) (1 FE_32) (1 FE_33) (1 FE_34) (1 FE_35) (1 FE_36) (1 FE_38) (1 FE_41) (1 FE_42) (1 FE_62) (1 FE_64) (1 FE_65) (1 FE_66) (1 FE_67) (1 FE_68) (1 TbpA) (1 Ton_system)

Appendix 2 - Net reactions of transmembrane iron transport subnetwork elementary flux modes

EFM	Net reaction
1	ATP_ext + HAEM_HOST_ext + PMF_ext = ADP_ext + APO_HAEM_CYTO_ext + 2 FE_INCORP
2	ATP_ext + HAEM_HOST_ext + PMF_ext = ADP_ext + APO_HAEM_CYTO_ext + 2 FE_STORED
3	ATP_ext + HAEM_HOST_ext + PMF_ext = ADP_ext + APO_HAEM_CYTO_ext + 2 FE_INCORP
4	ATP_ext + HAEM_HOST_ext + PMF_ext = ADP_ext + APO_HAEM_CYTO_ext + 2 FE_STORED
5	ATP_ext + HAEM_HOST_ext + PMF_ext = ADP_ext + APO_HAEM_CYTO_ext + 2 FE_INCORP
6	ATP_ext + HAEM_HOST_ext + PMF_ext = ADP_ext + APO_HAEM_CYTO_ext + 2 FE_STORED
7	ATP_ext + HAEM_HOST_ext + PMF_ext = ADP_ext + APO_HAEM_CYTO_ext + 2 FE_INCORP
8	ATP_ext + HAEM_HOST_ext + PMF_ext = ADP_ext + APO_HAEM_CYTO_ext + 2 FE_STORED
9	ATP_ext + HAEM_HOST_ext + PMF_ext = ADP_ext + APO_HAEM_CYTO_ext + 2 FE_INCORP
10	ATP_ext + HAEM_HOST_ext + PMF_ext = ADP_ext + APO_HAEM_CYTO_ext + 2 FE_STORED
11	ATP_ext + HAEM_HOST_ext + PMF_ext = ADP_ext + APO_HAEM_CYTO_ext + 2 FE_INCORP
12	ATP_ext + HAEM_HOST_ext + PMF_ext = ADP_ext + APO_HAEM_CYTO_ext + 2 FE_STORED
13	ATP_ext + HAEM_HOST_ext + PMF_ext = ADP_ext + APO_HAEM_CYTO_ext + 2 FE_INCORP
14	ATP_ext + HAEM_HOST_ext + PMF_ext = ADP_ext + APO_HAEM_CYTO_ext + 2 FE_STORED
15	ATP_ext + HAEM_HOST_ext + PMF_ext = ADP_ext + APO_HAEM_CYTO_ext + 2 FE_INCORP
16	ATP_ext + HAEM_HOST_ext + PMF_ext = ADP_ext + APO_HAEM_CYTO_ext + 2 FE_STORED
17	ATP_ext + HAEM_HOST_ext + PMF_ext = ADP_ext + APO_HAEM_CYTO_ext + 2 FE_INCORP
18	ATP_ext + HAEM_HOST_ext + PMF_ext = ADP_ext + APO_HAEM_CYTO_ext + 2 FE_STORED
19	ATP_ext + HAEM_HOST_ext + PMF_ext = ADP_ext + APO_HAEM_CYTO_ext + 2 FE_INCORP
20	ATP_ext + HAEM_HOST_ext + PMF_ext = ADP_ext + APO_HAEM_CYTO_ext + 2 FE_STORED
21	ATP_ext + HAEM_HOST_ext + PMF_ext = ADP_ext + APO_HAEM_CYTO_ext + 2 FE_INCORP
22	ATP_ext + HAEM_HOST_ext + PMF_ext = ADP_ext + APO_HAEM_CYTO_ext + 2 FE_STORED
23	ATP_ext + HAEM_HOST_ext + PMF_ext = ADP_ext + APO_HAEM_CYTO_ext + 2 FE_INCORP
24	ATP_ext + HAEM_HOST_ext + PMF_ext = ADP_ext + APO_HAEM_CYTO_ext + 2 FE_STORED
25	ATP_ext + HAEM_HOST_ext + PMF_ext = ADP_ext + APO_HAEM_CYTO_ext + 2 FE_INCORP
26	ATP_ext + HAEM_HOST_ext + PMF_ext = ADP_ext + APO_HAEM_CYTO_ext + 2 FE_STORED
27	ATP_ext + HAEM_HOST_ext + PMF_ext = ADP_ext + APO_HAEM_CYTO_ext + 2 FE_INCORP
28	ATP_ext + HAEM_HOST_ext + PMF_ext = ADP_ext + APO_HAEM_CYTO_ext + 2 FE_STORED

29	ATP_ext + HAEM_HOST_ext + PMF_ext = ADP_ext + APO_HAEM_CYTO_ext + 2 FE_INCORP
30	ATP_ext + HAEM_HOST_ext + PMF_ext = ADP_ext + APO_HAEM_CYTO_ext + 2 FE_STORED
31	ATP_ext + HAEM_HOST_ext + PMF_ext = ADP_ext + APO_HAEM_CYTO_ext + 2 FE_INCORP
32	ATP_ext + HAEM_HOST_ext + PMF_ext = ADP_ext + APO_HAEM_CYTO_ext + 2 FE_STORED
33	ATP_ext + HAEM_HOST_ext + PMF_ext = ADP_ext + APO_HAEM_CYTO_ext + 2 FE_INCORP
34	ATP_ext + HAEM_HOST_ext + PMF_ext = ADP_ext + APO_HAEM_CYTO_ext + 2 FE_STORED
35	ATP_ext + HAEM_HOST_ext + PMF_ext = ADP_ext + APO_HAEM_CYTO_ext + 2 FE_INCORP
36	ATP_ext + HAEM_HOST_ext + PMF_ext = ADP_ext + APO_HAEM_CYTO_ext + 2 FE_STORED
37	ATP_ext + HAEM_HOST_ext + PMF_ext = ADP_ext + APO_HAEM_CYTO_ext + 2 FE_INCORP
38	ATP_ext + HAEM_HOST_ext + PMF_ext = ADP_ext + APO_HAEM_CYTO_ext + 2 FE_STORED
39	ATP_ext + HAEM_HOST_ext + PMF_ext = ADP_ext + APO_HAEM_CYTO_ext + 2 FE_INCORP
40	ATP_ext + HAEM_HOST_ext + PMF_ext = ADP_ext + APO_HAEM_CYTO_ext + 2 FE_STORED
41	ATP_ext + HAEM_HOST_ext + PMF_ext = ADP_ext + APO_HAEM_CYTO_ext + 2 FE_INCORP
42	ATP_ext + HAEM_HOST_ext + PMF_ext = ADP_ext + APO_HAEM_CYTO_ext + 2 FE_STORED
43	ATP_ext + HAEM_HOST_ext + PMF_ext = ADP_ext + APO_HAEM_CYTO_ext + 2 FE_INCORP
44	ATP_ext + HAEM_HOST_ext + PMF_ext = ADP_ext + APO_HAEM_CYTO_ext + 2 FE_STORED
45	ATP_ext + HAEM_HOST_ext + PMF_ext = ADP_ext + APO_HAEM_CYTO_ext + 2 FE_INCORP
46	ATP_ext + HAEM_HOST_ext + PMF_ext = ADP_ext + APO_HAEM_CYTO_ext + 2 FE_STORED
47	ATP_ext + HAEM_HOST_ext + PMF_ext = ADP_ext + APO_HAEM_CYTO_ext + 2 FE_INCORP
48	ATP_ext + HAEM_HOST_ext + PMF_ext = ADP_ext + APO_HAEM_CYTO_ext + 2 FE_STORED
49	ATP_ext + HAEM_HOST_ext + PMF_ext = ADP_ext + APO_HAEM_CYTO_ext + 2 FE_INCORP
50	ATP_ext + HAEM_HOST_ext + PMF_ext = ADP_ext + APO_HAEM_CYTO_ext + 2 FE_STORED
51	ATP_ext + HAEM_HOST_ext + PMF_ext = ADP_ext + APO_HAEM_CYTO_ext + 2 FE_INCORP
52	ATP_ext + HAEM_HOST_ext + PMF_ext = ADP_ext + APO_HAEM_CYTO_ext + 2 FE_STORED
53	ATP_ext + HAEM_HOST_ext + PMF_ext = ADP_ext + APO_HAEM_CYTO_ext + 2 FE_INCORP
54	ATP_ext + HAEM_HOST_ext + PMF_ext = ADP_ext + APO_HAEM_CYTO_ext + 2 FE_STORED
55	ATP_ext + HAEM_HOST_ext + PMF_ext = ADP_ext + APO_HAEM_CYTO_ext + 2 FE_INCORP
56	ATP_ext + HAEM_HOST_ext + PMF_ext = ADP_ext + APO_HAEM_CYTO_ext + 2 FE_STORED
57	ATP_ext + HAEM_HOST_ext + PMF_ext = ADP_ext + APO_HAEM_CYTO_ext + 2 FE_INCORP
58	ATP_ext + HAEM_HOST_ext + PMF_ext = ADP_ext + APO_HAEM_CYTO_ext + 2 FE_STORED
59	ATP_ext + HAEM_HOST_ext + PMF_ext = ADP_ext + APO_HAEM_CYTO_ext + 2 FE_INCORP
60	ATP_ext + HAEM_HOST_ext + PMF_ext = ADP_ext + APO_HAEM_CYTO_ext + 2 FE_STORED

61	ATP_ext + HAEM_HOST_ext + PMF_ext = ADP_ext + APO_HAEM_CYTO_ext + 2 FE_INCORP
62	ATP_ext + HAEM_HOST_ext + PMF_ext = ADP_ext + APO_HAEM_CYTO_ext + 2 FE_STORED
63	ATP_ext + HAEM_HOST_ext + PMF_ext = ADP_ext + APO_HAEM_CYTO_ext + 2 FE_INCORP
64	ATP_ext + HAEM_HOST_ext + PMF_ext = ADP_ext + APO_HAEM_CYTO_ext + 2 FE_STORED
65	ATP_ext + FE_ext + PMF_ext = ADP_ext + FE_INCORP
66	ATP_ext + FE_ext + PMF_ext = ADP_ext + FE_STORED
67	ATP_ext + FE_ext + PMF_ext = ADP_ext + FE_INCORP
68	ATP_ext + FE_ext + PMF_ext = ADP_ext + FE_STORED
69	ATP_ext + FE_ext + PMF_ext = ADP_ext + FE_INCORP
70	ATP_ext + FE_ext + PMF_ext = ADP_ext + FE_STORED
71	ATP_ext + FE_ext + PMF_ext = ADP_ext + FE_INCORP
72	ATP_ext + FE_ext + PMF_ext = ADP_ext + FE_STORED
73	ATP_ext + FE_ext + PMF_ext = ADP_ext + FE_INCORP
74	ATP_ext + FE_ext + PMF_ext = ADP_ext + FE_STORED
75	ATP_ext + FE_ext + PMF_ext = ADP_ext + FE_INCORP
76	ATP_ext + FE_ext + PMF_ext = ADP_ext + FE_STORED
77	ATP_ext + FE_ext + PMF_ext = ADP_ext + FE_INCORP
78	ATP_ext + FE_ext + PMF_ext = ADP_ext + FE_STORED
79	ATP_ext + FE_ext + PMF_ext = ADP_ext + FE_INCORP
80	ATP_ext + FE_ext + PMF_ext = ADP_ext + FE_STORED
81	ATP_ext + FE_ext + PMF_ext = ADP_ext + FE_INCORP
82	ATP_ext + FE_ext + PMF_ext = ADP_ext + FE_STORED
83	ATP_ext + FE_ext + PMF_ext = ADP_ext + FE_INCORP
84	ATP_ext + FE_ext + PMF_ext = ADP_ext + FE_STORED
85	ATP_ext + FE_ext + PMF_ext = ADP_ext + FE_INCORP
86	ATP_ext + FE_ext + PMF_ext = ADP_ext + FE_STORED
87	ATP_ext + FE_ext + PMF_ext = ADP_ext + FE_INCORP
88	ATP_ext + FE_ext + PMF_ext = ADP_ext + FE_STORED
89	ATP_ext + FE_ext + PMF_ext = ADP_ext + FE_INCORP
90	ATP_ext + FE_ext + PMF_ext = ADP_ext + FE_STORED
91	ATP_ext + FE_ext + PMF_ext = ADP_ext + FE_INCORP
92	ATP_ext + FE_ext + PMF_ext = ADP_ext + FE_STORED

93	ATP_ext + FE_ext + PMF_ext = ADP_ext + FE_INCORP
94	ATP_ext + FE_ext + PMF_ext = ADP_ext + FE_STORED
95	ATP_ext + FE_ext + PMF_ext = ADP_ext + FE_INCORP
96	ATP_ext + FE_ext + PMF_ext = ADP_ext + FE_STORED

Appendix 3 - Raw data for Applikon Microreactor experiments 1

Isolate	Time (hours)	Growth (CFU/ml)		Protein (mg/ml)		Glucose (µg/ml)	
		Iron replete	Iron restricted	Iron replete	Iron restricted	Iron replete	Iron restricted
671/90	0	$3.0x10^{7}$	$3.2x10^{7}$	0.31	0.40	0	0
	2	$9.5x10^{8}$	$1.4x10^{8}$	0.52	0.57	102	207
	4	$1.0x10^{10}$	$2.3x10^{8}$	1.51	0.55	1534	0
	6	$2.7x10^{10}$	$3.0x10^{8}$	2.62	0.81	3136	680
	8	$3.2x10^{10}$	$1.5x10^{8}$	2.72	0.60	3139	0
45/04	0	$4.0x10^{7}$	$6.0x10^{7}$	0.00	0.00	0	0
	2	$7.0x10^{8}$	$1.2x10^{8}$	0.01	0.22	558	156
	4	$5.5x10^{9}$	$4.5x10^{8}$	0.31	0.13	1412	0
	6	$4.5x10^{10}$	$2.5x10^{9}$	1.44	0.62	3065	1218
	8	$7.0x10^{10}$	$7.5x10^{9}$	1.53	0.73	3065	2748
200038/A	0	$1.5x10^{8}$	$5.0x10^{7}$	0.00	0.00	0	0
	2	$2.0x10^{6}$	$4.5x10^{8}$	0.02	0.02	1000	0
	4	$4.0x10^{9}$	$6.0x10^{8}$	0.26	0.21	844	310
	6	$5.5x10^{10}$	$4.0x10^{9}$	1.50	0.72	2371	874
	8	$9.5x10^{10}$	$7.0x10^{9}$	1.47	0.68	3204	952
501249/A	0	$8.5x10^{7}$	$7.5x10^{7}$	0.00	0.00	0	0
	2	$1.0x10^{9}$	$5.0x10^{8}$	0.16	0.10	187	0
	4	$2.5x10^{9}$	$1.2x10^{9}$	0.69	0.31	146	0
	6	$1.4x10^{10}$	$1.5x10^{9}$	1.17	0.58	1595	0
	8	$1.3x10^{10}$	$1.8x10^{9}$	2.01	0.76	2929	238

These data represent a collation of raw data from graphs shown in **Figures 5.2**, **5.3** and **5.4** for growth rate, total protein content of bacterial pellets and glucose uptake by bacteria respectively.

Appendix 4 - Raw data for Applikon Microreactor experiments 2

Experiment	Time (hours)	Growth (CFU/ml)		Protein (mg/ml)		Glucose (µg/ml)	
		Iron replete	**Iron restricted**	**Iron replete**	**Iron restricted**	**Iron replete**	**Iron restricted**
1. Iron replete versus iron restricted, 37°C, pH 7.0	0	$1.8x10^{7}$	$1.9x10^{7}$	0.08	0.09	0	0
	2	$9.5x10^{8}$	$2.7x10^{8}$	0.35	0.23	218	73
	4	$1.2x10^{10}$	$1.7x10^{9}$	1.50	0.21	1357	571
	6	$7.5x10^{10}$	$8.5x10^{9}$	2.25	0.58	2687	85
	8	$1.2x10^{11}$	$5.5x10^{9}$	2.47	0.33	2680	94
2. 37°C versus 39°C, iron replete, pH 7.0		**37°C**	**39°C**	**37°C**	**39°C**	**37°C**	**39°C**
	0	$1.1x10^{8}$	$9.5x10^{7}$	0.03	0.05	0	0
	2	$9.0x10^{8}$	$8.0x10^{7}$	0.16	0.22	82	105
	4	$8.0x10^{9}$	$9.0x10^{8}$	1.05	1.32	670	1517
	6	$6.0x10^{10}$	$5.5x10^{9}$	1.97	1.93	2310	2673
	8	$5.5x10^{10}$	$8.0x10^{9}$	1.98	2.04	2310	2673
3. pH 6.0 versus pH 8.0, iron replete, 37°C		**pH 6.0**	**pH 8.0**	**pH 6.0**	**pH 8.0**	**pH 6.0**	**pH 8.0**
	0	$8.5x10^{7}$	$9x10^{7}$	0.03	0.06	0	0
	2	$2.3x10^{8}$	$1.3x10^{9}$	0.12	0.27	684	0
	4	$6.5x10^{8}$	$1.9x10^{10}$	0.14	1.02	1065	1874
	6	$8x10^{9}$	$6x10^{10}$	0.28	1.49	1524	1973
	8	$1.6x10^{10}$	$9x10^{10}$	0.84	1.87	2031	1973
4. pH 6.0 versus pH 8.0, iron replete, 30°C		**pH 6.0**	**pH 8.0**	**pH 6.0**	**pH 8.0**	**pH 6.0**	**pH 8.0**
	0	$5.5x10^{7}$	$5x10^{7}$	0.03	0.05	0	0
	2	$1.2Ex10^{8}$	$5x10^{8}$	0.03	0.03	0	0
	4	$5x10^{8}$	$1x10^{9}$	0.05	0.17	0	0
	6	$1.1x10^{9}$	$1.1x10^{10}$	0.16	0.61	0	367
	8	$9x10^{9}$	$6.5x10^{10}$	0.27	1.71	0	1786

These data represent a collation of raw data from graphs shown in **Figures 5.5**, **5.6**, **5.7** and **5.8** (**1, 2**, **3** and **4** respectively in table above) for growth rate, total protein content of bacterial pellets and glucose uptake by bacteria.